1 OF 4

PB

273357

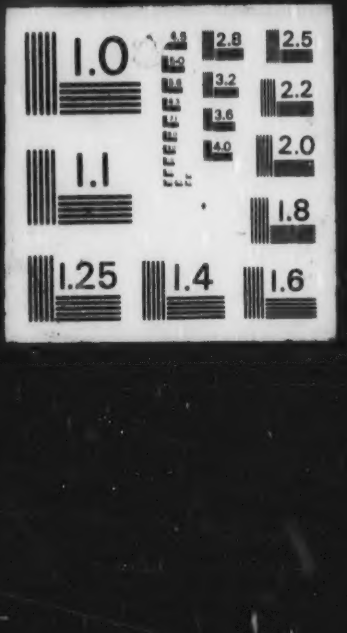
1.0
4.5
5.0
5.6
6.3
2.8
3.2
3.6
4.0
2.5
2.2
2.0
1.1
1.8
1.25
1.4
1.6

U.S. DEPARTMENT OF COMMERCE
National Technical Information Service

PB-273 357

Generation and Simulation of Metallic Particulate Air Pollutants by Electric Arc Spraying

West Virginia Univ, Morgantown

Prepared for

Industrial Environmental Research Lab, Research Triangle Park, N C

Sep 77

PB 273 357

EPA-600/2-77-201
September 1977

Environmental Protection Technology Series

UNITED STATES ENVIRONMENTAL PROTECTION AGENCY

REPRODUCED BY
NATIONAL TECHNICAL
INFORMATION SERVICE
U. S. DEPARTMENT OF COMMERCE
SPRINGFIELD, VA. 22161

RESEARCH REPORTING SERIES

Research reports of the Office of Research and Development, U.S. Environmental Protection Agency, have been grouped into nine series. These nine broad categories were established to facilitate further development and application of environmental technology. Elimination of traditional grouping was consciously planned to foster technology transfer and a maximum interface in related fields. The nine series are:

1. Environmental Health Effects Research
2. Environmental Protection Technology
3. Ecological Research
4. Environmental Monitoring
5. Socioeconomic Environmental Studies
6. Scientific and Technical Assessment Reports (STAR)
7. Interagency Energy-Environment Research and Development
8. "Special" Reports
9. Miscellaneous Reports

This report has been assigned to the ENVIRONMENTAL PROTECTION TECHNOLOGY series. This series describes research performed to develop and demonstrate instrumentation, equipment, and methodology to repair or prevent environmental degradation from point and non-point sources of pollution. This work provides the new or improved technology required for the control and treatment of pollution sources to meet environmental quality standards.

REVIEW NOTICE

This report has been reviewed by the participating Federal Agencies, and approved for publication. Approval does not signify that the contents necessarily reflect the views and policies of the Government, nor does mention of trade names or commercial products constitute endorsement or recommendation for use.

This document is available to the public through the National Technical Information Service, Springfield, Virginia 22161.

TECHNICAL REPORT DATA
(Please read Instructions on the reverse before completing)

1. REPORT NO.
EPA-600/2-77-201

2.

3. RECIPIENT'S ACCESSION NO.
PB275557

4. TITLE AND SUBTITLE
Generation and Simulation of Metallic Particulate Air Pollutants by Electric Arc Spraying

5. REPORT DATE
September 1977

6. PERFORMING ORGANIZATION CODE

7. AUTHOR(S)
B. Linsky, R. Hedden, M. Naylor, and F. Dimmick

8. PERFORMING ORGANIZATION REPORT NO.

9. PERFORMING ORGANIZATION NAME AND ADDRESS
University of West Virginia
Morgantown, West Virginia 26506

10. PROGRAM ELEMENT NO.
1AB012; ROAP 21ADM-025

11. CONTRACT/GRANT NO.
Grant R801858

12. SPONSORING AGENCY NAME AND ADDRESS
EPA, Office of Research and Development
Industrial Environmental Research Laboratory
Research Triangle Park, NC 27711

13. TYPE OF REPORT AND PERIOD COVERED
Grant Final; 7/73-1/75

14. SPONSORING AGENCY CODE
EPA/600/13

15. SUPPLEMENTARY NOTES IERL-RTP project officer for this report is Dennis C. Drehmel, Mail Drop 61, 919/541-2925.

16. ABSTRACT The report gives results of efforts to provide a generated output with an appropriate mass and concentration of fresh, dry, fine metal oxide particles for bench or pilot scale fine particulate collection research and development work. The work involved two electric arc aerosol generators: one using a single consumable electrode of welding wire; the other, two consumable wire electrodes of a commercially available electric arc metallizer. The generated aerosols were exhausted into a duct system and sampled using membrane filters. The single electrode generator produced 0.67 g/cu m of 0.1 micrometer diameter iron oxide particles as sampled by an Andersen Stack Sampler. The mass emission rate with an average of 1.95 g/min varied within a + or - 12% range. The double electrode generator produced submicron particles (measure by scanning electron microscopy). Mass volumetric concentrations ranged from 0.7 to 2.0 g/cu m for zinc oxide aerosols. The mass emission rate averaged 8.6 g/min for the zinc oxide aerosols and 7.7 g/min for the iron oxide aerosols. (The zinc oxide was ZnO and the iron oxide, Fe_3O_4.) The double electrode generator was further tested and validated for reproducibilities of total mass volumetric concentration and basic particle diameter distributions. Variables of operation were investigated to determine their effect on the mass volumetric concentration of the aerosol.

17. KEY WORDS AND DOCUMENT ANALYSIS

a. DESCRIPTORS		b. IDENTIFIERS/OPEN ENDED TERMS	c. COSATI Field/Group	
Air Pollution	Zinc Oxides	Air Pollution Control	13B	07B
Simulation	Iron Oxides	Particulate	14B	
Aerosols		Electric Arc Spraying	07D	
Metal Powder		Metallic Oxide Particles	11F	
Electric Arcs		Particle Collection	20C	
Metallizing			13H, 11C	

18. DISTRIBUTION STATEMENT
Unlimited

19. SECURITY CLASS *(This Report)*
Unclassified

20. SECURITY CLASS *(This page)*
Unclassified

21. NO. OF PAGES
336

22. PRICE
A15-A01

EPA Form 2220-1 (9-73)

EPA-600/2-77-201
September 1977

GENERATION AND SIMULATION OF METALLIC PARTICULATE AIR POLLUTANTS BY ELECTRIC ARC SPRAYING

by

B. Linsky, R. Hedden, M. Naylor, and F. Dimmick

University of West Virginia
Morgantown, West Virginia 26506

Grant No. R801858
ROAP No. 21ADM-025
Program Element No. 1AB012

EPA Project Officer: Dennis C. Drehmel

Industrial Environmental Research Laboratory
Office of Energy, Minerals, and Industry
Research Triangle Park, North Carolina 27711

Prepared for

U.S. ENVIRONMENTAL PROTECTION AGENCY
Office of Research and Development
Washington, D.C. 20460

ia

PREFACE

The growing concern about fine particles was barely detectable among air pollution specialists in the late 1950's. It surfaced in the emission inventory of the San Francisco Bay Area Air Pollution Control District Technical Report of 1958. By the early 1970's recognition of the need to control fine particles separately had been established. It became U.S. Environmental Protection Agency policy to deal with these microscopic and sub-micrometer particulates differently than larger ones from a technological control viewpoint, from an undesirable effects viewpoint, from a regulatory viewpoint, and from a measurement viewpoint.

The fine particles that were technically available for research and engineering development were either surrogates for realistic fine particulates, such as DOP, or were stale dusts that were redispersed in a gas stream. Some of the surrogates came from aqeous solutions or suspensions and were high in water vapor content as they entered the air or other gas streams. Caught in a dust collector weeks earlier and redispersed, the metal or metal oxide fine particulates were not fresh even though it is generally recognized that fresh metal fumes are often more reactive than stale ones.

There seemed to be a growing demand for a fresh dry fine particle generator of realistic metallic oxides such as a fine particle generating system with a fresh, dry particle output somewhat similar to that from an electric arc furnace. It was hoped that the mass per unit time (mass emission rate) and mass per unit volume of gases (mass volumetric concentration) would be sufficient to allow a realistically high dust-in-exhaust-gas stream for testing bench scale or small pilot scale dust collector to "improve the breed" of such collectors. The U.S. Environmental Protection Agency having an immediate need for such a fine particle generator because of work they were doing and extramural work they were having done for them on charged droplet fine particle scrubbers and other fine particle control equipment research and development purchased identical equipment to the metallizer generator when the ongoing findings of this research grant indicated a resonable possibility of success in mass volumetric concentration and mass emission rate of fine particles.

This report contains, as appendices, the theses and problem reports of the graduate students who did most of the research work on this project. As will be noted, most of the electron micrography and all of the elemental and chemical compound analytical work were done by a specialist contractor, Walter C. McCrone Associates. Much of the fine particle sizing was also done by the McCrone organization.

ABSTRACT

This research program was a pragmatic experimental activity that was conceived to provide a long-needed research tool for those concerned with very fine particles and their technological control. In order to try to provide a generated output with an appropriate mass and concentration of fresh dry fine metal oxide particles for bench or pilot scale collector research and development work, electric arc generators of fresh fine particle aerosols were modified and tested with zinc metallizing wire and with steel welding and metallizing wire at West Virginia University.

Work with two electric arc aerosol generators is reported; one generator employed a single consumable electrode of welding wire and the other generator employed two consumable wire electrodes of a commercially available electric arc metallizer. The generated aerosols were exhausted into a duct system and sampled using membrane filters.

The single electrode generator produced 0.67 grams per cubic meter of 0.1 micrometer diameter fresh iron oxide agglomerated particles as sampled by an Andersen Stack Sampler. The mass emission rate with an average of 1.95 grams per minute varied within a plus or minus 12 percent range. The basic particles that formed the 0.1 micrometer agglomerated particles were characterized to be log normally distributed with a mass median diameter of 0.0167 micrometer as observed and measured by electron microscopy.

The two consumable electrode aerosol generator produced agglomerated submicron particles (as measured by scanning electron microscopy) formed from 2-20 nanometer diameter basic particles (as measured by transmission electrode microscopy). Mass volumetric concentrations ranged from 0.7 - 2.0 grams per cubic meter for zinc oxide aerosols. The mass emission rate averaged 8.6 grams per minute for the zinc oxide aerosols and 7.7 grams per minute for the iron oxide aerosols. Selected area electron diffraction analyses found the zinc oxide to be ZnO and the iron oxide to be Fe_3O_4. The two electrode aerosol generator was further tested and validated for reproducibilities of total mass volumetric concentration and basic particle diameter distributions. Variables of operation were investigated to determine their effect on the mass volumetric concentration of the fresh dry fine particle aerosol produced by the generator.

This report was submitted in fulfillment of Grant No. R-801858-01-1 by West Virginia University under the sponsorship of the U. S. Environmental Protection Agency. This report covers the period July 20, 1973 to January 15, 1975, and work completed outside of the grant period through April 29, 1977, was included.

CONTENTS

Page

PREFACE ii

ABSTRACT iv

FIGURES vii

TABLES viii

CONVERSIONS FROM METRIC TO ENGLISH ix

ACKNOWLEDGMENTS x

A. INTRODUCTION 1

B. CONCLUSIONS AND RECOMMENDATIONS 6

C. EXPERIMENTAL PROCEDURES 11

Apparatus 12

Sampling 17

Analytic Techniques 19

Experimental Designs 19

D. RESULTS AND DISCUSSION 21

APPENDICES

1. THE HEDDEN REPORT 1-i

2. THE NAYLOR REPORT 2-i

3. THE DIMMICK REPORT 3-i

FIGURES

Number Page

1 Simplified diagram of aerosol generator apparatus (Hedden) 13

2 Metallizer equipment used by Naylor 15

3 Shrouded head metallizer equipment used by Dimmick 16

TABLES

Number		Page
1	Summary of mass volumetric concentration and emission rate with approximate range of agglomerated particle size indicated (Hedden)	22
2	Relative basic particle size frequency distribution in percent (Hedden)	24
3	Zinc oxide mass concentration mean and variance summary (Naylor)	25
4	Means and variances of zinc oxide basic particle size data (Naylor)	26
5	Analysis of variance for Latin Square experimental design mass volumetric concentration data (Dimmick)	28
6	Statistics for agglomerated samples (Dimmick)	29
7	Statistics for very fine basic particles (Dimmick)	30
8	Hedden-Naylor-Dimmick summary of results	31

CONVERSIONS FROM METRIC TO ENGLISH

1 meter = 10^{10} Å = 3.28 feet

1 meter/sec = 3.28 feet/sec

1 cubic meter (m^3) = 35.315 cubic feet (ft^3)

1 m^3/min = 35.315 ft^3/minute

1 gram = 15.43 grains = 2.2×10^{-3} pounds

1 gram/m^3 = 0.44 grain/ft^3 = 0.0624 pounds/1000 ft^3

1 gram/min. = 0.138 pounds/hr.

°C = (°F-32)/1.8

ACKNOWLEDGMENTS

The cooperation of several present and former materials identification specialists at West Virginia University is recognized and appreciated. They are named in the component reports and theses. Assistance beyond the ordinary level of equipment and service supplier's advice and guidance are also appreciated and recognized from Wall Colmonoy, Flamespray Industries, and McCrone's firms.

There were also inumerable discussants by phone and at various air pollution specialists' gatherings, ranging from a Gordon Research Conference through an Air Pollution Control Association session to several EPA supported conferences on fine particulates. It would not be possible to name all of the contributors of ideas, experiences, cautions, etc.

Considerable financial support, other than that which was provided in the research grant itself, was in the form of U.S. Environmental Protection Agency traineeships for graduate study from the Office of Air Pollution Manpower Development, as is shown in the component reports and theses.

Section A

INTRODUCTION

The need for a generator of fresh fine particle aerosols and the lack of a suitable generator led to the proposal of research and development of a fine particle aerosol generator for use in fine particle air pollution control research and development. The general purpose of this research was to prepare and characterize high mass volumetric concentration, fresh fine metallic oxide particle aerosols. In particular, the electric arc process of particle generation was chosen as most likely to provide the desired product. This required characterizing the fine particle aerosols and the mass concentrations produced by an electric arc aerosol generator.

Two electric arc aerosol generators were investigated and developed by graduate students at West Virginia University under the guidance of Professor Benjamin Linsky. Robert Hedden, having developed an initial single consumable electrode aerosol generator, reported results on a modified version of his generator in his Masters report. Michael Naylor and Fred Dimmick, working with a commercially available metallizer employing two consumable electrodes, reported results in their Masters reports. These three Masters of Science reports are the basis of this summary report; each of the Masters reports is attached as an appendix.

In order to place into proper perspective the information from these

Masters reports, a short developmental history from Hedden's first consumable electrode electric arc aerosol generator to the current form of the metallizer is presented. Again, differences in equipment configurations, differences in aerosol sampling methods and differences in analytic techniques are presented to provide insight into the background of the information.

During his graduate study, Robert Hedden developed a number of very fine particle generators which used an electric arc welder system. His systems changed based on his experience; one of his systems used two consumable wires, another used consumable wire and a non-consumable fixed electrode and another used one consumable wire and a non-consumable rotating electrode. He examined the last system in detail; it consisted of a consumable wire feed as the anode and a relatively non-consumable tungsten electrode as the cathode. Carbon steel welding wire was used for the anode. Runs were limited to 30 minutes due to the tungsten cathode being consumed after that length of time.

Modifications of Hedden's system were developed in 1973-74 by Professor Linsky, Robert Hedden, Dr. William Fischer, Arland Johansen, Michael McCawley, Rasool Nekooi and Dr. Richard Sears. This system consisted of using a Hobart continuous electric arc welder with two consumable wires from 2 separate heads each with its own wire feed motor and motor speed regulator. This system was unstable because of inadequate control over several factors including the guidance of the wires; for example, sometimes gaps between the wires were greater than 0.25 inch. Data collected using this system was insufficient to establish conclusive results.

In December, 1974, a commercial metallizer was found on the industrial consumer market that seemed to have suitable properties. The Electrospray metallizer unit (Wall Colmonoy Corp., Model VT-500) was selected after examining alternatives such as Model 10E metallizing gun of METCO, Inc.

The Electrospray metallizer was put into operation by Professor Linsky, Michael McCawley, Joe McCauley, Dr. Sears and Anthony Angotti. After establishing the generation system consisting of the metallizer, a collection barrel and an exhaust system for the aerosol, Robert Hedden, John Garbak, Don Stone and Mike Naylor proceeded to calibrate the equipment used in the process and tried to establish stability on generation runs. Even though reliable stability on runs was not established, periodic stable runs allowed some sampling.

Early work with the metallizer, which initially consisted of generating aerosols with metallizer steel wire (coated with copper), was followed by a change to 15 gauge zinc metallizing wire. Continued difficulty in establishing reliably stable generation runs occurred using the zinc wire.

In December, 1975, Naylor, Stone, and Dimmick made modifications and ran several successful runs with the zinc metallizing wire on the aerosol generator. Naylor collected samples in January, 1976 for his report.

During the summer cf 1976, Dimmick, Stone and Craig Repp worked on aerosol generation with steel welding wire and copper coated steel metallizing wire. After a few modifications and additions, Dimmick took samples with welding wire and metallizing wire.

Differences in generator configurations, in sampling methods, and in analytical techniques are evident when comparing the three Masters reports. The obvious differences between the Hedden design and the commercial metallizer design may overshadow the subtle differences in the generator configurations of Naylor and Dimmick. For example, Naylor positioned the separation and collection barrel vertically while Dimmick positioned the barrel horizontally; Dimmick employed an electrode tip shroud and Naylor did not. Hedden's power source was a constant voltage source; Naylor and Dimmick's was not. Also, Hedden's arc chamber was above atmospheric pressure and Naylor's and Dimmick's was below atmospheric pressure.

Differences in sampling methods center around two points: (1) methods used and (2) proficiency of each experimenter. Hedden used an Andersen Stack Sampler followed by a membrane filter. Naylor and Dimmick used membrane filters to collect particle diameter count and mass volumetric concentration samples. While Naylor's mass volumetric concentration samples were collected generally under isokinetic conditions, Dimmick's were not and Hedden did not report an isokinetic estimate.

Differences in analytical procedures may have led the research astray. In particular, Hedden employed typical electron microscopy techniques of particle measurement including dispersion of particle aggregates. Although Hedden explained that chained and agglomerated particles should be expected from electric arc production of aerosols, Naylor and Dimmick, through the McCrone organization, measured particles in the 2-20 nanometer range while an awareness of an apparent agglomerated-particle aerosol grew when properly loaded membrane filters were evaluated from scanning electron micrographs. Also, the inherent differences in sampling methods led to other differences in analytical measurements.

Despite the differences in equipment configuration, sampling techniques and analytical methods, the three Masters reports have fulfilled the objectives of aerosol characterization and apparatus investigation. Certainly some questions have been answered, some have been partially answered and many more have been raised. The report that follows should be taken in the light of the differences and similarities between each Masters report.

Section B

CONCLUSIONS AND RECOMMENDATIONS

Hedden concluded that based on the results of limited experimental tests the feasibility of employing an electric arc to produce aerosols of very fine iron oxide particles from a feedstock of consumable wire has been demonstrated. More than 30 grains per minute (1.95 g/min) of discrete, spherical particles with a mass median diameter of 0.0167 micrometers were repeatedly produced within a range of plus or minus 12 percent. Also, a conservative examination of the mass distribution data obtained from the Andersen Stack Sampler particle sizing technique indicated that approximately 75 percent of the particles have an effective diameter less than 0.1 micrometers.

Hedden recommended:

(1) With modification, the unit might be adapted for the production of aerosols of non-conductive refractory materials. This might be accomplished by replacing the wire torch with another non-consumable electrode holder, establishing an arc between them, and guiding the non-conductive feedstock into the high-intensity arc.

(2) Elimination of the tungsten electrode as one side of the arc could be accomplished by utilizing two wire torches and establishing an arc between the two consumable wire "electrodes."

(3) If agglomerating effects prove undesirable for a particular study, an ion generator or polonium grid could be employed to neutralize the charged particles.

(4) Optimization of main operating parameters - arc voltage, wire feed rate, and wire diameter - could significantly improve the feedstock-to-particulate conversion ratio of 4.75 percent.

Naylor concluded that for at least one operating condition, the generator can produce very fine agglomerated zinc oxide particles that are reproducible with respect to both the distribution of the basic particle diameters and mass volumetric concentration. Therefore, this metallizer is considered worthy of continued attention by researchers as a device for generating very fine particles.

The generation of mass concentration ranging from 0.67 - 2.05 g/sm^3 (1.5 - 4.7 grain/scf) was reproducibile at three of four operating conditions. The mass volumetric concentration was sensitive to changes in the operating conditions. The mass emission rate was 4.7 - 14.5 gram/minute.

Basic particle sizes ranged from 6.0 - 10.8 nm (0.006 - 0.0108 μm). At one operating condition, the basic particle diameters' mean and standard deviation were reproducibile, while at another the basic particle's mean, standard deviation and cumulative frequency distribution diameter was reproducibile. Comparatively, the mean particle diameters from these two operating conditions were significantly different.

Virtually all of the basic particles were agglomerated into chains or clusters of various sorts. The agglomeration initiated immediately after basic particle generation at the electric arc. Its fast rate undoubtedly resulted from the high initial number of basic particles per volume, their very fine particle size, sonic agglomeration from the noisy arcing process, and thermal turbulence of the gas stream near the arc.

At the one condition for which mass concentration was not reproducible the mean basic particle diameter was and is not considered to be reproducible.

In summary, Naylor recommended:

(1) Improve the research tool.

  a) Further development of equipment to improve operational quality.

  b) Investigation of other metals and expansion of generating and sampling program.

(2) Further study of the agglomeration of very fine particles.

  a) Define appropriate dimensions for describing the agglomerates.

  b) Based on these dimensions, determine whether or not the metallizer generates predictably reproducible distributions of sizes.

  c) If predictable reproducibility is established determine if there is a significant correlation between agglomerate size and such variables as chamber-duct retention time, number of very fine basic particles per unit volume, and diameters of the very fine particles.

  d) Related to "c" above, determine if there is a significant correlation between very fine basic particle diameter, agglomerate size and mass volumetric concentration.

(3) Use the research tool; for example, modify various experimental collection equipment designs to achieve and improve the effectiveness of small particle control.

Dimmick concluded that the electric arc generator produced an aerosol of agglomerated iron oxide fine particles in mass volumetric concentrations averaging 1.4 gm/m^3 and mass emission rates averaging 7.8 grams per minute. The generator showed some controllability of mass volumetric concentration and variability of very fine basic particle populations with respect to some operating variables. The analysis of the production of the mass volumetric concentration of the aerosol showed the mass volumetric concentration to be dependent on the wire feed rate and the open voltage across the electrodes.

The iron oxide fine basic particles,which composed the agglomerated particles having an estimated size of 0.4 μm, have been characterized to have means ranging from 5.4 nm to 9.1 nm (0.0054 μm to 0.0091 μm). Differences in size means and size distributions between sets of operating conditions indicated that changing the operation variables changed the size characteristics of the population of fine particles.

A simple comparative test for discerning the effect, if any, of changing the exhausting rate of the arc chamber on the aerosol's particle size was inconclusive. The agglomerated particle size was found not to change with an increase in exhausting rate. However, the very fine basic particle mean size was found to be greatly affected by the increase in exhausting rate. This change in generating properties indicated a need for further experimentation.

Dimmick recommended:

(1) Further investigation of the evidence found in the simple comparative test.

(2) The compressed air-jet that atomizes and quenches the melted and

vaproized metal should be studied to ascertain its effect on the aerosol's particle size mean and distribution. The open voltage would require very precise control if its effect on an aerosol's particle mean size or size distribution were to be investigated; a more appropriate power supply is needed.

(3) In the application of this aerosol generator, an on-line continuous mean size and size distribution analyzer, such as a Whitby-Liu mobility analyzer, would provide the necessary "before control equipment" and "after control equipment" data in an engineering evaluation of a piece of air pollution control equipment. Better control of the separation of the larger particles within the barrel could also help approximate real life circumstances.

The overall conclusion is that electric arc generation of fine particle aerosols provides an adequate emission rate at high enough mass volumetric concentrations to test fine particle control equipment. The fine particles are formed by agglomeration from many 2-20 nanometer sized particles with the metallizer generator.

An overall recommendation is to provide continual monitoring of the aerosol's particle size mean and distribution while further investigating any effects of the many independent variables present in the system. Although development is still needed, the electric arc generation of fresh fine metallic oxide particle aerosols provides a generating means for those interested in research and development of fine particle air pollution control technology.

Section C

Experimental Procedures

The two aerosol generators that were developed by Hedden and by Naylor and Dimmick use the energy from a direct current electric arc to heat materials - steel and zinc - in the production of fine particle aerosols. The heat (up to 7000°K) was provided from an arc between an electrode and the material to be melted (direct arc heating) or by an arc between two electrodes (indirect arc heating). In both direct and indirect heating, charged electrodes initiate an intense electric arc when brought into close proximity to each other. The result of this heat generating arc is the melting and vaporizing of the electrodes - particularly the anode.

In both generators, a nozzled gas (compressed air) jet converged about the zone of melted and vaporized materials. This jet had the effect of atomizing the melted materials into molten droplets as well as facilitating the condensation of the vaporized materials into very fine particles. These very fine particles, being newly formed, were considered to be fresh.

Simplistically, two products are produced by the electric arc aerosol generators : the solidified molten droplets from the atomizing spray and the solidified condensate of metallic vapors. Both generating apparatus incorporated settling chambers to separate the much larger particles from the product. Presumably, the fresh metallic fine particles were not affected by the gravimetric and centrifugal separation even though it became evident that the high particle number concentrations and the presence of abundant electric charges agglomerated the very fine basic particles into larger agglomerated particles - thereby increasing the effective size of the particles. This assumption does not exclude the possibility that discrete, very fine particles remain in the gas stream.

Apparatus

Hedden's final apparatus (Figure 1) consisted of an adjustable, constant voltage direct current power supply, a consumable electrode wire feed assembly with control panel, an arc chamber, a non-consumable tungsten electrode with cooled holder and shielding gas supply system, and a system to connect the arc chamber to an air mover upstream and a settling chamber and exhaust system with sampling port downstream.

The power supply utilized in Hedden's apparatus, conventionally used to provide power for semiautomatic welding processes such as gas shielded open air and submerged arc, was a direct current, self contained motor driven generator unit rated for a 100% duty cycle. This rating allowed continuous, uninterrupted production of power under full load. Once set, the output of a constant voltage power supply has essentially the same voltage no matter what the welding current may be. The voltage could be varied over a range of approximately 10 - 50 volts.

The automatic welding head assembly consisted of two main components: (1) the wire feed assembly with torch, and (2) remote control panel. The wire feed assembly combined an insulated wire supply reel, guides, drive motor with gear reduction box, and feed rolls, that constantly feed a consumable electrode wire through the air-cooled torch to the arc. The remote control

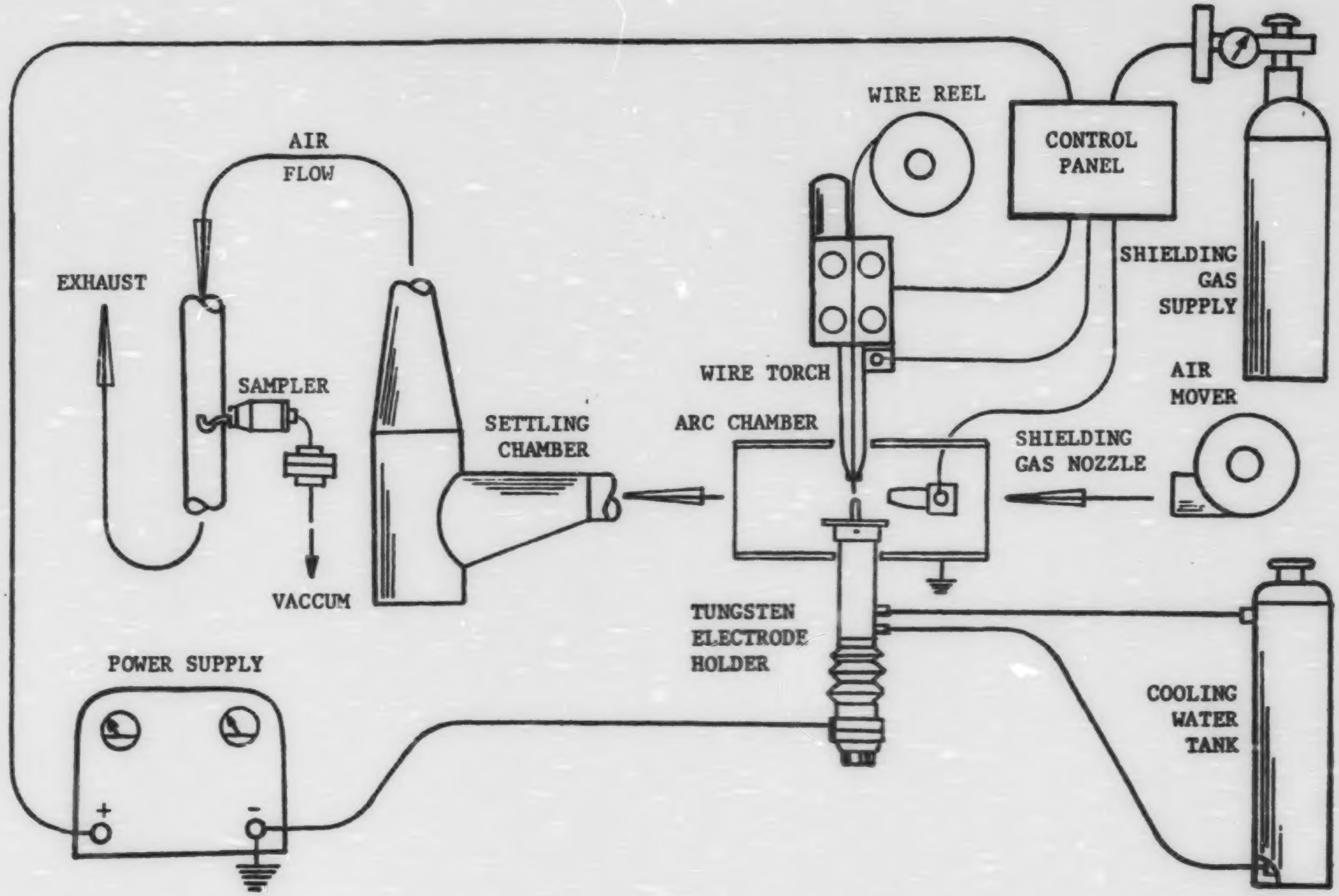
WIRE REEL
CONTROL PANEL
AIR FLOW
EXHAUST
SHIELDING GAS SUPPLY
WIRE TORCH
AIR MOVER
SAMPLER
SETTLING CHAMBER
ARC CHAMBER
SHIELDING GAS NOZZLE
VACCUM
TUNGSTEN ELECTRODE HOLDER
POWER SUPPLY
COOLING WATER TANK
+
-

Figure 1. Simplified diagram of aerosol generator apparatus (Hedden)

panel was electrically connected to both the welding machine and the non-consumable electrode holder cooling water supply through solenoid valves.

The arc chamber was fabircated from a 33 centimeter length of 12.7 centimeter (5 inches) diameter steel pipe. The attachments between the arc chamber and the wire feed assembly were designed to allow adjustment in all axes to obtain perfect alignment between the feed wire electrode and the non-consumable electrode. A shielding gas nozzle and supply system provided for displacing the air surrounding the non-consumable electrode thus preventing rapid consumption of the tungsten by oxidation .

Air flow through the system was provided by a "Gelman Hurricane Air Sampler" set on low speed. The ductwork leading from the arc chamber incorporated a settling chamber and elutriation column to separate the molten globules of steel from the gas stream. The duct leaving the elutriation column made a 180 degree turn before passing the sampling port and nozzle. An adequate length of straight duct was established to allow optimum positioning of the sample probe - a minimum of 10 duct diameters downstream and 5 duct diameters upstream from any disturbance to air flow.

The Naylor and Dimmick aerosol generating apparatus consisted of an electric arc two consumable electrode metallizer that incorporated an electric arc and a compressed air jet to spray melted and vaporized consumable wire electrodes, a 55 gallon oil drum that was used as the arc chamber and was connected to a supplemental air supply cleaned by a HEPA (High Efficiency Air Particulate) filter, a draft fan with exhausting ductwork from the oil drum, and a cloth filter particulate collector. (For Naylor's see Figure 2, for Dimmick's, Figure 3) The metallizer system supplied the necessary power and wire feed delivery. The ductwork and fan provided for exhausting and

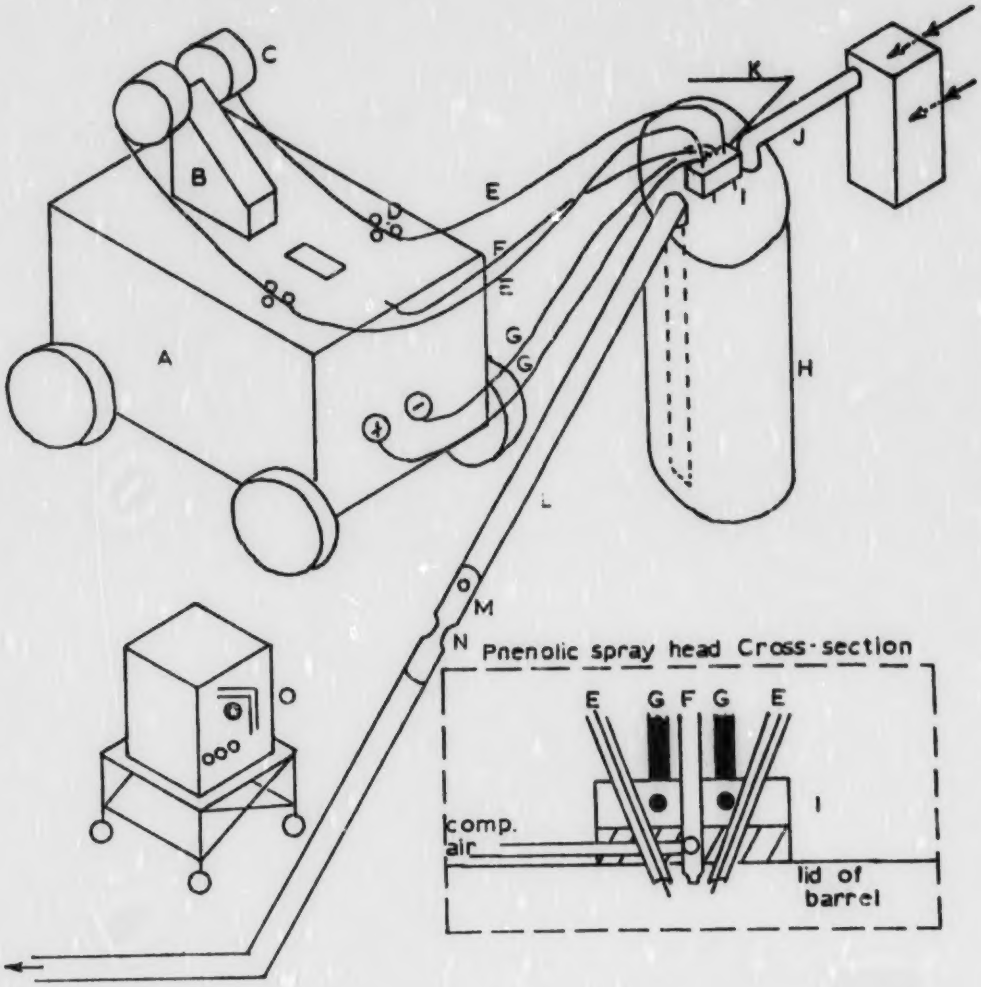
C
B
D
E
F
E
A
G
G
H
K
J
I
L
M
N
O
Phenolic spray head Cross-section
E
G
F
G
E
I
comp. air
lid of barrel

A) Power source of metallizer
B) Control console
C) Dual wire spools
D) Wire straightening, drive and conduit feed mechanism
E) Flexible conduit for wire
F) Flexible compressed air line - main air
G) High amperage electrical cable
H) 55 gallon barrel
I) Phenolic spray head
J) Dilution air from Hepa filter
K) Flexible compressed air line - secondary air
L) Exhaust duct - 6 inch diameter
M) Sampling port
N) Venturi
O) Stack sampler

Figure 2. Metallizer equipment used by Naylor

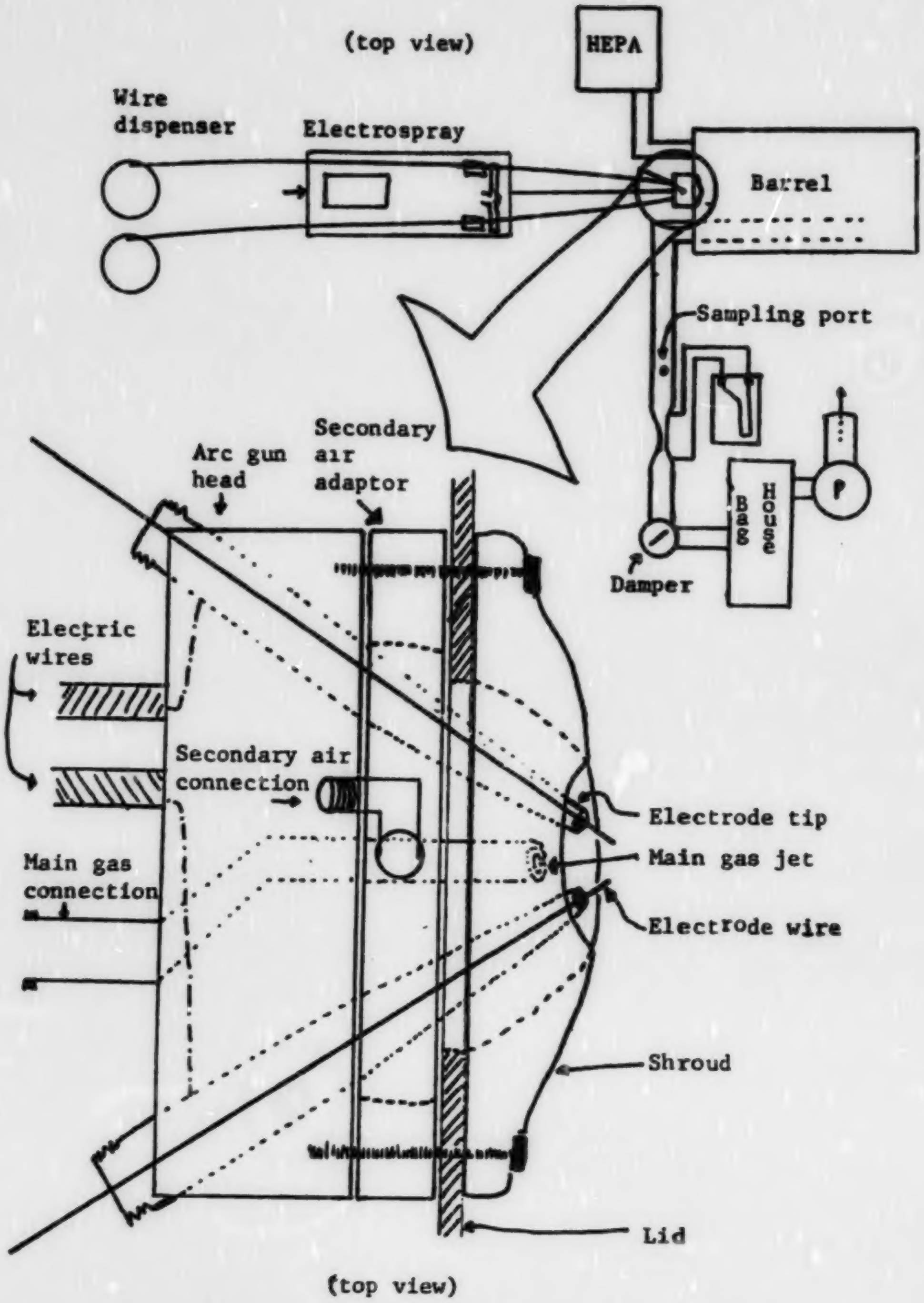
(top view)
HEPA
Wire dispenser
Electrospray
Barrel
Sampling port
P
Bag House
Damper
Arc gun head
Secondary air adaptor
Electric wires
Secondary air connection
Main gas connection
Electrode tip
Main gas jet
Electrode wire
Shroud
Lid
(top view)

Figure 3. Shroulded head metallizer equipment used by Dimmick

sampling the generated aerosol. The oversized baghouse cleaned the particle laden gas stream of most of the particulates before returning the process air to the atmosphere.

The metallizer of the Naylor and Dimmick apparatus is used commercially to provide coatings on metal or to fill in or build up worn areas on shafts, etc. It consisted of a non-constant voltage power source which converts 3 phase 220 volt alternating current to a direct current that is variable from 0 to 40 volts, up to about 400 amperes. A console was located on top of the power source from which air pressure to spray gas jet, consumable wire delivery rate, and arc open-circuit voltage are adjusted. Flexible conduits conveyed the wires from reels passing through the console to a phenolic spray head that guided the wires into fixed position electrode tips.

The spray head was fastened to the lid of a 55 gallon barrel with the electrodes extending through a slot into the barrel. The arcing takes place in the barrel. The larger particles of the metallized wire are directed by the high pressure air jet to the other end of the barrel where they are deposited. The dispersed air jet stream and a low pressure air stream entering through a HEPA filter conveyed the smaller particles through an exhaust duct past the sampling port to a cloth filter collector and exhaust blower.

Sampling

Hedden's system was allowed to operate for approximately one minute to establish steady-state conditions for sampling with steel welding wire. During this period the temperature of the exhaust gas stream stabilized producing a constant velocity past the sampling nozzle. A ten minute sampling period then commenced.

The sampling train consisted of a one-half inch (12.7 mm) stainless steel hook nozzle attached to an Andersen Stack Sampler, in series with an aluminum Millipore filter holder supporting a 47 mm diameter Gelman type GA-4 membrane filter to separate the fume from the sample gas stream.

A calibrated orifice was used to indicate instantaneous sample flow rate, with total flow rate recorded on a dry gas meter.

The fine particle aerosol mass concentration was determined gravimetrically. Also, each sample of collected fume was resuspended in 2 ml of a 1% nitrocellulose solution and dispersed by placing the test tube in an ultrasonic cleaner; the fume collected on the membrane filter was carefully scraped from the membrane and placed directly in 2 ml of the nitrocellulose solution and dispersed. A disposable pipette was used to place one drop of the solution on an uncoated electron microscope grid.

The metallizer generator was operated for at least two minutes before samples were taken either for mass conversion analysis or particle size distribution analysis. Randomly ordered samples were taken with a shut-off between each sampling run. Naylor took samples using zinc metallizing wire and Dimmick took samples using steel metallizing and welding wire.

Sampling for mass concentration data consisted of pre-trial determinations of isokinetic sampling conditions and then the actual sampling. After adjusting the stack sampler for isokinetic sampling, samples were taken such that at least 10 mg of mass was deposited on the tared filter.

Sampling the aerosol for subsequent particle size distribution and analysis consisted of estimating isokinetic conditions and then collection on appropriate membrane filters with sampling times of three, five and seven seconds. Then, the filters were enclosed in a plastic filter holder and were shipped by United Postal Service to McCrone Associates, Inc. in Chicago for analysis by scanning electron microscopy (SEM), transmission electron microscopy (TEM), and selected area electron diffraction SAED).

Analytic Techniques

Hedden used gravimetric and flow measurement techniques to determine a aerosol mass concentration. Hedden had electron micrograph from an RCA electron microscope at West Virginia University to measure particle diameter counts with the use of a semi-circle graticule.

Naylor and Dimmick used gravimetric and flow measurement with an RAC Stak sampler to determine aerosol mass concentration. Naylor and Dimmick both recieved fine basic particle measurements made by McCrone Associates using TEM and SEM. McCrone Associates also performed chemical identification using SAED. Naylor characterized the agglomerated particles from McCrone and Dimmick measured the agglomerated particles using the enlarged SEM photographs.

Experimental Designs

Hedden investigated the performance characterisitcs of the aerosol generator under semi-continuous operation. A series of three controlled test runs were made and a portion of the resultant fume was collected. All tests were conducted under identical conditions of arc voltage, wire feed rate, shielding gas flow rate, and dilution air flow rate. The test program was structured to determine the mass rate of production of iron oxide fume, the particle size (not recognized at first) distribution of that fume, and the degree of reproducibility of production rate and size distribution.

Naylor investigated the reproducibility of the metallizer aerosol generator using zinc metallizing wire. He used four settings with the generator to obtain data for particle size measurement and mass volumetric concentration determination. Naylor varied the consumable wire feed rate, open circuit voltage and the gas jet pressure.

Dimmick characterized the aerosols' particle size under four different operating conditions using steel welding wire. He also performed a simple comparative experiment investigating the effect of increasing the exhaust flow within the ductwork. Dimmick designed an experiment to investigate the effect of generator variables - wire feed rate, open circuit voltage, and gas jet pressure - on the aerosols' mass volumetric concentration.

Section D

Results and Discussion

Mass Volumetric Concentration and Emission Rate (Hedden)

With the mass of particulate in the sample gas stream determined gravimetrically, the average mass volumetric concentration of iron oxide fume in the sample gas stream was 0.292 grains/scf (668.1 mg/m^3). Assuming that the mass volumetric concentration of particulate matter in the total gas stream is the same as for the sample gas stream, the average total particulate production rate was calculated to be 30.08 grains/min (117.0 grams/hr). Total particulate emission rate, given in common units of measurement, is listed in Table 1.

Another performance factor directly related to the rate of production is the conversion ratio of consumable wire feed stock to very fine particles. The wire consumption rate was 5.43 lb/hr (2463 gram/hr). The average particulate production rate was 0.258 lb/hr (117.0 g/hr). Therefore, 5.43 pounds (2463 g) of wire was required to produce 0.258 pounds (117.0 g) of very fine particles for a conversion ratio of 4.75 percent.

Particle Sizing (Hedden)

Two methods were employed, with differing results, to determine particle size distribution: (1) an electron microscope and (2) an Andersen Stack Sampler.

Because of the high magnification, and consequently small field, of the electron microscope, photographic plates having a final magnification of 87,600 times were made of a minimum of three fields of each grid. Individual particles of iron oxide were spherical; and individual spherical particles

TABLE 1. Summary of mass volumetric concentration and emission rate with approximate range of agglomerated particle size indicated(Hedden)

STAGE	Approximate range of particle size (μm)	RUN 1		RUN 2		RUN 3		OVERALL	
		Collected weight (mg)	Cumulative percent total	Collected weight (mg)	Cumulative percent total	Collected weight (mg)	Cumulative percent total	Mean weight (mg)	Standard deviation (mg)
0	> 30	2.5	100.10	1.5	100.00	2.4	100.00	2.13	0.50
1	9.2-30	0.4	98.13	0.3	98.79	0.5	98.42	0.4	0.08
2	5.5-9.2	0.4	97.83	0.2	98.55	0.4	98.09	0.33	0.09
3	3.3-5.5	0.8	97.53	0.2	98.39	0.5	97.83	0.5	0.25
4	2.0-3.3	1.3	96.93	0.7	98.23	1.5	97.50	1.17	0.34
5	1.0-2.0	2.7	95.95	3.1	97.66	3.3	96.51	3.03	0.25
6	0.3-1.0	8.1	93.92	7.7	95.16	8.4	94.34	8.07	0.29
7	0.1-0.3	16.4	87.84	11.2	88.94	17.4	88.82	15.0	2.72
8	< 0.1	9.0	75.53	12.8	79.89	13.4	77.38	11.73	1.95
Filter	< 0.1	91.6	68.77	86.1	69.55	103.4	68.57	93.7	7.22
(1)	TOTALS	133.2	-	123.8	-	152.1	-	136.0	14.42
(2) Sample volume (scf)		7.23		7.21		7.17		7.20	-
(3) Mass volumetric concentr. (mg/scf)		18.42		17.17		21.21		18.89	2.1
(4) Volumetric flow rate (scfm)		103		103		103		103	-
(5) Emission rate (grams/min)		1.90		1.77		2.18		1.95	0.17

composing larger agglomerates were easily distinguished. The agglomerates were not assigned a composite or equivalent particle size but the basic particles composing an agglomerate were classified individually.

With a total of 12,355 basic particles sized the raw data was grouped into 10 classes with a basic particle size interval of 0.01 micrometers each to simplify calculation of various statistical values. Three basic particles exceeded 0.2 micrometers at 0.22, 0.25 and 0.24 micrometers. A simplified method for calculating the arithmetic mean and standard deviation of the basic particle size distribution was employed and relative particle size frequency was presented in Table 2.

The arithmetic mean size of the basic particles was found to be 0.022 micrometer with a standard deviation of 0.0163 micrometers. Using log-normal probability paper revealed an indication that the basic particle size distribution was log normal. The median, sometime known as the mass median diameter (MMD) divides the frequency distribution (by mass) in half and was found to 0.0167 micrometer.

The second method involved the relatively new Andersen Stack Sampler used in conjunction with a back-up membrane filter. Combining the mass distribution data with calibration information supplied by the manufacturer, cumulative particle (agglomerated) size mass distributions can be obtained and were presented in Table 1. Although this mass distribution data indicates approximately 69 percent of the sampled particulate passed through the Andersen Stack Sampler without collection, the previous data presented concerning the size of the discrete basic particles suggests that essentially all the particulate matter should have passed through the sampler without impacting on the collection plates.

Table 2. Relative basic particle size frequency distribution in percent(Hedden)

	Particle Size, micrometers										
STAGE	0.005-0.015	0.015-0.025	0.025-0.035	0.035-0.045	0.045-0.055	0.055-0.065	0.065-0.075	0.075-0.085	0.085-0.095	0.095 and >	
0	46.3	22.0	13.6	7.7	4.5	2.1	1.5	1.3	0.1	0.8	99.9
1	43.0	22.4	17.7	6.9	4.5	2.6	1.5	0.4	0.2	0.9	100.1
2	54.3	19.1	12.3	7.0	3.5	2.1	0.9	0.2	0.1	0.4	99.9
3	50.5	19.2	14.4	6.6	4.2	2.2	1.1	0.8	0.6	0.1	99.7
4	43.0	23.3	17.1	8.7	3.1	2.2	0.7	0.6	0.3	0.9	99.9
5	46.3	22.3	16.4	5.3	3.7	2.6	2.3	0.3	0.2	0.6	100.0
6	47.4	20.5	17.3	6.6	3.4	2.7	0.7	0.3	0.4	0.7	100.0
7	44.3	21.2	15.1	8.8	5.1	2.1	1.1	1.0	0.2	0.9	99.8
8	48.0	21.6	14.9	6.3	6.2	1.3	0.6	0.4	0.3	0.4	100.0
Filter	42.8	22.1	15.7	8.3	4.5	3.6	1.4	0.8	0.4	0.4	100.0
Mean	46.6	21.4	15.5	7.2	4.3	2.4	1.2	0.6	0.3	0.6	100.0
Standard Deviation	3.73	1.38	1.72	1.15	0.92	0.59	0.52	0.36	0.16	0.27	
Range	11.3	4.2	5.4	3.5	3.1	2.3	1.7	1.1	0.5	0.8	

Two methods were used to estimate the reproducibility of the relative particle size distributions---both using the mass distribuiton data obtained from the Andersen Stack Sampler and the back up membrane filter. The results of the three runs are presented in Table 1. The arithmetic mean and standard deviation for the weights found for each of the three runs on each stage of the sampler and membrane filter are shown. The second estimate of agglomerated size distribution reproducibility was obtained by calculating the arithmetic mean and standard deviation of the cumulative relative mass distribution for each of the various size intervals as shown in Table 2.

Mass Volumetric Concentration and Electron Diffraction (Naylor)

Naylor stated that the mass concentration results were more meaningful when the statistical parameters of mean, standard deviation, and coefficient of variation were calculated. The coefficient of variation is one indicator of reproducibility or precision of mass volumetric concentration generation. These parameters are summarized in Table 3.

Table 3. Zinc oxide mass concentration mean and variation summary (Naylor)

Condition	1	2	3	4
(1) Mean (g/sm^3)	1.03	0.68	2.05	1.12
(2) Stand. Dev. (g/sm^3)	0.20	0.05	0.14	0.10
(3) Coefficient of variation 100x(2)/(1)	19%	8.4%	6.9%	8.7%

Naylor tested the null hypothesis that the mean mass concentrations were equal using standard statisitcal methods. These hypothesis tests support the conclusion at the 5% level of significance that the mean of Condition 3 was greater than the mean of Condition 1, and that the mean of Condition 1 was greater than the mean of Condition 2.

Selected area electron diffraction results, as received from McCrone Associates, were compared to standard electron diffraction information (ASTM) and were found to indicate that the particles generated were ZnO.

Particle Sizing (Naylor)

The electron microscopy photographs of the zinc oxide samples were all similar in terms of particle appearance. Particle size means and variances were presented in Table 4. SEM photographs show agglomerates of different shapes and sizes. The agglomerates range in size from less than 0.1 μm to over 2 μm and appear to be interconnected. The shapes vary from spherical to chainlike. These agglomerates are composed of very fine particles as shown in the TEM photos of sample 101.

Table 4. Means and variances of zinc oxide basic particle size data (Naylor)

Sample #	101	125	133	134	104	128
Condition II	1	1	2	2	3	3
$\bar{D}$ (nm)	6.0	10.2	9.1	10.0	10.8	10.4
S^2 (nm^2)	14.6	29.2	35.6	41.1	28.1	22.0
S (nm)	3.8	5.4	6.0	6.4	5.3	4.7
Sample Size	297	280	350	280	376	281

The basic particles mean diameters for samples 101 ($\bar{D}_{101}$) and 125 ($\bar{D}_{125}$) of condition 1 were named significantly different by inspection. The values of the pairs $\bar{D}_{133}$ and $\bar{D}_{134}$ for Condition 2, and $\bar{D}_{104}$ and $\bar{D}_{128}$ for condition 3 were analyzed by a statistical method for significant difference. This analysis indicated that the two replicates for Conditon 2 have diameter means and variances that were not significantly different. The analysis also indicated that the means and variances for Condition 3 were not significantly different.

An important question is whether the means and variances for basic particle diameter populations generated under different conditions are different. Since the mean of Condition 1 cannot be estimated within a relatively tight range, only the relationship of Condition 2 to Condition 3 is examined. Hypothesis testing demonstrated that the mean basic particle diameters for Conditions 2 and 3 are significantly different. Thus changing the operating conditions apparently changed the mean basic particle diameters.

Mass Volumetric Concentration and Electron Diffraction (Dimmick)

The Latin Square analysis (Table 5) found the wire feed rate to be significant at the 0.01 significance level. This implied the wire feed rate had an effect on the resultant mass volumetric concentration. The variables of open voltage and jet pressure were not found to have any effect on the mass volumetric concentration of the aerosol even at the 0.1 significance level. The analysis of variance statistics for replication was also calculated and found to indicate a significant difference between trials at the 0.05 significance level but not the 0.01 significance level.

Table 5. Analysis of variance for Latin Square experimental design mass volumetric concentration data (Dimmick)

Variable	df	Sum of Squares	Mean Square	F_{cal}	$F_{\alpha=0.05}$	$F_{\alpha=0.01}$
Wire feed rate	3	1.473	0.4908	10.86	3.07	4.87
Open Voltage	3	0.319	0.1065	2.35	3.07	4.87
Main air-jet pressure	3	0.106	0.0352	0.77	3.07	4.87
Replication	1	0.335	0.3349	7.39	4.32	8.02
Experimental error	21	0.952	0.0453			
Total	31	3.185				

The SAS GLM analysis of the combination of the Latin Square and another set of data found the results to significantly describe the variability of all the data. With this total set of 40 observations, a statistical procedure calculated F statistics for determining the effect or noneffect of the independent variables in the experimental model. The procedure found the variables of wire feed rate, open circuit voltage, and sample replication to have a significant effect on the outcome: mass volumetric concentration of the gas stream.

The SAED analysis showed two possible resultant materials. Two different phases of iron oxide were possible: magnetite and maghemite.

Particle Sizing (Dimmick)

The size means of the agglomerates (Table 6) were found to be 0.41 μm (S=0.53 μm) for sample 715 and 0.40 μm (S=0.54 μm) for sample 714. These means were also found to be equal; this implied that they were from the same population. The coefficient of variances were rather large, thus the agglomerated particle distributions representative of the aerosols were not "monodisperse."

Table 6. Statistics for agglomerated samples (Dimmick)

Sample No.	Mean (μm)	Standard Deviation (μm)	Standard Error of the Mean (μm)	Coefficient of Variance (%)
714	0.40	0.54	0.03	135
715	0.41	0.53	0.03	129

The simple comparative analysis of increasing the duct exhausting velocity from 1300 fpm to 1850 fpm showed only a decrease in the agglomerated particle size from 0.41 μm to 0.40 μm. This difference was not significant at a 0.1 level of significnace.

Fine basic particle statistics were presented in Table 7. Statistical tests indicated a variety of results. The within group t-test analysis showed that the sample means in all the sets were equivalent within groups. The between group t-test analysis showed a variety of equal and unequal means. The within group very fine basic particle size distributions for sets 2, 3, and 4 were found to be equivalent. Size distributions between groups were found to be all different at an alpha level of 0.05. This implied that at three of four different operating conditions three different fine basic particle size distributions were generated. The t-test analysis between the two comparative samples 712 and 716 showed sample 712 to have a significantly

Table 7. Statistics for very fine basic particles(Dimmick)

Set Number	Sample No.	Number of Particles	Mean (nm)	Standard Deviation (nm)	Standard of Error of the Mean (nm)	Coefficient of Variance (%)
1	600	386	8.00	5.35	0.27	66.9
	601	446	7.83	4.56	0.22	58.2
	602	434	7.53	5.23	0.25	69.5
2	603	369	8.45	5.37	0.28	63.5
	604	368	8.32	5.51	0.29	66.3
	605	356	8.31	5.41	0.29	65.1
3	607	296	9.05	5.49	0.32	60.5
	611	274	8.57	5.40	0.33	62.9
4	609	298	7.86	5.40	0.31	68.8
	612	297	8.13	5.37	0.31	66.0
5	716	449	8.05	5.21	0.25	64.7
6	712	497	6.42	4.79	0.21	74.6

smaller very fine basic particle size than sample 716.

An overall characterization of the fine particle generators is presented in Table 8. This table list basic particle size statistics for the basic

Table 8. Hedden-Naylor-Dimmick summary of results

	Hedden (iron oxide)	Naylor (zinc oxide)	Dimmick (iron oxide)
Limit of microscope resolution (nm)	5	1	1
Width of diameter count interval (nm)	10	1	1
Mean basic particle diameter (nm)	22	6.0-10.8	6.4-9.1
Range of basic diameters (nm)	5->100	1-50	1-720
Standard deviation (nm)	16.3	3.8-6.4	4.7-5.5
Cumulative Frequency Distribution	log normal	normal	——
Mass volumetric concentration (gm/m^3)	0.67	1.21	1.38
Mass volumetric concentration (gm/m^3)	.61-0.75	.67-2.05	0.81-2.16
Mass emission rate (gm/min)	1.95	8.57	7.73
Percent conversion (%)	4.8	——	8-15

particles - not the agglomerated particles. Hedden did not directly measure what may be presumed to be the aerosol; that is, he measured agglomerated particles by inference from the Andersen Stack Sampler and not directly from micrographs. Naylor indicated a range of sizes for the agglomerated particles from less than 0.1 μm to greater than 2 μm. Dimmick measured the agglomerated particles and found an average size of 0.4 μm. The table also shows various production characteristics related to the efficiency of mass conversion from wire feed to particle aerosol.

A question that should be opened for discussion and research is centered around the physical explanation of the electric arc generation of fine particle aerosols. What are the relations and factors involved in the dichotomous formation of solidified molten droplets and agglomerated solid fine particles? Also, what effects on the chemical processes involved in the aerosol production does the dichotomous formation have?

ELECTRIC ARC GENERATION OF POLYDISPERSED IRON OXIDE AEROSOL IN AN AIR STREAM

PROBLEM

Submitted to the Graduate School
of
West Virginia University
In Partial Fullfillment of the Requirements for
the Degree of Master of Science in Engineering

by

Robert E. Hedden, B.S.

Morgantown
West Virginia
1972

ABSTRACT

Freshly formed metal and metal oxide particles in the sub-micron size range are known to have different behavior characteristics than those of collected, classified, aged, and redispersed particulates. In the past, significant quantities of freshly formed ultrafine particles have not been available for research work in air pollution control techniques, instrument calibration, emission simulation, animal inhalation or particle behavior studies. This has caused considerable difficulty in translating laboratory research to field application.

An experimental aerosol generator that supplies reproducible amounts of spherical, solid, fresh particles of metals and metal oxides directly in a hot or cooled gas stream is described in this report. The generator employs a direct current power source to create an arc between a relatively non-consumable tungsten cathode and a consumable feed-stock of wire. The feed-stock is vaporized in the high current density of the electric arc and particles are formed on cooling by a gas stream moving past the arc area.

Rate of continuous production of 0.1 micrometer diameter fresh iron oxide particles exceeds 100 grams/hour. The moving gas stream was sampled using a high temperature Andersen Stack Sampler probe followed by a membrane filter to obtain mass concentration. The size, shape and particle size distribution of the particles were determined using an electron microscope.

Other operating parameters, performance characteristics, and development background are discussed.

ACKNOWLEDGEMENTS

The author is grateful to all those who have contributed to the successful preparation of this report. Special appreciation is extended to his graduate advisor, Professor Benjamin Linsky, for his sincere interest in this study; and to Frank Noonan, then Director of Air Pollution Control Engineering Laboratories at West Virginia University, for his laboratory assistance and constructive criticism. Gratitude is also expressed to Dr. Howard W. Butler, Chairman of Mechanical Engineering, and Hasin T. Gencsoy, Professor of Mechanical Engineering, for making special equipment and facilities of their department available for this study. The cooperativeness of Don Garletts and Harold Martin of the Mechaincal Engineering Laboratory, and Fran Culler of the Civil Engineering Laboratory, during the mechanical design and fabrication of the apparatus was sincerely appreciated.

Special thanks is extended to Dr. M. R. Friedman of the Anatomy Department, West Virginia University School of Medicine, under whose guidance electromicroscopist Betsy Walker obtained numerous electronmicrographs of the material produced in this experiment. Further thanks is expressed to J. Reginald Dietz, Director of Research and Development for National Steel Corporation, Weirton, West Virginia, under whose direction R. E. Brien, Senior Research Metallurgist, prepared electronmicrographs of material collected from preliminary experiments.

The author also appreciated the encouragement and assistance given by Benjamin Eusebio and Bruce Harris, of what was then the National Air Pollution Control Administration, Cincinnati, Ohio.

Several training grants, 5 T01 AP0000 9-07 and 5 T01 AP0000 9-08, from what is now the Air and Water Programs Division of the U. S. Environmental Protection Agency made this study possible. The author is further indebted to the U. S. Bureau of Mines, Morgantown, West Virginia, for supplying the helium used in these experiments and to Two Thousand, Inc. for the use of the Andersen Stack Sampler.

TABLE OF CONTENTS

Page

ABSTRACT 1-ii

ACKNOWLEDGEMENTS 1-iii

LIST OF TABLES 1-vi

LIST OF FIGURES 1-vii

I. INTRODUCTION 1-1

II. LITERATURE REVIEW 1-5

III. APPARATUS 1-10

IV. EXPERIMENTAL 1-25

SAMPLING PROCEDURE 1-25

RESULTS 1-29

Mass Concentration and Rate of Production 1-29
Particle Size Distribution 1-34
Reproducibility of Production Rate and Relative Particle Size Distribution 1-49

V. CONCLUSIONS 1-52

VI. LIST OF REFERENCES 1-55

APPENDICES 1-58

APPENDIX A. Selected Bibliography of Readings Concerning Electric Arc Discharges 1-A-1

APPENDIX B. Developmental Background of the Tungsten Electrode Holder 1-B-1

APPENDIX C. Operating Procedure for Arc Aerosol Generator 1-C-1

APPENDIX D. Electron Microscope Particle Count Raw Data . . . 1-D-1

APPENDIX E. Statistical Calculations 1-E-1

LIST OF TABLES

Page

Table 1. Operating and sampling test conditions 1-27

Table 2. Weight (mass) distribution of particulate matter retained by the Andersen Stack Sampler and backup membrane filter 1-30

Table 3. Mass concentration and total production rate of iron oxide particles 1-31

Table 4. Electron microscope particle count data 1-36

Table 5. Relative particle size frequency distribution in percent from the data of Table 4 1-37

Table 6. Cumulative relative particle size distribution from data of Table 5 1-43

Table 7. Arithmetic mean and standard deviation of the cumulative relative mass distribution from data of Table 2 1-46

Table 8. Arithmetic mean and standard deviation of the weight (mass) distribution from data of Table 2 1-51

Table D-1. Electron microscope particle count raw data 1-D-1

Table E-1. Transformation for calculating the arithmetic mean and standard deviation from data of Table 4 1-E-1

Table E-2. Tabulation for calculating median and geometric mean from data of Table 4 1-E-2

Table E-3. Calculation of arithmetic mean and standard deviation of the relative frequency within each particle size interval from the data of Table 5 1-E-3

Table E-4. Calculation of arithmetic mean and standard deviation of the cumulative relative mass distribution from data of Table 7 1-E-7

Table E-5. Calculation of arithmetic mean and standard deviation of weight (mass) distribution from data of Table 8 1-E-8

LIST OF FIGURES

Page

Figure 1. Sketch of the components of a direct current arc 1-3

Figure 2. Graphical representation of thermal plasma in the arc region 1-3

Figure 3. Simplified diagram of aerosol generator apparatus . . . 1-11

Figure 4. Photographs showing assembled and exploded view of the non-consumable electrode holder 1-15

Figure 5. Photographs showing general arrangement of arc chamber apparatus 1-19

Figure 6. Simplified pictorial sketch of the arc chamber and ductwork system 1-23

Figure 7. Histogram representing particle size data from Table 5 1-38

Figure 8. Distribution curve representing data from Table 5 . . . 1-38

Figure 9. Ogive representing particle size data from Table 6 . . . 1-39

Figure 10. Cumulative distribution data from Table 6 plotted using normal probability scales 1-39

Figure 11. Cumulative particle size distribution data from Table 6 plotted using log-normal probability scales 1-40

Figure 12. Cumulative particle size distribution data from Table 7 plotted using log-normal probability scales 1-47

Figure B-1 Sketches showing developmental configurations of the tungsten electrode-arc chamber apparatus 1-B-3

Figure C-1. Simplified cross-sectional, plan view sketch showing location of components inside arc chamber 1-C-3

Figure C-2. Calibration curve of wire speed dial versus wire speed of 0.045 inch diameter wire 1-C-5

I. INTRODUCTION

The generation of significant quantities of solid aerosols with reproducibility as to mass, shape and particle size distribution is an essential *sine qua non* for research in air pollution control techniques, instrument calibration, emission simulation, animal inhalation and particle behavior studies, and in related fields of research (1,2,3,4). Therefore, the gas-solid phase system of a test aerosol is usually made up of components to simulate an actual natural or industrial situation.

Redispersion of collected, aged, and classified powders, the largest present source of significant quantities of solid aerosols, requires large energy inputs to overcome adhesive and agglomerating forces inherent in bulk powders (5). Even then, experience has shown that laboratory redispersions of particles exhibit different behavior characteristics than freshly formed particles (6,7). Significant quantities of freshly formed particles, synthesized in the same manner that they are produced industrially, have not been available for research work. These factors have caused specific difficulties in translating laboratory control engineering research and medical research to field applications and diagnosis.

One industrial process that is adaptable to the primary formation of solid aerosols in the laboratory is the heating of materials by the energy from a direct current electric arc. The heat is provided by an arc between an electrode and the material to be melted (direct arc heating) or by an arc between two electrodes (indirect arc heating).

Because the source of most of the heat is nonchemical, electric arc discharge heating is especially desirable in controlling contamination of the heated material.

The arc discharge occurs when two electrodes are brought into close proximity to one another such that a high electrical resistance is developed at their boundary and the tips begin to glow. This glow indicates the emission of electrons from the cathode, which because of high emission temperatures, up to 7000 K (8,9,10), produces ionization of the air. The bombardment of electrons received by the anode causes it to become white hot and to erode either by melting or vaporization. (Refer to Figure 1.)

In the actual direct current arc, the molecules of air dissociate. They lose some of their orbiting electrons and form a mixture of positive ions and electrons. This mixture of electrically charged atoms, and electrons, with their negative charge, is called thermal plasma (Figure 2). As a result, the ionized air becomes conductive to electricity and current flows without a mechanical connection between electrodes. Although a more detailed discussion of what happens in an electric arc is beyond the scope of this paper, a bibliography has been included in Appendix A listing specific readings which examine arc discharges.

In industry, the intense heat produced by electron activity in the electric arc is utilized for melting and refining of ferrous and nonferrous metals, and for the production of refractories. As the electric arc furnace is one of the most difficult to control sources of particulate emissions in industry, it is an appropriate and adaptable method for the simulation and primary formation of solid aerosols in the laboratory.

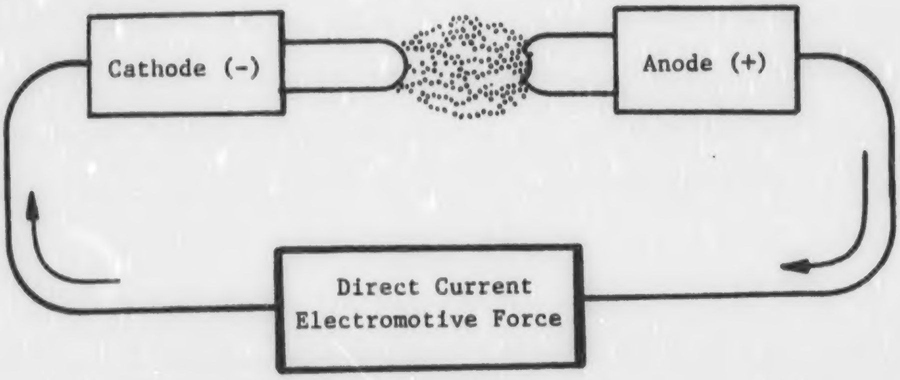
Cathode (-)
Anode (+)
Direct Current
Electromotive Force

Figure 1. Sketch of the Components of a Direct Current Arc

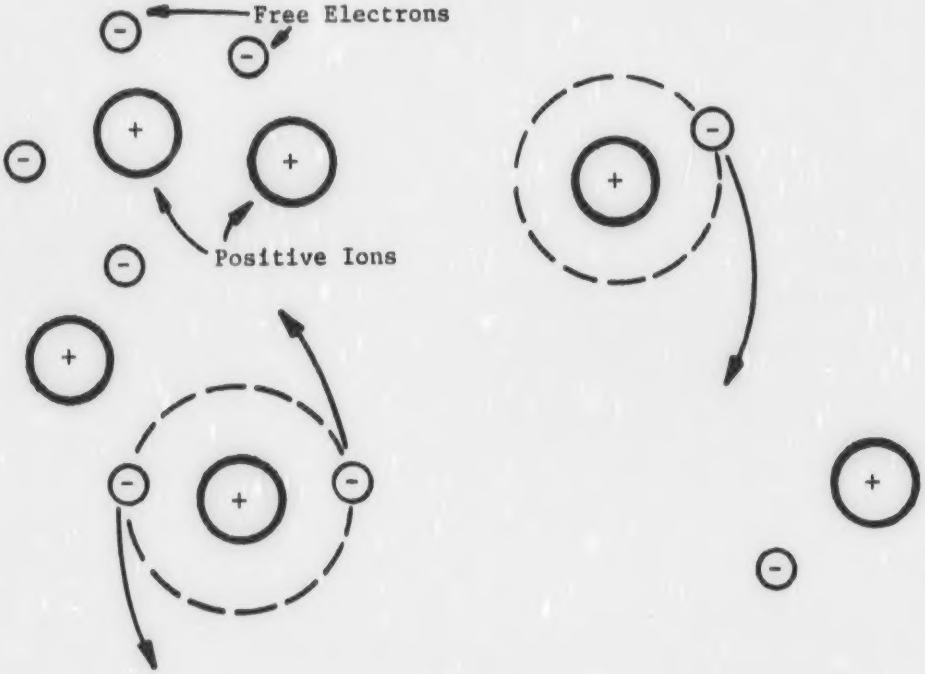
Free Electrons
Positive Ions

Figure 2. Graphical Representation of Thermal Plasma in the Arc Region

Using the technique of direct arc heating, an electric arc aerosol generator has been designed and built and has undergone limited tests to evaluate and maximize its performance characteristics and the properties of the aerosol produced. The generator appears suitable for production of particles of metals, oxides of metals, and other refractory materials, utilizing a constant potential, direct current power supply. An arc is sustained between a relatively nonconsumable tungsten cathode and a consumable feedstock of wire. Commercially available steel welding wire is the consumable feedstock used in the present investigation. The wire feed is maintained at a constant rate by a modified automatic welding head mechanism with a variable speed controller. A specially designed, water-cooled holder allows simultaneous manual advancement and rotation of the tungsten cathode to compensate for and maintain uniform erosion. The continuous arc discharge is contained in a 13 inch (33 cm) length of 5 inch (12.7 cm) standard steel pipe through which passes the entraining gas stream.

II. LITERATURE REVIEW

Many methods have been utilized to produce solid aerosols in significant and reproducible quantities for gas cleaning, animal inhalation and other aerosol research. In the past, aerosols of ultrafine solid particles made from materials to reproduce actual environments have not been available; this has caused difficulty in translating laboratory research to practical applications.

There are two basic types of aerosols: (1) aerosols which are homogeneous with respect to size, shape, and specific gravity, and (2) heterogeneous aerosols which simulate particles generated in nature or by an industrial process. Homogeneous aerosols are used for fundamental research and product testing and have uniform properties in order to minimize the number of variables which must be considered. This facilitates characterization of factors involved in a study and structuring standardized tests for determining acceptability of control and test equipment and working atmospheres. Although aerosols produced by homogeneous aerosol generators have many inherent advantages, the output concentrations from these generators is in the range of 0.1 to 10 milligrams per liter with flow rates of 1 to 4 liters per minute; further, dilution ratios of 10 to 100 are required to prevent agglomeration (11, 12). Consequently, these units are not adequate for the evaluation of gas cleaning equipment, where large volumes with high concentrations of particulate matter are required, as the concentration would be too low for realistic results.

For most applied and engineering research, heterogeneous aerosols are used. Silverman and Billings (13) have reviewed many of the methods and problems associated with generating solid aerosols in the laboratory for a variety of materials. A more complete treatise by Silverman on the generation of heterogeneous aerosols can be found in section 12.4.3 of the *Air Pollution Handbook* (14).

Of the many methods discussed by Silverman and Billings, only the redispersion method is capable of producing large quantities of solid aerosol for large scale laboratory testing. Large quantities -- grains to grams to tons -- are available with a wide variety of physical, electrical, and chemical characteristics for resuspension in a gas stream.

The major difficulty in dry dispersion of particles is limiting agglomeration. This limitation can be minimized by employing feeders utilizing techniques discussed by Olive (15) and by considering dispersion principles as discussed by Fuchs (16) to overcome bulk powder adhesive and agglomerating forces. However, the lower limit of particle diameter is 0.1 micrometers (17) and almost all aerosols produced from dry powders seem to be heterogeneous with respect to particle size.

The method which most closely approximates an actual industrial situation is that of direct attrition. "Fresh" aerosols can be produced by various mechanical and electro-mechanical means such as friction, evaporation, impact, explosion and condensation and burning. Small hammer and ball mills have been employed to produce fine materials on the order of 1 micrometer diameter. And a number of companies, most notably manufacturers of air filtration equipment, produce size reduction equipment usable as aerosol generators (18). There are many other primary methods reported in the literature but none have been capable of achieving wide acceptance because constant and reproducible production rates are very difficult to achieve in the submicron size range. At best, it is usually hoped a constant volumetric particle feed rate can be achieved but the resulting concentration and particle size distribution must still be determined by measurement.

The problems of reproducibility appear to be directly attributable to two major factors: (1) the control of the composition of the feedstock, and (2) the control of input energy, whether it be mechanical, chemical, electrical, and so forth.

In the aerosol generator under present consideration the feedstock is "common" welding wire available with various metal bases (aluminum, iron, chromium, copper, and nickel) in a wide range of trace metal compositions. Feed rate is controllable by one of a number of commercially available, constant speed, wire-feed motors. The energy input is electrical and is supplied by a constant voltage (CV) direct current power supply. An electrical potential is created between a consumable wire feedstock (the anode) and a relatively non-consumable tungsten electrode (the cathode). When the anode and cathode are brought in close proximity to each other, an intense electric arc is initiated which melts and evaporates a portion of the feedstock material. After leaving the vicinity of the electric arc, the vaporized metal rapidly condenses producing a desirable ultra-fine metal fume which can be conveyed by an air stream to sampling equipment, control devices, inhalation subjects, and so forth.

Although the use of an electric arc has been previously adapted for production of submicron particulates, vaporization of materials by this method has been primarily to obtain quantities of submicron particles as an end product in themselves. For example, Holmgren, *et. al.* (19) used various electric arc systems to generate particulates to be collected for later study of the particles using chemical analysis, x-ray diffraction, chemical reactivity tests, sinterability tests and electron microscopy. This and similar work by Harris, *et. al.* (20) has been performed to determine commercial applications and production methods for particulate materials. No consideration was given to maintaining the gas-solid phase system as a viable tool in itself.

The TAFA Division of the Humphreys Corporation (21) has developed a commercial carbon arc processing system capable of producing spherical particles. However, this system requires preliminary size reduction of the feed material as the feedstock must be in powder form. The end product in this system, once again the particles themselves, is produced by melting the powder (as compared to vaporization and subsequent condensation) whereupon each discrete particle assumes a spherical configuration. It is apparent that the size and mass of the spheroidal particles produced is directly limited by the size characteristic of the powder fed. Also, as opposed to a workable aerosol generator, the design emphasis of this unit is on the generation and immediate collection of the particles themselves. The inclusion of air or other gases is usually undesirable for their purposes.

In addition to carbon arcs, high voltage condenser discharge through thin foil and wire (22), and high voltage sparks (23) have been used to produce metallic aerosols for study in chambers. Truitt *et. al.* (24,25), under several studies for the United States Atomic Energy Commission, have used two "spark generators" which differ only in the power source. A Tesla coil was used as a power source for one and the high-frequency starter attachment on a welding machine supplied the power for the other. The electric "spark was set up across the axis of a 2-in. diameter glass pipe" between various metal electrodes. However, the design of the spark chamber limited aerosol generation to about one minute because of the mechanical limitations of electrode consumption. To avoid the problems of non-uniform and non-sustained generation, tanks, plastic bags, and stainless steel drums were used as holding chambers from which relatively small volumes, at rates up to 2 liters per minute, were withdrawn. Not only are mass concentrations and flow rates low and suitable only for small scale laboratory studies, but the problems of maintaining a constant aerosol particle size distribution by achieving a steady-state between agglomeration and preferential settling of these larger particles must be considered. Even then, the mass concentration of the aerosol will decrease due to settling.

In the present apparatus, the undesirable, as well as the desirable, characteristics of other uses of electric arcs have been integrated into the prototype of a continuous, steady state, and reproducible source of relatively large quantities of fresh metallic aerosol.

III. APPARATUS

The apparatus, diagrammatically sketched in Figure 3, consists of an adjustable, constant voltage, direct current power supply, a wire feed assembly with control panel, a non-consumable (tungsten) electrode holder with cooling system, an arc chamber, a shielding gas supply system, and a ductwork system connecting the chamber to an air mover upstream and a settling chamber and exhaust system, with sampling port, downstream.

The conventional use of the power supply[1] utilized in the present apparatus is to provide power for semiautomatic welding processes such as, gas shielded, open arc, and submerged arc. This "constant voltage (CV)" type of power source is a direct current, self-contained motor driven generator unit rated for a 100% duty cycle. This rating allows continuous, uninterrupted production of power under full load. Various instruments and controls are mounted on the front of the sheet metal enclosure of the motor-generator unit. In addition to an ammeter and voltmeter, a 110 volt receptacle, fuse holder, remote control receptacle, and electrode and ground terminals are located on the welding machine. Controls include start-stop pushbuttons and a field rheostat to regulate the output voltage. The voltmeter located on the machine reads open circuit voltage (while not welding) and arc voltage (while welding).

Once set, the output of a CV power supply has essentially the same voltage no matter what the welding current may be. The voltage can be

---

[1] Hobart Motor Driven Constant Voltage Welder for Automatic Welding, Model MC-900, Hobart Brothers Company, Troy, Ohio.

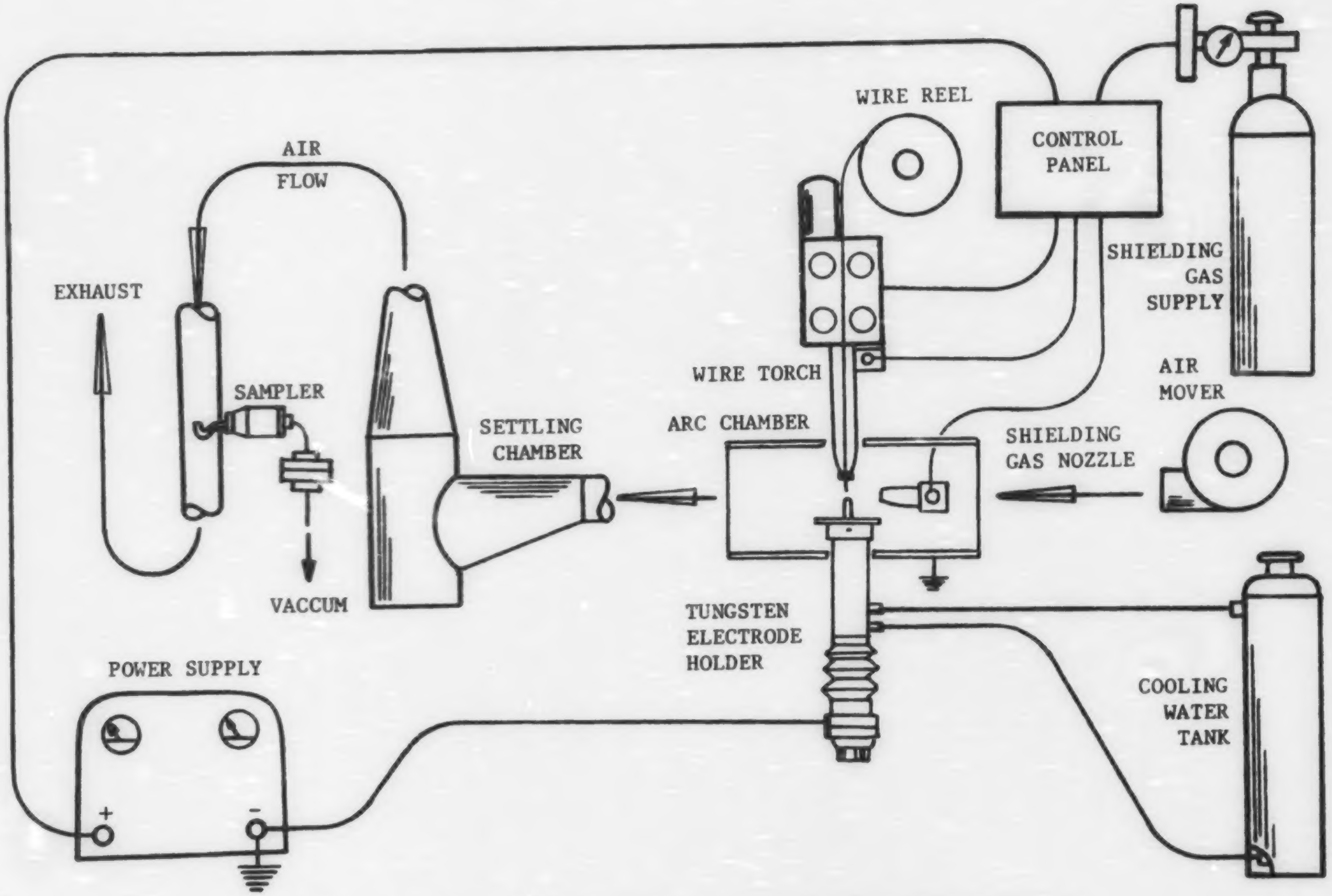
WIRE REEL
CONTROL PANEL
AIR FLOW
EXHAUST
SAMPLER
VACCUM
SETTLING CHAMBER
WIRE TORCH
ARC CHAMBER
SHIELDING GAS SUPPLY
AIR MOVER
SHIELDING GAS NOZZLE
TUNGSTEN ELECTRODE HOLDER
COOLING WATER TANK
POWER SUPPLY
+
-

Figure 3. Simplified diagram of aerosol generator apparatus

set over a range of approximately 10-50 volts; there is no current control on a CV type machine as the welding current flow is determined by the wire feeder. That is, as the wire feed speed is increased, the machine automatically supplies additional current, at the same constant voltage, to maintain the arc (26, 27). Thus, the wire feed speed control knob "sets" the welding current. The welding current is read on either the ammeter on the welding machine or the ammeter on the remote control panel for the "automatic welding head."

The automatic welding head assembly[2] consists of two main components: (1) wire feed assembly with torch, and (2) remote control panel. The wire feed assembly combines an insulated wire supply reel, guides, drive motor with gear reduction box, and feed rolls, to constantly feed a consumable electrode wire[3] through the air-cooled torch to the arc. The consumable electrode wire used in the present apparatus is solid steel (because an iron oxide fume was desired) and bare, except for a very thin coating of copper to prevent surface oxidation. The consumable wire is maintained at a positive (+) potential with respect to ground. The remote control panel is electrically connected to both the welding

---

[2] Hobart Automatic Welding Head, Model AI-22, Hobart Brothers Company, Troy, Ohio.

[3] The steel wire used is Hobart, Type 18 (E 705-G). The spool was further designated "6719-67, MIG 18B, .045." A typical wire trace element composition by per cent is given (27)

C	.12
Mn	1.90
Si	.80
P	.020
S	.020
Mo	.50

machine and the non-consumable electrode holder cooling water supply through solenoid valves.

The front of the control panel contains the following controls and instruments (28).

1. Fuse - This 4 ampere fuse fuses the input power to the control panel from the welding machine.
2. Ammeter - This ammeter indicates the amount of current flow at the arc.
3. Wire Speed Control - This controls the speed of the wire through the torch. (Figure C-2 is the calibration curve for this control).
4. Voltage Control - This controls the amount of voltage across the arc.
5. Voltmeter - This voltmeter indicates the amount of voltage across the arc.
6. Pilot Light - This light indicates when power is available at the control panel.
7. Wire Feed Control - This switch controls the direction of travel of the wire through the torch.
8. Inch Button - By depressing this button, the wire inches through the torch, forward or reverse, depending on the position of the "wire feed control."
9. Start and Stop Button - These start and stop the wire feed motor and therefore start and stop the arc.
10. Purge Button - This button purges the gas through the shielding gas nozzle.

11. On-Off Toggle Switch - This switch controls power to the control panel.

12. Water Valve - This valve controls the on and off cycle of water to the non-consumable electrode holder.

13. Gas Valve - This valve controls the on and off cycle of gas to the shielding gas nozzle.

The non-consumable electrode holder, shown in an exploded view in Figure 4, was designed and fabricated by the author. Materials of construction include stainless steel, steel and brass as indicated in the diagram. The non-consumable electrode is a 1/4 inch (6.35 mm) diameter tungsten arc welding electrode with a ground finish and 2 per cent thoria content. The ground finish is smoother and therefore makes better mechanical and electrical contact than the swaged type. Thoria is added to tungsten electrodes to improve arc stability, to make initiation of an arc easier, and to increase the amount of current carried per electrode diameter (29).

Several preliminary configurations of the tungsten electrode holder-arc chamber combination were constructed to investigate the feasibility of developing a workable semi-continuous model capable of achieving the desired result. Many of the problems encountered in the construction and operation of the models described in Appendix B have thus been eliminated in the construction of the present holder. Final design of the tungsten electrode holder involved three prime considerations: (1) compensation for electrode erosion, (2) electrical connection between power supply and electrode, and (3) dissipation of heat build-up.

Figure 4. Photographs showing assembled and exploded view of the non-consumable electrode holder

Figure 4a. Assembled view

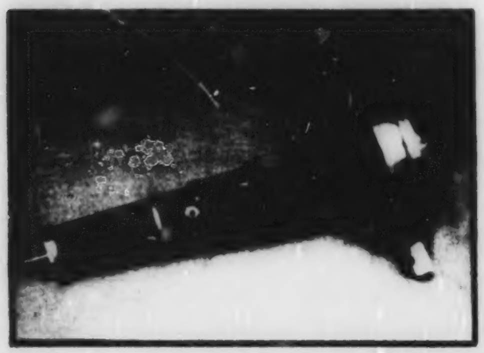

PARTIAL PARTS LIST[a]

1 Electrode guide (S)
2 Sliding seal components
3 Tungsten electrode
4 Feed screw (B)
5 Electrode holder body (M)
6 Cooling water fittings (B)
7 Rubber "O" ring
8 Packing retainer (A)
9 Silicone rubber packing
10 Feed screw guide (S)
11 Rubber bellows
12 Jam nut and lock washer (M)
13 Compression spring
14 Electrical connector
15 Rotating contact disks (B)
16 Plexiglas insulator
17 Feed screw knob

Figure 4b. Exploded view

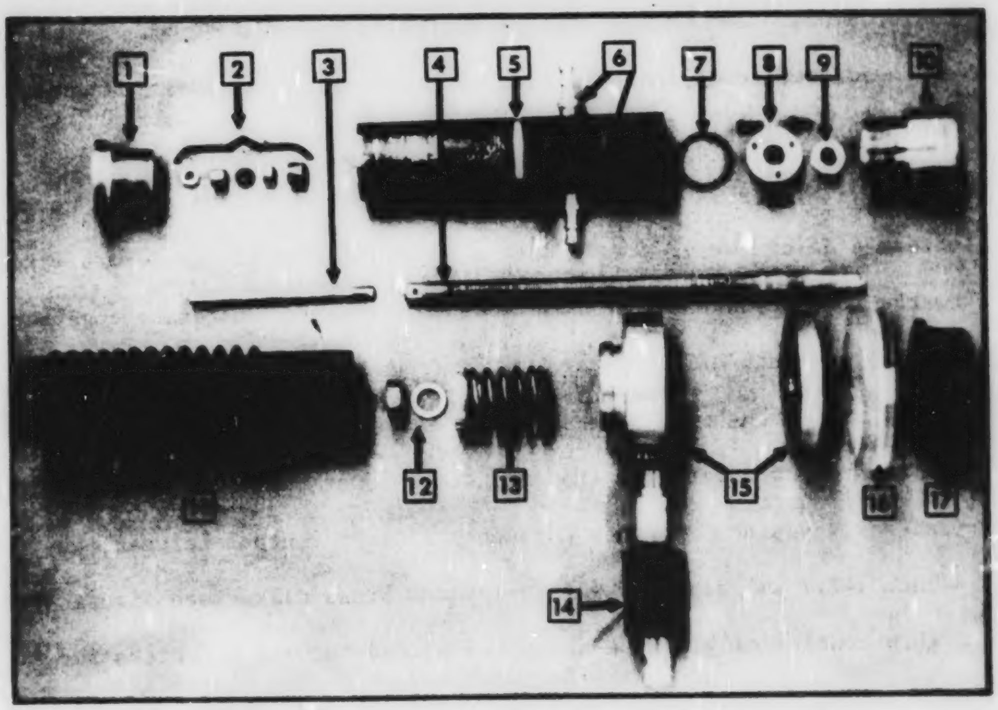

---

[a] Letter in parenthesis indicates material of construction: aluminum (A), stainless steel (S), brass (B), and mild steel (M).

Among other reasons, tungsten was chosen as a "non-consumable" electrode for its inherent property of having the highest melting point of all metals, 6170 F (3410 C) (30). But even with its refractory nature, the intense heat of the arc, the availability of air for oxidation, and the physical forces in the arc cause erosion of the electrode. The major portion of the erosion is due to melting of the electrode and subsequent removal of the molten material from the arc region by gravitational force, arc blow, and the moving gas stream. It is theorized a much smaller portion of the tungsten is lost by evaporization as its boiling point is 10,700 F (5927 C) (30). No trace of discrete tungsten particles could be detected on examination of the electronmicrographs of the collected fume as condensed tungsten has a morphology similar to that of iron oxide.

To advance the electrode into the arc, a manually operated screw feed with a pitch of 20 threads per inch (7.87 threads per cm) was employed. To compensate for the increased erosion rate on the downstream side of the electrode due to arc blow, the electrode was fixed to the feed screw causing the electrode and screw to rotate together. This arrangement allowed a relatively rounded point to be maintained in the arc throughout the tests.

Transfer of power from the stationary power supply to the rotating feed screw was accomplished through a sliding contact between two 4 inch (41.7 cm) diameter spring-loaded, brass disks (see Figure 4). A thin coating of graphite paste was placed between the disks for lubricating purposes and to improve conductivity. During the test the feed screw was turned approximately four revolutions per minute; upon disassembly no trace of arcing was observed between the contact surfaces of the disks.

To take advantage of electron flow, the tungsten electrode is grounded (-) making it the cathode of the direct current circuit. The characteristics of electron flow, negative to positive potential, cause the consumable wire (anode) to be bombarded with electrons from the relatively non-consumable cathode thereby concentrating the heat in the wire to be vaporized. At a current flow through the arc region of 150 amperes, the ratio of current density at the consumable wire versus that for the non-consumable tungsten electrode is approximately 30 to 1. Current density is defined as the current flow in amperes divided by the cross-sectional area of the conductor. The current density for the wire is,

$$\frac{\text{current}}{\text{area}} = \frac{150 \text{ amperes} \times 4}{\pi\ (0.045 \text{ inches})^2}$$

$$\text{current density (wire)} = 94{,}300 \text{ amperes/inch}^2$$

$$(= 14{,}620 \text{ amperes/cm}^2).$$

The current density in the tungsten electrode is,

$$\frac{\text{current}}{\text{area}} = \frac{150 \text{ amperes} \times 4}{\pi\ (0.25 \text{ inches})^2}$$

$$\text{current density (tungsten)} = 3056 \text{ amperes/inch}^2$$

$$(= 474 \text{ amperes/cm}^2)$$

As this is a direct current arc, the power (P) consumed in the arc is the product of electro-motive force (E), in volts, and current (I), in amperes.

Therefore,

$$P = EI$$

$$P = 23 \text{ volts} \times 150 \text{ amperes}$$

$$P = 3450 \text{ watts or } 11{,}775 \text{ Btu/hr}$$

$$(= 49.44 \text{ kg-calories/min}).$$

This relatively high rate of heat input to the system must be dissipated by one of the various methods of heat transfer: convection, radiation, or conduction. Air flow through the arc chamber past the arc region at the rate of 103 scfm (2.92 m^3/min) supplies significant cooling for the overall system. However, the major source of concern for heat build-up to adverse levels is the tungsten electrode holder itself. An easily replaceable 1/8 inch (3.175 mm) thick steel disk (see Figure C-1) is used to protect the exposed end of the electrode holder from arc splatter and to reflect the radiant energy of the arc. To dissipate the heat build-up in the tungsten electrode, a portion of which is conducted to the electrode holder through intimate metallic contact, the entire electrode holder is water cooled. Cooling water is supplied by a self-contained tank and pump assembly[4], through a solenoid valve located on the control panel assembly to the inlet port on the electrode holder. The return water flows unrestricted back to the holding tank which acts as a heat sink.

No attempt was made to cool the arc chamber itself as no problems of dimensional stability due to heat build-up were encountered. The arc chamber was fabricated from a 13 inch (33 cm) length of 5 inch (12.7 cm)

---

[4] Hobart Circoolator, S-3568B, Hobart Brothers Company, Troy, Ohio.

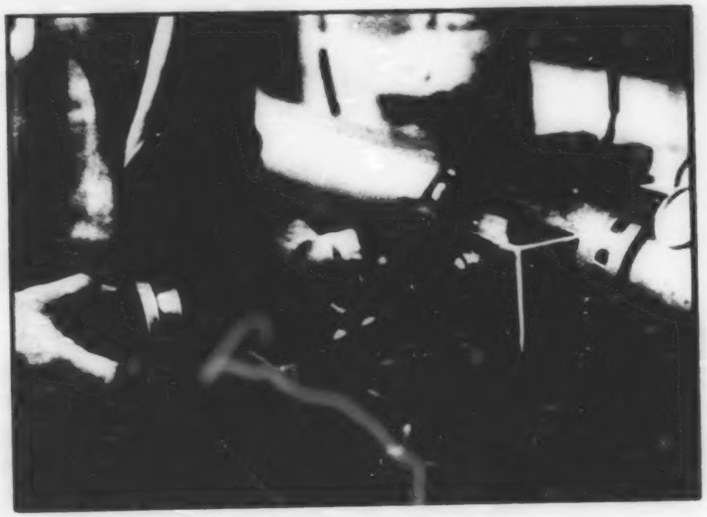

Figure 5a. Electrode holder being inserted into mounting block of arc chamber

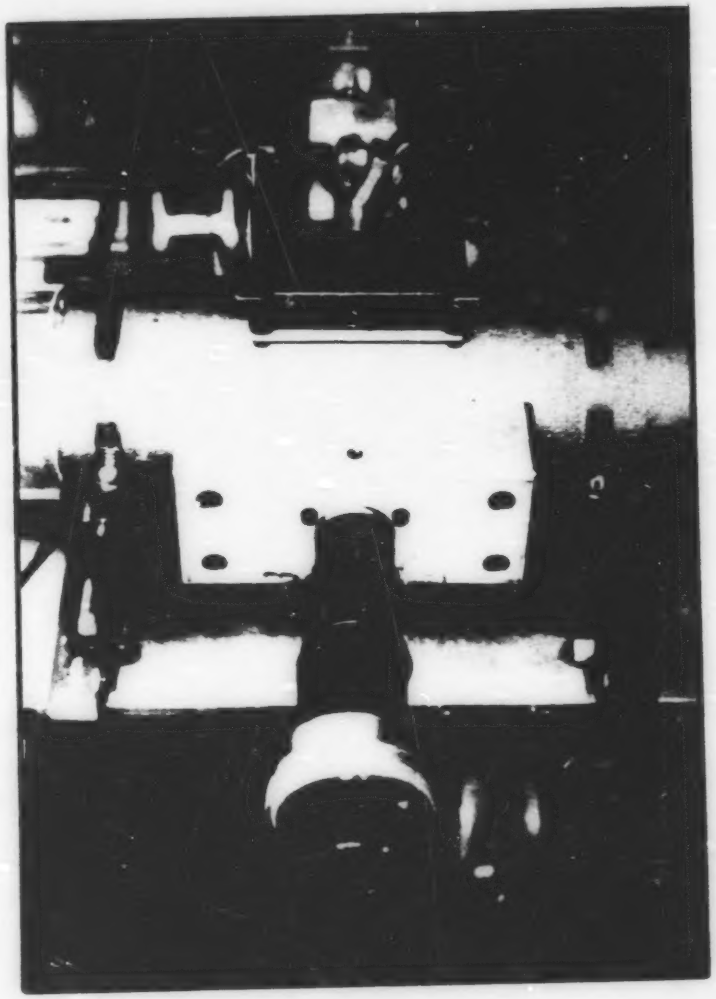

Figure 5b. Arc chamber mounting arrangement with electrode holder in place

Figure 5. Photographs showing general arrangement of arc chamber apparatus.

diameter, Schedule 40, steel pipe. The pipe axis was supported in a horizontal plane by steel supports (see Figure 5) attached to the chamber by stainless steel clamps; the steel supports were then bolted to a 20 x 24 inch (50.8 x 61.0 cm), 1/2 inch (12.7 mm) thick aluminum plate. (The wire feed assembly with torch are also bolted to this base plate through insulators. This arrangement assured positive orientation between wire feed torch, tungsten electrode holder and arc chamber.) The attachments between the chamber and the base plate, and between the wire feed assembly and base plate, are designed to allow adjustment in all axes to obtain perfect alignment between the feed wire and the non-consumable electrode.

The feed wire torch passes through the chamber wall 90 degrees to both the center line axis and the vertical tangent of the circular chamber. A concentric phenolic collar insulates the positive potential of the wire torch from the ground (-) potential of the chamber, base plate, and electrode holder. The tungsten electrode holder passes through an aluminum mounting block, milled to the contour of the arc chamber and bolted in place, on the same axis as the wire torch. A sliding fit exists between the mounting block and electrode holder, the latter being held in place by set screws. Various adjustments allow the arc to be maintained on the center line of the chamber. Refer to Appendix C, Figure C-1 for a detail of the positioning of the various components inside the arc chamber.

A 2 x 4 1/4 inch (5.1 x 10.8 cm) view window is located on the top of the chamber to allow visual evaluation of tungsten electrode erosion and observation of arc shape. The window is a standard lift-front, lens holder from a weldor's helmet modified to fit the chamber. A Shade Number 12 welding lens is used in the holder as protection from the injurious rays of the arc. The lift-front feature of the lens holder permits raising the window for a clear view of the interior of the chamber and the opening allows insertion of tools for making adjustments within the chamber.

Another salient feature of the arc chamber is the shielding gas nozzle and supply system. The shielding gas is supplied by a standard steel cylinder containing approximately 244 standard cubic feet ($6.91\ m^3$) of gas under a pressure of 2200 psig ($154.7\ kg/cm^2$). To reduce cylinder pressure to a usable level and assure constant flow, a single stage regulator and flowmeter is used and is mounted on top of the cylinder. A valve is used in the line to control flow through the flowmeter which is graduated in standard cubic feet of helium per hour (cfh). The gas flows to a solenoid on the control panel which shuts off the gas supply after the arc is extinguished, thus conserving the inert gas. From the solenoid, the gas flows to a ceramic nozzle located in the arc chamber which directs the gas at the tip of the tungsten electrode. Effective shielding of the tungsten electrode displaces the air surrounding the electrode preventing rapid consumption of the tungsten by oxidation. However, effective shielding is a difficult problem. Turbulence in the inert gas stream itself tends to pull in air; this problem is compounded by the relatively high velocity air stream being forced past the arc region. In an attempt to compensate for gas stream turbulence and maintain effective coverage of the electrode tip, an unusually high gas flow is used - 100 cubic feet per hour (47 l/min). Because of the relatively high rate of electrode consumption experienced it is still doubtful whether adequate coverage was obtained.

The usual choice of inert gas for shielding during tungsten inert gas (TIG) arc welding is between argon and helium. Each gas has its own particular advantages for different types of welding processes and materials. In the present apparatus, helium was the choice because of its availability. However, the choice of helium over argon appears advantageous for several reasons: (1) helium allows a 40 percent greater heat input per unit length of arc because of its higher ionization potential, and (2) it gives a more stable arc when using direct current power.

Figure 6 is a pictorial diagram of the arc chamber and its associated ductwork. Air flow through the system is provided by a "Gelman Hurricane Air Sampler" set on low speed. The air discharge of the blower passes through a 1 1/8 inch (28.6 mm) orifice, which limits flow to a nominal 100 cubic feet per minute (47.2 liters/second), through a detachable muffler into a 4 inch (10.2 cm) diameter horizontal duct. All ductwork throughout the system is fabricated from 22 gauge (0.794 mm) galvanized steel sheet. A transition piece connects the 4 inch (10.2 cm) diameter duct to a 2 foot (0.61 m) length of 5 inch (12.7 cm) duct leading directly to the arc chamber. From the chamber, a 2 foot (0.61 m) length of 5 inch round duct diverges into a 10 inch (25.4 cm) diameter section over a distance of 2 feet (0.61 m) and intersects a vertical duct at a 90 degree angle forming a tee. The bottom of the tee is closed by a removable

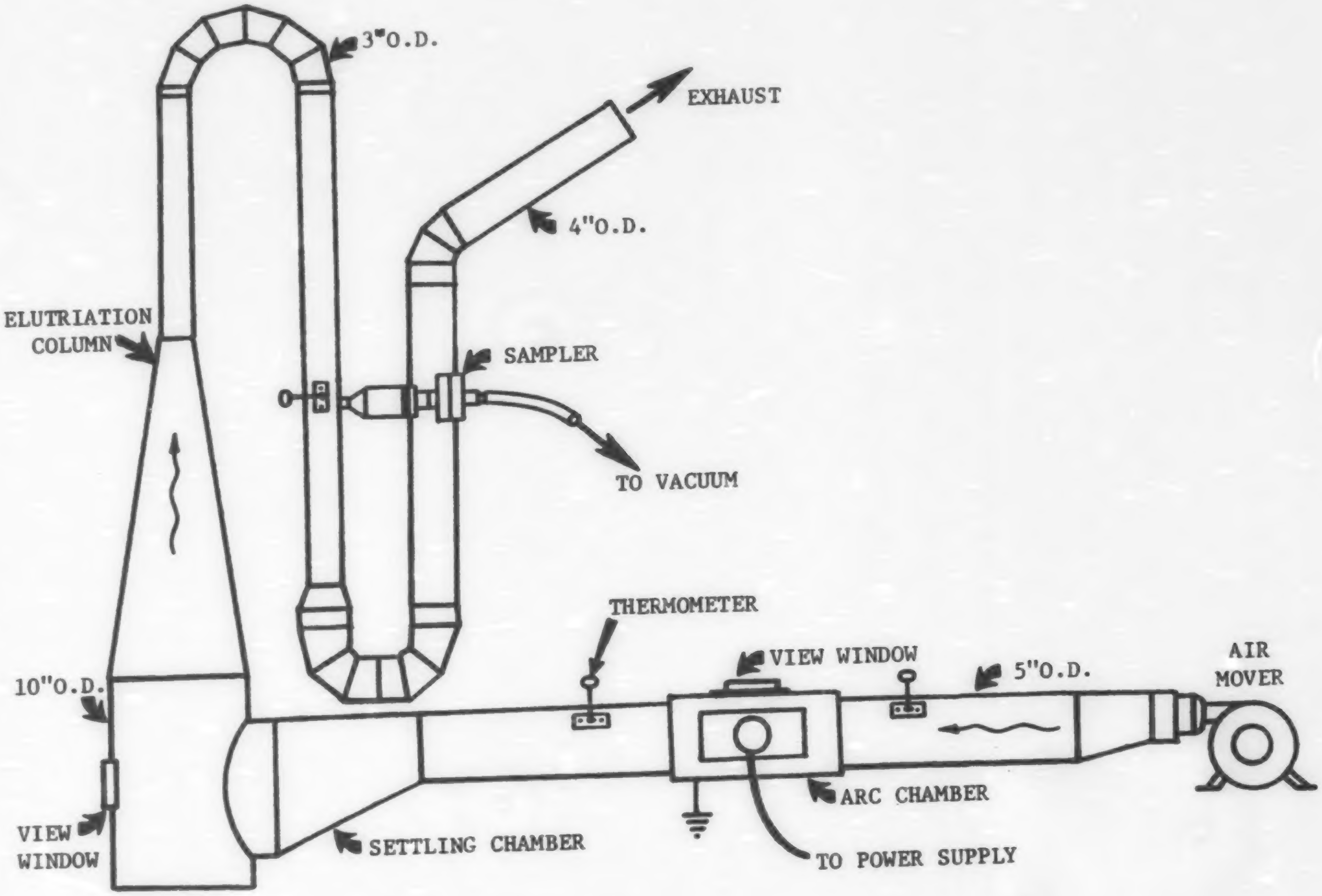
3"O.D.
EXHAUST
4"O.D.
ELUTRIATION COLUMN
SAMPLER
TO VACUUM
THERMOMETER
VIEW WINDOW
5"O.D.
AIR MOVER
10"O.D.
VIEW WINDOW
SETTLING CHAMBER
ARC CHAMBER
TO POWER SUPPLY

Figure 6. Simplified pictorial sketch of the arc chamber and duct work system

cap; the top of the tee converges over a 2 foot (0.61 m) length to a 3 inch (7.62 cm) diameter duct.

To separate the larger molten globules of steel from the gas stream, the ductwork leading from the arc chamber incorporates a settling chamber and elutriation column section in its design. The actual velocity in the 10 inch (25.4 cm) diameter vertical duct is 220 feet per minute (67.1 m/min) or 3.7 feet per second (1.12 m/sec). At this velocity steel particles larger than approximately 1/8 inch (3.175 mm) diameter are effectively eliminated from the gas stream by gravitational force. Further, inertial separation takes place in this section as the gas stream is caused to make a 90 degree change in direction.

A view window, again adapted from an arc weldor's helmet, is located on the vertical portion of the tee in such a manner as to allow observation of the arc by sighting through the inside of the 5 inch (12.7 cm) diameter duct.

The 3 inch (7.6 cm) duct leaving the elutriation column makes a 180 degree turn, and passes a 1/2 inch (12.7 mm) sampling nozzle. An adequate length of straight duct was established to allow optimum positioning of the sample probe -- a minimum of 10 diameters downstream and 5 diameters upstream from any disturbance to air flow. The 3 inch (7.62 cm) duct then diverges into a 4 inch (10.2 cm) duct, makes a 180 degree turn and exhausts the contaminated gas stream to the atmosphere through a roof ventilator.

Temperature sensors (bimetallic helix, dial thermometers) were placed in the duct at locations where significant temperature changes were expected to occur. A thermometer was also placed in close proximity to the sampling port. Location of thermometers is indicated on Figure 6.

* * *

A detailed procedure for the assembly and operation of the electric arc aerosol generator apparatus is found in Appendix C.

IV. EXPERIMENTAL

To investigate the performance characteristics of the aerosol generator under semi-continuous operation, a series of three controlled test runs were made and a portion of the resultant fume was collected. All tests were conducted under identical conditions of arc voltage, wire feed rate, shielding gas flow rate, and dilution air flow rate. Refer to Table 1 for a complete listing of test conditions. The test settings for voltage and wire feed were established on the bases of limited preliminary studies and are not claimed to be optimized values. The test program was structured to determine the mass rate of production of iron oxide fume, the particle size distribution of that fume, and the degree of reproducibility of production rate and size distribution.

SAMPLING PROCEDURE

After the arc was initiated according to the procedure outlined in Appendix C, the system was allowed to operate for approximately one minute to establish steady-state conditions for sampling. During this period the temperature of the exhaust gas stream stabilized producing a constant velocity past the sampling nozzle. A ten minute sampling period then commenced.

The sampling train consisted of a one-half inch (12.7 mm) stainless steel hook nozzle attached to an Andersen Stack Sampler[5], in series

---

[5] Andersen Stack Sampler manufactured by 2000 Inc., 5899 South State Street, Salt Lake City, Utah 84107.

Table 1. Operating and sampling test conditions

OPERATING PARAMETERS	English Units	Metric Units
Wire Feed Rate	200 inches/min	5.1 meters/min
Wire Diameter	0.045 inches	1.14 mm
Cathode Feed Rate[a]	0.2 inches/min	5.08 mm/min
Cathode Diameter	0.25 inches	6.35 mm
Arc Chamber Pressure	+0.72 inches W.C.	+1.34 mm Hg
Shielding Gas Flow Rate	100 cubic feet/hr	47.2 liters/min
Air Flow Rate	103 scfm	2.9 cubic meters/min

A power supply voltage control setting of 23 volts produced a current flow through the arc which fluctuated between 150 and 165 amperes.

SAMPLING PARAMETERS		
Sample Time	10 minutes per run	
Sample Rate	0.72 cfm @ 70F	20.41 lpm @ 21C
Exhaust Gas Temperature at Sample Port	167F	75C
Sample Nozzle Diameter	0.25 inches	6.35 mm
Ambient Temperature	70F	21C

[a] Cathode (tungsten electrode) was manually advanced approximately four turns per minute to compensate for erosion.

with an aluminum Millipore filter holder supporting a 47 mm diameter Gelman Type GA-4 membrane filter to separate the fume from the sample gas stream.

The Andersen Stack Sampler is approximately 2.75 inches (6.99 cm) in diameter and 5.0 inches (12.7 cm) in length, and weighs 3 pounds (1.36 kg). Construction is of stainless steel to withstand high temperatures and resist corrosion. The sample contains nine stages which are numbered 0 through 8, the number 8 stage having the same characteristics the number 2 stage has. The stages are 2.5 inches (6.35 cm) diameter gold plated brass plates with asbestos gaskets between the plates for spacing and sealing. Each stage has 300 air jets (holes) arranged in concentric circles, the holes decreasing in size moving from 0 through 7 (31). As the air flow through each stage is the same, the velocity of air through the air jets increases as hole size decreases. When the velocity imparted inertia of a particle is sufficient to overcome the aerodynamic drag, the particle will leave the gas stream and impact on the collection surface. Therefore, selective impaction of a particle on a particular plate depends on its aerodynamic dimensions - size, shape and density - and their relationship to gas velocity (32).

A calibrated orifice was used to indicate instantaneous sample flow rate, with total flow rate recorded on a dry gas meter.

Fume concentration was determined gravimetrically. After the sample was collected on the pre-weighed collection plates of the Andersen sampler and the back-up membrane filter, the plates and filter were dried at 248 F (120 C) for two hours. The plates and filter were then removed to a dessicator containing indicating type silica-gel and allowed to come to room temperature. When the plates and membrane filter were removed for weighing they were immediately placed on the enclosed balance pan and weighed. A small container of indicating-type silica-gel was placed in the balance enclosure. After the gravimetric determinations were made for Run 1, the collection plates were cleaned using minimal amounts of distilled water and a rubber policeman. The wash water from each plate was collected in separate test tubes, and the particulate allowed to settle for one week; the bulk of the water was then decanted and the remaining water evaporated in a drying oven. Each sample of collected fume was then resuspended in 2 ml of a 1% nitrocellulose solution[6] and dispersed by placing the test tube in an ultrasonic cleaner. The fume collected on the membrane filter was carefully scraped from the membrane and placed directly in 2 ml of the nitrocellulose solution and dispersed.

A disposable pipette was used to place one drop of the solution on an uncoated electron microscope grid. A separate grid was prepared using the solution containing particles from each collection plate and the membrane filter from Run 1. The 200 mesh grids (specimen screens) were bombarded by electrons and the projection recorded on photographic film for later particle size determination. An RCA Type EMU-4 electron microscope was used and produced a primary magnification of 29,200 times.

---

[6] No. 1120 Nitrocullulose Solution, 1%, 30 ml bottles. Ernest F. Fullan, Inc., P.O. Box 444, Schenectady, New York.

Table 2. Weight (mass) distribution of particulate matter retained by Andersen Stack Sampler and back-up membrane filter

	RUN 1			RUN 2			RUN 3		
STAGE	Weight (grams)	Percent Total	Cumulative Relative Frequency (Percent)	Weight (grams)	Percent Total	Cumulative Relative Frequency (Percent)	Weight (grams)	Percent Total	Cumulative Relative Frequency (Percent)
0	.0025	1.88	100.01	.0015	1.21	100.00	.0024	1.58	100.00
1	.0004	0.30	98.13	.0003	0.24	98.79	.0005	0.33	98.42
2	.0004	0.30	97.83	.0002	0.16	98.55	.0004	0.26	98.09
3	.0008	0.60	97.53	.0002	0.16	98.39	.0005	0.33	97.83
4	.0013	0.98	96.93	.0007	0.57	98.23	.0015	0.99	97.50
5	.0027	2.03	95.95	.0031	2.50	97.66	.0033	2.17	96.51
6	.0081	6.08	93.92	.0077	6.22	95.16	.0084	5.52	94.34
7	.0164	12.31	87.84	.0112	9.05	88.94	.0174	11.44	88.82
8	.0090	6.76	75.53	.0128	10.34	79.89	.0134	8.81	77.38
Filter	.0916	68.77	68.77	.0861	69.55	69.55	.1034	68.57	68.57
TOTAL	0.1332	100.01		0.1238	100.00		0.1521	100.00	

Table 3. Mass concentration and total production rate of iron oxide particles

	①	②	③	④	⑤	⑥	⑦	⑧	⑨	⑩
	Table 1		Table 1	15.43 ③/②	2288 ④	Table 1	④ X ⑥	.00857 ⑦	.0648 ⑦	3.89 ⑦
RUN	Sample Time	Total Sample Volume	Sample Weight	Mass Concentration		Total Gas Flow	Total Particulate Production Rate			
	(mins)	(scf)	(grams)	(gr/scf)	(mg/m^3)	(scfm)	(gr/min)	(lbs/hr)	(g/min)	(g/hr)
1	10	7.23	0.1332	0.284	649.8	103	29.25	0.251	1.90	113.8
2	10	7.21	0.1238	0.265	606.3	103	27.30	0.234	1.77	106.2
3	10	7.17	0.1521	0.327	748.2	103	33.68	0.289	2.18	131.0
AVE	10	7.20	0.1364	0.292	668.1	103	30.08	0.258	1.95	117.0

RESULTS

In all test runs to determine performance characteristics, identical apparatus and operating and sampling conditions were maintained as listed in Table 1.

Mass Concentration and Rate of Production

The mass of particulate in the sample gas stream was determined from the gravimetric differential between the tare weight of the clean Andersen collection plates and membrane filter and the weight of the plates and filter after sampling. The weight differential for each of the tests runs is shown in Table 2. Combining the information from Table 2 with knowledge of the total gas volume sampled and the sample time, the mass concentration of particulate matter in the sample gas stream was calculated. Average mass concentration of iron oxide fume in the sample gas stream was 0.292 grains/scf (668.1 mg/m^3). Assuming the mass concentration of particulate matter in the total gas stream is the same as for the sample gas stream, the average total particulate production rate was calculated to be 30.08 grains/min (117.0 grams/hr). Additional information concerning mass flow rate and mass concentration calculated for each run for both the sample and total gas streams is presented in Table 3. Total particulate production rate, given in various common units of measurement, is also listed in Table 3.

Another performance factor directly related to the rate of production is the conversion ratio of consumable wire feed stock to ultrafine particles. For the feed rate of 200 inches (5.1 m) per minute of 0.045 inch (1.14 mm) diameter mild steel wire, 12 thousand inches (305 m) are consumed in one hour. (Refer to Table 1). As there are 2210 inches per pound (25.46 m/kg) of wire (33), the wire consumption rate was

$$\frac{12{,}000 \text{ inches/hr}}{2{,}210 \text{ inches/lb}} = 5.43 \text{ lb/hr } (2.46 \text{ kg/hr}).$$

From Table 3, the average particulate production rate was 0.258 lb/hr (117.0 g/hr). Therefore, 5.43 pounds (2463 g) of wire was required to produce 0.258 pounds (117.0 g) of ultrafine particles for a conversion ratio of 4.75 percent. Although no complete mass balance was performed, the remaining portion of consumed metal can be accounted for by the following observations. A relatively large portion of the feed stock was not vaporized as some material melted and formed a puddle in the bottom of the arc chamber. A significant number of relatively larger particles, approximately 1000 micrometers, settled out in the settling chamber and elutriation column section of the ductwork. The loss of smaller particles is due to the electrophoretic and thermophoretic forces acting on the particles suspended in the gas stream. These forces cause the smaller particles to migrate to the walls of the ducting and attach themselves through various adhesive and electrostatic forces. A thin reddish-brown coating was observed on the inside of the ductwork after completion of the test program.

It is also interesting to note the number of discrete spherical particles generated at the above production rate. Considering a mass mean diameter of 0.022 micrometers and specific gravity of approximately

5.2 (34), the numerical generation rate is calculated in the following manner.

$$\text{Volume of single sphere} = \frac{1}{6}\pi d^3$$

$$= \frac{1}{6}\pi(0.022)^3 = 5.58 \times 10^{-6}\ \mu m^3$$

Specific gravity of $Fe_2O_3 = 5.2$

$$\text{Weight of single sphere} = 5.58 \times 10^{-6}\ \mu m^3 \times 10^{-12}\ cm^3/\mu m^3 \times 5.2\ g/cm^3$$

$$= 29.0 \times 10^{-18}\ \text{grams}$$

$$\text{Generation rate} = \frac{117.0\ g/hr}{29.0 \times 10^{-18}\ g/particle} \doteq 4 \times 10^{18}\ \text{particles/hr}$$

This is more than four quintillion particles per hour.

Particle Size Distribution

Two methods were employed, with differing results, to determine particle size distribution: (1) an electron microscope and (2) an Andersen Stack Sampler.

Because of the high magnification, and consequently small field, of the electron microscope, photographic plates were made of a minimum of three fields of each grid. The photographic plates were enlarged and printed on 8 x 10 inch (20.3 x 25.4 cm) photographic paper giving a final magnification of 87,600 times. The electron micrographs obtained in this manner have a two-dimensional appearance and discrete particles are readily discernible. Individual particles of iron oxide are spherical; and individual spherical particles composing larger agglomerates were easily distinguished. The particle size distribution data presented in Tables 4 and 5 and graphically represented in Figures 7, 8, 9, 10, and 11 are based on direct counts of discrete, spherical particles. That is, agglomerates are not assigned a composite or equivalent particle size but the particles composing an agglomerate are classified individually. A specially constructed semi-circle graticule was used to facilitate particle sizing.

Examination of the raw particle count data found in Appendix D lists thirty fields for which particle size determinations were made. The number of discrete particles observed on each 2.275 x 2.875 micrometer field ranged from 177 to 742 with an arithmetic mean of 412. A total of 12,355 particles were individually sized.

In order to simplify calculation of various statistical values, the raw data was grouped into 10 classes with a particle size interval of 0.01 micrometers each. Although the following mathematical descriptions of particle size were calculated on the assumption that all particles were classified in one of ten equal-interval classes, this was not exactly the case. As a small number of particles exceeded the upper boundary of the tenth class (0.105 micrometers), the tenth class was actually open-ended and contained all particles 0.095 micrometers in diameter and larger. This assumption introduces a slight error in the following calculations, but this error is relatively insignificant as only 30 particles of the 12,355 particles counted exceeded 0.105 micrometers. Three of these particles exceeded 0.2 micrometers at 0.22, 0.25 and 0.24 micrometers and were found on stages 5, 6, and 7, respectively.

Table 4. Electron microscope particle count data[a]

STAGE	Particle Size, micrometers										TOTALS
	0.005-0.015	0.015-0.025	0.025-0.035	0.035-0.045	0.045-0.055	0.055-0.065	0.065-0.075	0.075-0.085	0.085-0.095	0.095 and >	
0	522	248	153	87	51	24	17	15	1	9	1127
1	351	183	145	56	37	21	12	3	2	7	817
2	709	249	161	91	46	27	12	3	2	5	1305
3	431	164	123	56	36	19	9	7	5	1	851
4	773	419	308	157	56	39	13	10	5	16	1796
5	592	285	210	68	47	33	29	4	3	8	1279
6	345	149	126	48	25	20	5	2	3	5	728
7	436	209	149	87	50	21	11	10	2	9	984
8	749	336	233	98	97	20	9	7	4	6	1559
Filter	818	421	300	159	86	68	27	15	7	8	1909
TOTALS	5726	2663	1908	907	531	292	144	76	34	74	12355
RANGE	493	270	185	111	72	49	20	13	5	15	1181

[a] Refer to APPENDIX D for raw particle count data.

Table 5. Relative Particle Size Frequency Distribution in Percent from data of Table 4

STAGE	Particle Size, micrometers										
	0.005-0.015	0.015-0.025	0.025-0.035	0.035-0.045	0.045-0.055	0.055-0.065	0.065-0.075	0.075-0.085	0.085-0.095	0.095 and >	
0	46.3	22.0	13.6	7.7	4.5	2.1	1.5	1.3	0.1	0.8	99.9
1	43.0	22.4	17.7	6.9	4.5	2.6	1.5	0.4	0.2	0.9	100.1
2	54.3	19.1	12.3	7.0	3.5	2.1	0.9	0.2	0.1	0.4	99.9
3	50.5	19.2	14.4	6.6	4.2	2.2	1.1	0.8	0.6	0.1	99.7
4	43.0	23.3	17.1	8.7	3.1	2.2	0.7	0.6	0.3	0.9	99.9
5	46.3	22.3	16.4	5.3	3.7	2.6	2.3	0.3	0.2	0.6	100.0
6	47.4	20.5	17.3	6.6	3.4	2.7	0.7	0.3	0.4	0.7	100.0
7	44.3	21.2	15.1	8.8	5.1	2.1	1.1	1.0	0.2	0.9	99.8
8	48.0	21.6	14.9	6.3	6.2	1.3	0.6	0.4	0.3	0.4	100.0
Filter	42.8	22.1	15.7	8.3	4.5	3.6	1.4	0.8	0.4	0.4	100.0
Mean[a]	46.6	21.4	15.5	7.2	4.3	2.4	1.2	0.6	0.3	0.6	100.0
Standard Deviation[a]	3.73	1.38	1.72	1.15	0.92	0.59	0.52	0.36	0.16	0.27	
Range	11.3	4.2	5.4	3.5	3.1	2.3	1.7	1.1	0.5	0.8	

[a] Refer to APPENDIX E, Table E-3 for calculations.

Figure 7. Histogram representing particle size data from Table 5

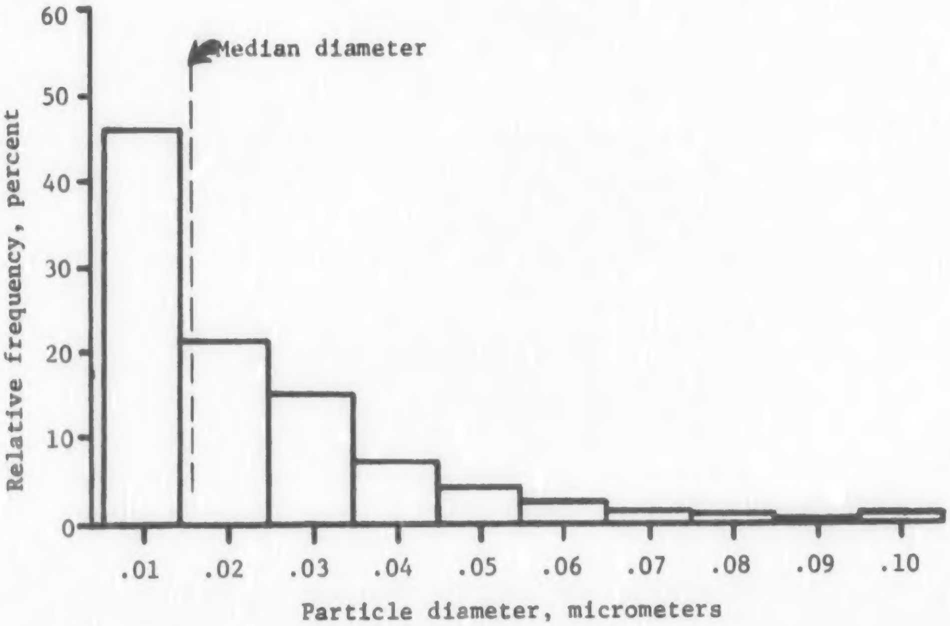

Figure 8. Distribution curve representing data from Table 5

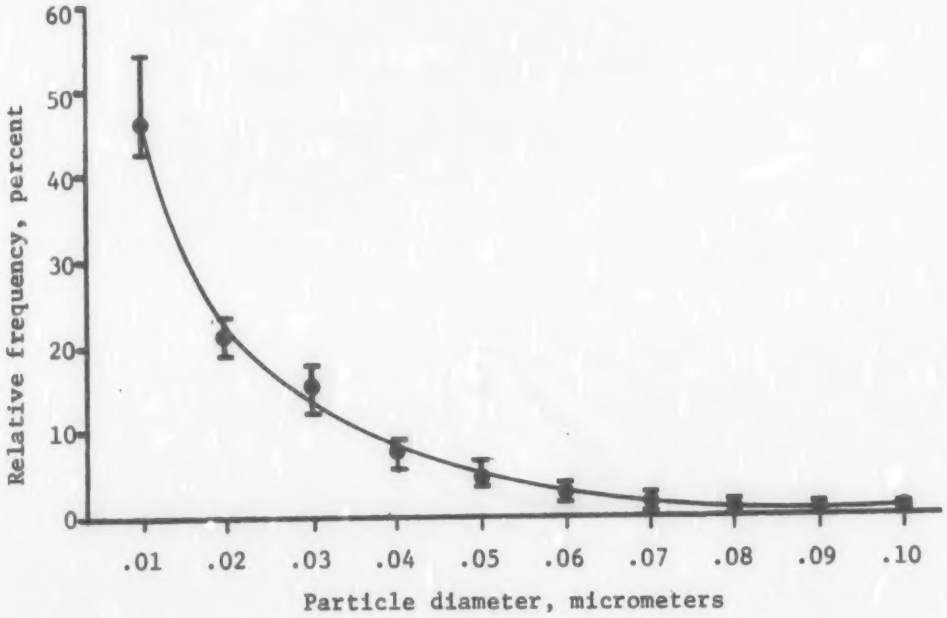

Figure 9. Ogive representing cumulative distribution data from Table 6

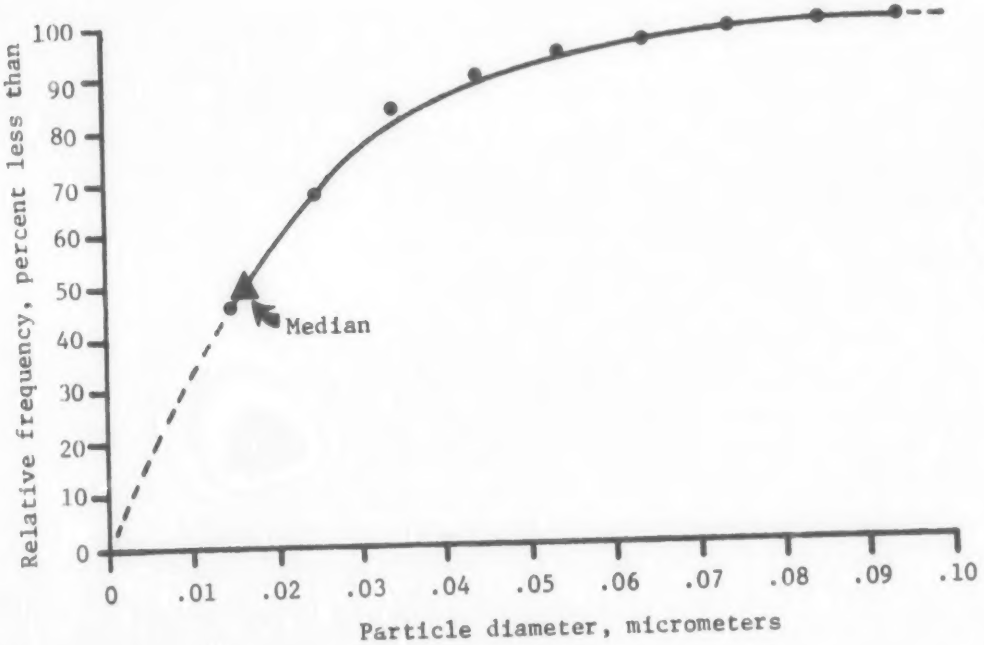

Figure 10. Cumulative distribution data from Table 6 plotted using normal probability scales

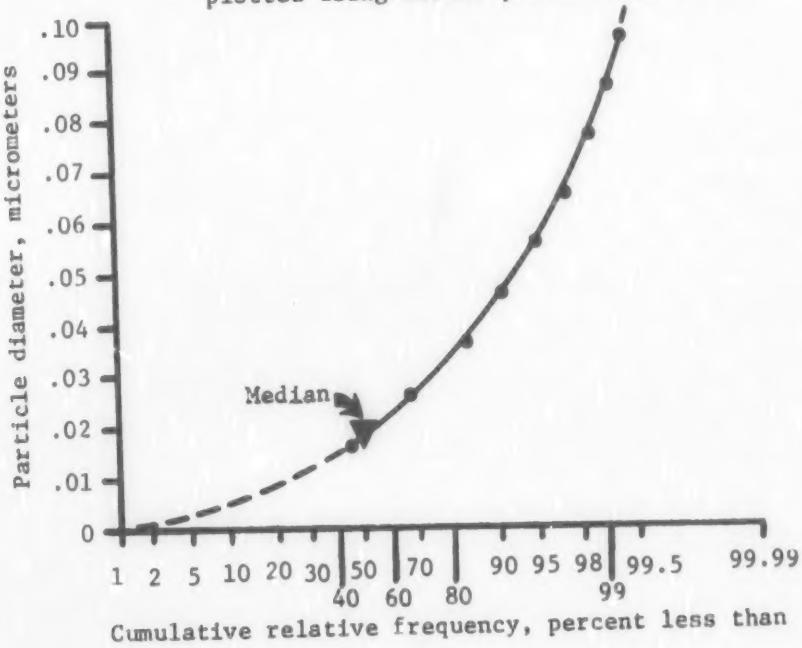

Figure 11. Cumulative particle size distribution data from Table 6 plotted using log-normal probability scales

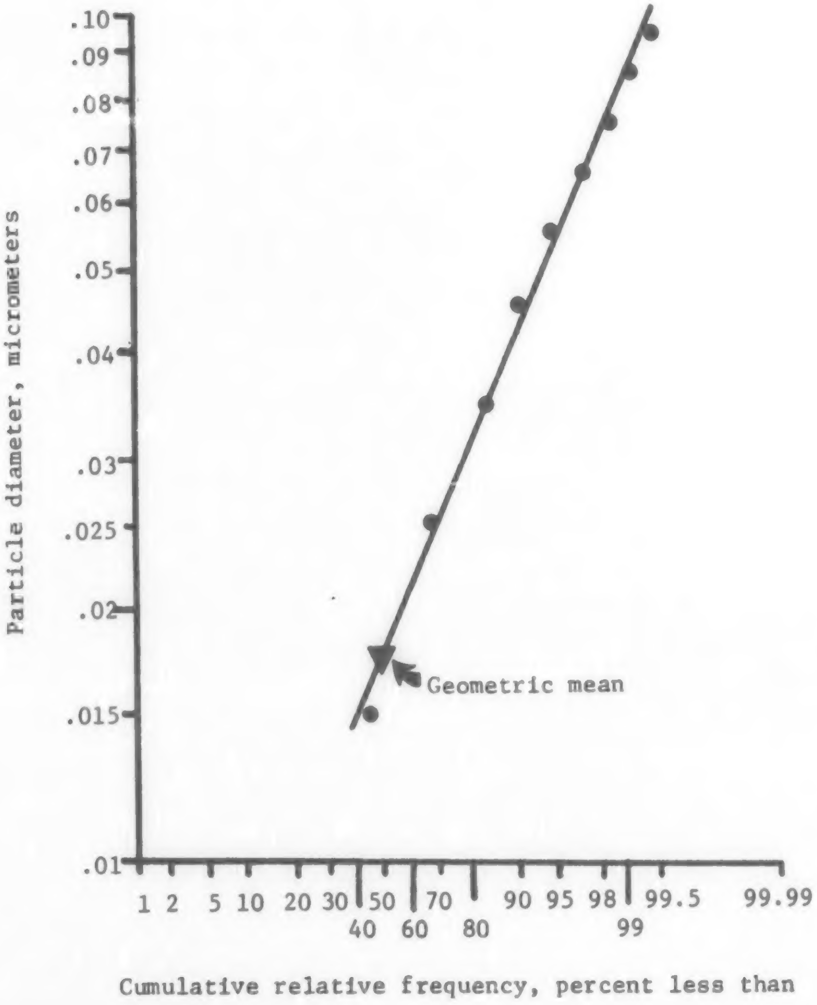

The raw particle count data of Appendix D has been somewhat reduced and presented in a more usable form in Table 4. A simplified method for calculating the arithmetic mean and standard deviation of the particle size distribution as described by Cadle [35] is employed. Calculation of the arithmetic mean, $\bar{d}$, is based on the following equations,

$$\bar{d} = c \frac{1}{n} \sum_{i=1}^{n} u_i f_i + d_o \frac{1}{n} \sum_{i=1}^{n} f_i$$

$$\bar{d} = c\bar{u} + d_o$$

where c is the class interval, n is the total number of particles counted, u_i is the class mark of the new scale (-1,0,1,2...8), d_o is the class mark corresponding to u_i 0, and f_i is the frequency for each class. Using the transformations found in Appendix E, Table E-1, the arithmetic mean is,

$$\bar{d} = .01 \left(\frac{2763}{12,355}\right) + 0.02$$

$\bar{d}$ = 0.022 micrometers

The equation for standard deviation (s) employs the same notation and is calculated using the following equation.

$$s = c\sqrt{\frac{1}{n} \sum_{i=1}^{n} u_i \; f_i \; -\bar{u}^{2}}$$

Using the values of Appendix E, Table E-1,

$$s = 0.01 \sqrt{\left(\frac{33451}{12355}\right) - \left(\frac{2763}{12355}\right)^{2}}$$

s = 0.0163 micrometers

In order to present the particle size distribution data in the several graphical forms of Figures 9, 10 and 11, it was necessary to transform the numerical distribution into a relative frequency distribution expressed in percent. The results of this conversion are presented on Table 6. The histogram and distribution curve of Figures 7 and 8, respectively, indicate a highly positive skewed distribution based on the particle size range examined. As the lower limit of resolution of the electron microscope was approximately 0.005 micrometers (50 Å), no information can be presented on particles that may have formed with diameters less than 0.005 micrometers.

The range of relative frequency found on each of the specimen screens for each size interval is also presented on Figure 8 and indicates the size distribution of discrete particles collected on each plate of the Andersen Stack Sampler and the membrane filter is approximately the same. Standard deviation of the relative frequency within each size interval is presented in Appendix G. The range of standard deviations also seems to indicate similar particle size distributions.

The cumulative frequency distribution tabulated in Table 6 is presented as an Ogive in Figure 9 and, more conventionally, using normal probability and log-normal probability scales in Figures 10 and 11 respectively. The log-normal scales of the latter reveal a relatively straight line indicating a log-normal particle size distribution.

Table 6. Cumulative distribution of data from Table 5

Class boundaries		Percent in Class	Percent less than upper class limit
L	U		
0.005	0.015	46.3	46.3
0.015	0.025	21.6	67.9
0.025	0.035	15.4	83.3
0.035	0.045	7.3	90.3
0.045	0.055	4.3	94.9
0.055	0.065	2.4	97.3
0.065	0.075	1.2	98.5
0.075	0.085	0.6	99.1
0.085	0.095	0.3	99.4
0.095	0.105[a]	0.6	100.

[a] Refer to page 34 for explanation of upper limit for this class.

The median and geometric mean are calculated using the procedures presented by Freund and Williams (36). By definition, the median divides the frequency distribution in half, *e.g.* there will be the same number of particles above the median size as there are below. For the present frequency distribution containing 12,355 ranked observations, the median corresponds to the calculated particle size of the 6178th particle. For the grouped data of Table 4 the median (M) is calculated using the following equation (37),

$$M = L + \frac{cJ}{f_M}$$

where L is the lower class boundary of the interval containing the median value, c is the class interval, J is the difference between the median observation and the cumulative frequency of all classes preceeding the class containing the median, and f_M is the frequency of the class containing the median. Using the tabulated values of Appendix F, the median is

$$M = .015 + \frac{0.01\ (6170-5726)}{2666}$$

$$M = 0.0167 \text{ micrometers.}$$

The median, sometimes known as the mass median diameter (MMD), has been graphically inserted in Figures 7 and 9. Inspection of Figure 9 confirms the calculated value of the median as the ogive curve representing the cumulative frequency distribution passes through coordinates of 50 percent cumulative relative frequency and 0.0167 micrometer particle diameter.

Geometric mean (G) is calculated based on the following relationship (38),

$$\log G = \frac{\Sigma \log x_i \ (f)}{n}$$

where x_i is the class mark of an interval, f is the frequency of that class interval, and n is the total number of observations (Σf). Again using the tabulated values found in Appendix F, the geometric mean is calculated as follows,

$$\text{Log } G = \frac{-27{,}715.1}{12{,}355} = \bar{2}.24322$$

$$\text{antilogarithm } \bar{2}.24322 = 0.01751$$

$$G = 0.0175 \text{ micrometers}$$

The geometric mean has been plotted on Figures 10 and 11 and at the "50 percent less than" point intersects the frequency distribution curves as expected.

By inspection of Table 4, the mode for this particle size distribution occurs in the 0.005-0.015 micrometer diameter interval.

As stated previously, two methods were employed to determine particle size distribution. The second method involved the relatively new Andersen Stack Sampler used in conjunction with a back-up membrane filter. Combining the mass distribution data of Table 2 with calibration information supplied by the manufacturer, cumulative particle size mass distribution can be obtained and is presented on Table 7. Although this mass distribution data indicates approximately 69 percent of the sampled particulate passed through the Andersen

Table 7. Arithmetic mean and standard deviation of cumulative relative mass distribution from data of Table 2

STAGE	Approximate range of particle size[a] (micrometers)	Upper Class Limit (micrometers)	RUN 1	RUN 2	RUN 3	Mean cumulative relative mass[c] (percent less than)	Standard deviation[c] (percent)	$\frac{s}{\bar{x}}$[c]
			Cumulative relative mass[b] (percent less than upper class limit)					
0	30 and larger	unknown	100.10	100.00	100.00	100.03	---	---
1	9.2-30	30	98.13	98.79	98.42	98.45	0.330	.0033
2	5.5-9.2	9.2	97.83	98.55	98.09	98.26	0.386	.0039
3	3.3-5.5	5.5	97.53	98.39	97.83	97.92	0.437	.0044
4	2.0-3.3	3.3	96.93	98.23	97.50	97.55	0.652	.0066
5	1.0-2.0	2.0	95.95	97.66	96.51	96.71	0.872	.0090
6	0.3-1.0	1.0	93.92	95.16	94.34	94.47	0.631	.0066
7	0.1-0.3	0.3	87.84	88.94	88.82	88.53	0.603	.0068
8	less than 0.1	0.1	75.53	79.89	77.38	77.60	2.188	.0281
Filter		0.1	68.77	69.55	68.57	68.96	0.518	.0075

[a] Farrell Yeates, *et. al.*, "Calibration and Evaluation of the Andersen Stack Sampler", Technical Report No. FY70 MCR-1, submitted to Two Thousand, Inc., Salt Lake City, Utah (April, 1970), p. 18.

[b] From Table 2.

[c] Refer to APPENDIX E, Table E-4 for calculations.

Figure 12. Cumulative particle size distribution data from Table 7 plotted using log-normal probability scales

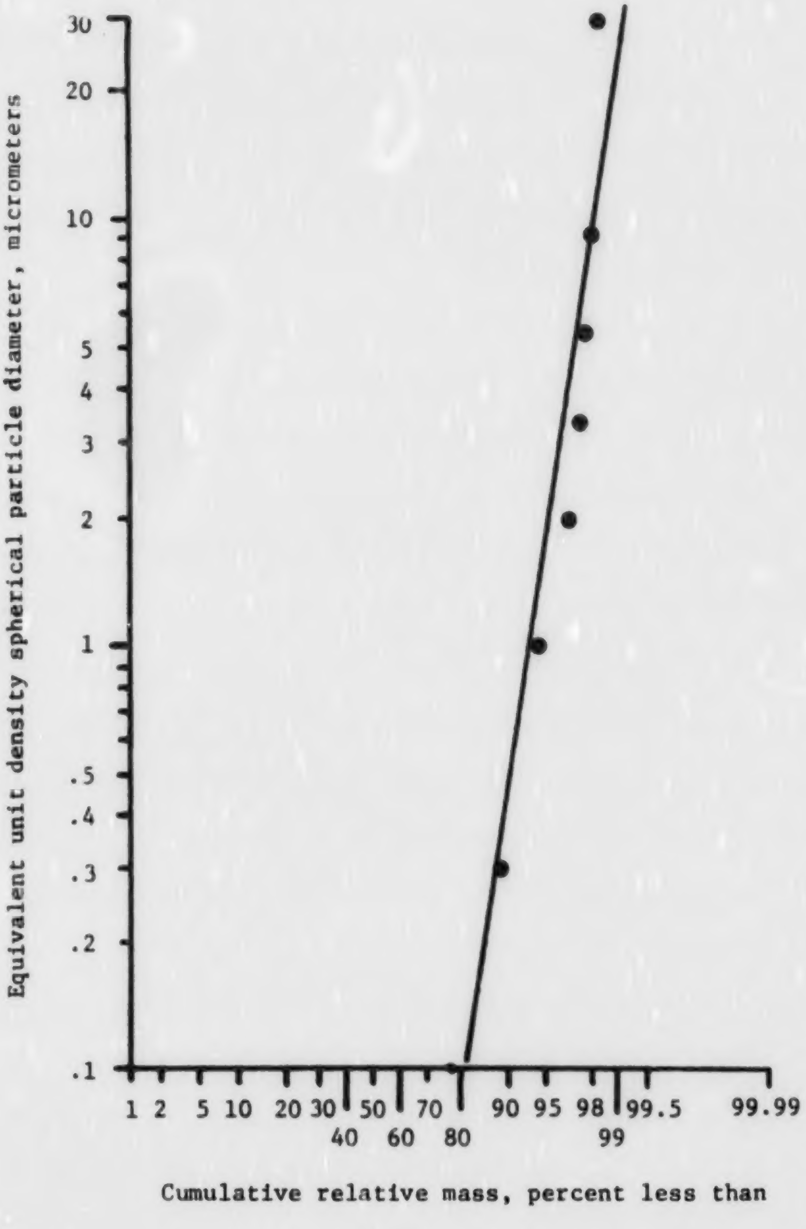

Stack Sampler without collection, the previous data presented concerning the size of the discrete particles suggests essentially all the particulate matter should have passed through the sampler without impacting on the collection plates. As the particles were produced in a direct current arc, it was expected that chains and agglomerates would form, thereby increasing the effective aerodynamic size of the particles. In fact, a limited number of these formations were observed on the electron micrographs. However, since the electron microscope sample preparation technique was designed to disperse any particle aggregates to facilitate counting, the effective size could not be confirmed by direct observation.

The Andersen Stack Sampler utilizes aerodynamic sizing to equate the size of all particles sampled---irrespective of shape or density---to the aerodynamic equivalence of unit density spheres. Vomela and Whitby (39) have made measurements on aggregates consisting of from 10 to 300 particles having a mass mean diameter of 0.05 micrometers and concluded the fluid drag on agglomerates of particles is nearly the same as that of a sphere having a volume equivalent to that of the aggregates. For example, a mass consisting of one hundred, 0.022 micrometer diameter particles is aerodynamically equivalent to one particle 0.1 micrometers in diameter. At present, the only calibration data available from the manufacturer is for unit density spheres and is listed on Table 7.

The mass distribution developed in Table 7 and presented graphically in Figure 12 is plotted as if the particles were spherical and of unit density. In reality this is known not to be the case as the specific gravity of iron oxide (Fe_2O_3) is in the range of 5.12 - 5.24 ([34]), thereby increasing the relative inertial force of spherical iron oxide particles when compared to the same size unit density spheres. That is, inside the sampler an iron oxide sphere will overcome the aerodynamic drag force and leave the turning gas stream (and impinge on the collection plate) at a much lower velocity than would the same size particle of unit density.

Reproducibility of Production Rate and Relative Particle Size Distribution

The production rate of particulate matter for each of the three runs was calculated and presented on Table 3 with the arithmetic mean calculated at 30.08 grains/min (1.95 g/min). As an indication of variability about the mean, the standard deviation (s) was calculated using the following equation,

$$s = \sqrt{\frac{\sum_{i=1}^{n} (x_i - \overline{x})^2}{n}}$$

where x_i represents an individual observation, $\overline{x}$ is the arithmetic mean, and n is the total number of observations.

x_i	$x_i-\overline{x}$	$(x_i-\overline{x})^2$
29.25	-0.83	.6889
27.30	-2.78	7.7284
33.68	3.60	12.9600

$\Sigma 21.3773$

Therefore,

$$s = \sqrt{\frac{21.3773}{3}} = 2.68 \text{ grains/min}$$

Two methods were used to estimate the reproducibility of the relative particle size distribution---both using the mass distribution data obtained from the Andersen Stack Sampler and membrane filter. The results of the three runs are presented in Table 2.

Table 8 presents the arithmetic mean and standard deviation for the weights found for each of the three runs on each stage of the sampler and the membrane filter. As a further, and possibly more meaningful, comparison of the standard deviations of the various stages with each other, the last column on Table 8 presents the standard deviation as a percent of the arithmetic mean of the weights. The mean and standard deviation of the total particulate mass captured during each run is also given and is another indicator of the reproducibility of production rate.

The second estimate of size distribution reproducibility is obtained by calculating the arithmetic mean and standard deviation of the cumulative relative mass distribution for each of the various size intervals. The results are presented on Table 7. Again the last column represents the standard deviation as a percentage of the mean, in this case the mean cumulative relative mass.

Table 8. Arithmetic mean and standard deviation of the weight (mass) distribution from data of Table 2

	RUN 1	RUN 2	RUN 3	$\bar{x}$	s	$\frac{s}{\bar{x}}$[a]
	Collected weight			Mean weight[a]	Standard deviation[a]	
STAGE	(milligrams)			(mg)	(mg)	
0	2.5	1.5	2.4	2.13	0.4496	0.2110
1	0.4	0.3	0.5	0.40	0.0812	0.2030
2	0.4	0.2	0.4	0.33	0.0943	0.2857
3	0.8	0.2	0.5	0.50	0.2449	0.4898
4	1.3	0.7	1.5	1.17	0.3398	0.2904
5	2.7	3.1	3.3	3.03	0.2493	0.0822
6	8.1	7.7	8.4	8.07	0.2867	0.0355
7	16.4	11.2	17.4	15.00	2.7178	0.1561
8	9.0	12.8	13.4	11.73	1.9482	0.1660
Filter	91.6	86.1	103.4	93.70	7.2171	0.0770
TOTALS	133.2	123.8	152.1	136.00	14.4202	0.1060
				Mean	1.3629	0.1997

[a] Refer to APPENDIX E, Table E-5 for calculations.

V. CONCLUSIONS

On the basis of the results of the limited experimental tests reported herein, the feasibility of employing an electric arc to produce aerosols of ultra-fine iron oxide particles from a feedstock of consumable wire has been demonstrated. Although little attempt was made to optimize the operating parameters, more than 30 grains per minute (1.95 g/min) of discrete, spherical particles with a mass median diameter of 0.0167 micrometers was repeatedly produced within a range of plus or minus 12 percent. Due to agglomeration, a limited number of aggregates and chains of particles were formed thereby increasing the mean effective aerodynamic size of the particle distribution. Even so, a conservative examination of the mass distribution data obtained from the Andersen Stack Sampler particle sizing technique indicates approximately 75 percent of the particles have an effective diameter less than 0.1 micrometers. If the agglomerating effects prove undesirable for a particular study, an ion generator or polonium grid could be employed to neutralize the charged particles. The rate of particle production is believed to be essentially uniform as the consumable wire was fed at a constant rate and the power supply was regulated at a constant voltage. It is felt the feedstock-to-particulate conversion ratio of 4.75 percent could be significantly improved through optimization of the main parameters: arc voltage, wire feed rate and wire diameter. The interior dimensions of the electrode holder coupled with an erosion rate of 0.2 inches (5.08 mm) per minute limited length of continuous production to approximately 30 minutes. Optimization of the above parameters complemented by improved shielding of the tungsten electrode should serve to reduce the erosion rate of the relatively non-consumable tungsten, thereby increasing the time interval between start-up and replacement of the tungsten electrode. A redesign of the electrode holder through addition of an automatic advancing mechanism capable of accepting longer tungsten electrodes could greatly improve the endurance of the generator.

The morphology of the iron oxide generated in this study closely approximates the characteristics of emissions from various heavy industrial processes: open hearth and basic oxygen steel making, scarfing, welding, plasma and oxygen-acetylene slab cutting, and of course, the electric arc furnace. As the behavior of collected and re-dispersed iron oxide particulate matter varies significantly from that of "fresh" iron oxide fume, the primary aerosol formation technique demonstrated here may prove invaluable for control equipment research. The practical implications of a device such as this are much more far-reaching. With no modification to the basic generator apparatus, essentially all metals and metal alloys could be vaporized in the electric arc producing oxides of most metals. Among hazardous metals of current interest because of their physiological effects are lead, chromium, beryllium, vanadian, tin and copper. To further increase the research applications, special cored wires can be produced to introduce additional contaminants into a system at a controlled rate along with a primary metal fume. The basic system is also amenable to introduction of gaseous constituents for study of possible or known synergistic relationships.

With modification, the unit could also be adapted for the production of aerosols of non-conductive refractory materials. This could be accomplished by replacing the wire torch with another non-consumable electrode holder, establishing an arc between them, and guiding the non-conductive feedstock into the high-intensity arc. Conversely, elimination of the tungsten electrode as one side of the arc could be accomplished by utilizing two wire torches and establishing an arc between the consumable wire "electrodes". This modification will inherently eliminate the problems of tungsten electrode erosion (requiring periodic replacement) and potential contamination of the solid phase of the aerosol. Ability of the generator to operate continuously would also be greatly enhanced.

LIST OF REFERENCES

(1) Lodge, James P., "Production of Controlled Test Atmospheres", Air Pollution, Arthur C. Stern, ed., Vol. 2, Academic Press, New York (1968) pp. 465-483.

(2) Amdur, Mary O., "The Physiological Response of Guinea Pigs to Atmospheric Pollutants", International Journal of Air Pollution, Vol. 1 (1959) pp. 170-183.

(3) Fuchs, N. A., The Mechanics of Aerosols, The Macmillan Company, New York (1964) p. viii-x.

(4) Silverman, Leslie, "Experimental Test Methods", Air Pollution Handbook, Paul L. Magill, Francis R. Holden and Charles Ackley eds., McGraw-Hill, New York (1956) pp. 12-1-12-2.

(5) Fuchs, op. cit., pp. 367-377.

(6) Ibid. p. 374.

(7) Silverman, op. cit., p. 12-20.

(8) Udin, Harry, Funk, Edward R., and Wulff, John, Welding for Engineers, John Wiley & Sons, Inc., New York (1954) p. 141.

(9) Holmgren, J. D., Gibson, J. O., and Sheer, C., "Some Characteristics of Arc Vaporized Submicron Particulates", Ultra Fine Particles, W. Kuhn, ed., John Wiley, New York (1963) p. 130.

(10) Amick, James and Turkevich, John, "Electron Microscopic Examination of Aerosols Formed in a Direct Current Arc", Ultra Fine Particles, W. Kuhn, ed., John Wiley, New York (1963) p. 147.

(11) Whitby, K. T., Lundgren, D. A., and Petersen, C. M., "Homogeneous Aerosol Generators", International Journal of Air and Water Pollution, Vol. 9 (1965) p. 265, 276.

(12) Silverman, Leslie and Billings, Charles E., "Methods of Generating Solid Aerosols", Journal of Air Pollution Control Association, Vol. 76, No. 6, (1956) p. 82.

(13) Ibid. pp. 77 ff.

(14) Silverman, "Experimental Test Methods", op. cit., pp. 12-19-12-38.

(15) Olive, T., "Solids Feeders", Chemical Engineering, Vol. 59, No. 11 (1952) pp. 163-178.

(16) Fuchs, *op. cit*. chapter VIII.

(17) Silverman, "Methods of Generating Solid Aerosols", *op. cit*. p. 77.

(18) Silverman, "Experimental Test Methods", *op. cit*., pp. 12-20, 12-22-12-23.

(19) Holmgren *et. al*., *op. cit*., p. 129.

(20) Harris, V., Holmgren, J. D., Korman, S., and Sheer, C., "Arc Decomposition of Rhodonite", *Electrochemical Society Journal*, Vol. 106, No. 10 (Oct. 1959) pp. 874-876.

(21) Tafa Division, Humphreys Corporation, 180 North Main Street, Concord, New Hampshire 03301.

(22) Karioris, Frank G., and Fish, Birney R., "An Exploding Wire Aerosol Generator", *Journal of Colloid Science*, Vol. 17, (1962) pp. 155-161.

(23) Silverman, "Methods of Generating Solid Aerosols", *op. cit*., p. 81.

(24) Davis, R. J., Truitt, J., and Gill, J. S., "Aerosol Studies in the Reactor Safety Program at Oak Ridge National Laboratory", *Journal of the Air Pollution Control Association*, Vol. 18, No. 10 (Oct. 1968), pp. 675-676.

(25) Truitt, J. and Davis, R. J., "The Function of Condensing Steam in Aerosol Scrubbers", Reactor Chemistry Division, Oak Ridge National Laboratory, Oak Ridge, Tennessee, unpublished report of research sponsored by the National Air Pollution Control Administration (1970).

(26) "Operation Instructions for Electric Motor Driver Constant Voltage Welder for Automatic Welding, Model MC-900, Specs 4136, 4210". Hobart Brothers Company, Troy, Ohio.

(27) "Hobart Welding Wire and Flux", Bulletin EW-382 (NWSA-630). Hobart Brothers Company, Troy, Ohio.

(28) "Installation-Operation-Maintenance Manual for Hobart Automatic Welding Head, Model AI-22, Specs 3974A." Hobart Brothers Company, Troy, Ohio.

(29) *Welding Data Book*, Robert N. Williams, ed., Industrial Publishing Company, Cleveland, Ohio (1967) pp. A/72-A/73.

(30) Rose, Arthur and Rose, Elizabeth, eds. *The Condensed Chemical Dictionary*, Van Nostrand Reinhold Company (1967) p. 982.

(31) Yeates, Farrel, *et. al*., "Calibration and Evaluation of the Andersen Stack Sampler", Technical Report No. FY70 MCR-1, submitted to Two Thousand, Inc., Salt Lake City, Utah (April 1970) p. 1.

(32) Andersen, A. A., "A Sampler for Respiratory Health Hazard Assessment", *AIHA Journal*, Vol. 27 (March-April 1966) pp. 160-165.

(33) Welding Data Book, *op. cit*., p. A/79.

(34) Rose, *op. cit*., p. 412.

(35) Cadle, Richard D., *Particle Size*, Reinhold Publishing Corporation, New York (1965) pp. 20-22.

(36) Freund, John E. and Williams, Frank J., *Modern Business Statistics*, Prentice-Hall, Englewood Cliffs, New Jersey (1958) pp. 60 ff.

(37) *Ibid*., p. 62.

(38) *Ibid*., pp. 66-68.

(39) Vomela, R. A. and Whitby, K. T., "The Charging and Mobility of Chain Aggregate Smoke Particles", *Journal of Colloid and Interface Science*, Vol. 25, No. 4 (December 1967) pp. 568-576.

APPENDICES

APPENDIX A	Selected Bibliography of Readings Concerning Electric Arc Discharges
APPENDIX B	Developmental Background of the Tungsten Electrode Holder
APPENDIX C	Operating Procedure for Arc Aerosol Generator
APPENDIX D	Electron Microscope Particle Count Raw Data
APPENDIX E	Statistical Calculations

APPENDIX A

Selected Bibliography of Readings Concerning Electric Arc Discharges

Aidala, Joseph B., "Electric Heating", in Chemical Engineers' Handbook, Robert H. Perry *et. al.*, eds., McGraw-Hill Book Co., New York (1963) pp. 25-41--25-42.

Fleming, John Ambrose, "Electric Lighting", in Encyclopaedia Britannica, 11th ed., vol. 16, Encyclopaedia Britannica Inc., New York (1910) pp. 659-666.

Jackson, Clarence E., "Welding", in Encyclopedia Americana, vol. 28, Americana Corp., New York (1969) pp. 599-603.

Rose, David John, "Conduction [of Electricity] in Gases", in Encyclopedia Britannica, vol. 8, Encyclopedia Britannica Inc., Chicago (1970) pp. 206-208.

Thomson, Joseph John, "Electric Conduction", in Encyclopaedia Britannica, 11th ed., vol. 6, Encyclopaedia Britannica Inc., New York (1910) pp. 884-887.

Udin, Harry, Funk, Edward R. and Wulff, John, Welding for Engineers, John Wiley and Sons Inc., New York (1954) pp. 114-115 and 136-169.

APPENDIX B

Developmental Configurations of the Arc Chamber and Electrode Holder Apparatus

Thoughts of utilizing an electric arc to create large, reproducible quantities of ultra-fine particles was precipitated by the author's experience with various welding and arc-cutting techniques, and knowledge of the characteristics of the resulting process emissions. Tungsten inert gas (TIG) welding techniques were first developed in the 1930's and have been refined for primary use in the aircraft industry for welding magnesium and aluminum. A refractory, "non-consumable", tungsten electrode is used to initiate an arc between the base metal and itself, and filler wire is manually fed into the molten puddle. Helium and/or argon is directed at the weld area to reduce oxidation of the tungsten electrode and molten metal in the weld. Tungsten arcs are also used as a heat source for cutting of metals. Another relatively recent development in the welding industry is the metal inert gas (MIG) process. It was not until 1948 that the first consumable electrode welding equipment was patented. This technique has now seen wide use in both automatic and semiautomatic applications.

The electric arc aerosol generator apparatus discussed in this report is a combination of equipment from these two welding processes. An automatic wire feed and torch assembly is used to feed consumable wire into an arc established between itself and a tungsten electrode using the constant potential MIG welder to supply the electromotive force. In order to establish the feasibility of proceeding with the design of a semi-continuous model, several preliminary arrangements were tried.

Figure B-1, pictorially illustrates, in a simplified manner, the evolutionary configurations investigated which lead to the design and construction of the arc chamber and electrode holder used to produce the results reported in this paper. Configuration I utilized a standard, rack mounted consumable electrode welding head and feed motor assembly (the same units used in the final configuration) to direct the wire at the tip of a one-eighth inch diameter tungsten electrode. The tungsten electrode was held in place be a compression-type, one-eighth inch brass tubing fitting (Swagelok[1] Part No. 200-1-2) bored through to allow the electrode to slide in and out of the chamber. By tightening and loosening the compression nut, the fitting acts as a chuck to lock the electrode in position. The pipe thread end of the fitting was place in a tapped hole in the arc chamber on the same centerline axis as the wire torch. The electrical hookup was greatly simplified as the tungsten electrode was placed at negative potential and the whole arc chamber could be safely and easily grounded. On the other side, passage of the wire torch through the chamber wall had to be insulated.

This configuration met with only limited success as the rate of tungsten melting and erosion was excessive, and continuous operation was limited to a maximum of thirty seconds. Two changes

---

[1] "Swagelok" fittings are manufactured by Crawford Fitting Company, Solon, Ohio 44139.

Figure B-1. Simplified sketches showing developmental configurations of the tungsten electrode-arc chamber apparatus

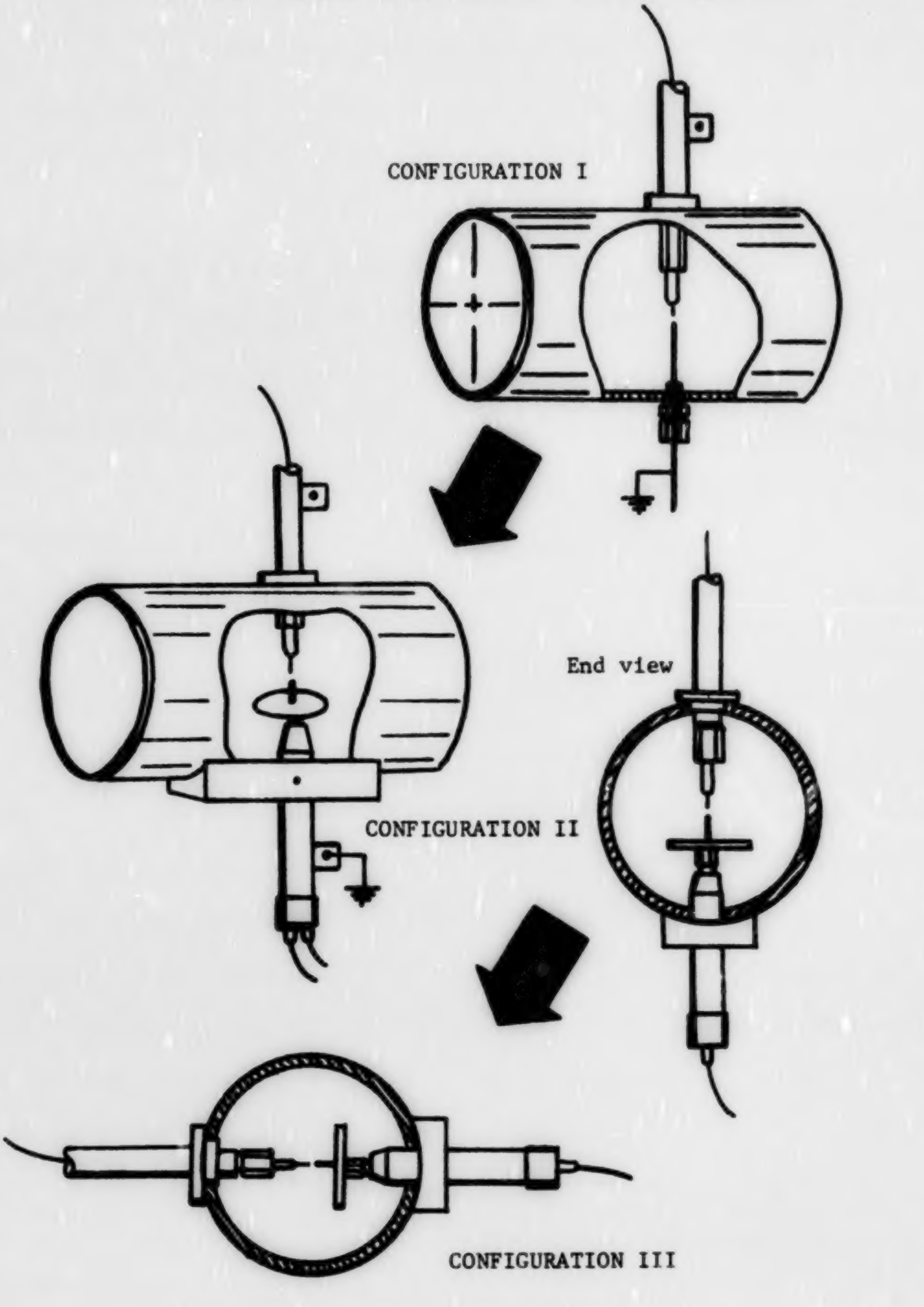
CONFIGURATION I
End view
CONFIGURATION II
CONFIGURATION III

were deemed appropriate to retard erosion and thereby increase operation time: (1) increase electrode diameter, and (2) supply a water-cooled electrode holder to dissipate heat.

Configuration II used the same wire torch arrangement, but the non-consumable electrode was increased in size to 0.25 inches in diameter and placed in a specifically constructed water-cooled holder. The holder was fabricated from an eight inch length of one inch standard pipe with a steel plug welded in one end. The plug was threaded and held a compression-type, stainless steel tubing fitting (Swangelok Part No. 400-1-316), again bored through to act as a water tight chuck to hold the tungsten electrode. The other end of the holder contained inlet and outlet fittings for the cooling water supply. An aluminum electrode holder mounting block was machined to fit the curvature of the chamber and bolted in place in such a manner as to locate the electrode centerline on the same axis as the consumable wire centerline. The holder was held in place by a set screw.

This configuration operated satisfactorily for up to two minutes before the build-up of molten wire and tungsten on the compression fitting forced a shut down. After melting one of the stainless steel fittings beyond use, a replaceable steel disc was placed over the end of the protruding electrode, as shown in Figure B-1, Configuration II, to protect the fitting and holder body from arc splatter and molten build-up. This addition did little to increase length of operation, as the same problem of build-up of molten metal recurred, this time on the disc protecting the holder.

To eliminate the problem of molten metal build-up it became obvious the arc chamber and its attachments could be rotated 90 degrees allowing the molten metal droplets to fall harmlessly to the bottom of the chamber. This change in orientation required substantial changes in the chamber mounts and fabrication of a special insulated mounting system for the feed motor and wire spool. The arrangement has been denoted Configuration III in Figure B-1.

With this change, length of operation was doubled, but this only meant continuous operation for a maximum of four minutes. It became apparent the limiting factor was excessive tungsten melting and erosion. Therefore, to increase endurance, a holder had to be designed to allow advancement of the electrode into the arc to compensate for melting and maintain uniform erosion. A water-cooled holder was finally designed and fabricated which satisfactorily incorporated these features. This unit, shown in Figure 4, was used successfully to obtain the results of this report.

APPENDIX C

Operating procedure for Arc Aerosol Generator

1. Assemble apparatus as shown in Figures 3, 5 and 6, omitting inlet duct.
2. Insert assembled cathode holder into arc chamber mounting block to blue line on holder and tighten set screws.
3. Place heat shield over end of cathode holder and tighten set screw by inserting allen wrench through view window opening.
4. Install shielding gas nozzle through view window opening.
5. Advance cathode by turning knob until tip is centered in gas nozzle outlet. Refer to Figure C-1.
6. Make electrical, shielding gas and water supply connections.
7. Turn on power to Control Panel only.
8. Set WIRE SPEED control dial to desired setting. (Refer to Figure C-2 for calibration curve for 0.045 inch diameter wire).
9. Clip off approximately 1/2 inch from protuding wire to remove any oxidized metal.
10. Place WIRE FEED switch in DOWN position.
11. Press INCH button until wire (anode) protrudes approximately 1/2 inch (12.7 mm) from torch tip. (See Figure C-1).
12. Adjust arc chamber on its slide mounts until gap between anode and cathode is approximately 1/8 inch (3.175 mm) and tighten hold down screws. (See Figure C-1).
13. Spray interior of arc chamber with welding splatter anti-stick spray.
14. Install inlet duct.
15. Close view window and secure with tape.
16. Turn on exhaust fan switch.
17. Turn on main power switch at buss and press START button on power supply.

18. Adjust VOLTAGE control dial on control panel to desired open circuit voltage. Voltage is read on power supply voltmeter.

19. Open valve on shielding gas tank.

20. Depress PURGE button on control panel and adjust gas flow to desired rate. Release button.

21. Turn on power to air blower (low speed) and water pump.

22. Depress PURGE button approximately one second and immediately press START button on control panel to initiate arc.

23. For continuous operation while conducting tests, manually turn feed screw on cathode holder to maintain tungsten tip centered in the axis of the shielding gas nozzle outlet.

24. To cease operating, place WIRE FEED switch in OFF position.

25. Press STOP button on power supply.

26. Allow shielding gas and cooling water to flow approximately 5 seconds for each 10 amperes of current flow, e.g. for a current flow of 150 amperes, flows should continue for 70 seconds after the arc is extinguished. Alternately, allow cooling water and air to circulate until air temperature immediately downstream from arc chamber cools to 100°F (38°C).

27. Press STOP button on Control Panel.

28. Close valve on shielding gas tank to conserve gas.

29. Turn off all power.

Figure C-1. Simplified cross-sectional, plan view sketch showing location of components inside arc chamber

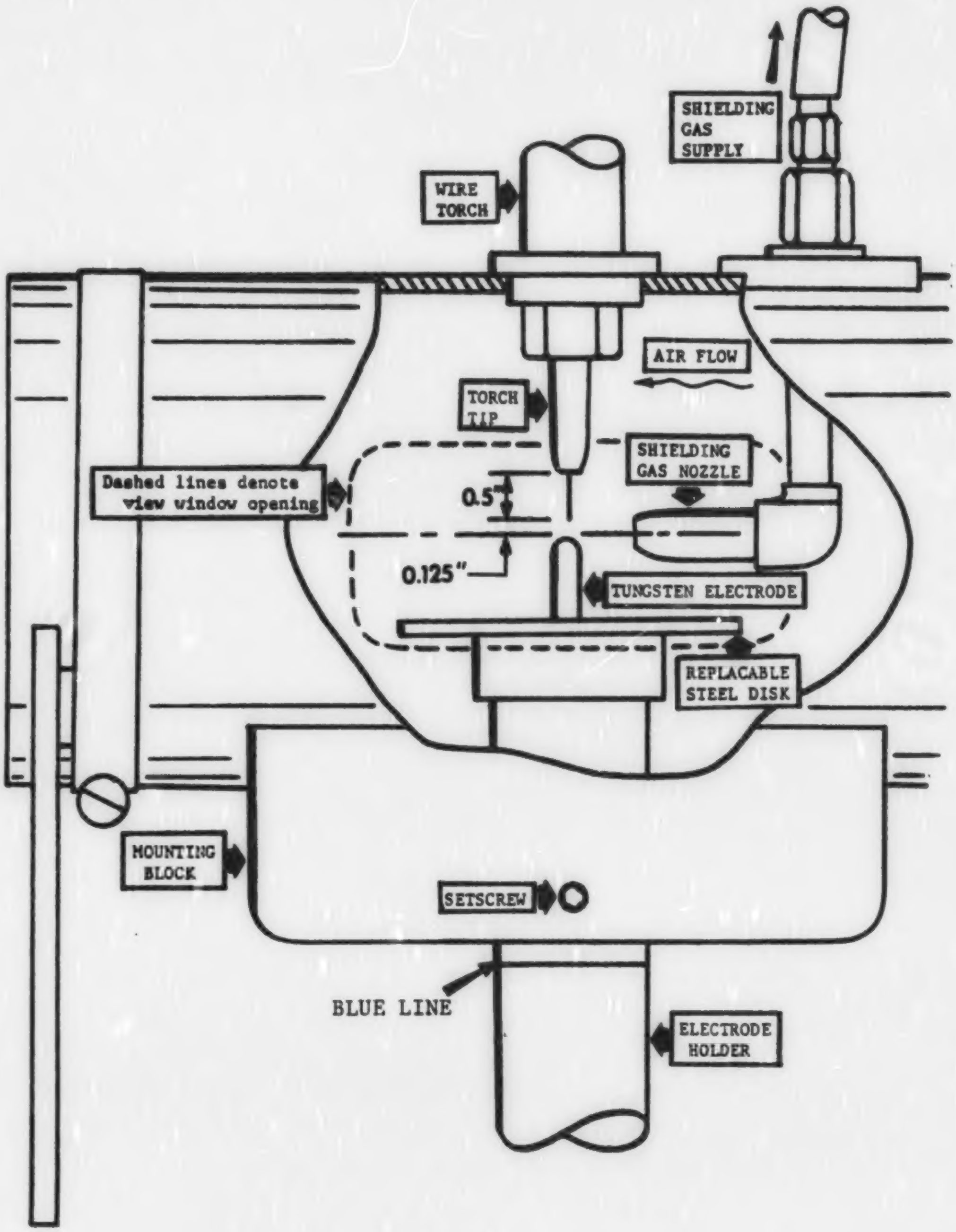
SHIELDING GAS SUPPLY
WIRE TORCH
AIR FLOW
TORCH TIP
SHIELDING GAS NOZZLE
Dashed lines denote view window opening
0.5"
0.125"
TUNGSTEN ELECTRODE
REPLACABLE STEEL DISK
MOUNTING BLOCK
SETSCREW
BLUE LINE
ELECTRODE HOLDER

Figure C-2. Calibration curve of wire speed dial versus wire speed of 0.045 inch diameter wire

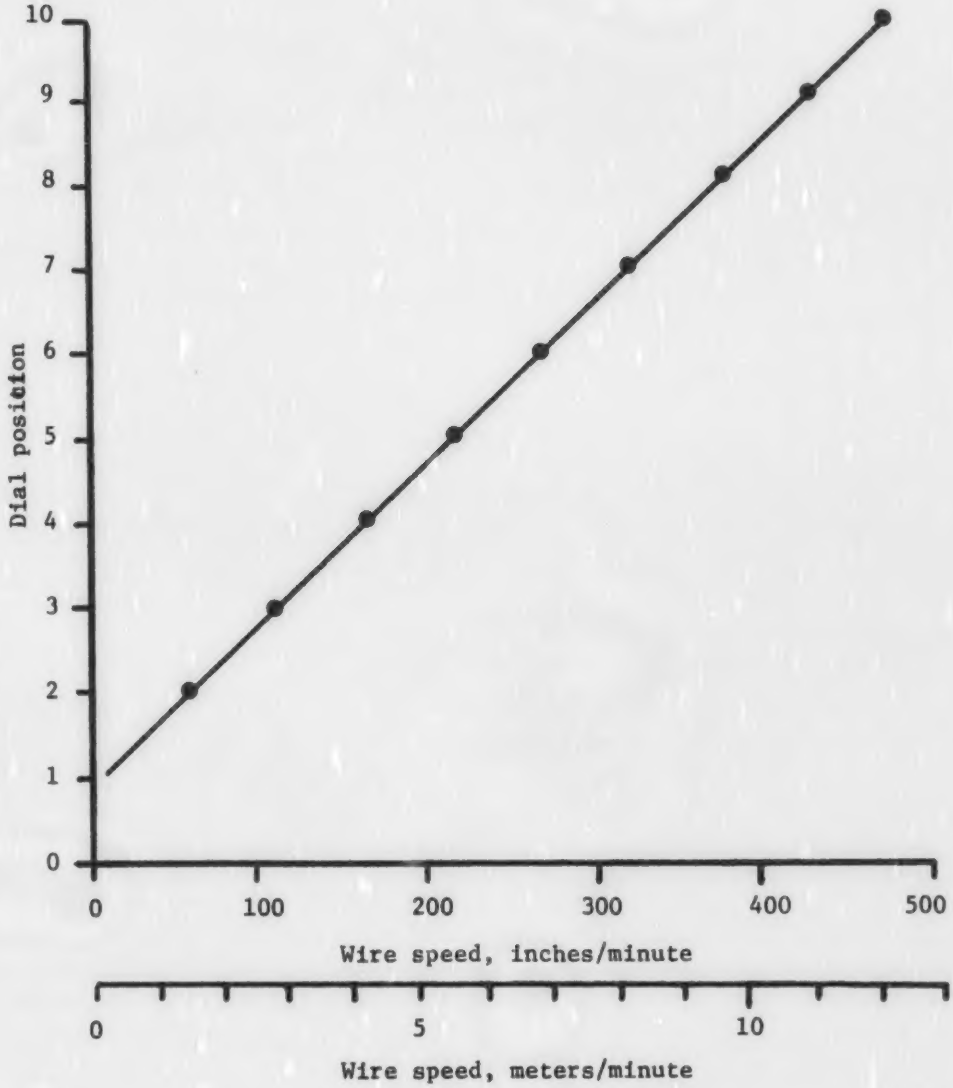

APPENDIX D

Table D-1. Electron microscope particle count raw data

STAGE	FIELD	Particle size, micrometers										TOTAL
		0.005-0.015	0.015-0.025	0.025-0.035	0.035-0.045	0.045-0.055	0.055-0.065	0.065-0.075	0.075-0.085	0.085-0.095	0.095 and >	
0	a	172	85	44	30	24	5	4	5	0	3	372
	b	232	112	65	33	14	16	9	7	1	4	493
	c	118	51	44	24	13	3	4	3	0	2	262
1	a	153	82	68	24	10	8	3	2	1	3	354
	b	111	63	46	9	19	8	8	0	1	2	267
	c	87	38	31	23	8	5	1	1	0	2	196
2	a	180	71	28	18	5	5	4	2	0	2	315
	b	391	97	89	50	20	10	6	1	1	3	668
	c	138	81	44	23	21	12	2	0	1	0	322
3	a	88	58	49	19	10	5	3	1	2	0	235
	b	132	18	22	15	2	2	3	2	3	1	200
	c	211	88	52	22	24	12	3	4	0	0	416
4	a	223	118	106	48	23	8	5	3	0	5	539
	b	281	148	84	57	15	17	5	3	3	7	620
	c	269	153	118	52	18	14	3	4	2	4	637
5	a	332	179	123	30	24	15	17	2	1	3	726
	b	131	36	29	15	9	6	3	1	2	5	237
	c	129	70	58	23	14	12	9	1	0	0	316

Table D-1 (continued). Electron microscope particle count raw data

STAGE	FIELD	Particle size, micrometers										TOTAL
		0.005–0.015	0.015–0.025	0.025–0.035	0.035–0.045	0.045–0.055	0.055–0.065	0.065–0.075	0.075–0.085	0.085–0.095	0.095 and >	
6	a	162	65	41	22	6	3	1	1	1	2	304
	b	106	49	57	18	8	4	2	0	1	2	247
	c	77	35	28	8	11	13	2	1	1	1	177
7	a	75	52	36	16	13	8	2	2	0	1	205
	b	171	84	50	25	18	8	2	6	1	3	368
	c	190	73	63	46	19	5	7	2	1	5	411
8	a	343	156	99	48	47	12	6	4	3	5	723
	b	179	77	59	19	23	6	1	1	1	0	366
	c	227	103	75	31	27	2	2	2	0	1	470
Filter	a	334	145	85	45	17	12	7	4	0	2	651
	b	157	142	81	45	38	28	11	4	5	5	516
	c	327	134	134	69	31	28	9	7	2	1	742
TOTAL		5726	2663	1908	907	531	292	144	76	34	74	12355
FIELD AVERAGE		158	89	64	30	18	9	5	3	1	2	565
STAGE AVERAGE		573	266	191	91	53	29	14	8	3	7	1236
RANGE		316	161	112	61	45	26	16	6	5	7	412

APPENDIX E

Table E-1. Transformation for calculating the arithmetic mean and standard deviation from data of Table 4

Class mark d_i	frequency f	u	uf	u^2f
0.01	5726	-1	-5726	5726
0.02	2663	0	0	0
0.03	1908	1	1908	1908
0.04	907	2	1814	3628
0.05	531	3	1593	4779
0.06	292	4	1168	4672
0.07	144	5	720	3600
0.08	76	6	456	2736
0.09	34	7	238	1666
0.10	74	8	592	4336
	n=12,355		Σ2763	Σ33,451

APPENDIX E

Table E-2. Tabulation for calculating median an geometric mean from data of Table 4

Class boundaries		Class mark		frequency	Cumulative frequency	
L	U	x_i	$\log x_i$	f		$-\log x_i(f)$
.005	.015	0.01	$\bar{2}.00000$	5726	5726	11452.0
.015	.025	0.02	$\bar{2}.30103$	2663	8389	6127.6
.025	.035	0.03	$\bar{2}.47712$	1908	10297	4726.3
.035	.045	0.04	$\bar{2}.60206$	907	11204	2360.1
.045	.055	0.05	$\bar{2}.69897$	531	11735	1433.2
.055	.065	0.06	$\bar{2}.77815$	292	12027	811.1
.065	.075	0.07	$\bar{2}.84510$	144	12171	409.7
.075	.085	0.08	$\bar{2}.90309$	76	12247	220.6
.085	.095	0.09	$\bar{2}.95424$	34	12281	100.4
.095	.105	0.10	$\bar{1}.00000$	74	12355	74.0
				n=12,355		Σ27,715.1

APPENDIX E

Table E-3. Calculation of arithmetic mean and standard deviation of the relative frequency within each particle size interval from the data of Table 5

x_i	$\bar{x}$	$x_i-\bar{x}$	$(x_i-\bar{x})^2$	s	$\frac{s}{\bar{x}}$
46.3	46.6	-0.3	0.09	3.726	0.0799
43.0		-3.6	12.96		
54.3		7.7	59.29		
50.5		3.9	15.21		
43.0		-3.6	12.96		
46.3		-0.3	0.09		
47.4		0.8	0.64		
44.3		-2.3	5.29		
48.0		2.0	4.00		
42.8		-3.8	14.44		
465.9			124.97		
22.0	21.4	0.6	0.36	1.386	0.0647
22.4		1.0	1.00		
19.1		-2.3	5.29		
19.2		-2.2	4.84		
23.3		1.9	3.61		
22.3		0.9	0.81		
20.5		-0.9	0.81		
21.2		-0.2	0.04		
21.6		0.2	0.04		
22.1		0.7	0.49		
213.7			17.29		
13.6	15.5	-1.9	3.61	1.720	0.1109
17.7		2.1	4.41		
12.3		-3.2	10.24		
14.4		-1.1	1.21		
17.1		1.6	2.56		
16.4		0.9	0.81		
17.3		1.8	3.24		
15.1		-0.4	0.16		
14.9		-0.6 0.	0.36		
15.7		0.2	0.04		
154.5			26.64		

Table E-3 (continued). Calculation of arithmetic mean and standard deviation of the relative frequency within each particle size interval from the data of Table 5

x_i	$\bar{x}$	$x_i-\bar{x}$	$(x_i-\bar{x})^2$	s	$\frac{s}{\bar{x}}$
7.7	7.2	0.5	0.25	1.146	0.1591
6.9		-0.3	0.09		
7.0		0.2	0.04		
6.6		0.6	0.36		
8.7		1.5	2.25		
5.3		-1.9	3.61		
6.6		-0.8	0.64		
8.8		1.6	2.56		
6.3		-0.9	0.81		
8.3		1.1	1.21		
72.2			11.81		
4.5	4.3	0.2	0.04	0.921	0.214
4.5		0.2	0.04		
3.5		-0.8	0.64		
4.2		-0.1	0.01		
3.1		-1.2	1.44		
3.7		-0.6	0.36		
3.4		-0.9	0.81		
5.1		0.8	0.64		
6.2		1.9	3.61		
4.5		0.2	0.04		
42.7			7.63		
2.1	2.4	-0.3	0.09	0.593	0.247
2.6		0.2	0.04		
2.1		-0.3	0.09		
2.2		-0.2	0.04		
2.2		-0.2	0.04		
2.6		0.2	0.04		
2.7		0.3	0.09		
2.1		-0.3	0.09		
1.3		-1.1	1.21		
3.6		1.2	1.44		
23.5			3.17		

Table E-3 (continued). Calculation of arithmetic mean and standard deviation of the relative frequency within each particle size interval from the data of Table 5

x_i	$\bar{x}$	$x_i-\bar{x}$	$(x_i-\bar{x})^2$	s	$\frac{s}{\bar{x}}$
1.5	1.2	0.3	0.09	0.516	0.430
1.5		0.3	0.09		
0.9		-0.3	0.09		
1.1		-0.1	0.01		
0.7		-0.5	0.25		
2.3		1.1	1.21		
0.7		-0.5	0.25		
1.1		-0.1	0.01		
0.6		-0.6	0.36		
1.4		0.2	0.04		
11.8			2.40		
1.3	0.6	0.7	0.49	0.357	0.596
0.4		-0.2	0.04		
0.2		-0.4	0.16		
0.8		0.2	0.04		
0.6		0.0	0.00		
0.3		-0.3	0.09		
0.3		-0.3	0.09		
1.0		0.4	0.16		
0.4		-0.2	0.04		
0.8		0.2	0.04		
6.1			1.15		
0.1	0.3	-0.2	0.04	0.156	0.521
o.2		-0.1	0.01		
0.1		-0.2	0.04		
0.6		0.3	0.09		
0.3		0.0	0.00		
0.2		-0.1	0.01		
0.4		0.1	0.01		
0.2		-0.1	0.01		
0.3		0.0	0.00		
0.4		0.1	0.01		
2.8			0.22		

Table E-3 (continued). Calculation of arithmetic mean and standard deviation of the relative frequency within each particle size interval from the data of Table 5

x_i	$\bar{x}$	$x_i - \bar{x}$	$(x_i - \bar{x})^2$	s	$\frac{s}{\bar{x}}$
0.8	0.6	0.2	0.04	0.267	0.444
0.9		0.3	0.09		
0.4		-0.2	0.04		
0.1		-0.5	0.25		
0.9		0.3	0.09		
0.6		0.0	0.00		
0.7		0.1	0.01		
0.9		0.2	0.04		
0.4		-0.2	0.04		
0.4		-0.2	0.04		
6.1			0.64		
				Σ 10.788	2.867
				Mean 1.079	0.287

Table E-4. Calculation of arithmetic mean and standard deviation of the cumulative relative mass distribution data of Table 7

STAGE	x_i	$\bar{x}$	$x_i-\bar{x}$	$(x_i-\bar{x})^2$	s	$\frac{s}{\bar{x}}$
1	98.13 98.79 98.42	98.45	-0.32 0.34 -0.03	.1024 .1156 .0009	0.330	0.0033
	295.34			0.2180		
2	97.83 98.55 98.09	98.26	-0.43 0.29 -0.17	.1849 .0841 .0289	0.386	0.0039
	294.47			0.2979		
3	97.53 98.39 97.83	97.92	-0.39 0.47 -0.09	.1521 .2209 .0081	0.437	0.0044
	293.75			0.3811		
4	96.93 98.23 97.50	97.55	-0.62 0.68 -0.05	.3844 .4624 .0025	0.652	0.0066
	292.66			0.8493		
5	95.95 97.66 96.51	96.71	-0.76 0.95 -0.20	.5776 .9025 .0400	0.872	0.0090
	290.12			1.5201		
6	93.92 95.16 94.34	94.47	-0.55 0.69 -0.13	.3025 .4761 .0169	0.631	0.0066
	282.42			0.7955		
7	87.84 88.94 88.82	88.53	-0.69 0.41 0.29	.4761 .1681 .0841	0.603	0.0068
	265.60			0.7283		

Table E-4 (continued). Calculation of arithmetic mean and standard deviation of the relative mass distribution data of Table 7

STAGE	x_i	$\bar{x}$	$x_i-\bar{x}$	$(x_i-\bar{x})^2$	s	$\frac{s}{\bar{x}}$
8	75.53	77.60	-2.07	4.2849	2.188	0.0281
	79.89		2.29	5.2441		
	77.38		-0.22	.0484		
	232.80			9.5774		
F	68.77	68.96	-0.19	.0361	0.518	0.0075
	69.55		0.59	.3481		
	68.57		-0.39	.1521		
	206.89			0.5363		

APPENDIX E

Table E-5. Calculation of arithmetic mean and standard deviation of weight (mass) distribution from data of Table 8

STAGE	RUN	x_i	$\overline{x}$	$x_i-\overline{x}$	$(x_i-\overline{x})^2$	s	$\frac{s}{\overline{x}}$
0	1	2.5	2.13	0.37	0.1369	0.4496	0.2110
	2	1.5		-0.63	0.3969		
	3	2.4		0.27	0.0729		
		6.4			0.6067		
1	1	0.4	0.40	0.00	0.0000	0.0812	0.2030
	2	0.3		-0.10	0.0100		
	3	0.5		0.10	0.0100		
		1.2			0.0200		
2	1	0.4	0.33	0.07	0.0049	0.0943	0.2857
	2	0.2		-0.13	0.0169		
	3	0.4		0.07	0.0049		
		1.2			0.0267		
3	1	0.8	0.50	0.30	0.0900	0.2449	0.4898
	2	0.2		-0.30	0.0900		
	3	0.5		0.00	0.0000		
		1.5			0.1800		
4	1	1.3	1.17	0.13	0.0169	0.3398	0.2904
	2	0.7		-0.47	0.2209		
	3	1.5		0.33	0.1089		
		3.5			0.3467		
5	1	2.7	3.03	-0.33	0.1089	0.2493	0.0822
	2	3.1		0.07	0.0049		
	3	3.3		0.27	0.0729		
		9.1			0.1867		
6	1	8.1	8.07	0.03	0.0009	0.2867	0.0355
	2	7.7		-0.37	0.1369		
	3	8.4		0.33	0.1089		
		24.2			0.2467		

Table E-5 (continued). Calculation of arithmetic mean and standard deviation of weight (mass) distribution from data of Table 8

STAGE	RUN	x_i	$\bar{x}$	$x_i-\bar{x}$	$(x_i-\bar{x})^2$	s	$\frac{s}{\bar{x}}$
7	1	16.4	15.00	1.4	1.9600	2.7178	0.1561
	2	11.2		-3.8	14.4400		
	3	17.4		2.4	5.7600		
		45.0			22.1600		
8	1	9.0	11.73	-2.73	7.4529	1.9482	0.1660
	2	12.8		1.07	1.1449		
	3	13.4		1.67	2.7889		
		35.2			11.3867		
F	1	91.6	93.70	-2.10	4.4100	7.2171	0.0770
	2	86.1		-7.60	57.7600		
	3	103.4		9.70	94.0900		
		281.1			156.2600		
TOTALS	1	133.2	136.00	-2.80	7.8400	(14.4202)	(0.1060)
	2	123.8		-12.20	148.8400		
	3	152.1		16.1	259.2100		
		409.1			415.8900		
					Σ	13.6289	1.9967
					Mean	1.3629	0.1997

VERY FINE PARTICLE
GENERATION BY ELECTRIC ARC:
SAMPLING AND ANALYSIS

PROBLEM

Submitted to the Graduate School
of
West Virginia University
In Partial Fulfillment of the Requirements for
the Degree of Master of Science in Engineering

by

Mike Naylor, B. S.

Morgantown,
West Virginia

1976

ABSTRACT

Established methods of generating useful reproducible concentrations of very fine particles for use in research possess various limitations. The development of an improved electric arc metal generating method used a new apparatus: a commercial electric arc metallizer. It is capable of generating very fine particles of the metals available in the form of metallizing or welding wire. The generation, sampling and analysis of zinc oxide particles are examined.

In addition to studying the effects of changing the arc metallizer's operating variables of air spray pressure and rate of wire consumption, the reproducibilities of total mass concentration and distribution of particle diameters were tested.

Particles were examined on Nuclepore 0.2 μm membrane filters by electron microscopy and electron diffraction. Particles were counted by diameter. Two replicate samples for each of three arc metallizer operating conditions were analyzed. One condition is not reproducible with respect to the mean diameter of sampled particles. The other two conditions are reproducible with respect to diameter means and variance. One of these conditions also has particle diameter distributions that are shown not significantly different. The mean diameters of the conditions are significantly different, indicating that by changing the air spray pressure and wirefeed rate, the particle diameters are changed.

The diameters of the particles generated at specific conditions

are distributed approximately normally. Mean diameters range from 6 to 11 nm (0.006 to 0.011 μm).

Virtually all of the very fine particles agglomerated, forming interconnecting chains. This phenomena apparently resulted from combined effects of the very fine particle diameters and the large initial concentration of the particles.

Mass concentrations were measured with Millipore 0.45 μm membrane filters. Four different operating conditions were defined, with three of them being the same as the ones used for particle sizing. These yield mean mass concentrations ranging from 0.65 to 2.0 gram/m^3.

For three of these conditions, the replicate mass concentration coefficient of variation (C.V.) is less than 9%. The fourth has a C.V. of 19%. This is the same condition for which the particle diameter means are not reproducible. The mass concentrations generated at different conditions are found significantly different by testing. The mass concentration is increased by increasing the air spray pressure or the rate of wirefeed or both.

Since the influence of the operating conditions has been demonstrated as well as varying levels of reproducibility for each condition, this metallizer is considered worthy of continued development and potential utilization by researchers as a device for generating very fine particles.

ACKNOWLEDGEMENTS

The investigator is grateful to his graduate advisor, Professor Benjamin Linsky, who introduced him to the topic of fine particle generation. He offered suggestions and encouragement in preparing for and writing this report.

For their research assistance, appreciation is extended to Dr. D. R. Sears, then Director of the Air Pollution Laboratories at WVU, and to graduate students, John Garbak, Don Stone and Fred Dimmick. The investigator thanks Fran Culler of the Civil Engineering Laboratory and Don Garletts of the Mechanical Engineering Laboratory for fabricating equipment parts.

The investigator acknowledges the suggestions from Charles Ghastin and Ed Morantz, sales representative for and developer of, respectively,the Wall Colmonoy electrospray metallizer.

The investigator expresses thanks to Richard Shimps of McCrone Associates for his advice on obtaining appropriate samples for electron microscopy.

The investigator appreciates the critical review of the statistical analysis by Dr. E. Z. Damewood of the Industrial Engineering Department at W.V.U.

Several types of financial assistance made this research possible. The metallizer and electron microscopy services were funded by Environmental Protection Agency Research grant R-801858-01-1, which was administered by Dennis Drehmel. The investigator received a study traineeship from EPA grant T-900487-10-0 and tuition compensation for one semester from the Civil Engineering Department at WVU.

TABLE OF CONTENTS

ABSTRACT 2-ii

ACKNOWLEDGEMENTS 2-iv

LIST OF FIGURES 2-viii

LIST OF TABLES 2-ix

CONVERSION FACTORS, EQUIVALENTS, AND ABBREVIATIONS 2-x

I. INTRODUCTION 2-1

II. REVIEW OF LITERATURE 2-3

III. EXPERIMENTAL 2-6

A. GENERATION 2-6

B. SAMPLING 2-7

1) General Considerations 2-7

2) Description of Sampling Components 2-11

3) Filters 2-12

4) Calculation of Nucleopore Efficiency 2-15

5) Sampling Procedure for Mass Concentration 2-16

6) Sampling Procedure for Electron Microscopy 2-21

7) Sensitivity of Results to Deviations from Isovelocity Sampling 2-22

C. ANALYTICAL TECHNIQUES 2-24

1) Mass Concentration Analytical Techniques 2-24

2) Particle Sizing and Identification Techniques . . 2-25

D. SELECTION OF EQUIPMENT OPERATING CONDITIONS FOR SAMPLING 2-26

IV. RESULTS 2-28

A. BRIEF EVALUATION OF EQUIPMENT OPERATION 2-28

B. SAMPLE NUMBER IDENTIFICATION 2-29

Page

1) Mass Concentration 29

2) Electron Microscopy and Electron Diffraction . . . 29

C. CHEMICAL COMPOSITION 29

1) Electron Diffraction Data 29

2) Assay of Wire 30

D. MASS CONCENTRATION 31

1) Means Testing 32

2) Analysis of Variance 32

E. PARTICLE SIZING BASED ON ELECTRON MICROSCOPY 33

1) Analysis 36

2) Computation of Means and Variances 36

3) Reproducibility Among Replicates 37

4) Differences Between Conditions 37

5) Frequency Distributions 38

i) Computation of Normal Distribution 47

ii) Goodness of Fit 47

F. AGGLOMERATION 48

G. COMPARISON WITH HEDDEN'S RESULTS 50

V. A. CONCLUSIONS 52

RECOMMENDATIONS 53

VI. LIST OF REFERENCES 56

VII. APPENDICES

Appendix A A-1

Appendix B B-1

Appendix C C-1

Page

Appendix D 2-D-1

Appendix E 2-E-1

Appendix F 2-F-1

Appendix G 2-G-1

Appendix H 2-H-1

LIST OF FIGURES

Figure		Page
1	Layout of Equipment	2-8
2	Schematic of EPA-RAC Sampling Train	2-9
3	Actual Stack Sampling Flow System	2-10
4	Schematic of Sampling Point and Venturi Meter	2-13
5	Exhaust Flow Versus Venturi Pressure Drop	2-14
6	Approximate Relationships of Sampling Nozzle	2-18
7	Typical Form for Mass Concentration Data	2-19
8	Plot of Line of Equal Bias as Function of R and K . .	2-23
9	Comparison of Cumulative Frequencies for Condition 2	2-41
10	Comparison of Cumulative Frequencies for Condition 3	2-42
11	Observed Frequency of Sample 134 and Normal Frequency	2-43
12	Observed Frequency of Sample 133 and Normal Frequency	2-44
13	Arithmetic Probability Plot of Sample 128 Diameters .	2-45
14	Log Probability Plot of Sample 128 Diameters	2-46
H-1	SEM Photograph of Sample 133 (5000 X)	2-H-2
H-2	SEM Photograph of Sample 133 (10,000 X)	2-H-2
H-3	TEM Photograph of Sample 101 (300,000 X)	2-H-3

LIST OF TABLES

Table		Page
1	Summary of Nuclepore Impaction, Interception, Diffusion and Total Collection Efficiencies	2-16
2	Summary of Possible Sampling Bias	2-23
3	Zinc Wire Sampling Conditions	2-27
4	Identification of Mass Concentration Samples	2-29
5	Identification of McCrone Samples	2-29
6	Electron Diffraction Data-Sample 104	2-30
7	Diffraction Data -- Sample 133	2-30
8	Standardized Zinc Oxide Mass Concentrations for All Samples	2-31
9A	Zinc Oxide Mass Concentration Mean and Variation Summary	2-31
9B	Mean Mass Concentration Matrix	2-32
10A	Zinc Oxide Particle Size Data	2-34
10B	Zinc Oxide Particle Size Data	2-35
11	Means and Variances of Zinc Oxide Particle Size Data .	2-37
12	Cumulative Observed and Expected Frequencies for Condition 2	2-39
13	Cumulative Observed and Expected Frequencies for Condition 3	2-40
14	Hedden-Naylor Data	2-50

CONVERSION FACTORS, EQUIVALENTS AND ABBREVIATIONS

acfm = actual cubic feet per minute

acmm = actual cubic meters per minute

$^{o}C = (^{o}F - 32)/1.8$

1 cm = 0.03281 ft.

cm/sec = 1.97 fpm

1 cubic meter (m^3) = 35.315 cubic feet (ft^3)

g/acf = gram/actual cubic feet

g/sm^3 = gram /standard cubic meter

1 grain = 0.0648 gram

1 grain = 1/7000 pound

grain/acf = grains/actual cubic foot

2.29 grains/scf = 1.00 g/sm^3

HEPA = high efficiency particulate air

mg/acf = milligrams/actual cubic foot

1 nm = 1×10^{-3} μm = 1×10^{-7} cm

SAED = selected area electron diffraction

SEM = scanning electron microscopy

scfm = standard cubic feet/minute

sm^3 = standard cubic meters

TEM = transmission electron microscopy

μm = 1×10^{-4} cm = 10^{+3} nm

INTRODUCTION

This report examines a method of producing in the laboratory reproducible concentrations of freshly made very small, metal oxide particles. The method represents a continuation of a long range project of the Air Pollution Engineering Laboratory, the goal of which is to develop a valid research tool to generate very fine freshly made particles for extended periods of time and to characterize these particles. The results of this project are applicable to the fields of respiratory, control equipment, instrument design, vegetation and cloud physics research.

The particle generator simulates general industrial electric arc processes. The concentrations of particles generated may be typical of those to which workmen are exposed.

A commercially available electric arc metallizer has been found that is potentially capable of delivering reproducible very small particles evolved from at least a dozen different metals. Metals in wire form are utilized by the machine as cousumable electrodes. "The wire passes through the high heat zone of the arc, becoming molten. Air pressure then sprays the molten particles onto the surface being coated."(1)

The process evolves metal vapor at high temperatures, which cools in an air stream and condenses into very fine particles commonly called metallurgical smoke or fresh metal fume. The nucleation of vapor is facilitated by the intense concentration of ions produced around the arc. Most of the original particles are believed to be formed by condensation on ions rather than by self nucleation.(2)

The unit particles are electrically charged. The complexes consist of long chains, frequently of hundreds of fine particles, most of which are too small to be resolved by the optical microscope so that electron microscopy must be used to observe their structure and form; electron diffraction shows the composition and nature of their surface regions more sensitively than Xray diffraction.(2)

The particles generated were analyzed for mass concentration and characterization, and distribution of sizes.

A problem report describing the historical development of the equipment in this project is presently being written by Don Stone.

REVIEW OF LITERATURE

The entire subject area of very fine particles is growing rapidly. Those working in the field know that the published literature has fallen far behind the real developments. This was clearly depicted during the Aerosol Measurement Workshop at Gainesville, Florida, in March 1976.

This literature review covers a few topics relating to very fine particle generation, sampling and analysis.

For years, Professor Linsky has pushed for recognition of small particles in air pollution separate from total emitted particulates. In 1958, he presented a paper explaining the need for such a listing by particles sizes in an emissions inventory.(3) He has also pointed out the lack of acceptable methods for producing fine fresh metal particles as distinguished from "stale particles."

Robert Hedden(4) developed a series of modifications of generators of very fine particles that utilized an electric arc welder with a consumable wire feedstock as an anode and a relatively nonconsumable tungsten cathode.

Hedden's literature review, which was not comprehensive, discussed the following limitations in particle generation to date (1972).

1) The homogeneous aerosol generators yield concentrations that are too dilute for air pollution control device research and development.

2) Higher concentrations can be achieved by redispersing large quantities of previously produced and collected powder but these particles lack the quality being "fresh" and are agglomerated.

3) Direct attrition methods -- friction, evaporation, impact, explosion and combustion approach the situations in the industrial environments but do not generally achieve particles smaller than one micrometer. Submicrometer ranges available are not reproducible due to control of feedstock and input energy.

4) Electric arc generators have been used previously but particle characterization was given little consideration

5) Finally, a high voltage continuous discharge method lacks the features of high concentration and runs lasting an hour or more.(4)

Hedden's equipment provided data which established reproducibility of mass concentration. For a particular set of operating conditions he indicated an average concentration of 0.65 gram/sm^3 (1.49 grain/scf) at standard conditions of 25°C and 760 mm. He also studied particles collected on one filter by electron microscopy. Due to limitations of time and money, he was not able to investigate the reproducibility of particle diameter sizes by count nor the influence of operating parameters on mass concentration and particle size. He used a carbon steel welding wire. Runs were limited to 30 minutes as the tungsten electrode would be consumed by that time.

Due to limited facilities, Hedden prepared the samples collected on membrane filters for electron microscopy analysis by dispersing the particles on a suitable grid. The dispersion probably altered agglomeration characteristics.

A major revision of Hedden's modifications was developed in 1973-74 by Hedden, Professor Linsky, Dr. William H. Fischer, Arland Johansen, Michael McCawley, Rasool Nekooi, and Dr. Sears.(5) The revised apparatus was an electric welder which used two consumable wires instead of one. This machine suffered stability problems due to inadequate control of the wires meeting and forming an arc. Gaps of greater than ½ inch resulted in unstable runs.(5) Mass concentrations were measured for varying voltage and rates of wire feed but, due to equipment limitations, the data was insufficient to establish conclusive results.

A method was cited by Brain(6) in 1974 for producing ferric oxide by combustion of iron pentacarbonyl. He observed concentrations in an animal exposure chamber ranging from 1.00 to 4.00 g/m^3 and noticed agglomerates of particles about 0.02μm in diameter averaging 0.4 μm in average count diameter. He said the diameters of the agglomerates were distributed log normally. While he argued that the iron oxides provide excellent test particles for animal exposure, his technique was obviously limited to iron oxide.

Hedden's size analysis of iron oxide particles also indicated a log normal distribution of diameters by count. However, neither Hedden nor Brain used statistical techniques of goodness to fit tests to check whether their observed size distributions were reasonably close to the generally claimed log normal distributions.

This report examines a method of producing metal oxide particles to determine its acceptability with respect to continuous generation, influence of operating conditions and reproducibility.

EXPERIMENTAL METHODS

GENERATION

The metallizer, manufactured by Flame Spray Industries,(1) has many commercial applications. It is widely used to provide coatings on metal or to fill in and build up worn areas on shafts, etc. One use for zinc wire in a continuous production line is to replace the rust proof coating along the machined or rolled threaded ends of electrical conduit that had been galvanized before the thread cutting.

The metallizer operates in a manner similar to an electric arc welder except that the product is blown onto another piece of material that is not connected electrically to the electrodes or power supply. The consumable wires are energized by the high amperage low voltage power source forming a plasma arc through which current will flow. The heating volatilizes more wire while the compressed air upstream dissipates and directs the condensing particles. A steady state of an arc generating fine fresh metal-oxide particles is established.

The specific metallizer used in this research (Fig. 1) consists of a power source which converts 3 phase 220 volt alternating current to direct current that is variable from 0 to 40 volts and up to about 400 amps; a console on top of the power source from which air pressure, wire feed rate, and open circuit voltage are adjusted; flexible conduits which convey wire, from reels secured to the console, to a phenolic spray head that guides the wires into fixed position electrode tips. Electrical cables transfer the direct current from the power source to the wires at the spray head.

The spray head was fastened to the lid of a 55 gallon barrel, with the electrodes extending through a slot into the barrel. The arcing takes place in the barrel. The larger particles of the metallized wire are directed by the high pressure air stream to the other end of the barrel where they are deposited.

A low pressure air stream entering through a HEPA (high efficiency particulate air filter) and the dispersed compressed air convey the much smaller particles through an exhaust duct to a cloth filter collector and exhaust blower (baghouse system). The entire layout of generation, exhaust and sampling is shown in Figure 1.

The size of the deposited particles in the barrel not drawn into the exhaust stream can be approximately calculated by treating the barrel as a cyclone. As estimated by the formulas and computations in Appendix A, the barrel bottom would collect 50% by weight of the particles 7 μm in diameter and 95% by weight of those 30 μm in diameter.

SAMPLING

General Considerations

To assure the best representation of the very fine particles, sampling was done under iso-velocity conditions. The procedure followed recommendations of the EPA Method Five(7) where possible. The recommended sampling train, as interpreted by Research Appliance Company,(8) is indicated in Figure 2. This was modified as shown in Figure 3.

The membrane filter holder was seated on top of the sampling

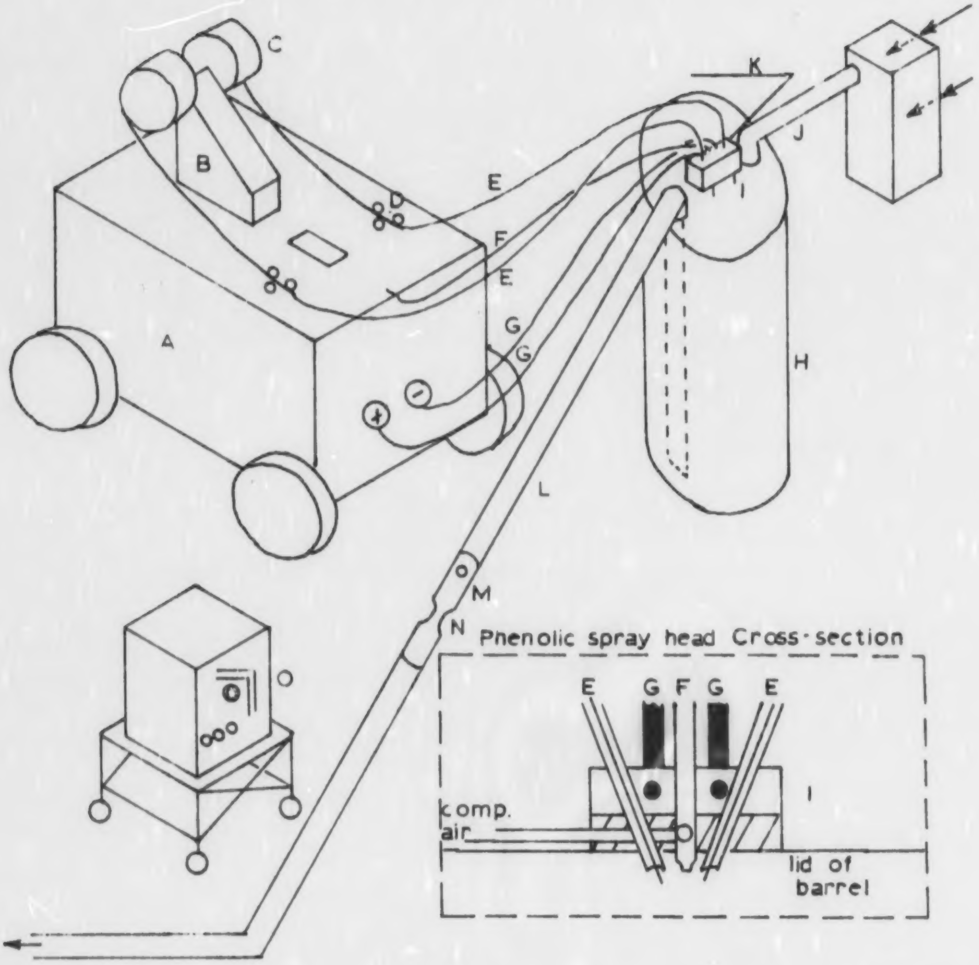
C
B
D
K
J
E
F
E
G
G
A
H
L
M
N
O
Phenolic spray head Cross-section
E
G
F
G
E
I
comp.
air
lid of
barrel

A) Power source of metallizer
B) Control console
C) Dual wire spools
D) Wire straightening, drive and conduit feed mechanism
E) Flexible conduit for wire
F) Flexible compressed air line - main air
G) High amperage electrical cable
H) 55 gallon barrel
I) Phenolic spray head
J) Dilution air from Hepa filter
K) Flexible compressed air line - secondary air
L) Exhaust duct - 6 inch diameter
M) Sampling port
N) Venturi
O) Stack sampler

Figure 1. Layout of equipment

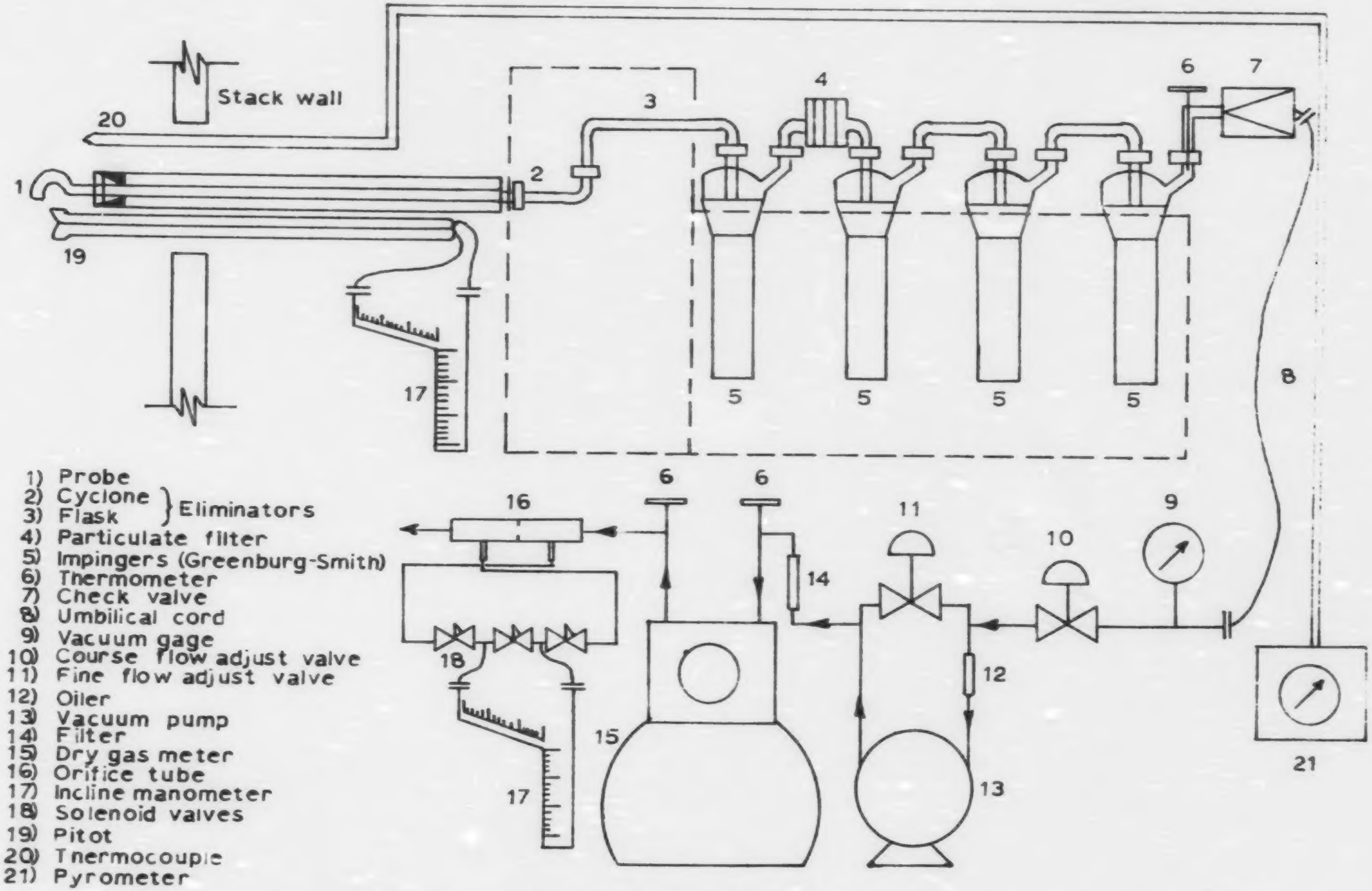
Stack wall
20
1
2
3
4
5
5
5
5
6
7
8
19
17
16
6
6
11
10
9
14
12
18
15
17
13
21
1) Probe
2) Cyclone
3) Flask
Eliminators
4) Particulate filter
5) Impingers (Greenburg-Smith)
6) Thermometer
7) Check valve
8) Umbilical cord
9) Vacuum gage
10) Course flow adjust valve
11) Fine flow adjust valve
12) Oiler
13) Vacuum pump
14) Filter
15) Dry gas meter
16) Orifice tube
17) Incline manometer
18) Solenoid valves
19) Pitot
20) Thermocouple
21) Pyrometer

Figure 2. Schematic of EPA-RAC sampling train

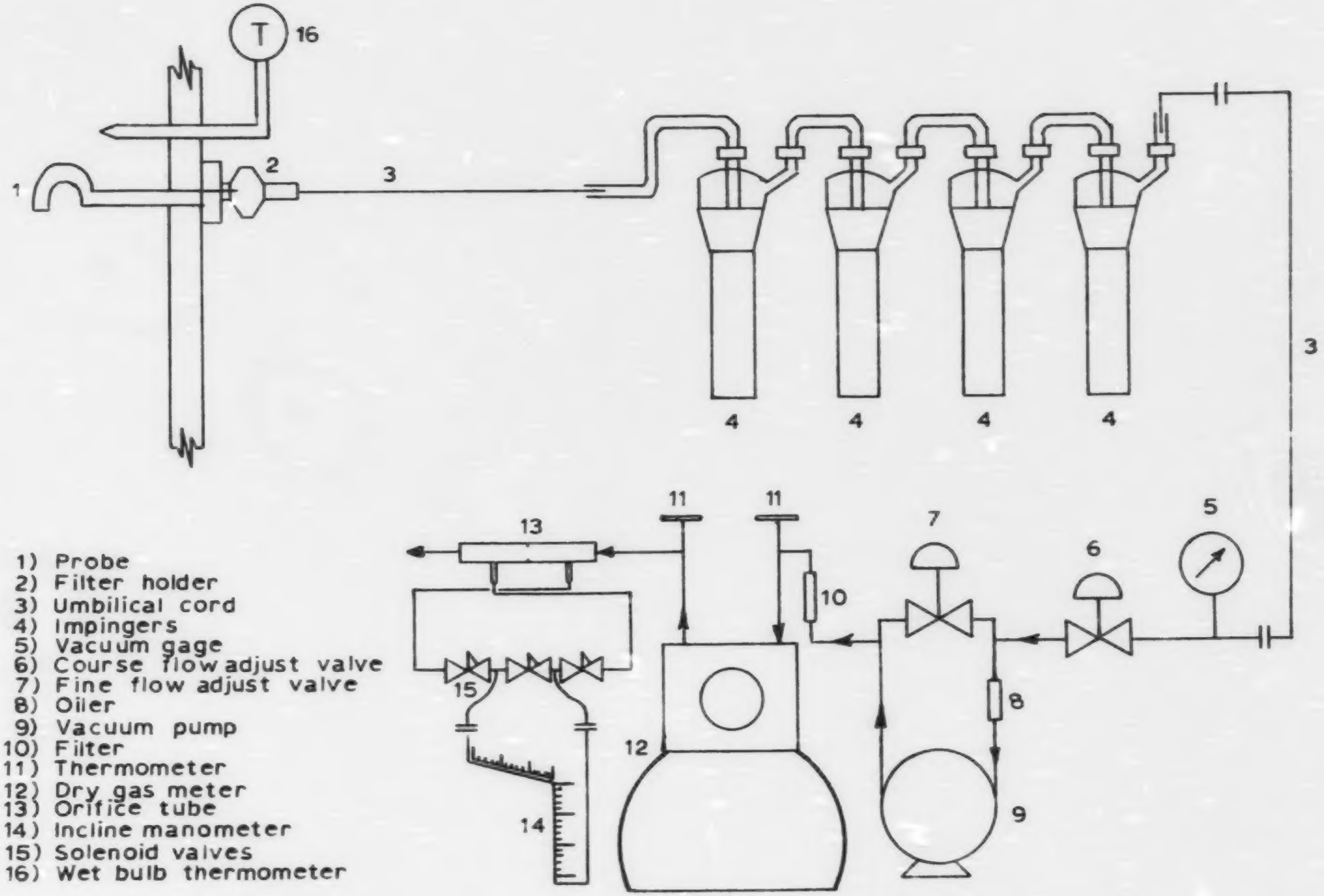
1
2
3
16
T
4
4
4
4
3
5
6
7
8
9
10
11
11
12
13
14
15
1) Probe
2) Filter holder
3) Umbilical cord
4) Impingers
5) Vacuum gage
6) Course flow adjust valve
7) Fine flow adjust valve
8) Oiler
9) Vacuum pump
10) Filter
11) Thermometer
12) Dry gas meter
13) Orifice tube
14) Incline manometer
15) Solenoid valves
16) Wet bulb thermometer

Figure 3. Actual stack sampling flow system

port, itself on top of the horizontally positioned duct. The intention was for the filter to trap all sizes of particles reaching it, differing from the arrangement in Figure 2 whereby the first impinger collects larger particles. A second difference in procedure was in the method of moisture measurement. A wet bulb thermometer was placed in the duct to determine the dew point. This was preferred to the method of monitoring the water levels in the impingers and measuring the weight gain of the silica gel impinger, as small incremental increases were anticipated.

Description of Sampling Components

The sampling train (Figure 3) consisted of the filter holder, filter cord to impingers, impingers, cord to the sampler, and the RAC stack sampler. Manometers were placed at the HEPA filter, venturi meter, and baghouse, in addition to the two contained in the sampler for monitoring orifice pressure drop and stack-velocity pressure. Also, thermometers are placed on the barrel lid near the spray head, 2 inches downstream of the sampling port, and at the baghouse.

Sampling Port. A ½ inch opening, 11 diameters from exhaust port on lid.

Probe. The S shaped straight-inlet nozzle was inserted into the air stream 1/3 diameter vertically from the port entrance.

Filter holder. The Gelman filter holder accepts 49 mm filters. The nozzle assembly is directly connected to the inlet of the holder.

Filters. Millipore filters, type HA, .45 μm pore diameter, were used to determine the mass concentrations which required collection times of several minutes. General Electric Nuclepore filters were employed for short duration particle sizing sampling. The filters are discussed further in the next sections.

Impingers. Moisture in the sampled air was removed by the series of four 1 liter impingers, chilled by an ice bath. The first two impingers each had 100 ml distilled water, the third was dry and the fourth 200 grams of dry silica gel.

RAC Stack sampler. The RAC Stack sampler Model 2343(5,6) consists of all elements downstream of the umbilical cord in Figures 2 and 3. It satisfies the specifications of the EPA Method V.(7)

Venturi Flow meter. A constriction was built into the ductwork about 5 diameters downstream from the sampling port (Figure 4). By a generally accepted stack sampling procedure,(9) velocity traverses along two perpendicular diameters at the sampling port location were tabulated as a function of the pressure drops measured by the manometer across the venturi. The velocities were averaged and corresponding flow rates were calculated. The data and calculations are presented in Appendix B. A plot of exhaust flow versus venturi pressure drop is shown in Figure 5.

Filters

Nuclepore filters (0.2 μm pore diameter) were selected for determining the distributions of particle diameters and for identifying the particles for the following reasons. Their smooth surface and better controlled pore size and frequency make them

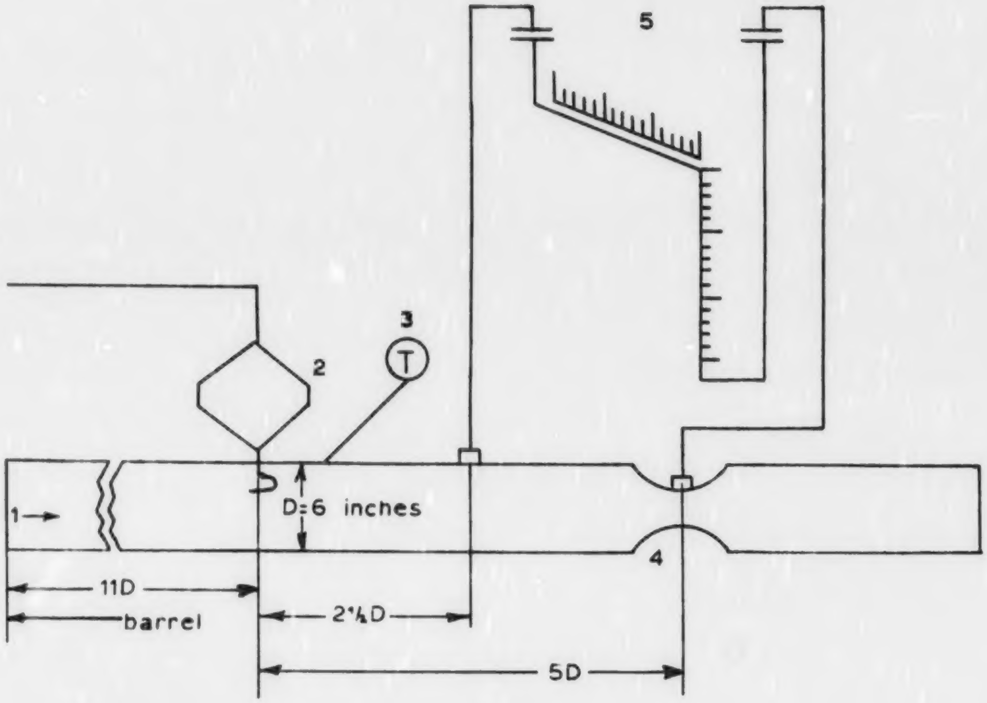
5
3
T
2
1→
D=6 inches
4
11D
barrel
2¼D
5D

1) Direction of air stream from chamber
2) Sampling nozzle and filter holder with cord to impinger
3) Thermometer
4) Venturi constriction with taps for static pressure
5) Incline manometer

Figure 4. Schematic of sampling point and venturi meter

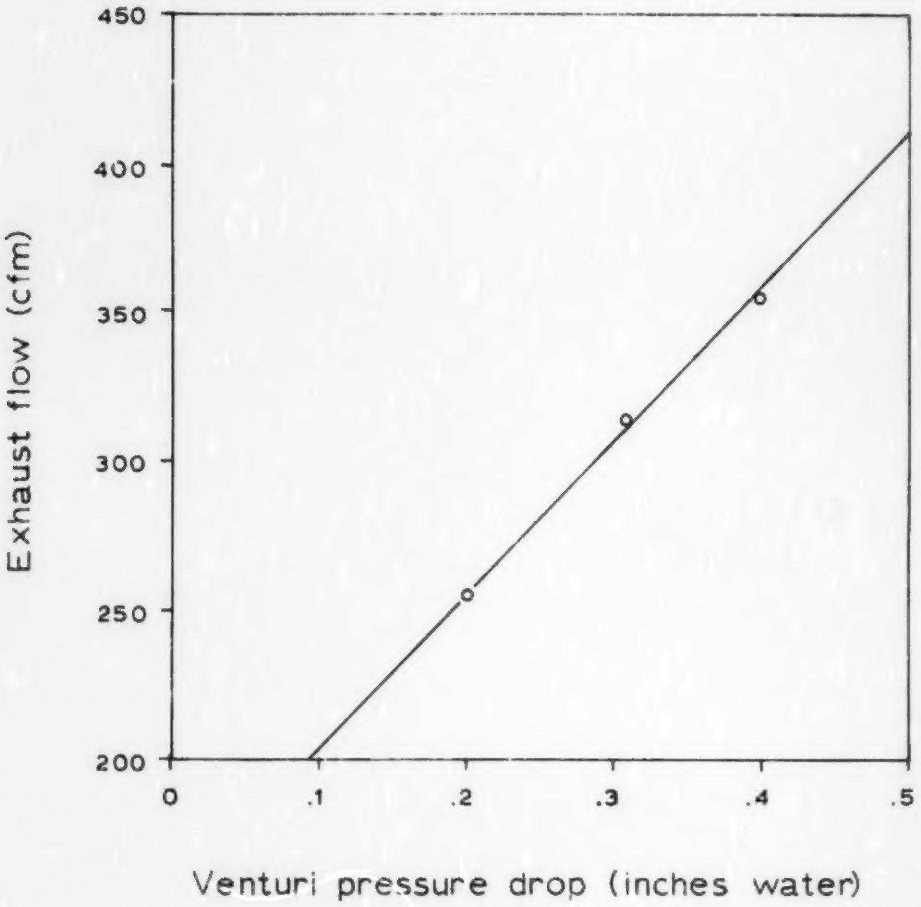

Figure 5. Exhaust flow versus venturi pressure drop

ideal for analysis by electron microscopy and electron diffraction.(10,11,12,13) The Millipore (Type HA, 0.45 μm pore diameter) filters were selected for determining the mass concentrations of the particles sampled. The Millipore filter's greater thickness (150 um) than the Nuclepore filters (12 μm) and its random fibrous structure allows the greater retention volume needed for several minutes of exposure in the particle stream.

The added advantage of the Nuclepore filters, which have simple straight through pores compared to the more "tortuous path" configuration of the Millipore membranes, is that they most closely approximate the popular model of filters used to predict particle collection efficiency.(11,12)

Calculation of Nuclepore Efficiency

One mathematical model for the study of membrane filters assumes a flat surface with equidistant parallel straight through pores. Since Nuclepore filters more closely resemble this model than other membrane filters the theory has been applied and corrected by Spurny, et. al.(14)

Three mechanisms: interception, diffusion, and impaction, contribute to the overall efficiency E_t. If the impaction efficiency is labeled as E_i, the diffusion efficiency as E_d, and the interception as E_r, then the respective efficiences are individually calculated and combined as follows:

$$E_t = E_i + E_d + 0.15\ E_r - E_i\ E_d - 0.15\ E_i\ E_r$$

In Appendix C, the individual efficiencies are defined, and appropriate values assumed are listed and efficiences are calculated. The following table summarizes the computed relationship between efficiences and particle size.

Table 1. Summary of Nuclepore Impaction, Interception, Diffusion and Total Collection Efficiencies (Pore Diam. = 0.2 μm)

Part. Dia. (μm)	E_i impact.	$.15E_r$ intercept.	E_d diffusion	E_t total
.02	.00	.00	1.00	1.00
.04	.00	.054	1.00	1.00
.10	.012	.11	1.00	1.00
.15	.028	.13	.993	1.00
.20	.05	.15	.962	1.00
.30	.447	1.00	.853	1.00

Sampling Procedure for Mass Concentration

The following steps outline the method followed by the experimenters when sampling for mass concentration. Before sampling: Measure atmospheric pressure at the equipment location. Dessicate the Millipore filters for two days and obtain tare weight to nearest 0.1 mg.

1) Equipment should be set up as in Figure 1. Metallizer has been running at a specific condition for at least two minutes and baghouse has been turned on. Millipore filter has been placed into holder.

2) Adjust flow at venturi meter. For a desired flow of 250 acfm (7.08acmm), for example, the manometer should indicate a pressure difference of 0.2 inches according to Figure 5.

3) Measure the velocity pressure of the exhaust stream at

the sampling nozzle location. Continuing the above example, this has been measured as 0.12 inches for 250 scfm. Compute stack velocity by $V_{stack} = 234\ (298 \times 0.12)^{\frac{1}{2}}\ \text{fpm} = 1400\ \text{fpm}$ (see Appendix B). Convert this to a nozzle flow yielding same velocity. Since the nozzle has an 1/8 inch diameter, with area of 0.000085 ft^2 the required nozzle flow is 0.12 scfm.

4) Make a preliminary run. Since isovelocity sampling is planned, the ratio of inlet nozzle velocity to duct velocity should be in the range of 0.9-1.1 (4). A preliminary run is necessary to check the rate of sampler pumping. Consult Figure 6 for an approximate setting for the orifice pressure drop. For .12 scfm, Δ_H(orifice) = 0.07 inches. This setting should be checked and manipulated after the probe has been inserted into the gas stream, described in step 6.

5) On a form similar to Figure 7, record HEPA filter ΔP_o, barrel (chamber) T, Average dry gas meter T at start, Meter CF start, and venturi ΔP.

6) Two to three persons are necessary. One person manually inserts probe into sampling port on a signal. A second person turns on sampling pump and timer at same signal. A third person gives the signal. All three monitor and note stack temperature, baghouse temperature, the temperatures and pressures in step 5 as well as the metallizer load voltage response, amperage, air pressure and quality of generation.

7) Upon signaling the end of the preliminary sampling period, about 2 minutes, remove the probe and turn off the pump.

8) Remove the filter from the holder and store in a covered

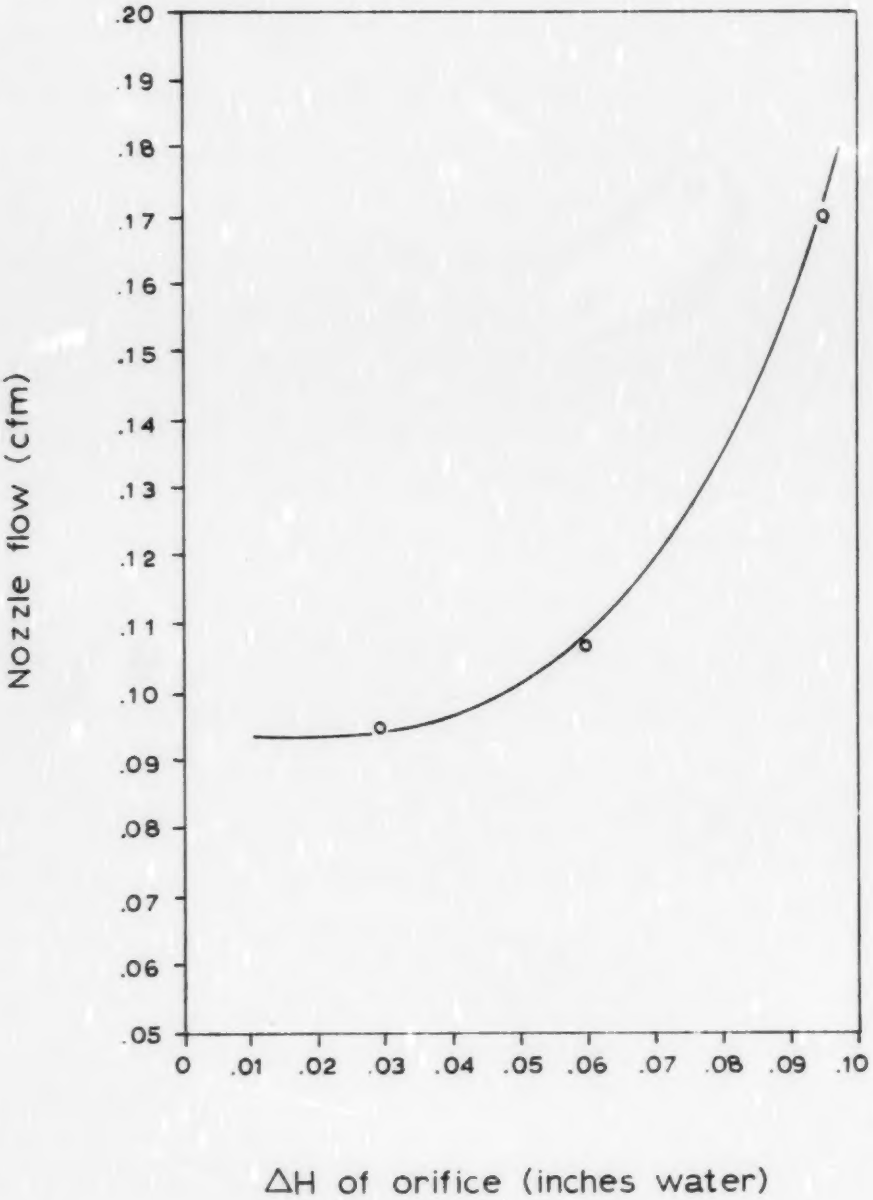

Figure 6. Approximate relationship of sampling nozzle flow to ΔH orifice of sample

Wire type __________ P_{bar}____________________

Wet bulb Temp._______________

1. Sample #
2. Barrel T(°C)
3. HEPA ΔP
4. $P_{duct} = P_{bar} - \textcircled{3}/13.6$
5. Venturi ΔP
6. Duct T (°C)
7. Bag T
8. Pitot ΔP
9. Wire feed rate
10. Amps
11. V_{open}
12. V_{load}
13. MAP
14. SAP
15. ΔH orifice
16. CF start
17. CF end
18. ΔCF
19. $\Delta TIME$
20. CFM = ⑱ / ⑲
21. $T_{meter_{start}}$
22. $T_{meter_{end}}$
23. Nozzle Vel.
24. V_{duct} =

$$\sqrt{234 \; \frac{29.92}{\textcircled{4}} \cdot (273+\textcircled{6})\textcircled{8}}$$

25. I ≈ ㉓/㉔

Figure 7. Typical form for Recording Mass Concentration Sampling Data

petri dish. With compressed air, blow the probe and holder inlet free of settled dust.

8) Note CF end. Approximate the isovelocity parameter by performing following computations.

Nozzle vel. = $\Delta CF/\Delta TIME \cdot (1/.000085 \text{ fpm})$

Stack Vel. = $234\ (.12 \times 29.92 \times T_{stack}(^{o}K)/P_{bar})^{\frac{1}{2}}$ (see Appendix B)

P_{bar} is the absolute total pressure at the sampling port.

I = Nozzle Vel/Stack Vel.

This is only approximate since it ignores moisture and meter temperature. But it is adequate for sampling. If the computed I is within the range of .9-1.1 then assume the sampler is properly adjusted and a sample may be taken by repeating the above steps. The sampling time should be designed to yield approximately a 10mg to 20mg deposit on the filter.

If the computed I is outside of the range, the ΔH on the pump must be changed in a direction that would bring the I ratio closer to unity. To achieve the acceptable ratio, another preliminary sample should be taken if the deviation is significant, otherwise take a sample and adjust the ΔH as necessary.

9) During one of the sampling periods, the wet bulb temperature should be measured and recorded. As a computation in Appendix D shows, the maximum moisture influence at the range of operating conditions was 4.4%, and thus this factor is not important in estimating the isovelocity factor.

10) At the end of all sampling for the day, place filters with samples that are considered satisfactory in a dessicator, laying

in the petri dish with the lid removed. After about 2 days, weigh them to the nearest 0.1 mg. (Weighing was not necessarily done in a dry environment.)

Sampling Procedure for Electron Microscopy

The goal in sampling with the Nuclepore filters was to obtain a deposit with a countable number of particles. When the loading is too intense, individual particles are not distinguishable. When loading is too light, the array of particles is too low to provide statistically satisfactory results. Isovelocity conditions are strived for but are difficult to confirm due to the short sampling time. Particle size sampling is usually done concurrently with mass sampling. Nuclepore filters are not dessciated and tared. The following steps outline the method followed.

1) Satisfy the first 3 steps on page 2-16. Place the Nuclepore filter into holder with glossy side toward sample stream.
2) Start the pump with the probe not in the exhaust stream. After about 5 seconds, insert the probe and direct the nozzle toward the stream and hold for an interval of 1 second to 4 seconds.
3) Repeat the above steps, using different holding times.
4) After collecting several filters, examine them visually and with an optical microscope. The filters should show a slight shadow or darkening due to the deposit. At a magnification of several hundred times, distinct particles should be apparent along with ample clean area.

Sensitivity of Results to Deviations from Isovelocity Sampling

According to Peterson, aerosol sampling is subject to two biases: velocity and inertial impaction. Bias is defined as (13, pg F-4).

> "Volumetric particle concentration or size distribution determined from probe sample divided by actual array of particles which existed in aerosol cloud."

He described work by Lundgren and Calvert in which the two sampling biases are referred to as R and K.

$R = V_o/V_c$

$K = (C\rho_p V_o D_p^2)/(18\mu D_c)$

where C = the Cunningham Correction factor =

$1 + 1.62 \times 10^{-5}/D_p + ((.55) \times 10^{-5}/D_p)\ \mathrm{EXP}(-.67 \times 10^{+5}\ D_p)$

V_o = Duct Velocity = (1400 fpm) = 711 cm/sec

V_c = Probe inlet velocity

D_p = particle diameter (cm)

ρ_p = particle density,

μ = viscosity = 185×10^{-6} poise (at 25°C)(ref. 16)

D_c = probe inlet diameter = 1/8 inch = .32 cm

Peterson developed the following graph, modified from Lundgren and Calvert data, that indicates "typical experimental sampler inlet bias for a straight inlet probe" plotted as a function of R and K.

Peterson said, (13, p. I-4)

> "As is quite often true in aerosol studies the . . .K is of primary importance. The range of maximum interest is the K value range from 0.01 to 1.0. Below 0.01 the sampling bias is low enough to be relatively unimportant. Above 1.0 the sampling bias is equal to the velocity ratio (R)."

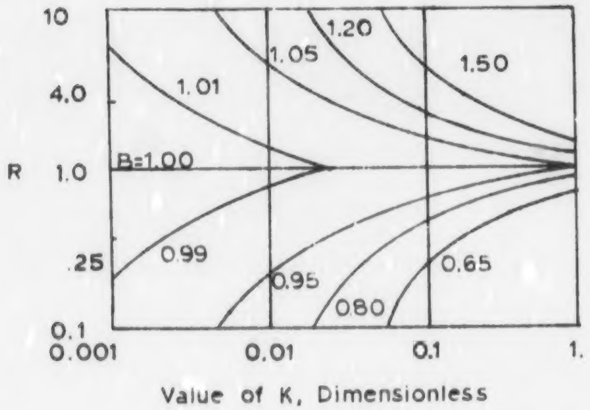

Figure 8. Plot of lines of equal bias as function of R and K (13, pg. L-5)

The above formula for K and graph of R and K are applied to predict the biases to which the particle sampling is subject. Since there are small fluctuations in the duct velocity pressure, after sampling has commenced, it is assumed the actual R could vary from 0.8 to 1.2. The following table summarizes the bias study for which computations are given in Appendix D.

Table 2. Summary of Possible Sampling Biases Duct Velocity - 711 cm/sec

Particle Diameter cm	μm	C	ρ_p	R	K	Bias (1.00 is left of ≠ sign)
1×10^{-4}	1.00	1.16	5	1.2	.039	< 1.03
1×10^{-4}	1.00	1.16	5	0.8	.039	$> .97$
1×10^{-4}	1.00	1.16	1	1.2	.0077	< 1.01
1×10^{-4}	1.00	1.16	1	0.8	.0077	$> .99$
1×10^{-6}	0.01	22.34	5	1.2	.0001	= 1.00
1×10^{-6}	0.01	22.34	5	0.8	.0001	= 1.00
1×10^{-6}	0.01	22.34	1	1.2	.0001	= 1.00
1×10^{-6}	0.01	22.34	1	0.8	.0001	= 1.00

For the most conservative assumptions, the maximum error, according to the Peterson article, would be 3%. If discrete particles on the order of 0.01 μm (10nm) are present, the sampling probe would show no significant bias to them.

Another bias that might occur during the particle sizing sampling would be a misalignment of the probe with respect to the exhaust stream. The filter is exposed while the probe is being positioned during which some misorientation necessarily occurs. Limited data by Lundgren and Calvert indicate an angular difference of 90° between inlet and stream flow for 2 μm particles gives a bias of less than 5%.(13) Therefore, the placing and removing of the probe probably causes little bias in the observed particle sizes and distribution. This problem could be expected to be insignificant in the mass concentration samples. An additional bias occuring is due to the depositing of particles along the walls of the probe and filter holder upstream of the filter.

ANALYTICAL TECHNIQUES

Mass Concentration Analytical Techniques

Compute the mass concentration of the sampled air by dividing the weight gain of a Millipore filter by the standardized volume of air pumped by the sampler. Dessicate the filters before and after use for approximately 48 hours. Weigh the filters on an analytical electro balance (approximate precision of ±0.5 mg). The balance scale indicates weights to the nearest 0.1 mg.

The mass concentration analyses are done by the experimenters.

Particle Sizing and Identification Techniques

Store the filtered samples individually in labeled, capped petri dishes. Send to Walter McCrone Associates, Chicago, Illinois, the contractor for microscopy analysis. McCrone examines the samples by transmission electron microscopy (TEM), scanning area electron microscopy (SEM), and selected area electron diffraction (SAED).

McCrone prepares samples for scanning electron microscopy by a replication process. See Appendix E. All of the original features on the filter surface, i.e., pore openings, and aggregates are preserved.

SEM photographs are most informative because of their three dimensional representation. Objects closer to the electron beam collector appear brighter than those farther away. The depth of field of the SEM is 300 to 500 times that available in a light microscope of the same magnification.(12) Photographs from McCrone indicated magnifications ranging from 5,000 x to 11,000 x. SEM is thus useful for studying particle shapes, porosity, aggregation and surface features.

The TEM allows inspection of individual particles by magnifications of up to several hundred thousands times but sacrifices the SEM's depth of field.

Using the TEM, particles are counted and sized by "hand" by observing about six areas of the deposit.(14)

High energy electron diffraction of an individual particle yields photographs showing a set of dark and light concentric bands, whose spacings and relative intensities depend upon the structure and composition of the specimen. The pattern formed by scattered electrons is scanned by a recording microphotometer. The calibrated output shows experimental diameters of circles from specific reflecting planes. These diameters are compared with the ASTM diameter, for the specified plane, to identify the sample material.(14)

SELECTION OF EQUIPMENT OPERATING CONDITIONS FOR SAMPLING

The metallizer manufacturer recommends that the electric arc be kept as small as possible without 'spitting' to achieve the most efficient metallizing.(1) The experimenters consider this condition as stable and observe that stability results in the following characteristics:

1. Particle generation is smoother and quieter.
2. The indicated amperage remains steady.
3. The load voltage is either equal to or a few volts less than the open circuit voltage setting, and does not oscillate about this level by more than one volt.

The experimenters assume that smaller particles and reproducibility will result from stable operating conditions.

The metallizer can be readily adjusted for rates of wire feed, air pressures to the arc (MAP and SAP) and open circuit voltage. The exhaust flow rate can also be adjusted by a damper and valve in the exhaust ductwork. It should be noted that the open circuit voltage is considered a dependent variable of the wirefeed rate. The wirefeed rate establishes the amperage across the arc.

With due consideration for the funds available for electron microscopy analysis, the following conditions were selected to examine the zinc wire fume.

Table 3. Zinc Wire Sampling Conditions

Condition	Wirefeed Rate	V_{open}	V_{load}	Amps	MAP	Flow	SAP
1	30	21	21	30	70	250	20
2	30	21	21	30	50	250	20
3	50	23	22	70	70	250	20
4	50	23	22	70	50	250	20

Notes: Wirefeed rate- percent of full rate, V_{open} - open circuit voltage, V_{load} - voltage across arc, MAP - main air pressure-psi, SAP- secondary air pressure, Flow- Exhaust flow in duct-scfm.

RESULTS

BRIEF EVALUATION OF EQUIPMENT OPERATION

As of April 1976 the experimental apparatus was considered moderately reliable by the experimenters. The equipment would not operate consistently satisfactory at established stable conditions. Specifically, many runs of zinc wire were interrupted when either of the wires jammed in the flexible conduit due to various friction affects. Also, the observed stabilities of steel wire at several operating conditions and of the zinc at condition four (Table 3) were not repeatable on different days.

It is important to note that the metallizer by itself is noisy and the use of the large particle collection drum adds to the noise. This noise, while not measured, interferred with communication between research personnel in a high ceiling room. If not corrected, it would reduce research work effectiveness, possibly interfere with the other research work nearby and could be expected to create stress in animals if the particles were used in animal quarters. The noise can undoubtedly be corrected by inherent design changes and by additional noise control materials.

SAMPLE NUMBER IDENTIFICATION

Mass Concentration

The zinc oxide samples shown in Table 4 were analyzed for mass concentration.

Table 4. Identification of Mass Concentration Samples

Sampling Condition	Sample Numbers
1	13, 19, 34, 45, 46
2	31, 32, 33, 44
3	15, 18, 35, 36
4	37, 38, 40

Electron Microscopy and Electron Diffraction

The zinc oxide samples shown in Table 5 were sent to Walter McCrone Associates for SEM, TEM and SAED analysis.

Table 5. Identification of McCrone Samples

Sampling Condition	Sample Numbers
1	101, 125
2	133, 134
3	104, 128

CHEMICAL COMPOSITION

Electron Diffraction Data

Selected area electron diffraction results, as received from McCrone Associates, are given in Tables 6 and 7. According to Richard Shimps of McCrone Associates, these tables indicate that the particles generated were ZnO.

Table 6. Electron Diffraction Data -- Sample 104

SAED Calculated diameters of Circles from Specific Reflecting Planes	ASTM Card S-0664 (Z_n0) diameters of Circles from Specific Reflecting Planes
Angstrom (0.1 nm)	Angstrom (0.1 nm)
2.814	2.816
2.592	2.602
2.463	2.476
1.903	1.911
1.622	1.626
1.498	1.477
1.378	1.379

Table 7. Diffraction Data -- Sample 133

SAED Calculated diameters of Circles from Specific Reflecting Planes	ASTM Card S-0664 (Z_n0) diameters of Circles from Specific Reflecting Planes
Angstrom (0.1 nm)	Angstrom (0.1 nm)
2.82	2.816
2.60	2.602
2.50	2.476
1.92	1.911
1.635	1.626
1.483	1.477
1.392	1.379

Assay of Wire

A typical assay of the Wall Colmonoy zinc wire (Platt #302) 15 gauge (.145 cm diameter)is

Zinc	99.99% +
Iron	.0015%
Cadium	.0015%
Lead	.002% Maximum

MASS CONCENTRATION

Mass concentration sampling data as observed are presented in Appendix F. Concentrations expressed as mg/acf are converted to mg/scf at the standard conditions of 760 mm mercury and 25° Centigrade. Table 8 summarizes the standardized concentrations expressed as g/sm^3.

Table 8. Standardized Zinc Oxide Mass Concentrations for all Samples

CONDITION	1		2		3		4	
REPLICATE	#	g/sm^3	#	g/sm^3	#	g/sm^3	#	g/sm^3
	13	0.87	31	0.74	15	1.91	37	1.03
	19	1.26	32	0.67	18	2.04	38	1.09
	34	1.00	33	0.62	35	2.02	40	1.23
	45	1.20	44	0.63	36	2.25		
	46	0.80						

The concentrations in Table 8 are more meaningful when the statistical parameters -- mean, standard deviation, and coefficient of variation (C.V.) are calculated. The coefficient of variation is one indicator of reproducibility or precision of concentration generation. These parameters are summarized in Table 9A.

Table 9A. Zinc Oxide Mass Concentration Mean and Variation Summary

Condition	1	2	3	4
(1) Mean (g/sm^3)	1.03	0.68	2.05	1.12
(2) Mean (grain/scf) ① x 2.29	2.36	1.56	4.69	2.56
(3) Stand. dev. (g/sm^3)	0.20	0.05	0.14	0.10
(4) Coefficient (③/①x 100) of variation	19%	8.4%	6.9%	8.7%

Table 9B. Mean Mass Concentration Matrix

	Wirefeed 30	Wirefeed 50
MAP 50	0.68 cond. 2	1.12 cond. 4
MAP 70	1.03 cond. 1	2.05 cond. 3

Row 4 of Table 9 indicates that the C.V.'s of conditions 2, 3, and 4 are less than 9% while condition 1 has a C.V. of 19%. Condition 1 is apparently much less reproducible.

Means Testing

A question relative to the values in Table 9B is whether the means are significantly different. The mean of condition 1 (X_1) is fairly close to $\bar{X}_4$ but two operating variables (wire feed rate and MAP) are different. A statistical method to test the other pairs of means is the Smith Satterthwaite test$^{(19)}$. This method is utilized by hypothesis tests applied (see Appendix G-1).

These hypothesis tests support the conclusion at the 5% level of significance that $\bar{X}_1 > \bar{X}_2$, $\bar{X}_3 > \bar{X}_2$ and $\bar{X}_3 > \bar{X}_1$. This implies that the mass concentration of zinc oxide particles is increased when air pressure or wirefeed rate or both are increased

Analysis of Variance

Another statistical analysis applicable to the mass concentration data is the analysis of variance. This is generally a more efficient and more powerful systematic approach of distinguishing experimental (random) error from variation due to different operating conditions.$^{(19)}$ However, appropriate experimental design to facilitate the analysis of variance would have required samples from several more wirefeed rates and MAP's instead of several replicates for each condition. Application of the two way classification analysis of variance as described on pp. 274-278 of ref. 19 yields results in contradiction to the hypothesis tests. But the contradiction is presumably caused by the insensitivity of the test at the minimum degrees of freedom of the two variables.

PARTICLE SIZING BASED ON ELECTRON MICROSCOPY

The electron microscopy photographs of the zinc oxide samples were all similar in terms of particle appearance. SEM photographs in Appendix H of sample 133, show agglomerates of different shapes and sizes. The agglomerates range in size from less than 0.1 μm to over 2 μm and appear to be interconnected. The shapes vary from spherical to chainlike. These agglomerates are composed of very fine particles as shown in the TEM photos for sample 101 (Fig. H-3). These particles, approximately circular and presumably spherical, have diameters of about 10 nm (.01 μm). These were the particles sized and counted by the McCrone organization. Since the agglomerates were interconnected, McCrone's group made the assumption that there was no meaningful method to count them for some appropriate dimension. The agglomeration is discussed more extensively later in the report.

Table 10 is a modified form of the zinc oxide particle sizing and count data as it was received from McCrone Associates. This table indicates the number of observed particle diameters in each one nanometer wide interval. Particles were not counted by

Table 10A. Zinc Oxide Particle Size Data

Size Range nm	Sample 101		Sample 104		Size Range nm	Sample 125	
	number	percent	number	percent		number	percent
20 → (a)	2	.67	24	6.36	20 →	26	9.29
19-20	0	-	2	.53	19-20	7	2.50
18-19	0	-	7	1.86	18-19	3	1.07
17-18	1	.33	17	4.52	17-18	1	1.07
16-17	1	.33	18	4.78	16-17	11	3.93
15-16	2	.67	24	6.38	15-16	9	3.21
14-15	3	1.01	16	4.25	14-15	9	3.21
13-14	2	.67	22	5.85	13-14	9	3.21
12-13	9	3.03	34	9.04	12-13	29	10.36
11-12	13	4.37	22	5.85	11-12	5	1.79
10-11	8	2.69	22	5.85	10-11	13	4.64
9-10	13	4.37	20	5.31	9-10	9	3.21
8-9	23	7.74	35	9.30	8-9	31	11.07
7-8	32	10.77	19	5.05	7-8	20	7.14
6-7	36	12.12	16	4.25	6-7	31	11.07
5-6	41	13.80	12	3.19	5-6	20	7.14
4-5	15	5.07	17	4.52	4-5	8	2.86
3-4	15	5.07	12	3.19	3-4	36	12.86
2-3	26	8.75	20	5.31	2-3	2	0.71
1-2	23	7.74	11	2.92	← 2	1	0.36
0-1	32	10.77	6	1.59			
Total	297	99.93%	376	99.90%		280	99.99%

(a) In samples 104, 125, 128, 133, 134 there were no more than 3 particles per 1 nm interval > 20nm. Particles were observed up to 50 nm. In this report particles > 20 nm are treated mathematically as belonging to an interval from 20-22nm. The investigator realizes that this assumption significantly influences the computation of statistical parameters.

Table 10B. Zinc Oxide Particle Size Data

Size Range nm	Sample 128 number	Sample 128 percent	Sample 133 number	Sample 133 percent	Sample 134 number	Sample 134 percent
20 → (a)	19	6.76	25	7.14	31	11.07
19-20	2	0.71	5	1.43	8	2.86
18-19	5	1.78	6	1.71	6	2.14
17-18	2	0.71	2	0.57	11	3.93
16-17	4	1.42	11	3.14	9	3.21
15-16	7	2.49	12	3.43	13	4.64
14-15	9	3.20	8	2.29	3	1.07
13-14	13	4.63	17	4.86	10	3.57
12-13	43	15.30	27	7.71	8	2.86
11-12	17	6.05	9	2.57	15	5.36
10-11	33	11.74	29	8.29	24	8.57
9-10	14	4.98	9	2.57	5	1.79
8-9	11	3.91	21	6.00	8	2.86
7-8	25	8.90	15	4.29	11	3.93
6-7	19	6.76	29	8.29	4	1.43
5-6	17	6.05	45	12.86	11	3.93
4-5	23	8.19	21	6.00	25	8.93
3-4	17	6.05	41	11.71	49	17.50
2-3	1	0.36	13	3.71	25	8.93
← 2	0	0.00	5	1.43	4	1.43
Total	281	99.99	350	100.00	280	100.01

(a) In samples 104, 125, 128, 133, 134 there were no more than 3 particles per 1 nm interval > 20 nm. Particles were observed up to 50 nm. In this report particles > 20 nm are treated mathematically as belonging to an interval from 20-22 nm. The investigator realizes that this assumption significantly influences the computation of statistical parameters.

mass or surface area.

Analysis

It was intended that the analysis of the particle size data would answer the following questions.

1) Are the particle size statistical parameters (mean, variance, distribution) from each replicate sample significantly different?
2) Are the statistical parameters from samples differing by one variable significantly different?
3) Do any theoretical statistical distributions reasonably fit the observed distributions?

Such an analysis would give a quantitative measure of the reproducibility potential and effect of the operating variables in addition to a characterization of the generated particles.

Computation of Means and Variances

The mean diameter for each sample can be calculated by

$$\bar{D} = \sum_{i=1}^{n} d_i f_i$$

where d_i = midpoint of size interval

n = number of intervals

f_i = decimal fraction of total within interval

$$\sum_{i=1}^{n} f_i = 1.00$$

The variance of the sample diameters can be computed from

$$S^2 = \sum_{i=1}^{n} x_i^2 f_i - \bar{D}^2$$

Table 11. Means and Variances of Zinc Oxide Particle Size Data

Sample #	101	125	133	134	104	128
Condition II	1	1	2	2	3	3
$\bar{D}$ (nm)	6.0	10.2	9.1	10.0	10.8	10.4
S^2 (nm^2)	14.6	29.2	35.6	41.1	28.1	22.0
S (nm)	3.8	5.4	6.0	6.4	5.3	4.7
Sample Size	297	280	350	280	376	281

Reproducibility Among Replicates

The mean diameters for samples 101 ($\bar{D}_{101}$) and 125 ($\bar{D}_{125}$) of condition 1 are significantly different by inspection.

The values of the pairs $\bar{D}_{133}$ and $\bar{D}_{134}$ for condition 2, and $\bar{D}_{104}$ and $\bar{D}_{128}$ for condition 3 are closer and are analyzed by a statistical method for significant difference in Appendix G-2.

This analysis indicates that the two replicates for condition 2 have diameter means and variances that are not significantly different. The analysis also indicates that the means and variances for condition 3 replicates are not significantly different.

Differences Between Conditions

An important question is whether the means and variances for particle diameter populations generated under different conditions are different. Since the mean of condition 1 cannot be estimated within a relatively tight range, only the relationship of condition

2 to condition 3 is examined. However, conditions 2 and 3 differ by two variables, and if the mean sizes are different there is a lack of data to distinguish variable influence.

Hypothesis testing in Appendix G-3 demonstrates that the mean particle diameters for conditions 2 and 3 are significantly different. Thus changing the operating conditions apparently changes the mean particle diameters.

Frequency Distributions

Another statistical parameter that provides useful information is the frequency distribution. The observed distributions are presented above in Table 10. The following two tables and two graphs indicate the cumulative frequency for conditions 2 and 3. In addition typical histograms representing observed frequencies and frequencies expected from the appropriate normal distribution are plotted.

The normal distribution provided a better fit to the observed distributions than did the log normal. This was found by calculating the maximum differences between the observed and expected (theoretical) distributions. This is examined statistically in the next section.

It was also attempted to decide which of the two fit better by plotting the data onto log normal and normal probability paper. By this method, data should plot as a straight line. However, this method was inconclusive as indicated by Figures 13 and 14.

Table 12. Cumulative Observed and Expected Frequencies for Condition 2

$\mu = 9.6 \qquad \sigma = 6.2$

d mm	Z	$F(d)_{133}$	F(Z)	$F(d)_{134}$	Maximum Diff. (a) (133)	(134)
≤ 2	-1.23	.014	.109	.014		
3	-1.06	.051	.145	.104		
4	- .90	.168	.184	.279		
5	- .74	.228	.230	.370		.140
6	- .58	.357	.280	.407		
7	- .42	.440	.337	.42	.103	
8	- .26	.483	.400	.46		
9	- .10	.543	.46	.49		
10	+ .06	.569	.52	.51		
11	+ .23	.652	.59	.59		
12	+ .39	.678	.65	.65		
13	+ .55	.755	.71	.67		
14	+ .71	.804	.76	.71		
15	+ .87	.827	.81	.72		
16	1.03	.861	.85	.77		
17	1.19	.893	.88	.80		
18	1.35	.898	.91	.84		
19	1.52	.916	.94	.86		
20	1.68	.930	.95	.89		

(a) The maximum absolute difference between observed (F(d)) and expected frequency (F(Z)).

Table 13. Cumulative Observed and Expected Frequencies for Condition 3

$\mu = 10.44 \quad \sigma = 4.9$

d_i	Z	$F(d)_{104}$	F(Z)	$F(d)_{128}$	Maximum Diff. (a)	
					(104)	(128)
1	-1.93	.016	.0268	-		
2	-1.72	.045	.043	-		
3	-1.52	.098	.064	.004		
4	-1.31	.130	.095	.064		
5	-1.11	.175	.134	.146		
6	- .91	.207	.181	.206		
7	- .70	.250	.242	.274		
8	- .50	.300	.309	.363		
9	- .29	.393	.386	.402		
10	- .09	.446	.464	.452		
11	+ .11	.505	.544	.569		
12	+ .32	.563	.626	.630		
13	+ .52	.654	.698	.783		.0844
14	+ .73	.712	.767	.829		
15	+ .93	.755	.824	.861	.0688	
16	+1.13	.818	.871	.886		
17	+1.34	.866	.910	.900		
18	+1.54	.911	.938	.907		
19	+1.75	.930	.960	.925		
20	+1.95	.935	.974	.932		

(a) The maximum absolute difference between observed (F(d)) and expected frequency (F(Z)).

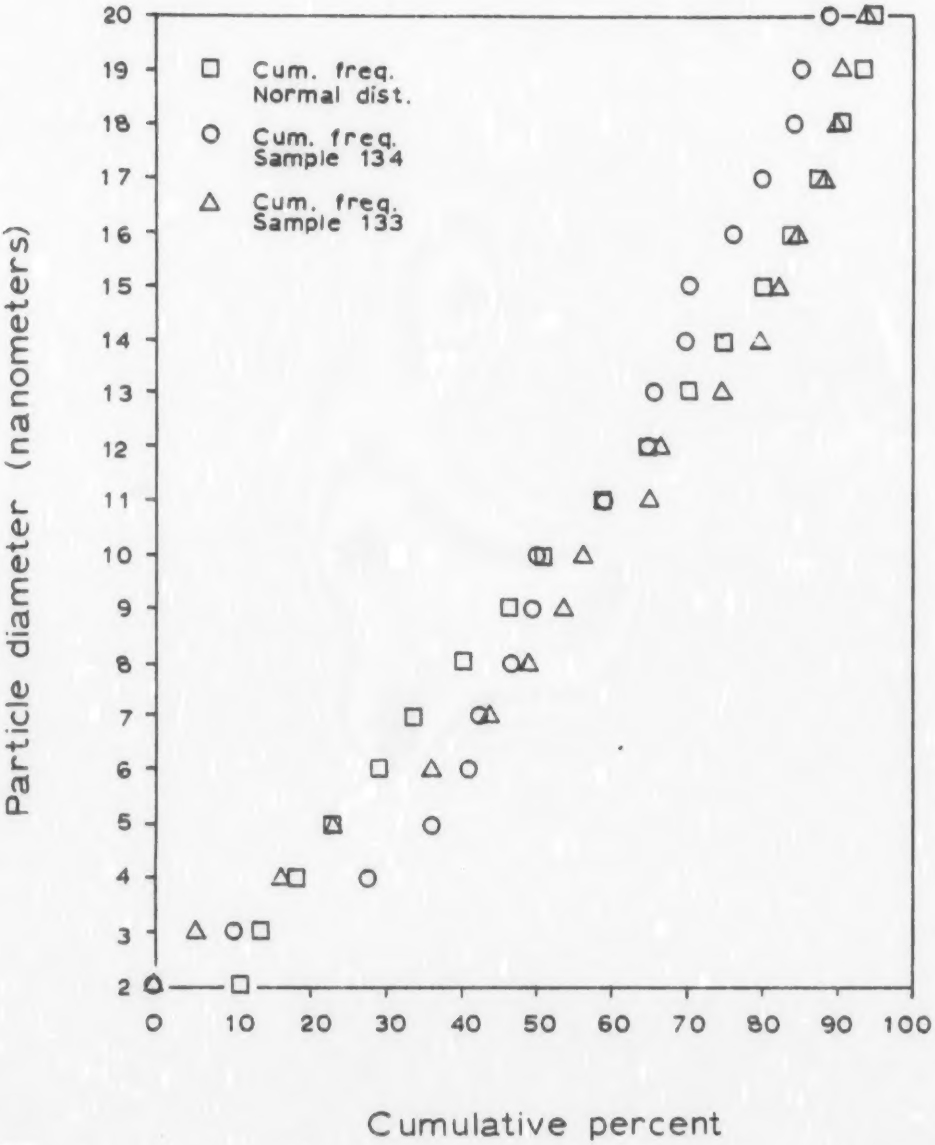

Figure 9. Comparison of cumulative frequencies for condition 2 (table 12)

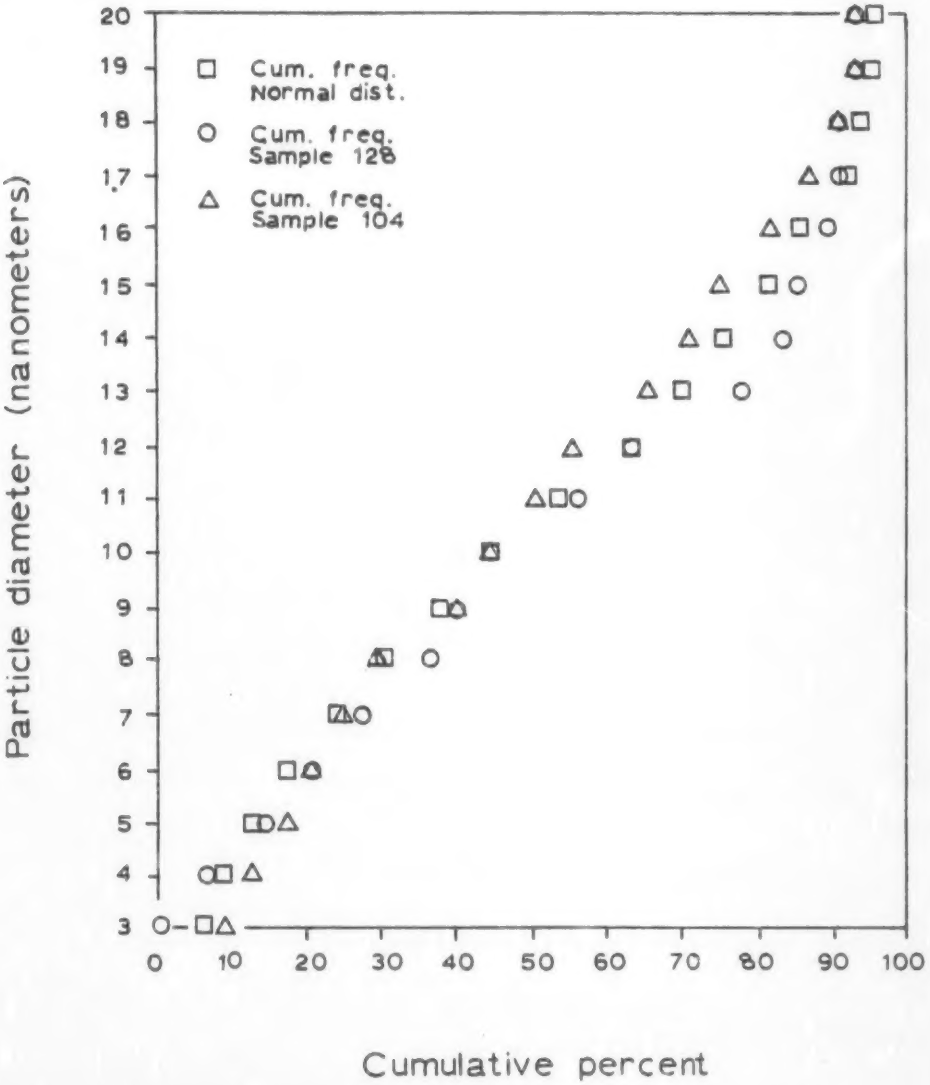

Figure 10. Comparison of cumulative frequencies for condition 3 (table 13)

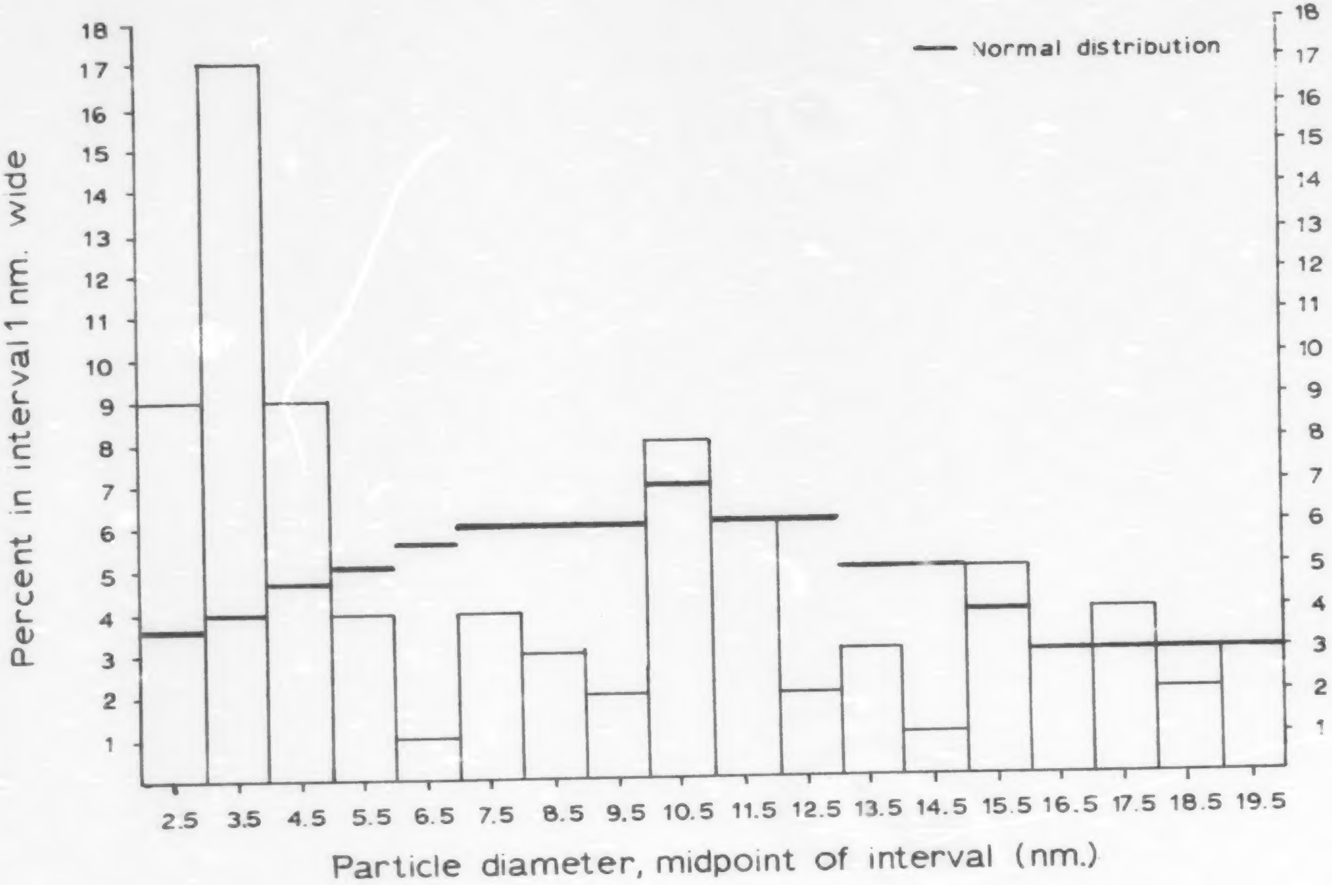

Figure 11. Observed frequency of sample 134 and normal frequency

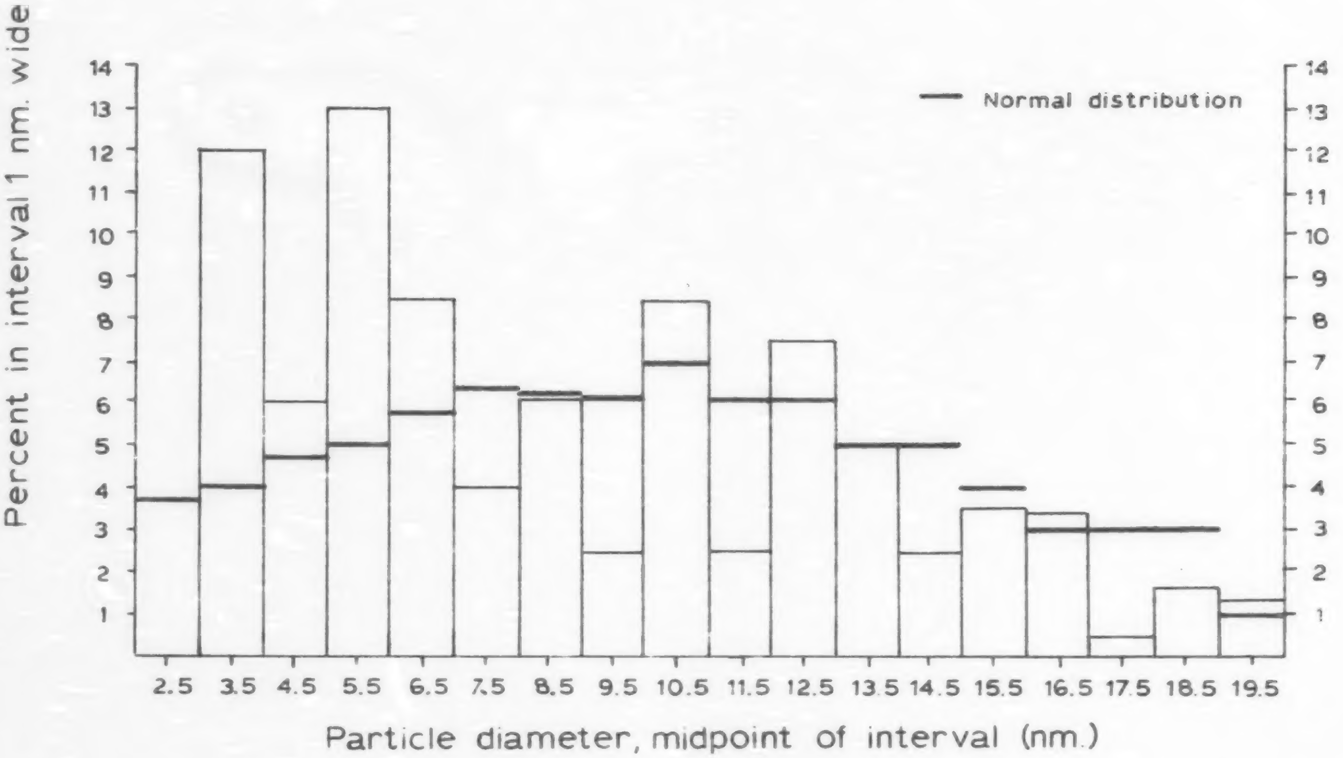

Figure 12. Observed frequency of sample 133 and normal frequency

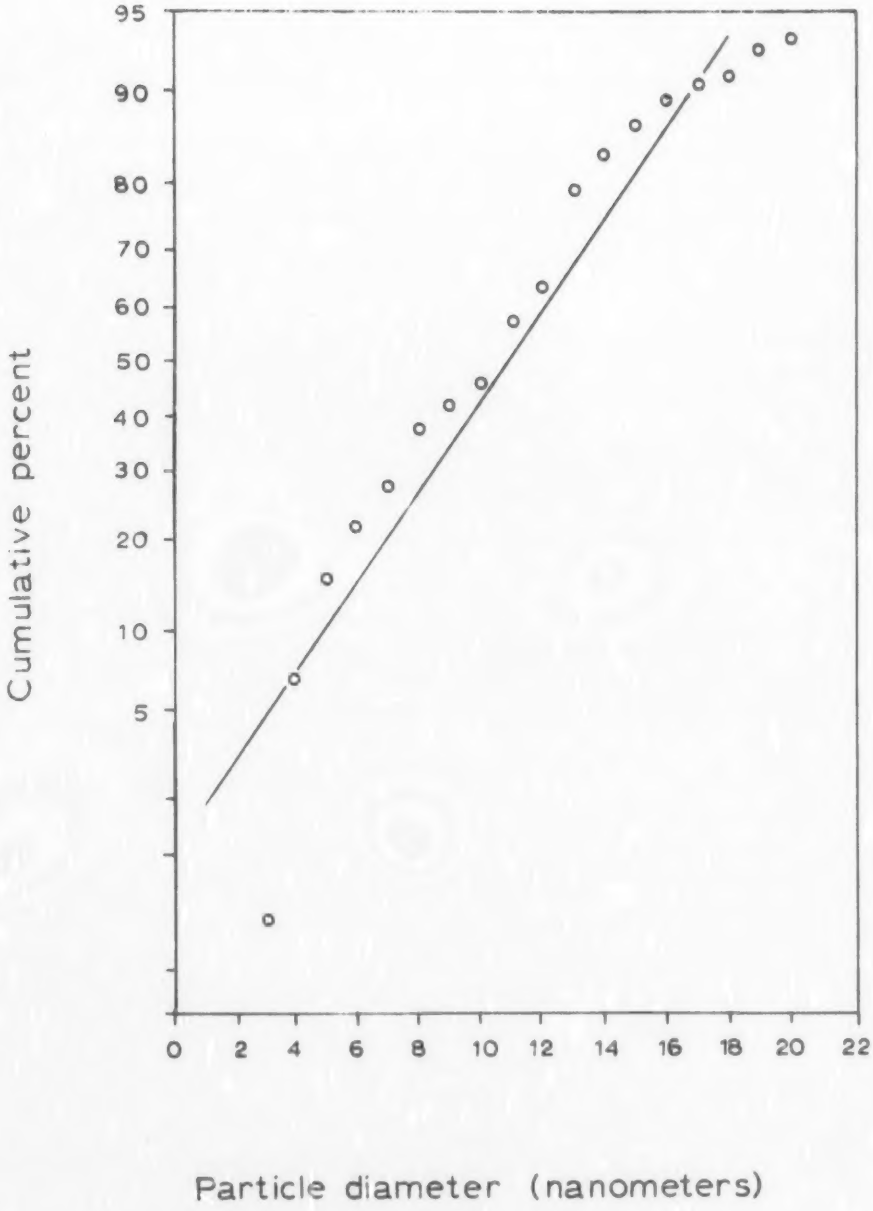

Figure 13. Arithmetic probability plot of sample 128 diameters

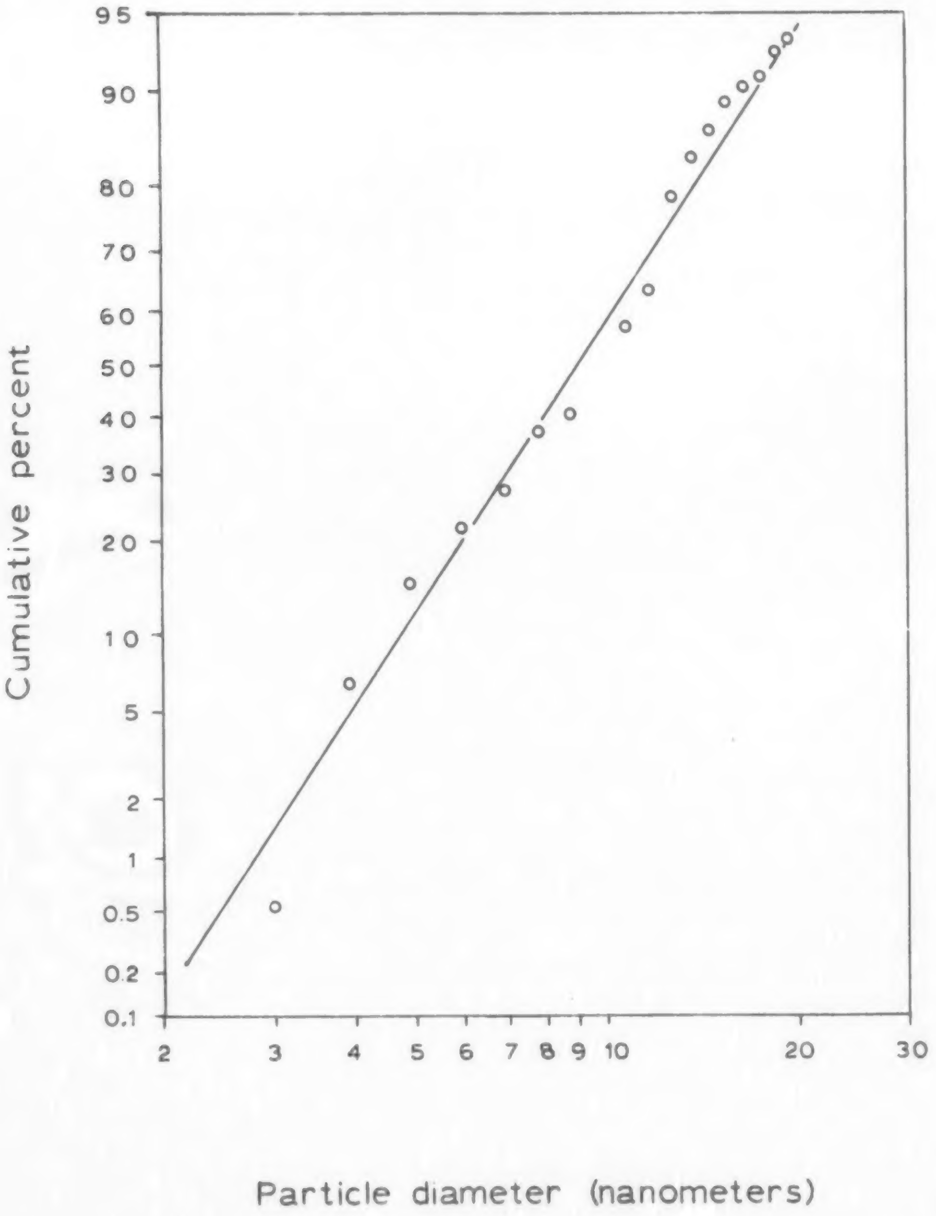

Figure 14. Log probability plot of sample 128 diameters

Computation of Normal Distribution

The cumulative normal distribution can be constructed from statistical tables by assuming values of μ and σ for the population of diameters (d_i). Tables(19) of the standard normal distribution give values of F(Z). F(Z) is the probability that $(Z_i = \frac{d_i - \mu}{\sigma}) \leq Z$

Goodness of Fit

Figures 9 and 10 show by inspection that the normal distributions provide an approximate fit to the observed data. Two of the statistical methods for testing goodness of fit are the Kolmogorov-Smirnov (K-S) test(19,20) and the chi square test.(19,21) The investigator used both methods and selected the K-S test for this report. The K-S test is a more powerful test for continuous distribution fitting.(25)

The one sample K-S test concerns the agreement between an observed distribution and a specified continuous distribution. The two sample K-S test concerns the agreement between two observed distributions. The test is (19, p. 222) "sensitive to population differences with respect to location, dispersion or skewness." Both tests are based on the maximum absolute difference between the two cumulative distributions.

In Appendix G-4 the one sample test is applied to samples 133, 134, 104, and 128. Only the distribution of diameters from sample 104 statistically fit an appropriate normal distribution. The two sample test is also applied to the replicates. The distributions of diameters for samples 133 and 134 of condition 2 are not significantly different, but the distributions for samples 104 and 128 are different.

AGGLOMERATION

An important question is where do the agglomerates originate? The available information does not directly answer this question. One reason why this question is important is that the agglomeration might be a peculiarity of only the generating equipment, the drum and duct system, the sampling processes, or of some combination of them.

Particle agglomeration is discussed in references 2, 7, 22 and 23. According to Green and Lane(22) the general equation "for the rate of coagulation (agglomeration) of an aerosol" is

$$\frac{-dn}{dt} = \frac{RT}{6\eta N} S\left[\frac{(r_1+r_2)^2}{r_1 r_2}\right]\left(1 + \frac{A\ell}{r}\right) n^2 \qquad (1)$$

where

$1 + \frac{A}{r}$ = Cunningham correction factor

A = .9 for smokes

ℓ = mean free path

$\ell = 9 \times 10^{-6}$ cm

r = particle radius = mean value of r_1 and r_2 (cm)

r_1 = radius of particle 1 (cm)

r_2 = radius of particle 2 (cm)

n = number of particles per cm^3

N = Avogadro's number = 6.0×10^{23}

R = gas constant = 8.3×10^7 for

$T = 293^{\circ}$ K

$\eta = 1.82 \times 10^{-4}$ poise

S = sphere of influence/particle radius

Green indicates that $\frac{1}{4}\left[\frac{(r_1+r_2)^2}{r_1 r_2}\right]$, which has a minimum of 1, has an average value of 1.27 when the range of radii $\frac{r_1}{r_2}$ in a uniformly polydisperse aerosol is 1-8.

$$\text{Then } \frac{-dn}{dt} = \frac{2}{3}\,\frac{RTS}{\eta N}\,\left(1+\frac{A\ell}{r}\right)n^2\ (1.27) \qquad (2)$$

$$= K\ \left(1+\frac{A}{r}\right)n^2\ (1.27) \qquad (3)$$

Green lists a table giving values of K for ferric oxide and magnesium oxide, among others, which are .66 and .83 x 10^{-9} cm^3/sec, respectively. By integrating the above equation, it follows

$$\frac{1}{n} - \frac{1}{n_o} = 1.27\ K\ \left(1 + \frac{A\ell}{r}\right)t \qquad (4)$$

For the zinc oxide particle we can let $r = 5 \times 10^{-7}$ cm (5nm)

$$\left(1 + \frac{A\ell}{r}\right) = 1 + 18 = 19$$

and assume $K = .7 \times 10^{-9}$. To estimate n_o, we can assume concentration=C

$1\ g/m^3 = 1 \times 10^{-6}\ g/cm^3$ and

$S.G. = 5;\ C = n_o\ 5.\frac{4}{3}\pi r^3\ \ g/cm^3$

$n_o = 3.83 \times 10^{11}$ particles/cm^3

Computing the time to reduce the initial number of particle n_o, to $\frac{1}{2}\, n_o$

$t_{\frac{1}{2}} = 1.55 \times 10^{-4}$ sec

This implies that the agglomeration takes place rapidly and well before the particles reach the sampling probe, an elapsed time of about 0.3 seconds. The agglomeration apparently commences close to the arc.

The agglomeration rate is substantially dependent upon n_o and particle size. If either variable were changed to give a combined change of 10^3 (toward smaller concentration and larger size) the $t_{\frac{1}{2}}$ would be altered to approximately the elapsed time.

Another factor in the agglomeration is that the particles are initially charged. (2,9) Aggregates of charged particles show pronounced tendency to be oriented in a chainlike fashion, indicating polarization. Since particles in arc smoke are highly charged, chain formation is not unexpected.(11)

COMPARISONS WITH HEDDEN'S RESULTS

Although earlier particle generator work at W.V.U. by Hedden(4) involved iron oxide, it is nevertheless interesting to compare some of his results to the zinc oxide results contained in this report.

The following table compares mass concentration and particle size data.

Table 14. Hedden-Naylor Data

	Hedden (iron oxide)	Naylor (zinc oxide)
Limit of microscope resolution (nm)	5	1
Width of diameter count interval (nm)	10	1
Mass concentration (gm/m^3)	.63	.67-2.05
Mean particle diameter (nm)	22	6.0-10.8
Range of diameters (nm)	5->100	1-50
Standard deviation (nm)	16.3	3.8-6.4
Cumulative Frequency Distribution	log normal	normal

Hedden apparently did not observe agglomerated particles. This was presumably caused by his procedure of resuspending the samples in solution and dispersing, rather than due to the fact that the metal oxides examined were different.

CONCLUSIONS

By a method described above, very fine zinc oxide particles were generated by a commercial electric arc metallizer fed by two wires and sampled using out-of-stack membrane and Nuclepore filters. At four different combined settings of air pressure to the arc and rate of wire consumption, mass concentrations were measured. At three of these settings particle diameters by count were measured by electron microscopy. The mass concentration means ranged from 0.67-2.05 g/sm^3 (1.5-4.7 grain/scf). The mean particle diameters ranged from 6.0-10.8 nm (0.006-0.0108 μm).

The generation of mass concentration was more precisely reproduced at three of the conditions. The mass concentration was sensitive to changes of the operating conditions.

Two samples from each of three conditions were observed by electron microscopy. At the one condition for which mass concentration was not reproducible, the mean particle diameter was and is not considered to be reproducible. At a second condition, the particle diameters' mean and standard deviation were reproducible, while at a third the mean, standard deviation and cumulative frequency distribution were reproducible.

The mean particle diameters of the second and third conditions were significantly different. The distribution of particle diameters from each sample is apparently approximated by an appropriate cumulative normal distribution. However, only one sample distribution, from the third condition, has a good fit, statistically.

Virtually all particles were agglomerated. The agglomeration initiates immediately after particle generation at the electric arc. Its fast rate results from a high initial number of particles per volume and very fine particle size.

RECOMMENDATIONS

The Flamespray model VT500 electrospray metallizer has demonstrated several important capabilities. For at least one operating condition, it can generate very fine agglomerated zinc oxide particles that are reproducible with respect to both the distribution of particle diameters and mass concentration.

Therefore, this metallizer is considered worthy of continued attention by researchers as a device for generating very fine particles. This attention would include, but not be limited to:

A. Improving the research tool.

    1) Further development of equipment to improve operational quality

        a. Improve the wire feeding of the softer metals to prevent interruptions of particle generation.

        b. Determine requirements for maintaining consistently stable operating conditions.

        c. Reduce the ambient noise levels caused by this metallizer.

    2) Investigation of other metals and expansion of generating and sampling program.

        a. Utilize different wire types and diameters.

        b. Determine the sensitivity to additional variables such as exhaust flow and secondary air pressure.

        c. Redesign the sampling program to facilitate an analysis of variance of mass concentration. Instead of two different wirefeed rates and MAP (main air pressure), these could be increased to 6 different ones. However, retain the present practice of collecting two replicate samples for electron microscopy analysis.

    3) Investigation of methods of sampling and measurement compatible with preserving freshness of particles. This would necessitate a definition of freshness and a method for preserving the sample during collection, during storage and transportation, and during analysis by electron microscopy, electron diffraction, x-ray diffraction, etc.

    4) Review of present sampling and measurement methods to determine if they reasonably utilize the best available technology.

    5) Further study of the agglomeration of very fine particles.

        a. Define appropriate dimensions for describing the agglomerates.

        b. Based on these dimensions, determine whether or not the metallizer generates predictably reproducible distributions of sizes.

        c. If predictable reproducibility is established determine if there is a significant correlation between agglomerate size and such variables as chamber-duct retention time, number of very fine particles per unit volume, and diameters of the very fine particles.

        d. Related to c, determine if there is a significant correlation between very fine particle diameter, agglomerate size and mass concentration.

B. Using the research tool.

    1) When a better understanding of this agglomeration is reached, modify the experimental equipment design to achieve predictable levels of exposure to mass concentrations, particle diameters, and agglomeration sizes found in various types of

occupational and community atmospheres.

2) Modify the experimental equipment design to achieve effectiveness of small particle control-equipment.

3) Investigation of the respiratory effects of fresh particles.

    a. What is the fate of agglomerated particles collected at various locations in the lung?

    b. What is the relationship between respiratory effects and particle age?

LIST OF REFERENCES

1. Wall Colmonoy Corporation, "Directions for Operating the Model VT-500 Colmonoy Electrospray Metallizer," Detroit, Michigan, 1973.

2. Green, H. L. and Lane, W. R., *Particulate Clouds: Dusts, Smokes and Mists*, 2nd edition, Van Nostrand Company, Co., Princeton, N. J., 1964.

3. Linsky, B., Smith, G., "Sources of Information on Air Pollution, *Proceedings* National Conference on Air Pollution, Washington, D.C., Nov., 1958.

4. Hedden, Robert, *Electric Arc Generation of Polydispersed Iron Oxide Aerosol in an Air Stream*,Problem Submitted to WVU, Morgantown, West Virginia, 1972.

5. Johansen, Arland, Unpublished Report, WVU, 1974.

6. Sears, D. R., "Fresh Metal Fumes Project -2," Laboratory Log at WVU, 1975.

7. Brain, Valberg, Sorokin, "An Iron Oxide Aerosol Suitable for Animal Exposures," *Environmental Research*, Vol. 7, No. 1, Feb., 1974.

8. "Method 5 - Determination of Particulate Emissions from Stationary Sources," *Federal Register*, Vol. 36, No. 27, 12123, 1971 pp. 24888-24890.

9. Research Appliance Company, "Instructions for RAC Stack Sampler," Gibsonia, Pa., 1971.

10. Joy Mfg. Co., "Methods for Determination of Velocity . . . Volume of Gases," *Bulletin No. W.P. 50, 19*70.

11. Davies, C. N., *Air Filtration*, Academic Press, N. Y., 1973.

12. Silverman, L., Billings, C., First, M., Particle Size Analysis in Industrial Hygiene, ACGIH and USAEC, Academic Press, 1971.

13. Air Sampling Instruments Committee, *Air Sampling Instruments* for Evaluation of Atmospheric Contaminants, ACGIH, 4th Edition, 1972.

14. Shimps, Richard, Walter McCrone Associates, series of Private Communications, Jan. 1976-Mar. 1976.

15. Spurny, Lodge, *et.al.*, "Aerosol Filtration By Nucleopore Filters," *Environmental Science and Technology*, Vol. 3, 1969, pp. 453-64.

16. CRC, Handbook of Chemistry and Physics, Van Nostrand, 1975.

17. "Electron Diffraction," Encyclopedia of Science and Technology, McGraw Hill, 1974.

18. Miller, Richard, Platt Industries, Private Communication, January 23, 1976.

19. Miller, I., Freund, J., Probability and Statistics, 12th Printing, Prentice Hall, Englewood Cliffs, N.J., 1965.

20. Kim, P. J. and Jennrich, R. I., "Tables of the Exact Sampling Distributions of the Two Sample Kolmogorov-Smirnov Criterion," Selected Tables in Mathematical Statistics, Harter and Owen, ed., Vol. 1, Markam Pub. Co., Chicago, 1970.

21. Mercer, Thomas, Aerosol Technology in Hazard Evaluation, ACGIH, Academic Press, N. Y., 1973.

22. Herdan, G., Small Particle Statistics, 2nd Edition, Academic Press, N. Y., 1960.

23. Hidy and Brock, ed., Topics in Current Aerosol Research, Part 2, Vol. 3, 1st edition, Pergamon Press, N. Y., 1972.

24. Danielson, John A., Air Pollution Engineering Manual, U. S. Department of H.E.W., No. 999-AP-40, Cincinnati, Ohio, 1967.

25. Damewood, E. Z., West Virginia University Industrial Engineering, Private Communication, April 16, 1976.

APPENDIX A

COLLECTION EFFICIENCY OF THE BARREL

An empirical formula by Lapple(24, pg 95) is "sufficiently accurate for an engineering estimation of many cyclone applications." He defines D_{pc} as the diameter of those particles collected with 50 percent efficiency. After determining D_{pc} by the formula following, the collection efficiency of particles D_p can be determined by a graph showing cyclone efficiency versus D_p/D_{pc}.

$$D_{pc} = \left(\frac{9\mu b}{2N_e V_i \rho_p \pi}\right)^{1/2}$$

where μ = gas viscosity = $(183\times10^{-4} \times .672\times10^{-3})$ lb mass/ sec ft.

b = cyclone inlet width = 0.08 ft

N_e = effective turns = ½ (For cyclones may vary from ½-10)

V_i = gas inlet velocity = 44 fps

ρ_p = particle density = 5.6(s.g.) x 62.4
= 349 lb/ft^3

b, V_i, are estimated as spread and velocity of compressed air stream reaching arc

$$D_{pc} = \left(\frac{9 \times (183 \times 10^{-4})(.672 \times 10^{-3})(.08)}{2(\frac{1}{2})44(349)\pi}\right)^{1/2} = 2.4 \times 10^{-5} \text{ ft}$$

$$= 7.31 \times 10^{-4} \text{ cm} = 7.3 \ \mu\text{m}$$

50% by weight of the 7.3 um particles are collected.

For 95% efficiency $D_p/D_{pc} = 4$, according to Figure 48, pg. 95, ref. 24.

$$D_p = 4 \times 7.3 \ \mu\text{m} = 29 \ \mu\text{m} \approx 30 \ \mu\text{m}$$

APPENDIX B

COMPUTATION OF STACK GAS VELOCITY, VELOCITY TRAVERSES, AND STACK FLOW

According to reference 10, the velocity at a stream line in a flue V_s, can be determined from the following

Using standard pitot tube

$$V_s(\text{fps}) = 3.90 \quad \frac{29.92}{P_s} \times \frac{1.00}{Gd} \times HT_s$$

P_s = absolute pressure in flue in inches mercury

Gd = specific gravity of gas referred to that of air

H = velocity head in inches of water = ΔH

T_s = flue gas temperature in degrees Kelvin assuming Gd = 1

$$V_s = 3.90 \left(\frac{29.92}{P_s} \Delta HT_s\right)^{\frac{1}{2}} \text{fps} = 234 \left(\frac{29.92}{P_s} \Delta HT_s\right)^{\frac{1}{2}} \text{fpm}$$

APPENDIX B

Table B-1. Velocity Traverses for Different Venturi Pressure Drops (6)

Venturi ΔP .20 inches water

% of duct diameter	Pitot ΔP in water	ν fpm	Pitot ΔP in water	ν fpm	
6.2%	.09	1201	.10	1266	
25	.12	1387	.12	1387	vertical
75	.12	1387	.12	1387	traverse
93.8%	.09	1201	.09	1201	
6.2%	.10	1266	.11	1328	
25	.12	1387	.12	1387	horizontal
75	.12	1387	.11	1328	traverse
93.8%	.08	1133	.08	1133	

(1) $\bar{\nu}$ = 1298 fpm
for 6" duct Area = .197 ft^2
(2) Q = 256 cfm

Venturi ΔP = .31 inches water

% of duct diameter	Pitot ΔP in water	ν fpm	Pitot ΔP in water	ν fpm	
6.2%	.11	1328	.17	1651	
25	.17	1651	.18	1699	vertical
75	.18	1699	.19	1746	traverse
93.8%	.14	1498	.14	1498	
6.2%	.15	1551	.17	1651	
25	.18	1699	.19	1746	horizontal
75	.18	1699	.17	1651	traverse
93.8%	.12	1387	.12	1387	

$\bar{\nu}$ = 1596 fpm Q = 314 cfm

Venturi ΔP = .40 inches water

% of duct diameter	Pitot ΔP in water	ν fpm	Pitot ΔP in water	ν fpm	
6.2%	.14	1498	.17	1651	
25	.20	1791	.23	1921	vertical
75	.24	1962	.24	1962	traverse
93.8%	.18	1699	.18	1699	

(continued)

Venturi ΔP = .40 inches water (continued)

% of duct diameter	Pitot ΔP in water	ν fpm	Pitot ΔP in water	ν fpm	
6.2%	.22	1879	.23	1921	
25	.24	1962	.24	1962	horizontal
75	.22	1879	.21	1835	traverse
93.8%	.15	1551	.15	1551	

$\bar{\nu} = 1795$ $Q = 354$ cfm

(1) Velocities are calculated by using "standard air tables" and assuming standard conditions of 760 mm and 70°F. This introduces only a small error.

(2) Flows are calculated by the formula

$$Q = \bar{\nu} \cdot A \text{ where } A = \pi(3/12)^2 = .197 \text{ ft}^2$$

The values of Venturi ΔP and Q are plotted in Figure 5.

APPENDIX C

EFFICIENCY OF NUCLEOPORE FILTERS

Definitions of Individual Efficiencies:

1) Partial efficiency of impaction

$$E_i = \frac{2E_i'}{(1+e)} - \frac{(E_i')^2}{(1+e)^2}$$

where

$$E_i' = 2\ \mathrm{STK}\sqrt{e} + 2\ \mathrm{STK}^2(d)\exp\left[\frac{1}{\mathrm{STK}\sqrt{e}}\right] - 2\mathrm{STK}^2 e$$

$e = \sqrt{P}/(1 - \sqrt{P})$

P = filter porosity = .094 (ref. 21)

STK (Stokes number) = $mq/(6\eta r R_o)$

m = mass of single particle (gm)

r = radius of particle (cm)

q = face velocity at filter

R_o = pore radius of clean filter = 0.1×10^{-4} cm

η = viscosity of air (poise)

$\eta = 185 \times 10^{-6}$ poise T 25°C

q = 3 cm/sec when V_o = 711 cm/sec

$e = \sqrt{.094}/(1 - \sqrt{.094}) = .44$

Assume specific gravity = 1 (conservative)

$m = 4/3\ \pi r^3$

Table C-1. E_i for Values of Particle Diameter

D um	r $\times 10^{-4}$ cm	m gm	STK —	E_i' —	E_i' —
.1	.05	1.25×10^{-16}	6.74×10^{-3}	.0089	.012
.15	.075	$.42\times10^{-15}$	1.51×10^{-2}	.020	.028
.2	.10	1.00×10^{-15}	2.7×10^{-2}	.0358	.0497
.3	.15	1.41×10^{-14}	2.43×10^{-1}	.322	.447

2) Partial efficiency of diffusion

$E_D = 1 - .81904 \exp\left[-3.6568\, N_D\right] - \ldots$

where

$$N_D = \frac{LDP}{R_o^2 q}$$

L = filter thickness (cm) = 12×10^{-4} cm

D = aerosol particle diffusivity (cm^2/sec)

P = filter porosity = 0.094

R_o = pore radius = 0.1×10^{-4} cm

q = 3 cm/sec

Table C-2 E_D for Values of Particle Diameters

Diam. um	D (ref.11)	N_D	E_D
.02	1.4×10^{-4}	52.6	1.00
.04	3.6×10^{-5}	13.7	1.00
.10	6.8×10^{-6}	2.58	1.00
.15	3.4×10^{-6}	1.29	.993
.20	2.2×10^{-6}	.84	.962
.30	1.24×10^{-4}	.47	.853

3) Partial efficiency of Interception

$E_R = N_R(2-N_R)$

$N_R = r/R_o$ if $N_R > 1$ efficiency is 1

r = particle radius

$R_o = 0.1 \times 10^{-4}$ cm

Table C-3. E_R for Values of Particle Diameter

D um	r 10^{-4}cm	N_R	E_R	$.15E_R$
.04	.02	.2	.36	.054
.10	.05	.5	.75	.11
.20	.10	1.00	1.00	.15
.21	.105	1.05	1.00	1.00

The partial efficiencies are tabulated and combined in Table 1.

APPENDIX D

COMPUTATIONS FOR K IN TABLE 2

$$C = 1 + \frac{1.62}{D_p} 10^{-5} + \frac{.55\text{x}10^{-5}}{D_p} \text{EXP}(-.67 \text{ x } 10^5 D_p)$$

D_p	C
$1 \text{ x } 10^{-4}$	1 + 1.62 + .0000677 = 1.16
$1 \text{ x } 10^{-6}$	1 + 16.2 + 5.14 = 22.34

APPENDIX E

PROCEDURE FOLLOWED BY McCRONE ASSOCIATES FOR ELECTRON MICROSCOPY AND ELECTRON DIFFRACTION

Shimps outlines analytical procedures practiced by McCrone Associates in the following excerpted letter. (14)

> "The sampling procedure is our standard one for both the SEM and TEM examinations.
>
> For the TEM, a square of filter 3 mm on a side is cut out and placed sample side down on a TEM grid with a carbon substrate. This preparation is then placed on a stainless steel mesh support on a cold finger in a condensation washer where the filter dissolves and thus deposits the sample material on the carbon substrate.
>
> For the SEM, a square of filter is cut and placed on adhesive on an SEM stub. First carbon and then gold is vacuum evaporated on the specimen so that it may be examined in the SEM."

APPENDIX F

MASS CONCENTRATION DATA

The following -1 tables represent a condensed tabulation of most of the data observations for each sample during the sampling. Each -1 table is followed by a -2 table which includes net sample weight, mass concentration at actual conditions (gm/acf) and mass concentrations at standard conditions (gm/scf).

Although moisture in the air stream was monitored, sampled volumes were not corrected for it as the correction was small. The following calculations give conservative estimates of the corrections.

a. given: $T_{STACK} = 30^{o}C$

Rel Humid = 25%

$P_{bar} = 28.4$ in.

Vapor Pressure = 31.824 mm = 1.25 in (ref. 16)

Percent Moisture in air - $\frac{V.P.x(R.H.)}{P_{bar}} = R = 1.10\%$

b. given: Same as a) except Rel. Humid - 100%

Percent Moisture = $\frac{1.25 \times 100\%}{28.4} = 4.4\%$

Condition a was probably not exceeded during the sampling. The equation for the isovelocity factor I is

$$I = \frac{T_{STACK}(P_{STD}/T_{STD})(V_{MSTD} + V\ _{STD})}{\Delta Time\ V_{STACK}\ P_{bar_{STACK}}\ A_{nozzle}}$$

$$= \left(\frac{V_{m_{ACT}}}{\Delta Time\ V_{STACK}\ A_{nozzle}}\right) X \left[\left(\frac{T_{STACK}}{P_{bar_{STACK}}}\right)\left(\frac{P_{bar}}{T_{m_{AVC}}}\right)(1+R)\right]$$

$$= (\quad I' \quad) \times (\quad C \quad)$$

where P_{STD} = 29.92 inches

T_{STD} = 298°K

$V_{m_{STD}}$ = standardized meter dry volume

$V_{w_{STD}}$ = volume of water vapor

V_{STACK} = STACK gas velocity

A_{nozzle} = .000085 ft^2 (1/8 in)

P_{bar} = Atm P at dry gas meter

$T_{m_{AVG}}$ = average dry gas meter temperature

$R = V_{w_{STD}}/V_{m_{STD}} = 0$

I' = approximate I

C = Correction factor

Tables -1 also provide the I' and C numbers. In tables -2, actual concentrations are standardized by multiplying by 1/SC where

$$ACF \times \frac{P_{meter}}{P_{STD}} \times \frac{T_{STD}}{T_{meter}} = ACF \times SC$$

Table F-1A. Zinc Sampling Data as Observed
Pitot ΔP = .12   SAP = 20 psi

	Sample #	13	15	18	19	31	32
	Date	1/6/75	1/6	1/14	1/14	2/14	2/14
	P_{bar}	29.34	29.34	29.11	29.11	29.51	29.51
	Chamb T	19	20	17.5	16.5	19°	19°
2	HEPA ΔP	.60	.60	.4	.4	.90	.9
3	P_{STACK}=①-②/13.6	29.30	29.30	29.08	29.08	29.4	29.4
	Venturi ΔP	.20	.20	.20	.20	.20	.20
	STACK T(°C)	17	19	19	19	23	19
	Wirefeed	30	50	50	30	30	30
	Amps	25	60	60	30	30	30
	MAP	70	70	70	70	50	50
	ΔH orif	.07	.065	.065	.065	.065	.062
	ΔCF	.389	.350	.256	.325	.481	.392
	Δ Time(min.)	3	3	2	2.51	3.5	3
	acfm	.130	.117	.128	.130	.137	.131
	T_{mave}(°F)	72	72	74	76	71	74
4	Nozzle vel.	1529	1376	1506	1529	1616	1539
5	Stack vel.	1394	1399	1404	1404	1409	1397
	I' = ④/⑤	1.10	.98	1.07	1.09	1.15	1.10
	Rel Humid	12%	12%	20%*	20%*	20%*	20%*
	C	.98	.99	.99	.98	1.01	.99

Table F-2A. Standardized Mass Concentration Data

$I = I' \times C$	1.08	.97	1.06	1.07	1.16	1.09
Net wt. gain	.0095	.0188	.0144	.0114	.0101	.0074
gm/acf	.0244	.0536	.0563	.0350	.0210	.0190
1/sc	1.010	1.010	1.024	1.024	1.007	1.007
gm/scf	.0246	.0541	.0577	.0358	.0211	.0191

* estimated

Table F-1B. Zinc Sampling Data as Observed
Pitot ΔP = .12 SAP = 20 psi

Sample #	33	34	35	36	37	38
Date	2/14	2/14	2/14	2/14	2/18	2/18
P_{bar}	29.51	29.51	29.51	29.51	28.54	28.54
Chamb T	20°	20°	28	28	31	29
HEPA ΔP	1.09	1.09	1.09	1.09	1.0	.8
P_{STACK} in.	29.43	29.43	29.43	29.43	38.47	28.49
Vent. ΔP	.20	.19	.21	.21	.20	.20
Stack T(°C)	20	23	25	26	28	24
Wirefeed	30	30	50	50	50	50
Amps	30	30	70	70	70	70
MAP	50	70	70	68	50	50
ΔH orif	.06	.058	.055	.055	.055	.052
ΔCF	.816	.779	.476	.487	.395	.539
Δ Time(min.)	6.0	6.0	4.0	4.0	3.0	4.0
acfm	.136	.129	.119	.122	.132	.135
T_{mave}(°F)	75	77	79	78	66	64
Nozzle vel.	1600	1527	1400	1432	1549	1585
Stack vel.	1401	1409	1416	1418	1439	1431
I' =	1.15	1.09	.99	1.01	1.07	1.11
Rel. Humid	20%*	20%*	20%*	20%*	20%*	20%*
C	.99	.99	1.00	1.00	1.03	1.00

Table E-2B. Standardized Mass Concentration Data

$I = I' \times C$	1.14	1.08	.99	1.01	1.10	1.11
Net wt. gain	.0143	.0218	.0268	.0305	.0113	.0163
gm/acf	.0175	.0280	.0563	.0626	.0286	.0302
1/sc	1.013	1.013	1.018	1.018	1.025	1.025
gm/scf	.0177	.0284	.0573	.0637	.0293	.0310

Table F-1C. Zinc Sampling Data as Observed

Pitot ΔP = .12 SAP = 20 psi

Sample #	40	44	45	46
Date	2/18	2/18	2/25	2/25
P_{bar}	28.54	28.54	29.11	29.06
Chamb T	30	23.5	27	30
HEPA ΔP	.8	.8	.70	.70
P_{STACK}	28.48	28.48	29.06	29.06
Vent ΔP	.20	.20	.20	.215
Stack T	25	22	28	28
Wirefeed	50	30	30	30
Amps	70	30	25	25
MAP	50	50	70	70
ΔH orif	.05	.05	.04	
ΔCF	.478	.471	.766	.355
Δ Time	4	4.11	6.0	2.79
acfm	.120	.115	.128	.127
T_{mav}	63.5	63	79	80
Nozzle vel.	1406	1348	1502	1497
Stack Vel.	1434	1424	1427	1427
I'	.98	1.06	1.05	1.05
Rel. Humid	20%	20%	25%	25%
C	1.01	1.00	1.01	1.00

Table E-2C. Standardized Mass Concentration Data

$I = I' \times C$	.99	1.06	1.06	1.05
Net weight gain	.0162	.0082	.0260	.0081
6) gm/acf	.0339	.0174	.0339	.0228
7) 1/sc	1.025	1.025	1.0056	1.0056
8) gm/scf	.0347	.0178	.0341	.0229

APPENDIX G

G-1. HYPOTHESIS TESTS OF THE MEANS OF THE MASS CONCENTRATIONS

The Smith Satterthwaite test requires no assumption in equality of variance, which makes it a powerful test. It does assume that the observed values in a given sample are normally distributed, however.

Generally:

H_0: $\mu_1 = \mu_2$

H_1: $\mu_1 > \mu_2$

Reject H_0 if $t' > t_\alpha$

where μ_1 = true but unknown condition #1 population of mass concentrations

H_0 = Null hypothesis

H_1 = First alternative hypothesis

$$t' = \frac{\overline{X}_1 - \overline{X}_2}{\frac{S_1^2}{n_1} + \frac{S_2^2}{n_2}}$$

$$\nu = \text{degrees of freedom} = \frac{\left(\frac{S_1^2}{n_1} + \frac{S_2^2}{n_2} \right)^2}{\frac{(S_1^2/n_1)^2}{n_1 - 1} + \frac{(S_2^2/n_2)^2}{n_2 - 1}}$$

t_α = value in tables for t as function of ν and α

α = significance level = probability of rejecting the null hypothesis when it is true.

$\overline{X}_1$ = observed mean of sample #1

S_1 = standard deviation from sample #1

n_1 = number of observations in sample #1

Specifically, for $\bar{X}_1$ and $\bar{X}_2$ (see Table 9A)

H_o: $\mu_1 = \mu_2$

H_1: $\mu_1 > \mu_2$

$\alpha = 0.05$

$t' = 3.2$ $\nu = 2.2$

$t_\alpha = 2.8$ (Table IV, ref. 19)

$t' > t_\alpha$

H_o is rejected. Therefore we conclude $\mu_1 > \mu_2$

Considering $\bar{X}_1$ and $\bar{X}_3$

H_o: $\mu_3 = \mu_1$

H_1: $\mu_3 > \mu_1$

$\alpha = 0.05$

$t' = 7.43$ $\nu = 6.94$

$t_\alpha = 1.9$

$t' > t_\alpha$

H_o is rjected. Therefore we conclude $\mu_3 > \mu_1$

Continuing with $\bar{X}_2$ and $\bar{X}_3$

H_o: $\mu_3 = \mu_2$

H_1: $\mu_3 > \mu_2$

$\alpha = 0.05$

$t' = 18.4$ $\nu = 3.8$

$t_a = 2.15$

$t' > t_\alpha$

H_o is rejected. Therefore we conclude $\mu_3 > \mu_2$

G-2. HYPOTHESIS TESTS OF THE MEANS AND VARIANCES OF REPLICATE PARTICLE SIZE DATA

This method(19) employs a simpler hypothesis procedure than described in G-1 because the sample sizes are well over 30, thus eliminating the need for a degrees of freedom calculation. The first criterion for replicate reproducibility is equality of the true mean diameters.

Generally $H_0\colon \mu_1 = \mu_2 \qquad (\bar{D}_1 > \bar{D}_2)$

$H_1\colon \mu_1 \neq \mu_2$

μ_1 = true but unknown diameter of replicate 1 > population

$\bar{D}_1$ = mean of replicate 1 (best estimate of μ_1)

$$Z^* = \frac{\bar{D}_1 - \bar{D}_2}{\left((S_1^2/n_1) + (S_2^2/n_2)\right)^{1/2}}$$

Reject H_0 if $Z^* > Z_{\alpha/2}$

For condition 2 (see Table 11);

$D_1 = 10.8 \qquad S_1^2 = 35.59 \qquad n_1 = 350$

$D_2 = 9.1 \qquad S_2^2 = 41.14 \qquad n_2 = 280$

$$Z^* = \frac{10.0 - 9.1}{\left(\frac{35.6}{350} + \frac{41.1}{280}\right)^{1/2}} = 1.73$$

For $\alpha = 0.05 \qquad Z_{\alpha/2} = 1.96$

$Z^* < Z_{\alpha/2}$

H_0 cannot be rejected. Therefore we conclude $\mu_1 = \mu_2$

For condition 3:

$\bar{D}_1 = 10.8$ $S_1^2 = 28.14$ $n_1 = 376$

$\bar{D}_2 = 10.4$ $S_2^2 = 21.96$ $n_2 = 281$

$Z^* = 0.92$ $Z_{\alpha/2} = 1.96$ $\alpha = 0.05$

$Z^* > Z_{\alpha/2}$

H_0 cannot be rejected. Therefore we conclude $\mu_1 = \mu_2$.

A second criterion for replicate reproducibility is equality of the true variances. Generally

H_o: $\sigma_1^2 = \sigma_2^2$

H_1: $\sigma_1^2 \neq \sigma_2^2$

Reject H_o if $F > F_{\alpha/2}\ (n_1-1,\ n_2-1)$

where $F = S_1^2/S_2^2$

n = sample size

Applying this to conditions with means that are not significantly different, for condition 2

$S_1^2 = 41.14$ $n_1-1 = 279$

$S_2^2 = 35.59$ $n_2-1 = 349$

$$F = \frac{41.14}{35.59} = 1.16$$

for $\alpha = 0.02$ $F_{\alpha/2}(279,\ 349) = 1.32$

$F < F_{\alpha/2}$ and H_0 cannot be rejected. Therefore we conclude $\sigma_1^2 = \sigma_2^2$.

For condition 3 $S_1^2 = 28.14$ $S_2^2 = 21.96$

$$F = \frac{28.14}{21.96} = 1.28$$

for $\alpha = 0.02$ $F_{\alpha/2}\ (375,\ 280) = 1.32$

$F < F_{\alpha/2}$ and H_0 cannot be rejected.

Therefore we conclude $\sigma_1^2 = \sigma_2^2$.

G-3. HYPOTHESIS TESTS OF THE MEAN DIAMETERS OF CONDITIONS 2 AND 3

Generally, the analysis is similar to the ones for replicate reproducibility. The means and variances for each condition are first averaged.

For condition 3

Let $\bar{D}_1 = \frac{376(10.8) + 281(10.4)}{376 + 281}$

$\bar{D}_1 = 10.6$

$S_1^2 = \frac{376(28.14) + 281(21.96)}{376 + 281}$

$S_1^2 = 25.50$

$S_1 = 5.05$

For condition 2

$\bar{D}_2 = \frac{9.13(280) + 9.99(350)}{280 + 350} = 9.6$

$S_2^2 = \frac{280(41.14) + 350(35.59)}{280 + 350} = 38.06$

$S_2 = 6.17$

H_0: $\mu_1 = \mu_2$

H_1: $\mu_1 \neq \mu_2$

$$Z^* = \frac{\bar{D}_1 - \bar{D}_2}{\left((S_1^2/n_1) + (S_2^2/n_2)\right)^{1/2}} = \frac{1.0}{0.32} = 3.17$$

For $\alpha = 0.05$ $\quad Z_{\alpha/2} = 1.96$

$Z^* > Z_{\alpha/2}$ and H_0 is rejected . Therefore we conclude $\mu_1 \neq \mu_2$. The mean sizes of particles from conditions 2 and 3 are therefore considered to be significantly different.

G-4. KOMOGOROV - SMIRNOV FITNESS TESTING

Applying the one sample test to the samples in condition 2 (Table 12)

D_{max} (sample 133) = 0.103

for $\alpha = 0.05$ $D\alpha = 1.36/\sqrt{n}$ n = sample size = 350 $D_{\alpha} = 0.073$ (19)

$D_{max} > D\alpha$ Sample 133 does not fit the given distribution at 5% level of significance

D_{max} (sample 134) = 0.140

for $\alpha = 0.05$ n = 280 $D\alpha = 0.081$

$D_{max} > D\alpha$. Sample 134 does not fit the given distribution at the 5% level of significance.

The two sample test is also applied at $\alpha = 0.05$.

$D_{\alpha} = 0.12$ reference (20)

$D_{max} = (0.37-0.23) = 0.14$

$D_{max} > D_{\alpha}$. Therefore Samples 133 and 134 have significantly different distributions.

Applying the one sample test to the condition 3 samples (Table 13)

$D_{max_{104}} = 0.0688$ n = 376 $\alpha = 0.05$ D $= 0.070$

$D_{max} < D_{\alpha}$

Sample 104 fits the normal distribution

$D_{max_{128}} = 0.0844$ n = 281 $D_{\alpha} = 0.081$ $\alpha = 0.05$

$D_{max} > D_{\alpha}$; Sample 128 does not fit the distribution.

Applying the two sample test to condition 3 samples

$D_\alpha = 0.12$ at $\alpha = 0.05$ (19)

$D_{max} = (0.83-.71) = 0.12$

$D_{max} < D_\alpha$; Samples 104 and 128 do not have significantly different distributions.

G-5. SUMMARY OF STATISTICAL TESTS

The above statistical tests, applied to mass and size count data are summarized.

Mass Concentration-Comparing Conditions

$\mu_1 > \mu_2$ $\mu_3 > \mu_2$ $\mu_3 > \mu_1$

Particle Sizing

Replicate Reproducibility

Condition 1	Condition 2	Condition 3
$\mu_{101} \neq \mu_{125}$	$\mu_{133} = \mu_{134}$	$\mu_{104} = \mu_{128}$
	$\sigma_{133} = \sigma_{134}$	$\sigma_{104} = \sigma_{128}$

Differences between conditions

$\mu_2 \neq \mu_3$

Frequency Distribution

a) Closeness of fit to normal distribution
133 and 134 do not fit
104 fits but 128 does not

b) Closeness of fit to each other - Reproducibility
133 and 134 are different
104 and 128 fit

APPENDIX H

ELECTRON MICROSCOPY PHOTOGRAPHS

The following photographs were selected by the investigator as typical of all the photographs of the 6 samples analyzed by McCrone Associates.

The reproductions are not altered with regard to magnification. The prints are reproduced from negatives made by Copycat, Inc., Morgantown, using the McCrone photographs.

Figures H-1 and H-2 indicate the light colored chain like agglomerates against the porous Nucleopore filter background. The "dark holes" represent the 0.2 μm pores.

Figure H-3 represents the composition of part of an agglomerate. The particles here are dark and are distinguished by light borders.

Figure H-1. SEM Photograph of Sample 133 (5000X). 1 cm. ≈ 2 μm.

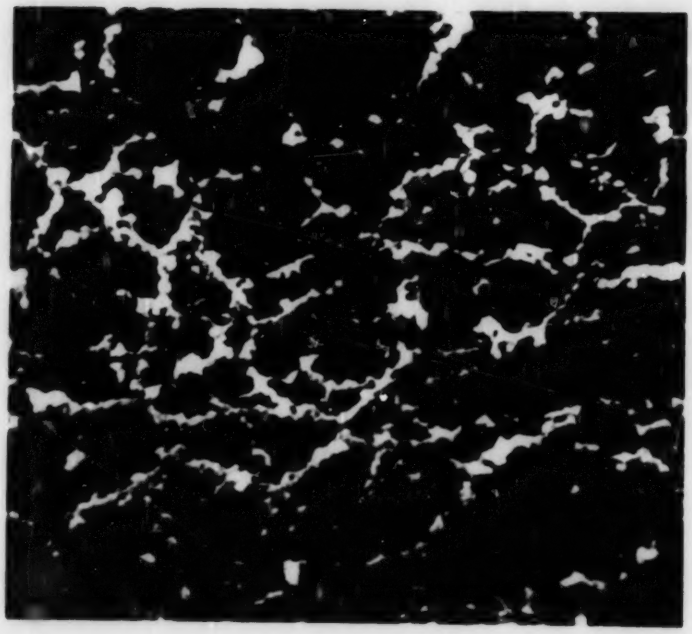

Figure H-2. SEM Photograph of Sample 133 (10000X). 1 cm. ≈ 1 μm.

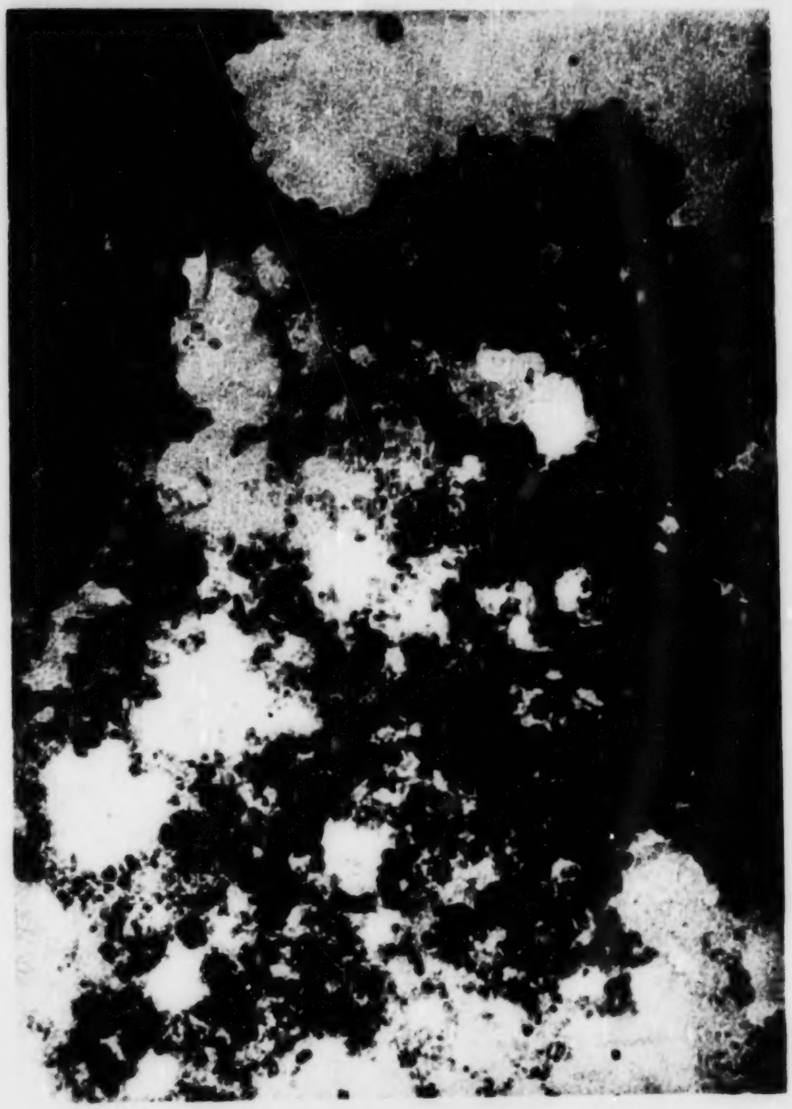

Figure H-3. TEM Photograph of Sample 101
(300,000X)

ELECTRIC ARC GENERATION
OF
FRESH IRON OXIDE AEROSOLS

THESIS

Submitted to the Graduate School
of
West Virginia University
In Partial Fulfillment of the Requirements For
The Degree of Master of Science in Engineering

by

William Fred Dimmick II, A.B.

Morgantown,
West Virginia

1977

ABSTRACT

ELECTRIC ARC GENERATION OF FRESH IRON OXIDE AEROSOLS

The development of a fresh metal oxide fine particle aerosol generator was needed to provide necessary true-to-life conditions for testing air pollution control and measurement equipment. A generator of fresh aerosols was considered to be applicable to toxicological studies. An electric arc metallizer employing dual consumable electrode wires was developed for fresh metal oxide aerosol generation with the guidance of Professor Benjamin Linsky. The present engineering problem consisted of characterizing the aerosols produced by the generator when metallizing steel feed stock and investigating the influence of operation variables on the conversion of mass from solid wire to aerosol particles.

Generation of fine particle aerosols was done using a commercially available electric arc metallizer to spray melted and vaporized feed stock electrode wires into a 55 gallon barrel. The spray generated aerosol was exhausted through a duct work.

The generated aerosols were sampled on membrane filters for subsequent particle size count analysis using scanning electron microscopy and transmission electron microscopy. The same samples were analyzed for chemical composition by selected area electron diffraction.

Membrane filters were also used to capture mass samples for determining the mass concentration of the aerosol in the exhausting duct works. The mass concentration was used as the dependent variable in a Latin Square designed experiment where operation adjustments of the equipment as manufactured were the independent variables. These independent variables were the wire feed rate, the open voltage across the arc, and the

pressure of the compressed air jet used to form the spray.

The data shows the aerosols to be composed of agglomerated particles formed from very fine magnetite particles. The agglomerated particles had a mean size of 0.4 μm by count whereas the very fine particles have mean count diameters ranging from 0.0054-0.009 μm (5.4-9nm). At three different operating conditions three different very fine particle means were found. Each of these conditions produced an unique particle size distribution.

The mass concentration Latin Square experimental design found the wire feed rate and the open voltage to influence changes in the mass concentration of the aerosol. A maximum mass concentration was found to be approximately 2 gm/m^3. The variability produced by replication of a data set was found to be significant.

In conclusion, the generator was found to produce very fine ferrous particles that agglomerated into submicron sized particles. Evidence suggests that, with further characterization of the agglomerated very fine particle aerosols, the generator will produce true-to-life fresh aerosols with reproducible properties. The aerosol mass concentration was considered to be adequate for testing of air pollution control and measurement equipment.

ACKNOWLEDGMENT

The author wishes to graciously thank everyone involved in the completion of the research. His major professor and advisor, Professor Benjamin Linsky, introduced him to the field and concepts of fine particles. His colleague Mike Naylor taught him the set up and operation of the aerosol generating apparatus. Don Stone and Craig Repp, fellow graduate students, helped in the collection of samples. Craig Repp and the author designed and built a metallizing wire dispenser to deliver feedstock from 50 pound wire coils to the generating apparatus.

The author expresses gratitude for helpful suggestions from Mr. Charles Ghastin of the Wall Colmonoy Corporation and Mr. Richard Shimps of McCrone Associates. Suggestions and questions from Dr. S. R. Borbash of the Industrial Engineering Department at West Virginia University guided the researcher's statistical analysis.

The author was a graduate air pollution trainee under Environmental Protection Agency grant numbers T900567010 and T900567020. The financial support for this research was funded as part of Environmental Protection Agency grant R-801858-01-1.

The author thanks his wife, Linda, for her patience during the time of his presently completed studies.

TABLE OF CONTENTS

Page

ABSTRACT 3-ii

ACKKNOWLEDGEMENT 3-iv

LIST OF TABLES 3-vii

LIST OF FIGURES 3-ix

LIST OF SYMBOLS, ABBREVIATIONS, AND CONSTANTS 3-x

INTRODUCTION 3-1

STATEMENT OF ENGINEERING OBJECTIVES 3-2

REVIEW OF PERTINENT LITERATURE 3-3

PROCEDURE 3-6

  Equipment and Materials 3-6
  Operation of Generator Apparatus 3-10
  Sampling 3-11
  Phenomenon Characterization Techniques 3-11
  Experiment: Analysis of Phenomenon 3-13
  Data 3-16

ANALYSIS OF DATA 3-30

  Agglomerates 3-30
  Fine Particles 3-33
  Mass 3-46

DISCUSSION OF RESULTS 3-51

  Agglomerates 3-51
  Fine Particles 3-51
  Chemical Composition 3-53
  Mass Analysis 3-54

CONCLUSIONS 3-57

BIBLIOGRAPHY 3-60

APPENDICES 3-62

  Appendix A 3-63
  Appendix B 3-64
  Appendix C-1 Particle Sizing Pictures 3-65
  Appendix C-2 Sizing of the Agglomerates 3-66

TABLE OF CONTENTS (continued)

Appendix C-3 Mass Concentration Data 3-68
Appendix D-1 Latin Square 3-81
Appendix D-2 T Test Procedure 3-84
Appendix D-3 ANOVA 3-88
Appendix D-4 Stepwise Procedure 3-89
Appendix D-5 GLM and Residual Plots 3-92
Appendix E 3-100

LIST OF TABLES

Page

1. Hobart steel metallizing wire (HB 18) Assay 3-10
2. Aerosol generator operating conditions for particle size analysis 3-14
3. Comparison study operating conditions 3-14
4. Determination of orthogonal data collection points 3-15
5. Agglomerated data corrected for magnitude of magnification: sample 715 3-17
6. Agglomerated data corrected for magnitude of magnification: sample 714 3-17
7. Very fine particle distributions: set 1 3-18
8. Very fine particle distributions: set 2 3-20
9. Very fine particle distributions: set 3 3-22
10. Very fine particle distributions: set 4 3-23
11. Very fine particle distributions: samples 712 and 716 3-24
12. Selected area electron diffraction data 3-25
13. Diffraction lines for magnetite and maghemite 3-25
14. Latin square mass concentration data summary (gm/m^3) 3-26
15. Orthogonal mass concentration data summary (gm/m^3) 3-27
16. A listing of all the mass concentration data 3-28
17. Two means equality test hypothesis decision-making criteria 3-31
18. Statistics for agglomerate samples 3-33

LIST OF TABLES (continued)

19. Statistics for fine particle distributions 3-40

20. Within group t-statistics for fine particle samples 3-41

21. Between group t-statistics for fine particle samples 3-42

22. Within group chi-square statistics 3-44

23. Between group chi-square statistics 3-45

24. Analysis of variance for latin square experimental design 3-47

25. SAS ANOVA for latin square experimental design data 3-48

26. SAS GLM table for orthogonal data 3-49

27. SAS GLM table for all of the data 3-50

28. Raw data for agglomerated particle count 3-67

29. Mass data for first latin square experiment . . . 3-71

30. Mass data for second latin square experiment . . . 3-75

31. Mass data for orthogonal experiment 3-79

32. Formula and definitions for latin square analysis of variance 3-82

33. Calculation table for latin square design 3-83

34. SAS T Test table 3-87

35. Stepwise regression procedure for dependent variable Y 3-90

36. SAS GLM table including residuals 3-93

37. Relating wire feed rate and percent mass converted 3-100

LIST OF FIGURES

Page

1. Equipment set up with close up of arc gun assembly 3-8
2. Example of data sheet 3-12
3. Set 1 frequency distributions 3-35
4. Set 2 frequency distributions 3-36
5. Set 3 frequency distributions 3-37
6. Set 4 frequency distributions 3-38
7. Sample 712 and 716 frequency distributions 3-39
8. Histograms of agglomerated particles 3-52
9. SEM picture sample 715 3-65
10. SEM picture sample 714 3-65
11. Explanation of data sheet and mass calculation symbols 3-70
12. Graph: wire feed rate versus standard residual 3-96
13. Graph: open voltage versus standard residual 3-97
14. Graph: predicted outcome (Yhat) versus standard residual 3-98
15. Graph: order of presentation versus standard residual 3-99
16. Wire feed rate calibration 3-101

LIST OF SYMBOLS, ABBREVIATIONS AND CONSTANTS

ANOVA = analysis of variance

GLM = general linear model

T Test = a statistical test based on the t-distribution

SS = sum of squares

df = degrees of freedom

Yhat = predicted outcome from an estimated descriptive equation

SEM = scanning electron microscopy

TEM = transmission electron microscopy

SAED = selected area electron diffraction

lines

d Å = diffraction lines in angstroms (Å)

HEPA = high efficiency particulate air

R# = reynolds number

P_{bar} = ambient barometric pressure

P_{duct} = pressure in exhaust duct

HEPA Δp = pressure drop across HEPA filter

Venturi Δp = pressure drop across calibrated venturi

Pitot Δp = velocity pressure differential as measured by a standard pitot tube

Duct T = temperature in exhaust duct

Bag T = temperature within bag house

V_{open} = open voltage across electrodes

AMPS = electrical current in amperes

LIST OF SYMBOLS, ABBREVIATIONS AND CONSTANTS (continued)

MAP = main air jet pressure at machine

SAP = secondary air supply pressure

ΔH orifice = manometer differential on RAC sampler

CF start = dry gas meter reading before sampling

CF end = dry gas meter reading after sampling

ΔCF = sample volume

ΔT = time of sampling in minutes

$T_{meter-start}$ = temperature of RAC thermometer at beginning of sampling

$T_{meter-end}$ = temperature of RAC thermometer at end of sampling

V_{duct} = velocity of gas stream in exhaust duct

STP = standard temperature (273 °K) and pressure (1 atmosphere)

$gm/m^3 = gm/sm^3$ = grams per standard (STP) cubic meters

gm/a_{cf} = grams per actual cubic feet

fpm = feet per minute

g = acceleration due to gravity

ρ = density

μ = dynamic viscosity

d = circular diameter

LIST OF SYMBOLS, ABBREVIATIONS, AND CONSTANTS (continued)

1Å = 10^{-10}m = 10^{-8}cm = 10^{-7}mm = 10^{-4} μm = 10^{-1}nm

grains/ft^3 x 2.288 = grams/m^3

(°F-32) x 5/9 = °C

ft^3/minute x 0.0283 = m^3/minute

diameter = a physical quantity

INTRODUCTION

The generation of fresh dry metal aerosols for experimental analysis, whether it is testing fabric filters for particle penetration or examining the effect of inhaled cadium oxide particles on hamster kidneys, is a necessity for proper similitude to many industrial events. The known discrepancy between the occurrence of brass fever after exposure to "fresh" zinc oxide fumes and the lack of occurrence with exposure to stale, redispersed zinc oxide fumes (14) expresses the validity of discriminating between fresh and stale particles. Again, the fact that the emission of fine particles as air pollutants has received increasing attention in the past nineteen years (7) implies the concurrent need of fine particle aerosol generators for evaluation of engineering designs. Eugene Grassel (4) states recent scrutiny of fine particles in the atmosphere is producing an aerosol generator market.

A characteristic of fine particulate aerosols is the small rate at which the particles settle due to the force of gravity. In Appendix A, it is shown that a 0.5 μm diameter solid spherical particle with a unit density of one gram per cubic centimeter falls less than one-half centimeter in one hour (approximately four and a half inches per day). This property virtually eliminates the possibility of fine particles settling quickly by gravity to earth's surface. Presumably, the particles are blown about the atmosphere by winds.

Fine particles can absorb and scatter light. Aerosols with particles in the size range of visible light extinguish light (8). Waggoner and Charlson (18) state that blue hazes in mountainous areas may or may not be due to scattering by particles. There should be no haze unless there are particles between the observer and the mountain if the mountain is closer than 10 km (7 miles). They also say that light scattering increases with humidity, but for relatively hygrophobic systems the increase may be very slight. Certainly extinction increases with an increase in the light extinguishing particle number in the atmosphere.

As shown in Appendix B, a unit density spherical particle of diameter 0.1 μm weighs one thousand times greater than a unit density spherical particle with a 0.01 μm diameter. Any air pollution emission criterion that relies only on measurement by weight is not including all the proper physically descriptive information. The importance of characterizing an aerosol by its particle size distribution has been known in industrial hygiene for decades. Measurement of a fine particulate aerosol without considering the size distribution is incomplete.

STATEMENT OF ENGINEERING OBJECTIVE

Further research with the Electrospray aerosol generator (as described in Equipment and Materials) was needed to provide more information leading to a better engineering characterization for the uses of the equipment and its output. A statistical-design approach was incorporated with the object of furthering the knowledge of the variables of solid feed material to particle mass concentration conversion. These variables as represented in this research were (1) the open voltage across the arc, (2) the wire feed rate, and (3) the pressure of main gas jet which impinges upon the arc to form the metallizing spray. All of these variables were obtainable from adjustment mechanisms routinely supplied as part of the metallizer. The dependent variable (the outcome) was the aerosol mass concentration.

Further characterization of the aerosol produced by the Electrospray aerosol generator was also an objective. Naylor (10) reported on the results of Electrospray production of zinc oxide particle aerosols from zinc consumable electrodes. In the current research, carbon steel wire was used to produce iron oxide aerosols for fine particle size distribution analysis. Both the aerosol characterizing analysis and the mass conversion analysis are analyses in the sense that they examine a system by looking at some of its elements and their relations. A simple comparative experiment also observed the effect on aerosol characteristics of faster gas and particle removal from the chamber (barrel) where the gas and the particles received direct line-of-sight radiation from the arc.

REVIEW OF PERTINENT LITERATURE

Holmgren *et.al*. (6) reported a technique for production of fine particles in a high intensity arc. The feed material was incorporated in the anode and was vaporized as a consequence of the extreme temperatures produced by the arcing. They explained that due to a sudden drop in temperature of the vapor, as it was carried away from the arc, fine particles were formed by condensation.

Particles that ranged from 100 Å to 1000 Å (as measured by electron microscopy) were produced. Mass production rates of 10-20 lb/hr (76-152 gm/min) under a practical running condition were reported for generation of oxide-type materials.

Holmgren et.al. reported the production of Fe_2O_3 particles with an 'equivalent sphere diameter' of 658 Å (65.8 nm, 0.0658 μm). They described the aerosol particles as roughly spheroidal with a distinct trend toward a hexagonal outline. They stated that dispersion about the mean varied with the physical properties of the feed material.

Pfender and Boffa (12) described a method of generating fine particle aerosols in a high intensity arc. Their apparatus included transpiration cooling of the anode to facilitate the production of smaller particles. They stated that with low intensity arcs coagulated and chainlike particles with poorly controlled size distributions are produced. They referenced Holmgren et.al. to state that better results are obtained with high intensity arcs.

Pfender and Boffa (12) reported generation of monodisperse spheroidal shaped particles with a diameter ranging from approximately 100 to 1000 Å as measured by a Whitby analyzer. They did not report the criterion used to determine monodispersity nor the mass production rate.

Formenti et.al. (3) reported the production of fine metal oxide particle aerosol from diffusion burning of volatile metallic chlorides in a hydrogen oxygen flame. They reported generating particles with a range of diameters of 100-2000 Å. They stated that the diameter of the particles and their morphology are controlled by (1) the temperature of the flame, (2) the concentration of chloride injected into the burner, and (3) the residence time of the chloride vapor in the flame. They reported production of Fe_2O_3 particles in a mixture of alpha and gamma phases. They did not report aerosol size distribution dispersity or mass production rate.

Grassell (4) discussed the development of aerosol generators for industrial research with respect to fine particles aerosols. Two basic criteria were used to evaluate the propriety of an aerosol for filter medium testing. These criteria were (1) sufficient quantity of the aerosol for testing a 1000 cfm system and (2) the aerosol should reflect problems of both penetration and cleanability observed in real life situations. Grassell reported the need and development of an aerosol generator for testing air cleaners exposed to diesel exhaust. The generator built from an acetylene burner was relatively stable with day to day reproducibility of filter media loadings varying by a factor of 10 when using repetitive settings of controls.

Robert Hedden (5) working with Linsky developed an arc generator of a fine particle aerosol. A single consumable electrode functioning as an anode was vaporized by the heat generated by the arc. The vaporized metal condensed as it was quenched by a passing air stream to form fine particles. The iron oxide particles were sized by electron microscopy to have an average diameter of 22 nm (220 Å). The mass production rate was found to be 1.95 gm/minute. Hedden characterized by weight the aerosol as containing 75% particles with effective diameter less than 0.1 μm.

Mike Naylor (10) working with Dr. Richard Sears under Linsky reported experimental results on a two consumable wire electrode, electric arc aerosol generator. Naylor produced zinc oxide aerosols with the generating apparatus. The apparatus consisted of a commercially available electric arc metallizer, a settling barrel and an aerosol exhausting system. The same generator unit was employed to produce aerosols for this report.

The consumable electrodes were melted and vaporized in the intense heat of the arc and subsequently the vapor condensed into fine particles in an air stream. These fine particles were found in agglomerated chains as well as individually. Naylor reported a range of average diameter sizes from 6-11 nm as measured by transmission electron microscopy (TEM). A mass concentration of 0.65-2.0 gm/m^3 was found by Naylor at approximately 7.8 m^3/minute. This is a production rate of 5-15.6 gm/minute.

Amson (1) stated that even though erratic behavior of the consumable-electrode arc system is not rare, choosing a suitable power source and ambient gas with suitable settings for the open-circuit voltage and the wire electrode feed speed often leads to the system operating in a 'quasi-steady state' mode. He reported that the electrode voltage drop plays a very small part in the behavior of the consumable electrode system. A decisive part is played by the electrode stick out only when high resistivity electrodes are employed. The electrode stick out is the portion of the electrode wire from the current transfer tip to the arc.

PROCEDURE

Equipment and Material

The aerosol generating apparatus consisted of an Electrospray metallizer that used an electric arc and a compressed air jet to spray melted and vaporized consumable wire electrodes, a 55 gallon oil drum connected to a supplemental air supply cleaned by a HEPA (High Efficiency Air Particulate) filter, a draft fan with accompanying duct works from the oil drum, and a cloth filter particle collector (See Figure 1). The metallizer system supplied the necessary power and material feed delivery. The duct work and fan provided for exhausting and sampling the aerosol. The baghouse cleaned the particle laden gas stream of most of the particulates.

The metallizer (19) consisted of a power source, dual wire feeding system, and an electric arc "gun." The metallizer power supply was a three phase, 230 volt, 60 cycle AC to DC solid state full wave rectifier. The DC supply could be varied from 20 to 40 volts. The wire feeding system consisted of a reproducibly variable drive motor connected to a pair of interlocking pinch rollers (with tension adjustments), wire straighteners, and wire conduits for simultaneous delivery of the dual feedstock wire electrodes to the arc gun.

The electric arc gun provided the transfer of electric current to the consumable feedstock electrodes and atomization and quenching of the products of the arc. The gun also provided a stationary structure for proper electrode alignment and consistent impingement of the main gas (compressed air) jet on the arc zone by the spray nozzle.

The arc gun was mounted through a cutaway in the lid of the oil drum. A tip shroud which reduced entrainment of particles through the arc zone was mounted on the arc side of the lid. A spacer bar between the gun assembly and the barrel lid permitted connection of a second air supply.

The 55 gallon barrel was set horizontally in a rack to facilitate connection with the metallizer. The barrel's lid clamp was used to hold the lid "air tight" against a tape gasket. An arc gun opening, a

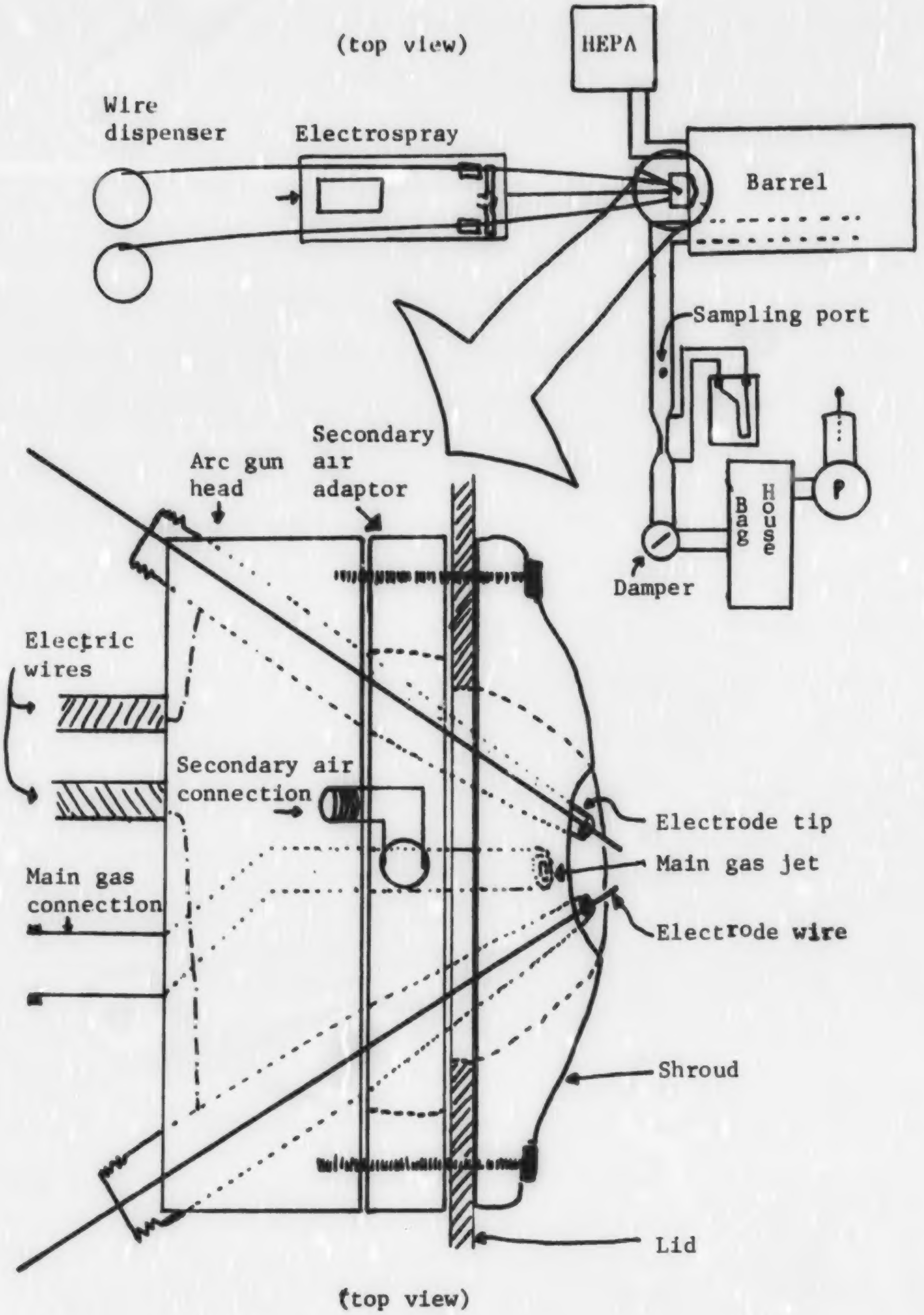
(top view)
HEPA
Wire dispenser
Electrospray
Barrel
Sampling port
Bag House
P
Damper
Arc gun head
Secondary air adaptor
Electric wires
Secondary air connection
Main gas connection
Electrode tip
Main gas jet
Electrode wire
Shroud
Lid
(top view)

Figure 1. Equipment set-up with closeup of arc gun assembly.

filtered diluting make-up air inlet, and an exhaust air outlet were provided in the lid.

The barrel functioned as a settling chamber for the larger particles. Particles larger than 30 μm in diameter were collected with an efficiency of approximately 95% by weight (10). The separation occurred from gravity and a centrifugal force created by the 180 degree rotation of the gas stream upon entering the exhaust duct.

The exhaust duct began one third the distance from the bottom of the barrel. After leaving the barrel, the duct was immediately directed for a straight run of at least 20 pipe diameters to the exhaust system to the baghouse. At a point 10 pipe diameters from the last duct disturbance, the sampling port was located. A calibrated venturi flow meter was placed between the sampling port and the exhaust pipe system to the baghouse. After the venturi, a damper was placed for adjustment of the total air stream flow rate. The cloth filter and fan completed the exhaust duct system.

The sampling train consisted of an RAC stack sampler with Greenburg-Smith impinges connected to the sampling probe. A S-hook nozzle was connected to a membrane filter holder. The filter holder retained an appropriate filter for collecting the aerosol samples.

The stack sampler provided for adjustment of probe tip entrance velocity as well as a measurement of dry gas volumetric flow. The impinger system cooled and then dewatered the gas for measurement by the dry gas meter.

Membrane filters were used to collect samples for subsequent particle count or mass analysis. Membrane filters with 0.45 μm pore sizes were used for mass analysis and filters with 0.20 μm pore sizes were used for particle count analysis. The 0.20 μm membrane filters were also chosen because they provided good surface properties for electron microscopic particle counting.

The wire used in this research was stainless steel welding or metallizing wire. Hobart steel welding wire (HB #18) was used for production of fine particle aerosols for particle count and morphologic analysis. Wall Colmonoy wire #10 was used to produce fine particle aerosols for mass analysis. The following was an assay of the Hobart steel wire (16):

Table 1. Hobart steel metalizing wire (HB 18) assay

Fe	96.84%
Mn	1.90%
Si	0.65%
Mo	0.45%
C	0.12%
P	0.02%
S	0.02%

Operation of Generator Apparatus

The Electrospray control unit was operated with spray settings within the range recommended by Wall Colmonoy (19). The settings for the wire feed rate varied within 30-60 (see Appendix E for units), the open voltage ranged from 20-31 volts, and the main jet pressure ranged from 40-60 psi. The experimenter set the control variables and began operation. If the apparatus ran without sputtering (an audio characteristic of inefficient operation) for two minutes, the apparatus was considered operating stably. The closed voltage (voltage across arc during operation) was not used as a criterion for stability.

Sampling

After generation for at least two minutes, samples were taken either for mass conversion analysis or particle size distribution analysis. Consecutive randomly ordered samples were taken with a two minute shut down between each sampling run.

Sampling for mass analysis consisted of pre-trial determination of isokinetic sampling conditions and then the actual sampling. After adjusting the stack sampler for isokinetic sampling as suggested by the accompanying operation manual (13), samples were taken such that at least 10 mg of mass was deposited on the tared filter. All necessary data was recorded before and during the trials on a form such as in Figure 2.

Sampling the aerosol for subsequent particle size distribution analysis consisted of estimating isokinetic conditions and then collection on appropriate membrane filters with sampling times of three, five and seven seconds. Then, the filters were enclosed in a plastic filter holder and were shipped by United Postal Service to McCrone Associates, Inc. in Chicago for analysis by scanning electron microscopy (SEM), TEM, and selected area electron diffraction (SAED).

Phenomenon Characterization Techniques

The sizing of the fine particles was done by McCrone Associates through TEM with a particle size count of an enlarged photomicrograph. The fine particles counted by size were believed to agglomerate into larger particles prior to sampling. The size limits that the McCrone laboratory considered appropriate for adequate TEM characterization ranged from less than 2 nm to greater than 20 nm by increments of 1 nm.

Wire Type: P_{bar}: Dry Bulb Temperature:
Date: Wet Bulb Temperature:

Sample #

Barrel Temp (°C)

$\boxed{3}$ HEPA Δp

$P_{duct} = P_{bar} - \frac{\boxed{3}}{13.6}$

Venturi Δp

Duct T (°C)

Bag T (°C)

Pitot Δp

Wire Feed Rate

Amps

V_{open}

MAP

SAP

Δ H orifice

CF start

CF end

$\boxed{4}$ Δ CF

$\boxed{5}$ Δ Time

$T_{meter\text{-}start}$

$T_{meter\text{-}end}$

$\boxed{6}$ Nozzle Velocity

CFM ($\boxed{4}$ / $\boxed{5}$)

$\boxed{7}$ $V_{duct} = 234\sqrt{\frac{29.92}{P_{duct}} \cdot (273 + T_{duct})(\text{Pitot } \Delta p)}$

$I = \boxed{6} / \boxed{7}$

Figure 2. Example of data sheet

SEM was used to check samples for the proper laoding (particles per area) necessary for TEM particle sizing. SAED analysis was performed to determine phase characteristics of the particulate matter.

Sizing the agglomerates of fine particles characteristic of the aerosol was done by the experimenter with SEM photomicrographs. SEM negatives were enlarged noting the actual enlargement onto Kodak RC paper as suggested by Mr. Richard Shimps of McCrone Associates (17). The particles were sized with an uncalibrated clear plastic metric ruler. A minimum of 150 particles were counted by size and then corrected to actual size with the known magnitude of magnification.

Mass determination analysis was done by the experimenter weighing the exposed sample membrane filters on an analytical balance accurate to ± 0.5 mg. With the mass determined by the TARE method and sampling volumetric flow (STP) determined, an iron oxide mass concentration was found.

Experiment: Analysis of Phenomenon

Four sets of samples were taken at four different operating conditions for particle size analysis. The conditions were shown in Table 2.

Two sets of samples were taken under identical conditions with the exception that the gas stream velocity within the duct work was varied. These conditions were shown in Table 3.

Mass samples were taken to conform to a Latin Square experimental design. The Latin Square design is explained in Appendix D-1. Two Latin Square designs were randomly chosen and operating conditons (variables) were designated to the statistical design structure. The

Table 2. Aerosol generator operating conditions for particle size analysis

Sample Numbers	Condition Set Number	Wire Feed Rate	Open Voltage	Main Jet Pressure (psi)
600	1	25	20	60
601		25	20	60
602		25	20	60
603	2	25	20	45
604		25	20	45
605		25	20	45
607	3	50	22	60
611		50	22	60
609	4	50	22	45
612		50	22	45

Table 3. Comparison study operating conditons

Sample Number	Condition Set Number	Wire Feed Rate	Open Voltage (volts)	Main Jet Pressure (psi)	Velocity of Gas Stream (fpm)
715	5	50	22	60	1300
716		50	22	60	1300
712	6	50	22	60	1850
714		50	22	60	1850

samples for the structure were randomly ordered and then the samples were taken. Two trials, the second trial a replicating trial, were performed; the trials occurred on different days.

Another set of mass samples were taken to supplement the Latin Square design. A collection of orthogonal points were selected about an observed maximum point in each of the operating variables; a wire feed rate of 60, an open voltage of 29, and a main jet pressure of 45 were considered midpoints. A unit "distance" was added to and subtracted from each midpoint to develop a resulting eight orthogonal samples as follows in Table 4.

Table 4. Determination of orthogonal data collection points

	Wire Feed Rate	Open Voltage (Volts)	Main Jet Pressure (psi)
Midpoint value	60	29	45
Unit distance	5	1	5
Resulting points			
Additive	65	30	50
Subtractive	55	28	40
Resulting samples Condition			
1	65	28	40
2	55	28	50
3	55	30	40
4	65	30	40
5	65	30	50
6	65	28	50
7	55	30	50
8	55	28	40

These resultant sampling conditions were randomly order and then samples were taken.

Data

The aerosol size distributions found for the agglomerated fine particles of sample 714 and 715 were presented in Tables 5 and 6. The percentages of the total number of particles and the cumulative percentages were also given. The raw data uncorrected for the different magnifications were presented in Table 27.

The fine particle size distributions found for the various sets of operating conditions were presented in Tables 7, 8, 9, 10, and 11. The percentages and cumulative percentages were also given.
SEM pictures of the agglomerated very fine particles were shown in Appendix C-1.

In Table 12, the results of the SAED analysis were presented. In Table 13, ASTM electron diffraction lines were given for magnetite (Fe_3O_4) and maghemite (γ-Fe_2O_3).

The mass concentration data from the two Latin Square designs was presented in Table 14. The mass concentration data from the orthogonal collection of data was presented in Table 15. Table 16 contains a listing of all the mass concentration data. The data and method of mass concentration calculation for the Latin Square and the orthogonal designs were presented in Appendix C-3.

Table 5. Agglomerated data corrected for magnitude of magnification: sample 715

Class Mark (μm)	Frequency	Cumulative Frequency	Percent	Cumulative Percent
0.09	141	141	47.0	47.0
0.28	56	197	18.7	65.7
0.43	31	228	10.3	76.0
0.61	23	251	7.7	83.7
0.78	10	261	3.3	87.0
0.96	7	268	2.3	89.3
1.1	11	279	3.7	93.0
1.3	4	283	1.3	94.3
1.5	4	287	1.3	95.7
1.7	3	290	1.0	96.7
1.8	1	291	0.3	97.0
2.3	1	292	0.3	97.3
2.6	8	300	2.7	100.0

Table 6. Agglomerated data corrected for magnitude of magnification: sample 714

Class Mark (μm)	Frequency	Cumulative Frequency	Percent	Cumulative Percent
0.09	156	156	55.3	55.3
0.27	41	197	14.5	69.9
0.46	19	216	6.7	76.6
0.64	17	233	6.0	82.6
0.82	14	247	5.0	87.6
1.0	8	255	2.8	90.4
1.2	7	262	2.5	92.9
1.4	3	265	1.1	94.0
1.6	3	268	1.1	95.0
1.7	6	274	2.1	97.2
2.3	2	276	0.7	97.9
2.5	1	277	0.4	98.2
2.6	1	278	0.4	98.6
2.7	4	282	1.4	100.0

Table 7. Very fine particle distributions set 1

Sample 600

Class Mark (nm)	Frequency	Cumulative Frequency	Percent	Cumulative Percent
1.5	13	13	3.4	3.4
2.5	53	66	13.7	17.1
3.5	53	119	13.7	30.8
4.5	37	156	9.6	40.4
5.5	33	189	8.6	49.0
6.5	23	212	6.0	54.9
7.5	18	230	4.7	59.6
8.5	10	240	2.6	62.1
9.5	18	258	4.7	66.8
10.5	19	277	4.9	71.8
11.5	19	296	4.9	76.7
12.5	17	313	4.4	81.1
13.5	21	334	5.4	86.5
14.5	4	338	1.0	87.6
15.5	7	345	1.8	89.4
16.5	7	352	1.8	91.2
17.5	9	361	2.3	93.5
18.5	3	364	0.8	94.3
19.5	6	370	1.6	95.9
21	16	386	4.1	100.0

Sample 601

Class Mark (nm)	Frequency	Cumulative Frequency	Percent	Cumulative Percent
1.5	8	8	1.8	1.8
2.5	37	45	8.3	10.1
3.5	55	100	12.3	22.4
4.5	65	165	14.6	37.0
5.5	45	210	10.1	47.1
6.5	20	230	4.5	51.6
7.5	15	245	3.4	54.9
8.5	25	270	5.6	60.5
9.5	55	325	12.3	72.9
10.5	16	341	3.6	76.5
11.5	40	381	9.0	85.4
12.5	7	388	1.6	87.0
13.5	9	397	2.0	89.0
14.5	13	410	2.9	91.9
15.5	13	423	2.9	94.8
16.5	2	425	0.5	95.3
17.5	2	427	0.5	95.7
18.5	3	430	0.7	96.4
19.5	6	436	1.4	97.8
21	10	446	2.2	100.0

Table 7. Continued

Sample 602

Class Mark (nm)	Frequency	Cumulative Frequency	Percent	Cumulative Percent
1.5	24	24	5.5	5.5
2.5	79	103	18.2	23.7
3.5	57	160	13.1	36.8
4.5	21	181	4.8	41.7
5.5	25	206	5.8	47.5
6.5	43	249	9.9	57.4
7.5	20	269	4.6	62.0
8.5	20	289	4.6	66.6
9.5	22	311	5.1	71.7
10.5	13	324	3.0	74.7
11.5	33	357	7.6	82.3
12.5	16	373	3.7	85.9
13.5	2	375	0.5	86.4
14.5	6	381	1.4	87.8
15.5	9	390	2.1	89.9
16.5	9	399	2.1	91.9
17.5	12	411	2.8	94.7
18.5	2	413	0.5	95.2
19.5	9	422	2.1	97.2
21	12	434	2.8	100.0

Table 8. Very fine particle distributions set 2

Sample 603

Class Mark (nm)	Frequency	Cumulative Frequency	Percent	Cumulative Percent
1.5	2	2	0.5	0.5
2.5	45	47	12.2	12.7
3.5	58	105	15.7	28.4
4.5	34	139	9.2	37.6
5.5	29	168	7.9	45.5
6.5	18	186	4.9	50.4
7.5	13	199	3.5	53.9
8.5	18	217	4.9	58.8
9.5	30	247	8.1	66.9
10.5	11	258	3.0	69.9
11.5	16	274	4.3	74.2
12.5	14	288	3.8	78.0
13.5	12	300	3.3	81.3
14.5	19	319	5.2	86.5
15.5	7	326	1.9	88.3
16.5	7	333	1.9	90.2
17.5	11	344	2.9	93.2
18.5	4	348	1.1	94.3
19.5	7	355	1.9	96.2
21	14	369	3.8	100.0

Sample 604

Class Mark (nm)	Frequency	Cumulative Frequency	Percent	Cumulative Percent
1.5	3	3	8.8	0.8
2.5	51	54	13.8	14.6
3.5	66	120	17.9	32.6
4.5	18	138	4.9	37.5
5.5	33	171	9.0	46.5
6.5	19	190	5.2	51.6
7.5	13	203	3.5	55.2
8.5	14	217	3.8	59.0
9.5	39	256	10.6	69.6
10.5	8	264	2.2	71.7
11.5	21	285	5.7	77.4
12.5	12	297	3.3	80.7
13.5	9	306	2.4	83.2
14.5	10	316	2.7	85.9
15.5	5	321	1.4	87.2
16.5	7	328	1.9	89.1
17.5	7	335	1.9	91.0
18.5	5	340	1.4	92.3
19.5	9	349	2.4	94.8
21	19	368	5.2	100.0

Table 8. Continued

Sample 605

Class Mark (nm)	Frequency	Cumulative Frequency	Percent	Cumulative Percent
1.5	4	4	1.1	1.1
2.5	41	45	11.5	12.6
3.5	56	101	15.7	28.3
4.5	42	143	11.7	40.1
5.5	21	164	5.8	46.0
6.5	19	183	5.3	51.4
7.5	17	200	4.7	56.1
8.5	17	217	4.7	60.9
9.5	29	246	8.1	69.1
10.5	9	255	2.5	71.6
11.5	17	272	4.7	76.4
12.5	12	284	3.3	79.7
13.5	12	296	3.3	83.1
14.5	11	307	3.0	86.2
15.5	5	312	1.4	87.6
16.5	8	320	2.2	89.8
17.5	8	328	2.2	92.1
18.5	4	332	1.1	93.2
19.5	8	340	2.2	95.5
21.	16	356	4.4	99.9

Table 9. Very fine particle distributions set 3

Sample 607

Class Mark (nm)	Frequency	Cumulative Frequency	Percent	Cumulative Percent
1.5	1	1	0.3	0.3
2.5	16	17	5.4	5.7
3.5	47	64	15.8	21.6
4.5	40	104	13.5	35.1
5.5	20	124	6.7	41.8
6.5	24	148	8.1	50.0
7.5	6	154	2.0	52.0
8.5	12	166	4.0	56.0
9.5	11	177	3.7	59.7
10.5	9	186	3.0	62.8
11.5	19	205	6.4	69.2
12.5	18	223	6.0	75.3
13.5	10	233	3.3	78.7
14.5	12	245	4.0	82.7
15.5	11	256	3.7	86.4
16.5	9	265	3.0	89.5
17.5	5	270	1.6	91.2
18.5	6	276	2.0	93.2
19.5	6	282	2.0	95.2
21	14	296	4.7	99.9

Sample 611

Class Mark (nm)	Frequency	Cumulative Frequency	Percent	Cumulative Percent
2.5	13	13	4.7	4.7
3.5	54	67	19.7	24.4
4.5	46	113	16.7	41.2
5.5	12	125	4.3	45.6
6.5	25	150	9.1	54.7
7.5	8	158	2.9	57.6
8.5	4	162	1.4	59.1
9.5	7	169	2.5	61.6
10.5	7	176	2.5	64.2
11.5	28	204	10.2	74.4
12.5	14	218	5.1	79.5
13.5	10	228	3.6	83.2
14.5	7	235	2.5	85.7
15.5	8	243	2.9	88.6
16.5	5	248	1.8	90.5
17.5	5	253	1.8	92.3
18.5	1	254	0.3	92.7
19.5	5	259	1.8	94.5
21	15	274	5.4	99.9

Table 10. Very fine particle distributions set 4

Sample 609

Class Mark (nm)	Frequency	Cumulative Frequency	Percent	Cumulative Percent
1.5	18	18	6.0	6.0
2.5	55	73	18.4	24.4
3.5	22	95	7.3	31.8
4.5	16	111	5.3	37.2
5.5	26	137	8.7	45.9
6.5	22	159	7.3	53.3
7.5	20	179	6.7	60.0
8.5	18	197	6.0	66.1
9.5	18	215	6.0	72.1
10.5	7	222	2.3	74.4
11.5	12	234	4.0	78.5
12.5	9	243	3.0	81.5
13.5	8	251	2.6	84.2
14.5	6	257	2.0	86.2
15.5	8	265	2.6	88.9
16.5	5	270	1.6	90.6
17.5	6	276	2.0	92.6
18.5	8	284	2.6	95.3
19.5	3	287	1.0	96.3
21	11	298	3.6	100.0

Sample 612

Class Mark (nm)	Frequency	Cumulative Frequency	Percent	Cumulative Percent
1.5	16	16	5.3	5.3
2.5	47	63	15.8	21.3
3.5	23	86	7.7	28.9
4.5	19	105	6.3	35.3
5.5	22	127	7.4	42.7
6.5	21	148	7.0	49.8
7.5	26	174	8.7	58.5
8.5	17	191	5.7	64.3
9.5	13	204	4.3	68.6
10.5	11	215	3.7	72.3
11.5	12	227	4.0	76.4
12.5	12	239	4.0	80.4
13.5	11	250	3.7	84.1
14.5	8	258	2.6	86.8
15.5	5	263	1.6	88.5
16.5	4	267	1.3	89.8
17.5	7	274	2.3	92.2
18.5	8	282	2.6	94.9
19.5	6	288	2.0	96.9
21	9	297	3.0	99.9

Table 11. Very fine particle distributions for samples 712 and 716

Sample 712

Class Mark (nm)	Frequency	Cumulative Frequency	Percent	Cumulative Percent
1.5	26	26	5.2	5.2
2.5	148	174	29.7	35.0
3.5	63	237	12.6	47.6
4.5	39	276	7.8	55.5
5.5	24	300	4.8	60.3
6.5	19	319	3.8	64.1
7.5	23	342	4.6	68.8
8.5	24	366	4.8	73.6
9.5	21	387	4.2	77.8
10.5	20	407	4.0	81.8
11.5	14	421	2.8	84.7
12.5	11	432	2.2	86.9
13.5	13	445	2.6	89.5
14.5	10	455	2.0	91.5
15.5	11	466	2.2	93.7
16.5	11	477	2.2	95.9
17.5	10	487	2.0	97.9
18.5	4	491	0.8	98.7
19.5	2	493	0.4	99.1
21	4	497	0.8	99.9

Sample 716

Class Mark (nm)	Frequency	Cumulative Frequency	Percent	Cumulative Percent
1.5	17	17	3.7	3.7
2.5	49	66	10.9	14.6
3.5	66	132	14.6	29.3
4.5	47	179	10.4	39.8
5.5	35	214	7.7	47.6
6.5	28	242	6.2	53.8
7.5	19	261	4.2	58.1
8.5	23	284	5.1	63.2
9.5	18	302	4.0	67.2
10.5	18	320	4.0	71.2
11.5	15	335	3.3	74.6
12.5	19	354	4.2	78.8
13.5	23	377	5.1	83.9
14.5	17	394	3.7	87.7
15.5	12	406	2.6	90.4
16.5	9	415	2.0	92.4
17.5	6	421	1.3	93.7
18.5	11	432	2.4	96.2
19.5	9	441	2.0	98.2
21	8	449	1.7	100.0

Table 12. Selected area electron diffraction data

Sample	602	604	611	609
lines d Å	1.478	1.485	1.489	1.476
	1.615	1.615	1.615	1.615
		1.710	1.706	
	2.094	2.10	2.10	2.11
	2.526	2.526	2.526	2.517
	2.97	2.97	2.962	2.961

Sample	712	716
lines d Å	1.257	-
	1.320	-
	-	1.487
	1.628	1.618
	1.721	1.713
	2.106	2.101
	2.54	2.53
	2.96	2.97

Table 13. Diffraction lines for magnetite and maghemite

	Magnetite, Fe_3O_4 ASTM Card 19-629	Maghemite, γ-Fe_2O_3 ASTM Card 15-615
lines d Å	1.266	1.008 s
	1.328	1.702 s
	1.485	2.089 s
	1.616	2.521 s
	1.715	2.950 s
	2.099	
	2.532	
	2.967	

s = lines marked with s include those of the spinel structure

Table 14. Latin square mass concentration data summary (gm/sm^3)

Main Air Pressure (psi)

Replicate 1

Open Voltage (Volts)	40	45	50	55
25	0.92 A	1.11 B	1.37 C	1.03 D
27	1.19 B	1.28 C	1.74 D	0.81 A
29	1.51 C	1.77 D	1.07 A	1.48 B
31	1.70 D	1.05 A	1.31 B	1.18 C

Wire Feed Rates:

A - 30
B - 40
C - 50
D - 60

Main Air Pressure (psi)

Replicate 2

Open Voltage (Volts)	40	45	50	55
25	1.00 A	1.22 B	1.46 C	1.81 D
27	1.50 B	1.55 C	1.83 D	1.15 A
29	1.43 C	1.38 D	1.13 A	1.38 B
31	1.67 D	1.19 A	1.92 B	1.26 C

Table 15. Orthogonal mass concentration data summary (gm/m^3)

	Main Air Pressure (psi)			
Open Voltage (Volts)	40	50	40	50
28	1.44	1.52	1.44	1.70
29	1.51	1.41	1.71	2.13
Wire Feed Rate	45		55	

Table 16. A listing of all the mass concentration data

Sample Number	Mass Concen. (gm/m^3)	Temp. in Exhaust Duct (°C)	Wire Feed Rate	Open Voltage (Volts)	Main Air Pressure (psi)
563	2.16	82	50	31	55
702	2.13	90	55	30	50
562	1.92	62	40	31	50
566	1.83	80	60	27	50
581	1.81	80	60	25	55
554	1.77	85	60	29	45
558	1.74	80	60	27	50
705	1.71	95	55	30	40
550	1.7	72	60	31	40
707	1.7	85	55	28	50
564	1.67	80	60	31	40
565	1.55	77	50	27	45
704	1.52	80	45	28	50
529	1.51	68	50	29	40
703	1.51	72	40	30	40
561	1.5	71	40	27	40
560	1.48	70	40	29	55
576	1.46	76	50	25	50
701	1.44	72	45	28	40
706	1.44	85	55	28	40
573	1.43	68	50	29	40
700	1.41	70	45	30	50
571	1.38	58	40	29	55
575	1.38	76	60	29	45

Table 16. Continued

Sample Number	Mass. Concen. (gm/m^3)	Temp. in Exhaust Duct (°C)	Wire Feed Rate	Open Voltage (volts)	Main Air Pressure (psi)
555	1.37	76	50	25	50
546	1.31	73	40	31	50
548	1.28	74	50	27	45
572	1.22	65	40	25	45
553	1.19	73	40	27	40
568	1.19	57	30	31	45
549	1.18	75	50	31	55
569	1.15	58	30	27	55
570	1.13	54	30	29	50
547	1.11	64	40	25	45
556	1.07	60	30	29	50
552	1.05	53	30	31	45
559	1.03	70	60	25	55
582	1.0	59	30	24	40
557	0.92	57	30	25	40
551	0.81	60	30	27	55

ANALYSIS OF DATA

Agglomerates

In the comparative experiment samples 715 and 714 were chosen as representative of the agglomerates found in the samples. The agglomerates measured by the experimenter were found to have means of 0.41 μm (S=0.53 μm) and 0.40 μm (S=0.54 μm) as shown in Appendix C-2. The following analysis used the student t-test for determining the equality of expected populations of two different samples. The implication was that the means were equal if the difference between the two means was equal to zero.

The null hypothesis that the difference between the two means was equal to zero:

$$H_o: \; u_1 - u_2 = 0$$

was tested against the alternative hypothesis that the difference was not equal to zero,

$$H_A: \; u_1 - u_2 \neq 0.$$

To determine which hypothesis was true, the t-test statistic was used. This statistic was determined by the following general formula:

$$t_{cal} = \frac{\bar{x}_1 - \bar{x}_2}{S_{\bar{x}p}}$$

where $\bar{x}_1 - \bar{x}_2$ was greater than or equal to zero and $S_{\bar{x}p}$ was the pooled standard deviation as defined in Appendix D-2. The t_{cal} value was compared to a tabulated $t_{\alpha/2}$ (v) statistic value where the α- error was equal to 0.10 and the degrees of freedom (v) were set equal to infinity because the sample sizes were much larger than 30. As shown in Appendix D-2, the hand calculations showed the t value to be 0.194. The $t_{\alpha/2}$ ($v=\infty$) value was found to be 1.645.

The criteria for hypothesis test was as follows:

Table 17. Two means equality test hypothesis decision-making criteria

If $t_{cal} \leq t_{\alpha/2}$, then H_o is accepted
and H_A is rejected.

If $t_{cal} > t_{\alpha/2}$, then H_o is rejected
and H_A is accepted.

Because $t_{cal} < t_{\alpha/2}$, the null hypothesis, H_o: $u_1-u_2=0$, is accepted. This implied that the two sample means came from the same population; this was tested for 90% confidence.

The above student t-test was only applicable if the variances of the samples came from the same population. The F-statistic was used to determine if the variances came from the same population. Where

$$F_{cal} = \frac{S_1^2}{S_2^2}$$

with S_i^2 equal to the variance of sample i and F_{cal} having an F-distribution with degrees of freedom v_1 for s_1 and v_2 for s_2 was compared to a tabulated $F_\alpha(v_1,v_2)$ and found to be less than or equal to the F_α value, the variances were considered to be from the sample population. If the variances were different, the Smith-Satterthwaite test (9) was used to determine the equality of two means.

The F_{cal} was found to be 1.05 and $F_\alpha(v_1,v_2)$ was not found in any statistical table. But, if both of the degrees of freedom (v_1 and v_2) approach large values (> 100), values of $F_\alpha(v_1,v_2)$ approach 1.00. It was assumed that F_{cal} was greater than F_α and therefore the Smith-Satterthwaite test was needed for the t-statistic test for equality of means.

The hypothesis testing using the Smith-Satterthwaite t-statistic is the same as the equivalent variance t-test with the exception that the t-value was found by the following equation:

$$t_{cal} = \frac{\bar{x}_1-\bar{x}_2}{\sqrt{\frac{S_1^2}{n_1}+\frac{S_2^2}{n_2}}}$$

and that the degrees of freedom (df) were found by the following equation:

$$df = \left[\frac{S_1^2}{n_1}+\frac{S_2^2}{n_2}\right]^2 \div \left[\frac{\left(S_1^2/n_1\right)^2}{n_1-1}+\frac{\left(S_2^2/n_2\right)^2}{n_2-1}\right]$$

The t_{cal} value was found to be 0.225 with degrees of freedom 576. The $t_{\alpha/2}$ value was still 1.635. The outcome of the hypothesis that the means were equal was not changed by the fact that the variances were not equal.

The coefficient of variance was also calculated for each sample distribution and was presented in Table 1. along with the means ($\bar{x}$), standard deviation (S), and standard errors of the mean for each sample. The coefficient of variance was an indicator of the monodispersity of a size distribution (2) and is given by the following formula:

$$C.V. = S/\bar{x}$$

The coefficient of variance for the agglomerate size distributions of samples 714 and 715 were 1.35 and 1.29, respectively. Any sample size distribution with a coefficient of variance less than 0.10 (2) was considered monodisperse.

Table 17. Statistics for agglomerate samples

Sample No.	Mean (μm)	Standard Deviation (μm)	Standard Error of the Mean (μm)	Coefficient of Variance (%)
714	0.40	0.54	0.03	135
715	0.41	0.53	0.03	129

Fine Particles

The fine particle size distribution data was broken down into six sets of data contingent on the six sets of conditions. Two basic tests were performed on the fine particle size distribution data: (1) within group t-test for equality of means and between group t-test for equality of means and (2) within group and between group chi squared test for equality of frequency distributions. Plotted frequency distribution were shown in Figures 3, 4, 5, 6, and 7.

The SAS T-TEST and MEANS (15) procedures were employed to determine relevant statistics for the data. The MEANS procedure calculated the means, standard deviations, standard errors of the mean, and the coefficients of variance as presented in Table 19. The T-TEST procedure calculated the F-statistic for comparison of two sample variances and the t-statistic for determination of mean equality. A summary of the t-test statistics for the within group analysis was presented in Table 20. A summary of t-test statistics for between group analysis was presented in Tables 20 and 21. The tables were structured for presentation of statistics concerning the intersecting samples.

The statistic in the middle of each block was the t-value calculated for the two mean t-test where

$$t = \frac{x_1 - x_2}{S^{-}_{xp}}$$

with the hypothesis that the means of the intersecting samples were equal. The box above the t-value was checked if the variances of the two samples were considered to be unequal; this implied that the t-value had been determined by the Smith-Satterthwaite t-statistic. The value beneath the t-value was the probability that the t-value could be exceeded due to random error in the sampling.

The equality of the frequency distributions were tested by the use of the SAS FREQUENCY (15) procedure. Chi-squared statistics were determined by the FREQUENCY procedure and presented for within and between groups in Tables 22 and 23 respectively.

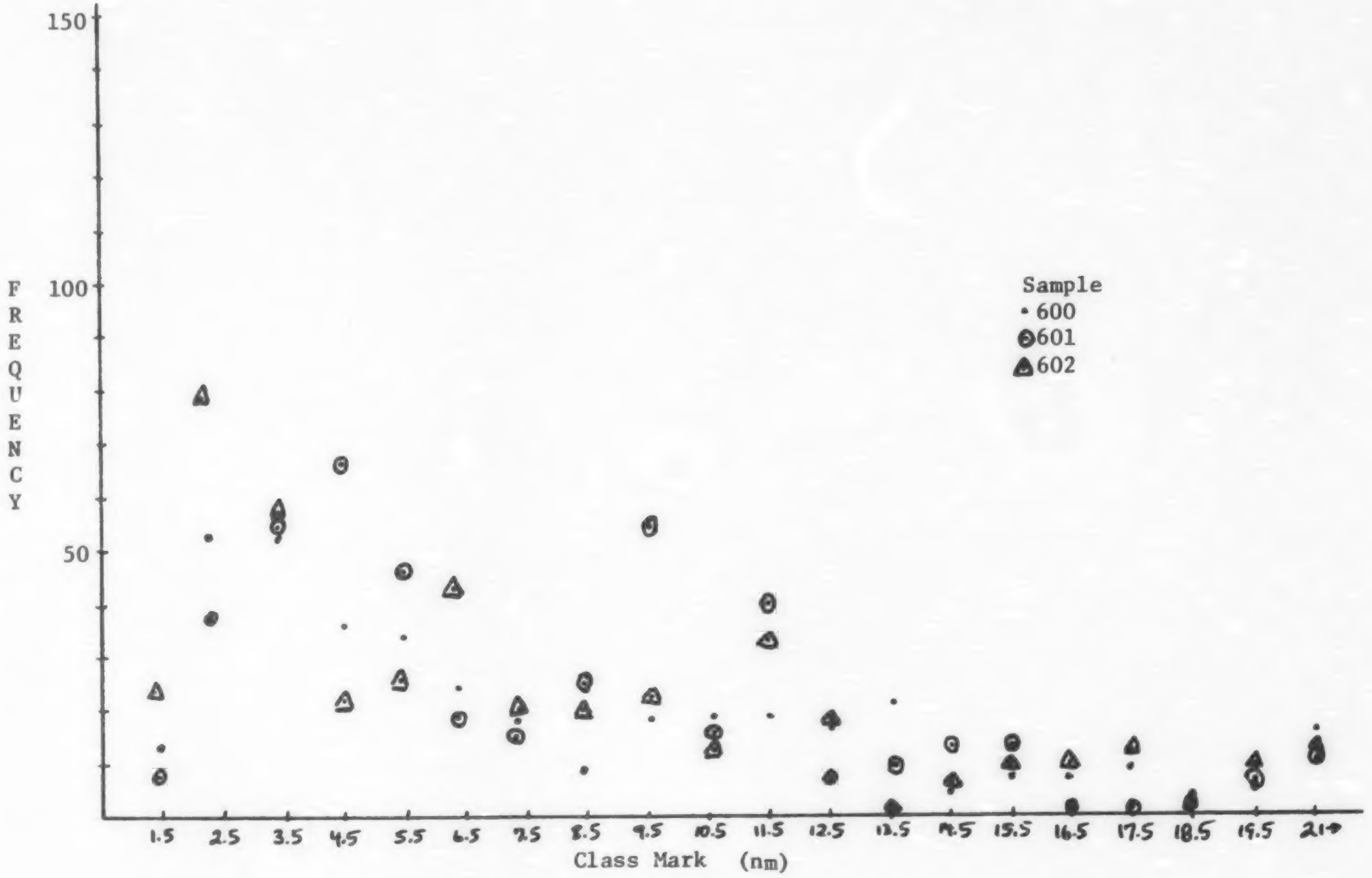

Figure 3. Set 1 frequency distributions.

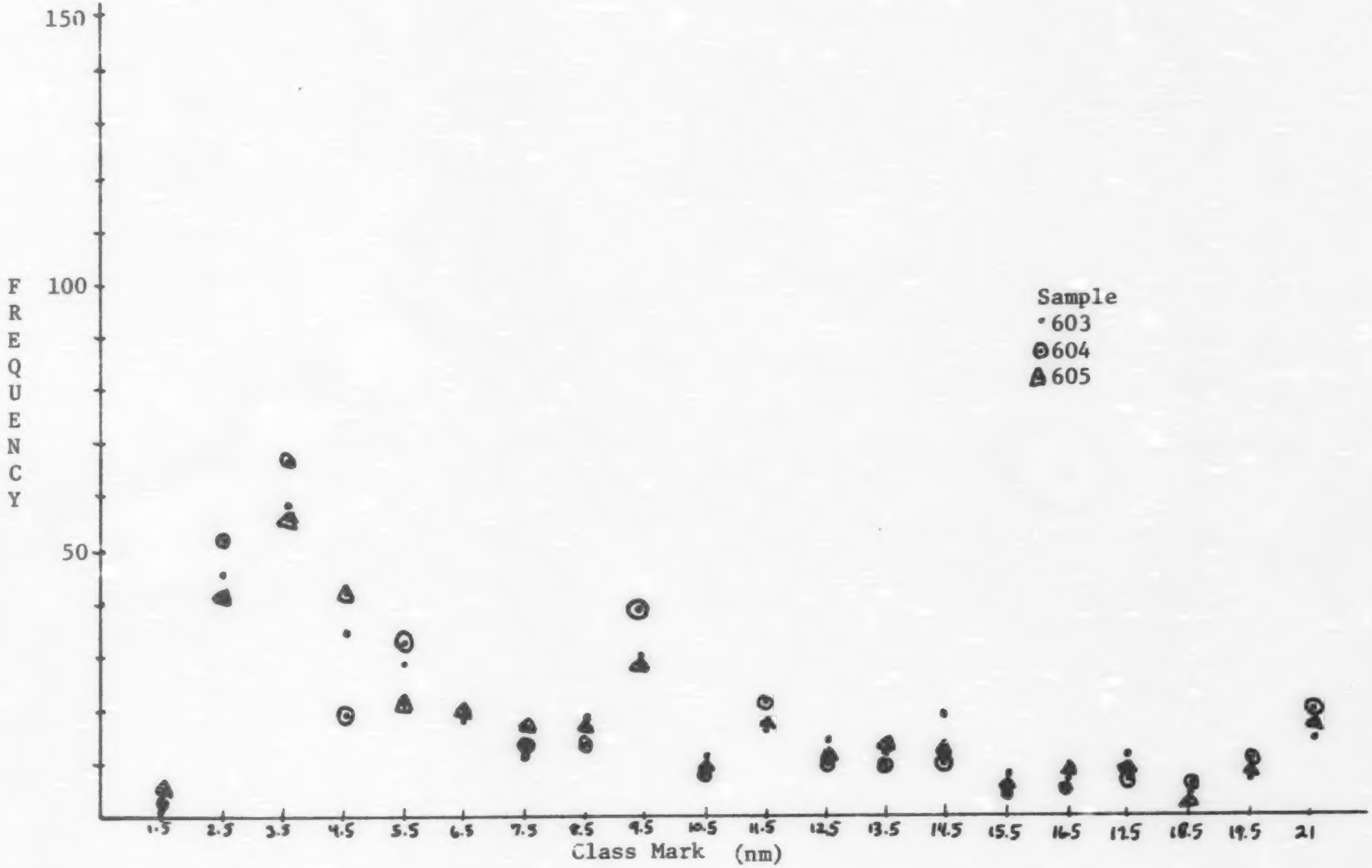

Figure 4. Set 2 frequency distributions.

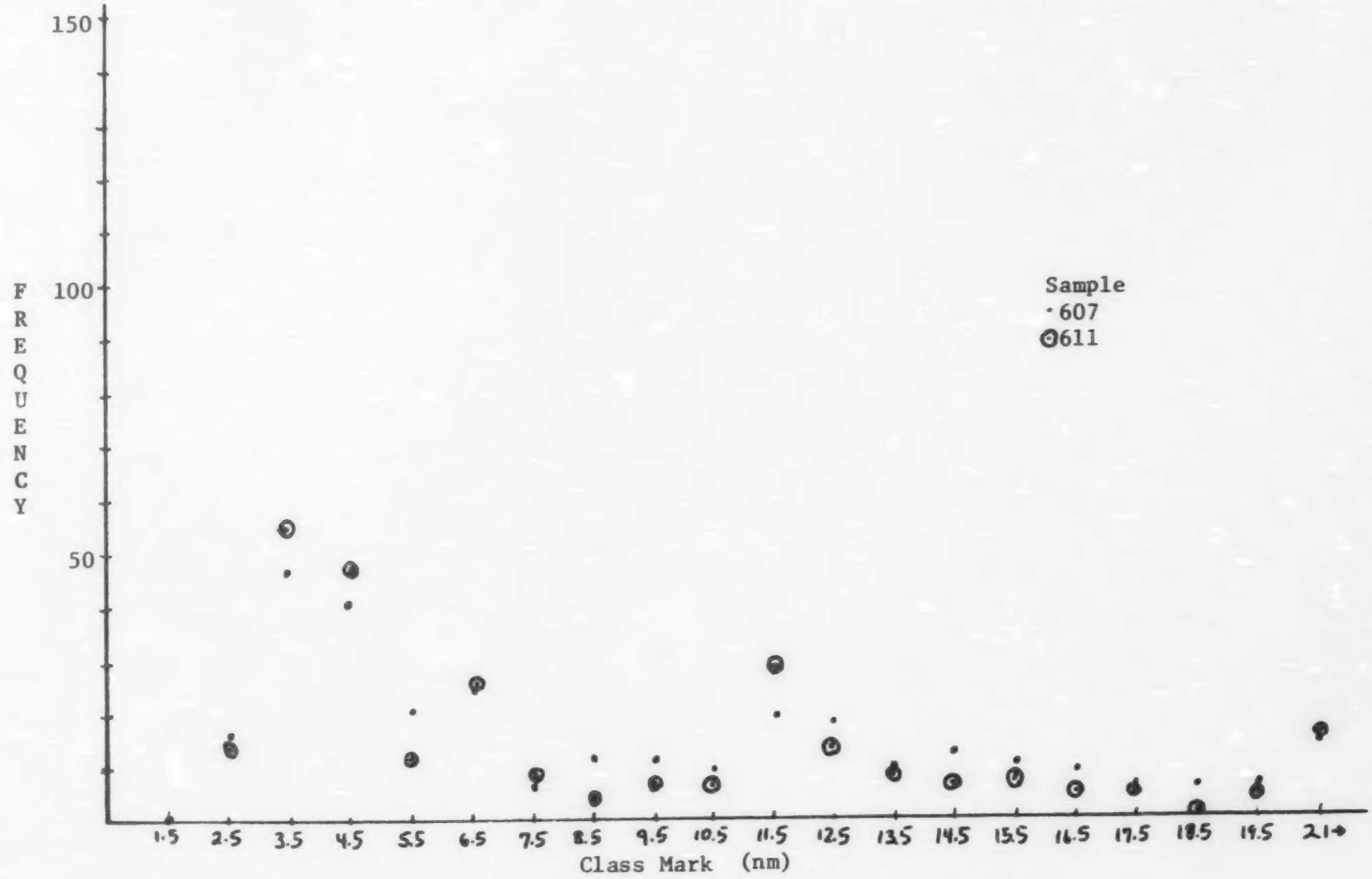

Figure 5. Set 3 frequency distributions.

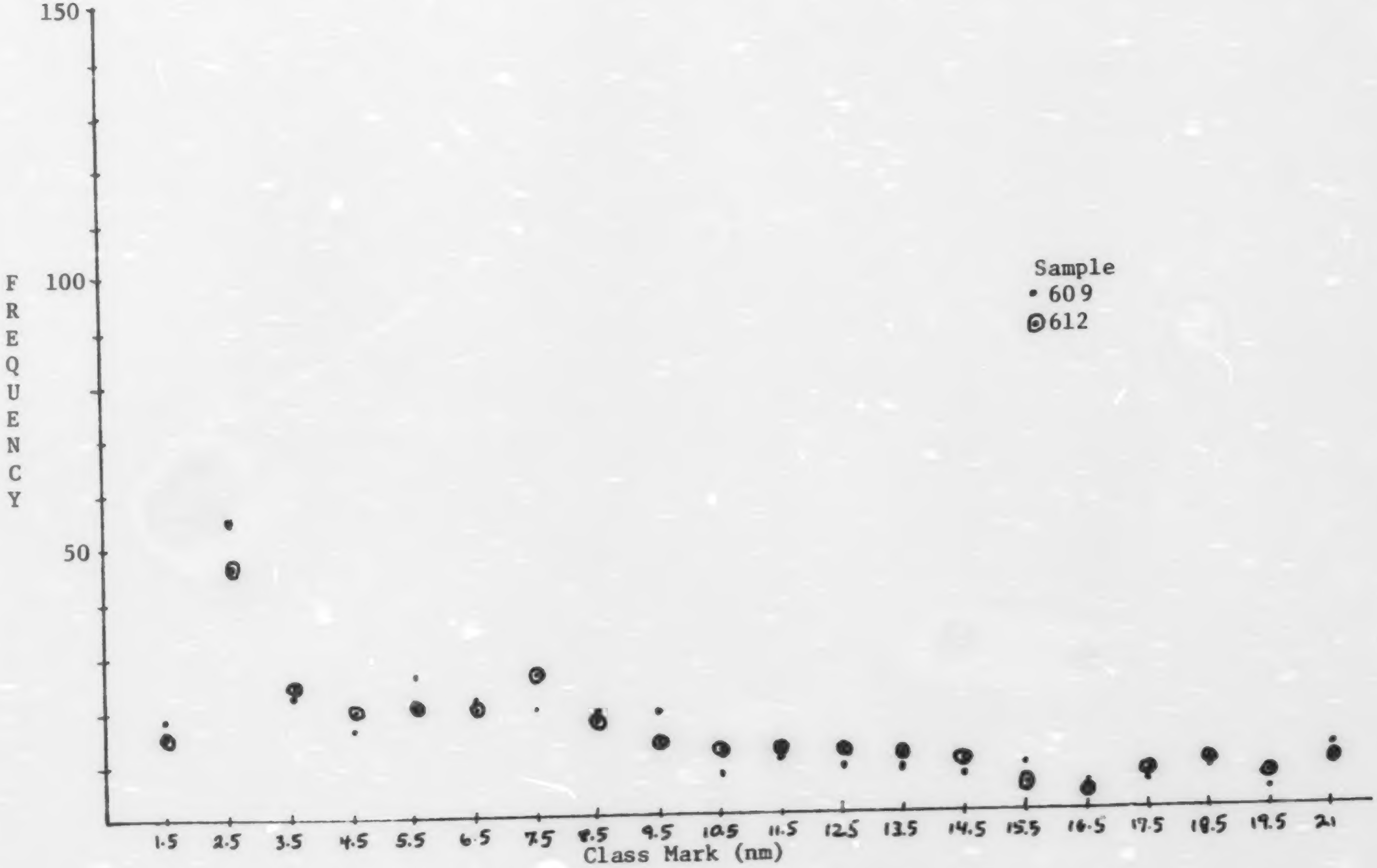

Figure 6. Set 4 frequency distributions.

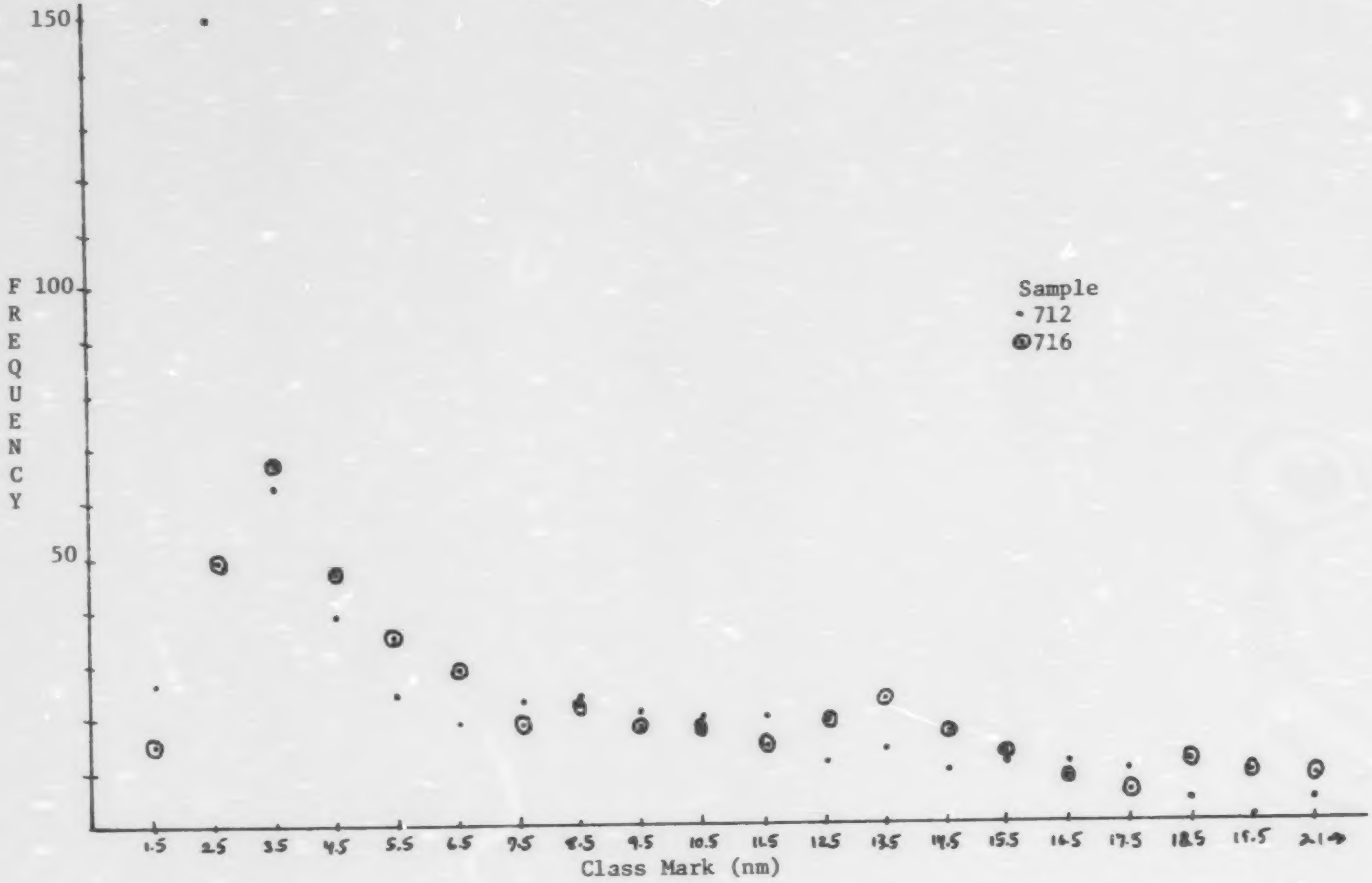

Figure 7. Samples 712 and 716 frequency distributions.

Table 19. Statistics for fine particle distributions

Set Number	Sample No.	Number of Particles	Mean (nm)	Standard Deviation (nm)	Standard of Error of the Mean (nm)	Coefficient of Variance (%)
1	600	386	8.00	5.35	0.27	66.9
	601	446	7.83	4.56	0.22	58.2
	602	434	7.53	5.23	0.25	69.5
2	603	369	8.45	5.37	0.28	63.5
	604	368	8.32	5.51	0.29	66.3
	605	356	8.31	5.41	0.29	65.1
3	607	296	9.05	5.49	0.32	60.5
	611	274	8.57	5.40	0.33	62.9
4	609	298	7.86	5.40	0.31	68.8
	612	297	8.13	5.37	0.31	66.0
5	716	449	8.05	5.21	0.25	64.7
6	712	497	6.42	4.79	0.21	74.6

Table 20. Within group t-statistics for fine particle samples

600	601	602	Sample Number
-	☑ 0.496 0.62	☐ 1.28 0.20	600
	-	☑ 0.919 0.36	601
		-	602

603	604	605	Sample Number
-	☐ 0.302 0.76	☐ 0.328 0.74	603
	-	☐ -0.026 0.98	604
		-	605

607	Sample Number
☐ 1.04 0.30	611

609	Sample Number
☐ 0.629 0.53	612

716	Sample Number
☑ -5.02 0.001	712

Table 21. Between Group t-statistics for fine particle samples

Sample Number	603	604	605	607	611	609	612	716	712
600	☐ -1.14 0.25	☐ -0.80 0.42	☐ 0.78 0.44	☐ -2.52 0.12	☐ -1.36 0.18	☐ 0.34 0.73	☐ -0.33 0.74	☐ -0.15 0.88	☑ 4.56 0.001
601	☑ -1.75 0.08	☑ -1.36 0.18	☑ -1.33 0.19	☑ -3.17 0.001	☑ -1.91 0.06	☑ -0.07 0.94	☑ 0.80 0.42	☑ -0.69 0.49	☐ 4.63 0.001
602	☐ -2.46 0.02	☐ -2.03 0.04	☐ -2.06 0.04	☐ -3.80 0.002	☐ -2.57 0.01	☐ 0.83 0.41	☐ -1.53 0.13	☐ -1.51 0.13	☑ 3.35 0.008

Sample Number	607	611	609	612	716	712
603	☐ -1.43 0.15	☐ -0.30 0.76	☐ 1.40 0.16	☐ 0.74 0.46	☐ 1.05 0.29	☑ 5.76 0.001
604	☐ -1.71 0.09	☐ -0.59 0.55	☐ -1.08 0.28	☐ 0.43 0.67	☐ 0.70 0.49	☑ 5.29 0.001
605	☐ -1.74 0.08	☐ -0.62 0.54	☐ 1.06 0.29	☐ 0.40 0.69	☐ 0.67 0.50	☑ 5.27 0.001

Table 21. Continued

Sample Number	600	601	602	603	604	605	607	611	609	612
716	☐ -0.15 0.88	☑ -0.69 0.49	☐ -1.51 0.13	☐ 1.05 0.29	☐ 0.70 0.49	☐ 0.67 0.50	☐ 2.50 0.01	☐ 1.29 0.20	☐ -0.50 0.62	☐ 0.20 0.84
712	☑ 4.56 0.001	☐ 4.13 0.001	☑ 3.35 0.008	☑ 5.76 0.001	☑ 5.29 0.001	☑ 5.27 0.001	☑ 6.86 0.001	☑ 5.53 0.001	☑ 3.79 0.001	☑ 4.54 0.001

Sample Number	609	612	716	712
607	☐ 2.67 0.008	☐ 2.06 0.04	☐ 2.50 0.01	☑ 6.86 0.001
611	☐ 1.59 0.11	☐ 0.98 0.33	☐ 1.29 0.20	☑ 5.53 0.001

Sample Number	716	712
609	☐ -0.50 0.62	☑ 3.29 0.001
612	☐ 0.20 0.84	☑ 4.54 0.001

Table 22. Within group chi-squared statistics

Sample Number	600	601	602
600	-	67.2 0.0001	44.6 0.0008
601		-	99.98 0.0001
602			-

Sample Number	603	604	605
603	-	14.8 0.733	6.98 0.994
604		-	17.93 0.527
605			-

Sample Number	611
607	17.69 0.543

Sample Number	612
609	7.154 0.993

Sample Number	716
712	71.77 0.001

Table 23. Between group chi-squared statistics

Sample Number	607	611	609	612
603	29.8 0.055	56.1 0.0001	49.8 0.0001	45.1 0.0007
604	51.7 0.0001	73.9 0.0001	47.9 0.0003	51.8 0.0001
605	28.5 0.074	45.6 0.0006	46.3 0.0005	39.7 0.0036

Sample Number	607	611
609	77.7 0.0001	109.9 0.0001
612	67.7 0.0001	96.6 0.0001

Mass

The Latin Square data was organized and presented in the Latin blocks in Table 14. The Latin Square analysis of variance calculations were carried out in Appendix D-1 with a summary presented in Table 24. The data was also analyzed using the SAS ANOVA procedure. This data was shown in Table 25. This table was explained in Appendix D-3.

The data taken about an expected midrange of operating variables was analyzed by the SAS GLM (15) procedure and was presented in Table 26.

All of the mass data, that is, both the Latin Square and the orthogonal data sets were analyzed by the SAS GLM and STEPWISE procedure. The SAS GLM table was presented in Table 27. The STEPWISE procedure used a statistical method to develop a "best-fit" linear model for the prediction of the dependent variable-mass concentration of aerosol within the gas stream. In Appendix D-4, this procedure was described.

The "best-fit" linear model was analyzed for its aptness with respect to its predictive ability using the SAS GLM procedure and associated calculations for model residual analysis. This procedure was described in Appendix D-5.

Table 24. Analysis of variance for latin square experimental design mass data

Variable	df	Sum of Squares	Mean Square	F_{cal}	$F_{\alpha=0.05}$	$F_{\alpha=0.01}$
Wire feed rate	3	1.473	0.4908	10.86	3.07	4.87
Open Voltage	3	0.319	0.1065	2.35	3.07	4.87
Main air-jet pressure	3	0.106	0.0352	0.77	3.07	4.87
Replication	1	0.335	0.3349	7.39	4.32	8.02
Experimental error	21	0.952	0.0453			
Total	31	3.185				

Table 25. SAS ANOVA for latin square experimental design mass data

Dependent Variable: Y, Mass Concentration

Source	Sum of Squares	df	Mean Square	F Value
Model	2.23	10	0.22	4.94
Error	0.95	21	0.045	PR>F
Corrected Total	3.18	31		0.0010

R-Square	C.V.
0.70	15.4

Std. Dev.	Y Mean
0.21	1.38

Source	df	ANOVA SS	F Value	PR>F
Wire feed rate	3	1.47	10.86	0.0002
Voltage	3	0.32	2.36	0.1004
Air Pressure	3	0.11	0.81	0.5042
Replication	1	0.33	7.35	0.0131

Table 26. SAS GLM table for orthogonal data

Dependent Variable: Y, Mass Concentration

Source	df	Sum of Squares	Mean Square	F Value
Model	3	0.26	0.08	2.41
Error	4	0.14	0.03	PR>F
Corrected Total	7	0.40		0.2079

R-Square	C.V.
0.64	11.8

Std. Dev.	Y Mean
0.19	1.61

Source	df	Type I SS	F Value	PR>F
Wire feed rate	1	0.15	4.20	0.1099
Voltage	1	0.054	1.51	0.2864
Air Pressure	1	0.054	1.51	0.2864

Table 27. SAS GLM table for all of the data

Dependent Variable Y, Mass Concentration

Source	df	Sum of Squares	Mean Square	F Value
Model	13	2.81	0.22	5.12
Error	26	1.09	0.042	PR>F
Corrected Total	39	3.90		0.0002

R-Square	C.V.
0.71	14.4

Std. Dev.	Y Mean
0.21	1.43

Source	df	Type I SS	F Value	PR>F
Wire feed rate	5	1.94	9.21	0.0001
Voltage	4	0.37	2.22	0.0946
Air Pressure	3	0.16	1.27	0.3063
Replication	1	0.33	7.87	0.0094

DISCUSSION OF RESULTS

Agglomerates

The size means of the agglomerates were found to be 0.41 μm (S=0.53 μm) for sample 715 and 0.40 μm (S=0.54 μm) for sample 714. These means were also found to be equal; this implied that they were from the same population. The coefficient of variances were rather large, thus the agglomerated particle distributions representative of the aerosols were not "monodisperse."

The simple comparative analysis of increasing the duct exhausting velocity from 1300 fpm to 1850 fpm showed only a decrease in particle size from 0.41 μm to 0.40 μm. This difference was not significant at a 0.1 level of significance.

The distribution of the agglomerates was not normally distributed about the mean as shown in Figure 8. This fact indicated an inadequacy of this analysis because the t-test for equality of means assumed the sample distributions to be normally distributed. Therefore, the analysis of the agglomerate distributions was, at least, a characterization of the aerosol. While this was true, the analysis still served to illustrate the t-test for equality of mean technique.

Fine Particles

The within group t-test analysis showed that the sample means in all the sets were equivalent within groups. T-test hypothesis and implications were outlined in Appendix D-2. Set 2 t-test analysis showed a very small difference within this group of operating conditions. The variance of this set of samples were also considered equal by the F-test as set forth in Appendix D-2. Certainly, these three sample

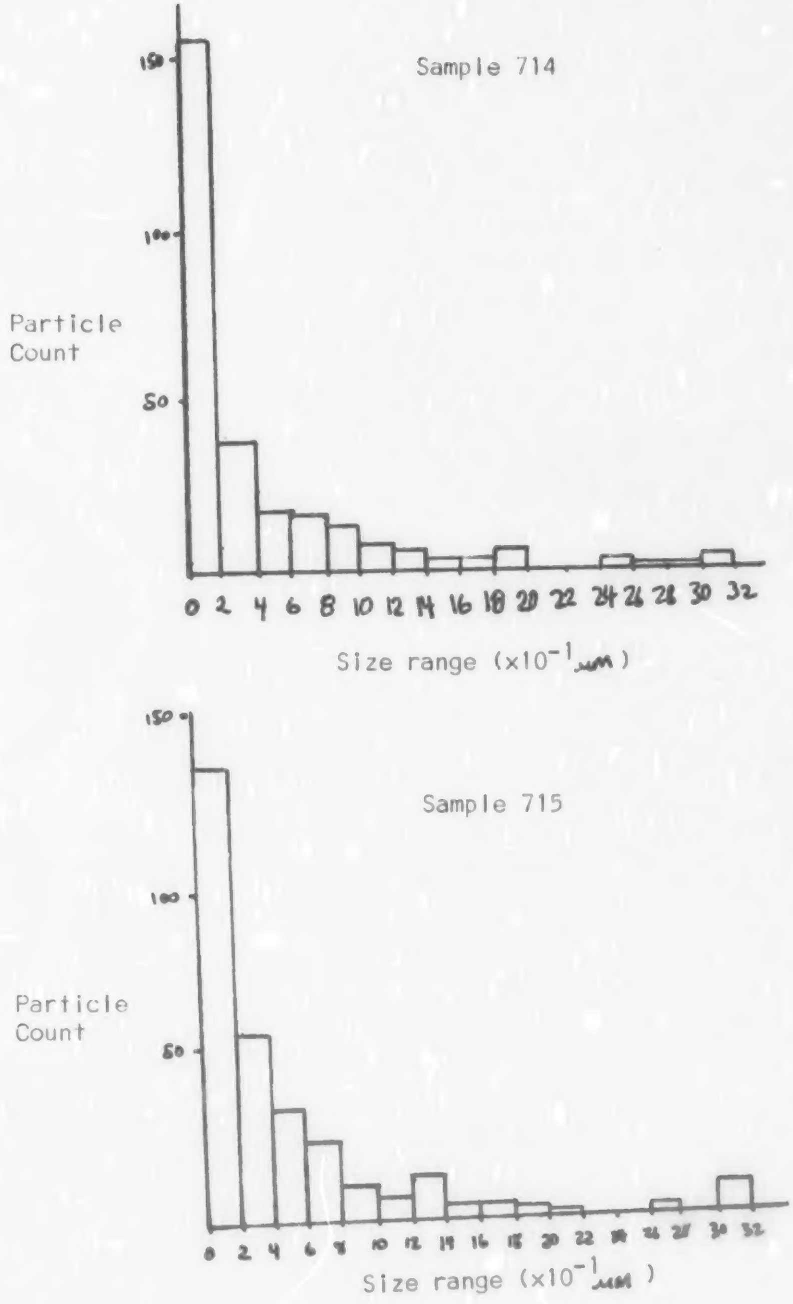

Figure 8 Histograms of agglomerated particles

populations (set 2) were representative of the same aerosol parent population.

The between group t-test analysis showed a variety of equal and unequal means. Table 21 showed that the means of set 1 were all different than the means in set 3. Three of the four means in the combination of set 3 and set 4 were different. Five of the six means in the combination of set 1 and set 4 were equal. The majority of the means of the combination of set 1 and set 2 were unequal.

The t-test analysis between the two comparative samples 712 and 716 showed sample 712 to have a significantly smaller very fine particle size than sample 716. In fact, sample 712 was found to have a mean much smaller than other samples taken. The increase in the exhausting rate of the barrel was the only known difference in the operating conditions and most likely had the observed effect on the means and variances of the fine particle size distributions. Even with this information, the simple comparative experiment was not considered to be conclusive because of the small number of samples.

The within group very fine particle size distributions for sets 2, 3, and 4 were found to be equivalent. Size distributions between groups were found to be all different at an alpha level of 0.05. This implied that at three of four different operating conditions three different fine particle size distributions were generated.

Chemical Composition

The SAED analysis showed two possible resultant materials. Two different phases of iron oxide were possible: magnetite and maghemite. Mr. Richard Shimps of McCrone said: There is difficulty in deciding which one may truly be present, or if both are present. This stems from the fact that the strongest diffraction lines of each material are the same since the strongest lines of maghemite are those which include the spinel structure. (17) Magnetite was considered to be present with a possibility of maghemite being present.

Mass Analysis

The Latin Square experimental design was analyzed by two analyses of variance methods; as expected, the Latin Square hand calculation and the SAS ANOVA procedure resulted in the same values for the statistics. The F statistic in ANOVA was used to determine if the particular variable had any effect on phenomenon of gas stream particulate mass concentration. The test was explained in Appendix D-3.

The Latin Square analysis found the wire feed rate to be significant at the 0.01 significance level. This implied the wire feed rate had an effect on the resultant mass concentration. The variables of open voltage and jet pressure were not found to have any effect on the mass concentration of the aerosol even at the 0.1 significance level. The analysis of variance statistics for the effect of replication was also calculated and found to indicate a significant difference between trials at the 0.05 significance level but not the 0.01 significance level.

As explained in Appendix D-3, the SAS ANOVA procedure also analyzed the variance of the data to determine if the variability of the data was a consequence of random error (noise) in the collection of the data or a consequence of the changing of the experimental variables. The F test value for this test was found to conclude that the variability was a consequence of the experimental variables at the 0.01 significance level.

The SAS GLM procedure found this particular set of operating points to insignificantly describe the variability of the orthogonal data. Even though this was found, the wire feed rate was found to be almost significant at the 0.1 significance level.

The SAS GLM analysis of the combination of the Latin Square and Orthogonal data found the data to significantly ($\alpha = 0.01$) describe the variability of all the data. With this total set of 40 observations, the SAS GLM procedure calculated a F statistic for determining the effect or noneffect of the independent variables in the experimental model. The procedure found the variables included in the model to have a significant effect on the outcome: mass concentration of the gas stream. That was, the GLM procedure determined that the wire feed rate, the open voltage across the arc, and the sample replication variables affected the results of the experiment.

The SAS STEPWISE procedure determined a "best-fit" linear equation for the prediction of mass concentration in the gas stream. The equation was

$$Y = -0.81 + 0.01\ (WF) + 0.048\ (V)$$

where Y is the mass concentration (gm/m^3), WF is the wire feed rate (range 30-60), and V is the open voltage (range 25-31 volts). By the SAS GLM procedure the intercept beta value (-0.81) was significant at the 0.11 level. The wire feed rate beta value (0.019) was significant at the 0.001 level and the open voltage beta value (0.048) was significant at the 0.01 level. It was found that the prediction of mass concentration was not to be predicted by the gas jet pressure variable. The variability in the data brought about by the replication factor was ignored in this analysis because it was not a controlled independent variable.

The analytical method of investigating the aptness of the model developed by the SAS GLM procedure by plotting a standardized residual was presented in Appendix D-5. The difference between the observed outcome and the predicted outcome - the residual - at a collected data point was expected to be zero assuming a perfect fit of the model. A real model was expected to have residuals scattered evenly about zero for all the data points used to determine the model.

Plots of the independent variables against the standard residual were expected to evaluate nonlinearity of the regression function: the model. Plots were shown in Appendix D-5 (Figures 12 and 13) and were interpreted as showing that the model, indeed, fitted a linear function.

A plot of the predicted values of the model against the standard residual was expected to evaluate nonconstancy of error variance. If the standard residual increased or decreased as the predicted value changed, the error variance was considered not to be constant throughout the model's predictive range. As shown in Appendix D-5 (Figure 14), this was the case with the predictive model determined by the SAS GLM procedure. The implication of this fact was that the error variance was larger when the predicted value was larger; this meant that the variability of gas stream mass concentration can be expected to be greater when larger mass concentrations are being considered.

A plot of the collection order with respect to the time sequence of the data against the standard residuals was expected to evaluate nonindependence of the error terms. The implication of this was that the ordering of the sample collection was not random. The residual plot in Appendix D-5 (Figure 15) showed the sampling order to be random.

CONCLUSION

The iron oxide aerosol has been characterized by count with a particle size mean of 0.4 μm. The inherent limitations in this analysis, e.g. choice of magnification, nonnormality of sample distribution, indicates that the mean is probably less than 0.4 μm. It should be noted that most of the particles were measured to be less than 0.1 μm.

The iron oxide fine particles that formed by agglomeration into the aerosol particles have been characterized to have means ranging from 5.4 nm to 9.1 nm (0.0054 μm to 0.0091 μm). The size means and size distributions of samples at given operating conditions were found to be equal. This implied that a specific operating set up generated a particular population of fine particles. Differences in size means and size distributions between sets of operating conditions indicated that changing operation variables changed the characteristics of the population of fine particles generated.

The simple comparative test for discerning the effect on size of changing the exhausting rate of the arc chamber was inconclusive. The agglomerated fine particle aerosol size was found not to change with an increase in exhausting rate. However, the fine particle mean diameter size was found to be greatly affected by the increase in exhausting rate. The evidence of this change in generating properties indicated a need for further experimentation.

The analysis of the production of the mass concentration of the aerosol showed that a linear expression aptly fitted the data. The predictive model showed the mass concentration to be a function of the wire feed rate and the open voltage across the electrodes. The model predicted a range of 1.0 to

1.8 gm/m^3 with a concurrent increase of wire feed and voltage. The generation of a particular mass concentration should therefore be predictable given adequate preliminary characterization for at least this material.

With respect to possible suggestions for further development of the Electrospray aerosol generator, there are two areas that require further work. The first area concerns the control of variables, such as the wire feed rate, the open voltage, and the main comressed air-jet. The second area concerns application precautions.

The wire feed delivery should be smooth - free of delivery impedance. The wire straighteners should control the curvature of the wire for consistent contact area at the arc. It was felt that the straighteners and the pinch rollers imparted an oscillating tension to the wire and consequently an oscillating arc contact area. This behavior was observed as a sound changing in pitch during operation and as an oscillating - up and down - motion of the wire as it left the electrode tips.

The open voltage would require very precise control if its effect on the aerosol's particle mean size or size distribution were to be investigated. The compressed air-jet that atomizes and quenches the melted and vaporized metal should be studied to ascertain its effect on the aerosol's particle size mean and distribution. Possibly, variables related to the agglomeration of the very fine particles could be studied. Also the effect of the temperature of the particle laden gas stream from the barrel to the sampling port could be studied.

In the application of this aerosol generator, an on-line continuous mean size and size distribution analyzer, such as a Whitby-Liu mobility analyzer, would provide the necessary before control equipment and after control equipment data in an engineering evaluation of a piece of air pollution control equipment. Control of the separation of the larger particles within the barrel could also be used to help approximate real life circumstances.

In conclusion, the electric arc generator produced an iron oxide aerosol of agglomerated fine particles in mass concentration averaging 1.4 gm/m^3. The generator showed controllability of mass concentration and variability of fine particle populations with respect to operating variables. The resultant conclusion of this report is that the generator is controllable and, with detailed characterization of the aerosol below 0.5 μm that the generator would fill a much needed service in production of standard, fresh aerosols for engineering evaluations of bench or pilot scale air pollution control equipment and source sampling (stack testing) equipment.

BIBLIOGRAPHY

1. Amson, J. D.; "Electrode Voltage in the Consumable-Electrode Arc System." Journal of Physics D: Applied Physics, Vol. 5, 1972.

2. Davies, C. N.; Aerosol Science, Academic Press, 1966

3. Formenti, M., Julliet, F., Meriavdeau, P., Teichner, S. J., and Vergnon, P.; "Preparation in a Hydrogen-Oxygen Flame of Ultrafine Metal Oxide Particles" in Aerosol and Atmospheric Chemistry, edited by G. M. Hidy, Academic Press, 1972, pp. 45-50.

4. Grassel, Eugene E.; "Aerosol Generation for Industrial Research and Product Testing," in Fine Particles: Aerosol Generation, Measurement, Sampling, and Analysis, edited by Benjamin Y. H. Liu, Academic Press, 1976, pp. 145-173.

5. Hedden, Robert; Electric Arc Generation of Polydispersed Iron Oxide Aerosol in an Air Stream, problem report submitted to West Virginia University, Morgantown, West Virginia, 1972.

6. Holmgren, J. D., Gibson, J. O., and Sheer, C.; "Some Characteristics of Arc Vaporized Submicron Particles, " Journal of the Electrochemical Society, Vol. 111, No. 3, March 1964, pp. 362-369.

7. Linsky, B., and Smith, G.; "Sources of Information on Air Pollution," Proceedings, National Conference on Air Pollution, Washington, D. C., November 1958.

8. Magill, P. L., Holden, F. R., and Ackley, C; Air Pollution Handbook, McGraw-Hill Book Company, 1956, section 6.

9. Miller, I., and Friend, J. E.; Probability and Statistics for Engineers, Prentice-Hall, Inc., 1965.

10. Naylor, Mike; Very Fine Particle Generation by Electric Arc: Sampling and Analysis, problem report submitted to West Virginia University, Morgantown, West Virginia, 1976.

11. Neter, J. and Wasserman, W.; Applied Linear Statistical Models, Richard D. Irwin, Inc., 1974.

12. Pfender, B. and Boffa, C. V.; "Generation of Ultrafine Aerosols with a Transpiration Cooled Anode in a High Intensity Arc," The Review of Scientific Instruments, Vol. 41, No. 5, May, 1970, pp. 655-657.

13. Research Appliance Company; "Model 2443 Staksampler: Description, Operating Instruction, and Procedures," Gibsonia, Pa., 1972.

14. Rohrs, Lloyd; "Metal-Fume Fever from Inhaling Zinc Oxide," AMA Achieves of Industrial Health, Vol. 16, No. 1, July 1957, pp. 42-47.

15. SAS INSTITUTE, INC.; A USER'S GUIDE TO SAS 76, Raleigh, North Carolina, 1976.

16. Sears, D. R.; "Fresh Metal Fume Project-2," Laboratory Note Book at West Virginia University, Morgantown, West Virginia 1975.

17. Shimps, Richard; Walter McCrone Associates, private communications from April to December 1976.

18. Waggoner, A. P., and Charlson, R. J.; "Measurements of Aerosol Optical Parameters," in Fine Particles: Aerosol Generation, Measurement, Sampling and Analysis, edited by Benjamin Y. H. Liu, Academic Press, Inc., 1976, pp. 511-535.

19. Wall Colmonoy Corporation; "Model UT-500 Colmonoy Electrospray Metallizer, Direction for Operating," Detroit, Michigan, 1973.

20. Western Precipitation Group - Bulletin WP-50; "Methods for Determination of Velocity Volume, Dust, Nd Mist Content of Gases," Joy Manufacturing Company, Los Angeles, California.

Appendix A

Assuming that a particle is spherical and that its Reynolds number is small enough to indicate laminar flow, it is possible to calculate the terminal velocity of the particle by the following expression:

$$V_t = \frac{d^2(\rho_p - \rho_f)g}{\mu}$$

where d is the diameter of the particle, ρ_p is the density of the particle, ρ_f is the density of the fluid, g is the acceleration due to gravity, and μ is the dynamic viscosity of the fluid.

Assuming a particle of diameter 0.5 μm with a unit density of (1gm/cm^3) in an atmospheric fluid (20 °C,1 atmosphere), the formula yields

$$V_t = \frac{(5 \times 10^{-7} m)^2 (1 \times 10^3 Kg/m^3 - 1.2 kg/m^3)(9.81 m/s^2)}{1.82 \times 10^{-3} Kg/m \quad s}$$

$$V_t = 1.4 \times 10^{-6} m/s = 0.48\ cm/hr$$

$$V_t = 0.19\ in/hr = 4.58\ in/hr$$

$$R\# = \frac{V \cdot d \quad \rho_p}{DV}$$

$$R\# = \frac{(1.4 \times 10^{-6} m/s)(5 \times 10^{-7} m)(1 \times 10^3 Kg/m^3)}{1.82 \times 10^{-3}\ Kg/m \quad s}$$

$$R\# = 3.8 \times 10^{-7}$$

A particle with above assumptions will have a terminal velocity of less than one half centimeter per hour; this particle has a Reynolds number small enough to indicate laminar flow; this satisfied the second assumption necessary for use of this terminal velocity expression.

Preceding page blank

Appendix B

The mass of an assumed spherical particle is given by the following expression:

$$M = \rho(4\pi r^3/3)$$

$$M = \rho\pi d^3/6$$

where r is the radius of the particle, ρ is the density of the particle, and d is the diameter of the particle.

The ratio of the masses of two spherical particles with different diameter but equivalent densities is given by:

$$M = M_1/M_2$$

$$M = (\rho\pi d_1{}^3/6)/(\rho\pi d_2{}^3/6)$$

$$M = d_1{}^3/d_2{}^3$$

with the assumption of equal density spherical particles with diameters of 0.1 μm and 0.01 μm, the larger particle is 1000 times heavier than the smaller particle at the same point on the Earth's surface.

Appendix C-1 Particle Sizing Pictures

The following pictures were presented to show the SEM pictures used to measure the agglomerated particles.

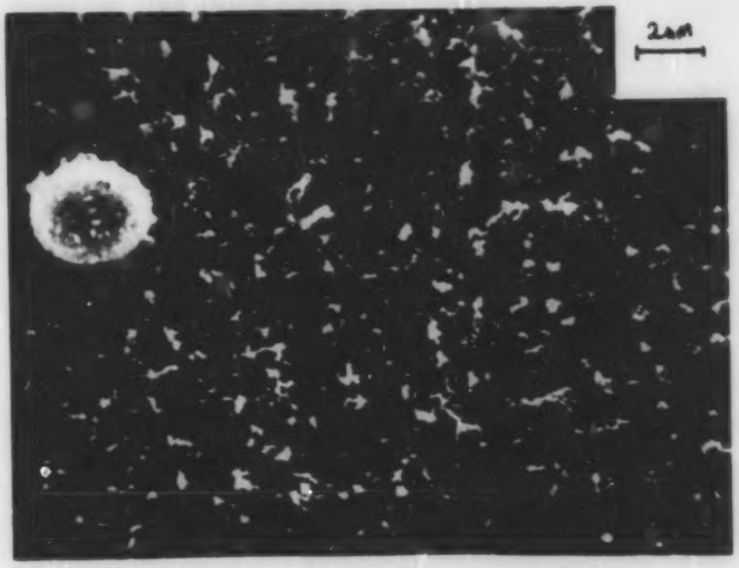

Figure 9. SEM picture sample 715

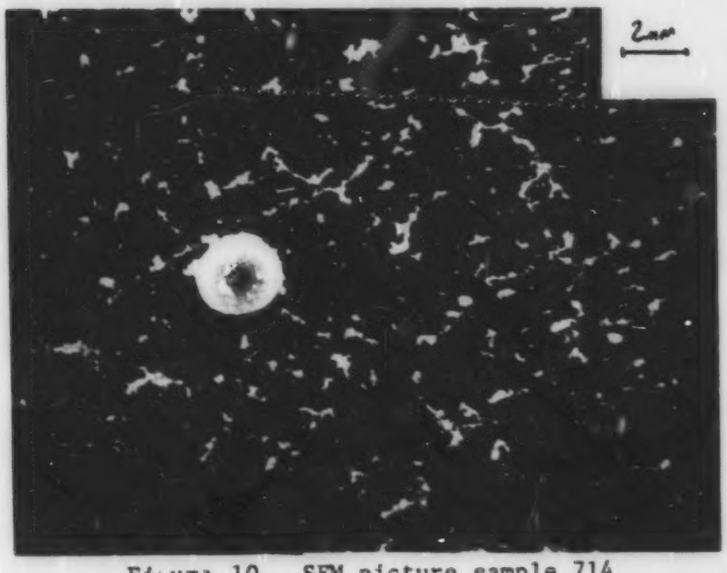

Figure 10. SEM picture sample 714

Appendix C-2 Sizing of the Agglomerates

The agglomerated particles were measured with a clear plastic metric ruler. The photomicrographs were enlarged such that a measurement of 2 mm would approximately correspond to 0.2 μm. The maximum horizontal - across the photograph - and the maximum vertical distance a particle covered were measured and averaged to give an average particle diameter. With known magnification, the actual size was determined by the following expression:

$$\text{Real Size} = \frac{\text{Image Size}}{\text{Magnitude of Magnification}} .$$

Groups ranging from less than 2 mm to greater than 30 mm by increments of 2 mm were used in counting the number of particles within a range. Class marks were assigned to each group interval. The raw data is presented in Table 28. The SAS MEANS procedure determined the statistics presented in Table 18.

The photographs from the SEM negative were not exceptionally clear; that is, the particles did not have sharp edges. This effect would be a factor in both sample measurements; therefore it was felt the results were not affected by this extraneous variable.

Appendix C-1 Particle Sizing Pictures

The following pictures were presented to show the SEM pictures used to measure the agglomerated particles.

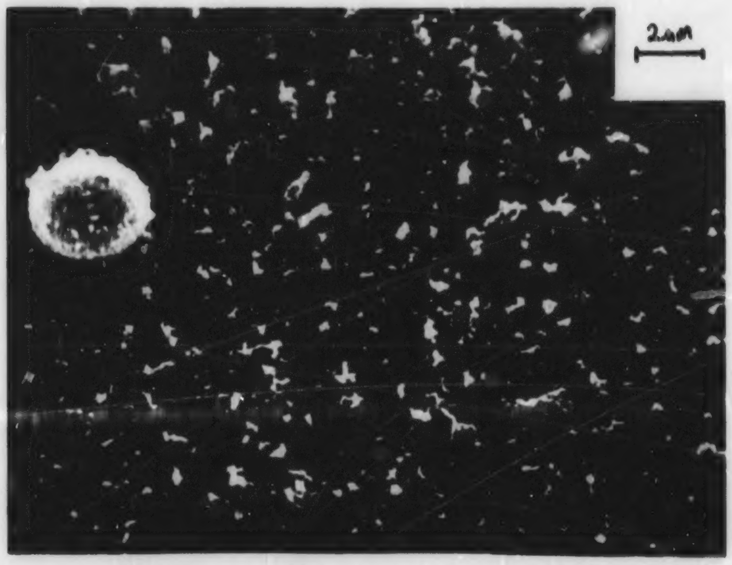

Figure 9. SEM picture sample 715

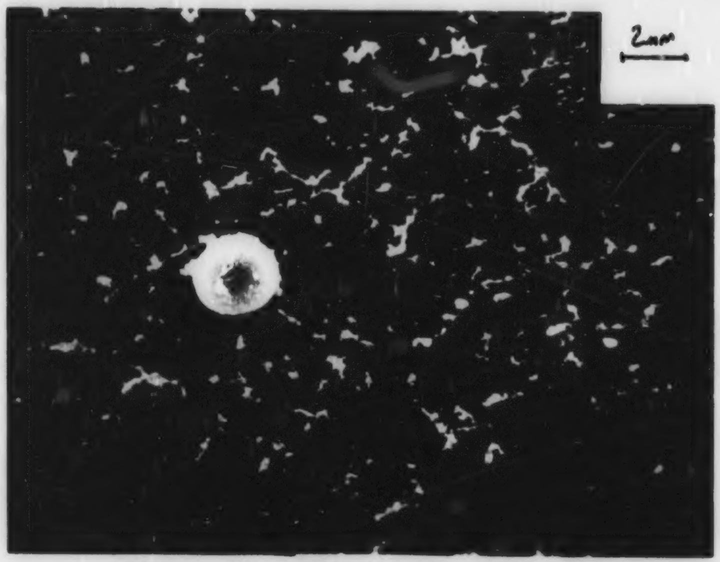

Figure 10. SEM picture sample 714

Table 28. Raw data for agglomerated particle count

Sample #		714	715
Magnifier (1) Negative		5000	5000
(2) Enlargement		23/10.5	23/10
Range	Class Mark	Count	Count
Less than 2mm	1 mm	156	136
2 to 4 mm	3 mm	41	56
4 to 6 mm	5 mm	19	31
6 to 8 mm	7 mm	17	23
8 to 10 mm	9 mm	14	10
10 to 12 mm	11 mm	8	7
12 to 14 mm	13 mm	7	11
14 to 16 mm	15 mm	3	4
16 to 18 mm	17 mm	3	4
18 to 20 mm	19 mm	6	3
20 to 22 mm	21 mm	0	1
22 to 24 mm	23 mm	0	0
24 to 26 mm	25 mm	2	0
26 to 28 mm	27 mm	1	1
28 to 30 mm	29 mm	1	0
Greater than 30 mm	31 mm	4	8

Appendix C-3 Mass Concentration Data

The mass concentration data is presented in the following three sets of tables. The top listings in each table are some of the data taken during sampling. The bottom listings are the calculated values for determining the mass concentration (STP) and indicator of isokenitic conditions (10,13).

After finding the net weight of a mass sample, STP mass concentration can be found by dividing the ratio of the mass collected to the volumetric flow through the filter by a correction factor sc. This factor compensates for the differences in temperature and pressure relative to standard temperature (298°K) and pressure (29.92 in.) by the following formula:

$$V_{STD} = V_{Meter} \times \frac{P_{Meter}}{29.92\text{ in.}} \times \frac{298\ ^\circ K}{T_{Meter}} = V_{Meter} \times \text{ sc.}$$

This calculation assumes the negligible influence of water in the duct gas stream (10,20); the relative humidity was found to be less than 20%. Symbols are explained in Figure 11.

The isokenitic factor was approximated by the ratio of the nozzle velocity to the stack velocity:(I'). It was expected to provide an adequate target for approximating isokenitic; as can be seen in the concentration raw data tables, the samples were not taken isokenitically. The sample nozzle velocity was mostly greater than the gas stream velocity. The approximation (I') is transformed into the isokenitic relation (I):

$$I = \frac{(T_{STACK}/T_{STD})(P_{STD}/P_{STACK})(V_{m\ STD} + V_{w\ STD})}{(Vel_{STACK})(\Delta Time)(Area\ of\ Nozzle)} ,$$

by multipling approximation (I') (10) by the correction factor c which is given in Figure 11.

V_{STD} is STP volumetric flow

V_{Meter} is volumetric flow (cfm)

P_{Meter} is Atmospheric pressure at stack sampler (in.Hg)

T_{Meter} is Average temperature of stack sampler thermometer (°F)

Δp HEPA is Δp across HEPA filter (in. H_2O)

Pilot Δp is standard pilot p at point of sampling (in. H_2O)

SAP is secondary air supply (psi)

Stack T (T_{STACK}) is temperature of duct (°C)

P_{STACK} is gage pressure of sampling duct (in.Hg)

Wire feed rate is 30-60 (corresponding to 37 to 86 gm/min)

MAP is main air jet pressure (psi)

Open Voltage is voltage across arc prior to operation (volts)

CF is dry gas meter volumetric flow (ft^3)

Time is time of sampling (sec)

Area of Nozzle is $(1/4 \cdot 1/12)^2(\pi/4)$ (ft^2)

Nozzle Velocity is CFM area of nozzle (ft/min)

Stack Velocity is $234\sqrt{\frac{29.92}{P_{STACK}}\quad(273 + T_{STACK})(\text{Pilot}\,\Delta p)}$

Isokenetic approximation is $\frac{\text{Nozzle Velocity}}{\text{Stack Velocity}}$

$$C = \frac{T_{STACK}}{P_{barStack}} \cdot \frac{P_{bar}}{T_{meters}} \cdot (1 + R)$$

R = % water in gas stream

Figure 11. Explanation of data sheet and mass calculation symbols

Table 29. Mass data first latin square experiment

(1) Pitot ΔP = 0.065   Date 7/5/76
SAP = 20 psi   (2) P_{bar} = 28.98 in Hg

Sample #	529	546	547	548
(3) Δp HEPA	0.5	0.5	0.55	0.6
(4) P_{Stack} = (2) - (3)/13.6	28.92	28.92	28.93	28.93
(5) Stack T (C)	68	73	64	74
Wire Feed Rate	50	40	40	50
MAP	40	50	45	45
Open Voltage	29	31	25	27
(6) CF	0.359	0.412	0.372	0.399
(7) Time	1 min	1 min	1 min	1 min
T_{Meter}	76	77.5	79.5	80.5
(8) Nozzle Velocity =	1053	1209	1091	1170
(9) Stack Velocity =	1121	1129	1114	1131
Isokenetic estimate (I')	0.94	1.08	0.98	1.03
C	1.15	1.16	1.13	1.16
I = I' x C	1.08	1.24	1.11	1.19
gm/acf	0.0428	0.0371	0.0315	0.0362
gm/sm^3	1.51	1.31	1.11	1.28
sc	0.97	0.968	0.964	0.96

Table 29. (Continued)

(1) Pitot ΔP = 0.065 Date 7/5/76

SAP = 20 psi (2) P_{bar} = 28.98 in Hg

Sample #	549	550	551	552
(3) Δp HEPA	0.6	0.65	0.65	0.7
(4) P_{Stack} = (2) - (3)/13.6	28.93	28.93	28.93	28.93
(5) Stack T (C)	75	72	60	53
Wire Feed Rate	50	60	30	30
MAP	55	40	55	45
Open Voltage	31	31	27	31
(6) CF	0.364	0.383	0.386	0.401
(7) Time	1 min	1 min	1 min	1 min
T_{Meter}	81.75	83.5	84	87
(8) Nozzle Velocity =	1068	1124	1132	1176
(9) Stack Velocity =	1133	1127	1107	1096
Isokenetic estimate (I')	0.93	1.00	1.02	1.07
C	1.16	1.15	1.10	1.08
I = I' x C	1.00	1.15	1.12	1.16
gm/acf	0.0334	0.0481	0.0228	0.0297
gm/sm^3	1.18	1.70	0.81	1.05
sc	0.96	0.957	0.956	0.951

Table 29. (Continued)

(1) Pitot ΔP = 0.065 Date 7/5/76

SAP = 20 psi (2) P_{bar} 28.98 in Hg

Sample #	553	554	555	556
(3) Δp HEPA	0.7	0.65	0.65	0.65
(4) P_{Stack} = (2) - (3)/13.6	28.93	28.93	28.93	28.93
(5) Stack T (C)	73	85	76	60
Wire Feed Rate	40	60	50	30
MAP	40	45	50	50
Open Voltage	27	29	25	29
(6) CF	0.389	0.390	0.382	0.380
(7) Time	1 min	1 min	1 min	1 min
T_{Meter} (F)	88.5	88.25	88.75	89
(8) Nozzle Velocity =	1141	1144	1121	1115
(9) Stack Velocity =	1129	1148	1133	1107
Isokenetic estimate (I')	1.01	1.00	0.99	1.01
C	1.14	1.18	1.15	1.10
I = I' x C	1.15	1.18	1.14	1.11
gm/acf	0.0336	0.0502	0.0388	0.0303
gm/sm^3	1.19	1.77	1.37	1.07
sc	0.949	0.950	0.950	0.947

Table 29. (Continued)

(1) Pitot ΔP = 0.065 Date 7/5/76

SAP = 20 psi (2) P_{bar} = 28.98 in Hg

Sample #	557	558	559	560
(3) Δp HEPA	0.65	0.65	0.65	0.70
(4) P_{Stack} = (2) - (3)/13.6	28.93	28.93	28.93	28.93
(5) Stack T (C)	57	80	70	70
Wire Feed Rate	30	60	60	40
MAP	40	50	55	55
Open Voltage	25	27	25	29
(6) CF	0.370	0.378	0.400	0.383
(7) Time	1 min	1 min	1 min	1 min
T_{Meter}	89.75	90	90.25	90.5
(8) Nozzle Velocity =	1085	1190	1173	1124
(9) Stack Velocity =	1102	1140	1124	1124
Isokenetic estimate (I')	0.98	0.97	1.04	1.00
C	1.08	1.16	1.13	1.04
I = I' x C	1.06	1.13	1.08	1.04
gm/acf	0.0260	0.0493	0.0291	0.042
gm/sm^3	0.92	1.74	1.03	1.48
sc	0.946	0.946	0.945	0.945

Table 30. Mass data second latin square experiment

(1) Pitot ΔP = 0.06 Date 7/11/76
SAP = 20 psi (2) P_{bar} = 29.05 in Hg

Sample #	561	562	563	564
(3) Δp HEPA	0.5	0.5	0.5	0.5
(4) P_{Stack} = (2) - (3)/13.6	29.01	29.01	29.01	29.01
(5) Stack T (C)	71	62	82	80
Wire Feed Rate	40	40	50	60
MAP	40	50	55	40
Open Voltage	27	31	31	31
(6) CF	0.389	0.350	0.340	0.352
(7) Time	1 min	1 min	1 min	1 min
T_{Meter}	80	81	82	82
(8) Nozzle Velocity =	1141	1026	974	1033
(9) Stack Velocity =	1089	1006	1097	1094
Isokenetic estimate (I')	1.06	1.02	0.89	0.94
C	1.15	1.12	1.18	1.17
I = I' x C	1.22	1.14	1.05	1.10
gm/acf	0.0425	0.0543	0.0611	0.0473
gm/sm^3	1.50	1.92	2.16	1.67
sc	0.966	0.964	0.962	0.962

Table 30. (Continued)

(1) Pitot ΔP = 0.06 Date 7/11/76

SAP = 20 psi (2) P_{bar} = 29.05 in Hg

Sample #	565	566	582	568
(3) Δp HEPA	0.5	0.5	0.5	0.5
(4) P_{Stack} = (2) - (3)/13.6	29.01	29.01	29.01	29.01
(5) Stack T (C)	77	80	59	57
Wire Feed Rate	50	60	30	30
MAP	45	50	40	45
Open Voltage	27	27	25	31
(6) CF	0.369	0.335	0.393	0.375
(7) Time	1 min	1 min	1 min	1 min
T_{Meter}	80.5	80	82	82
(8) Nozzle Velocity =	1082	983	1153	1100
(9) Stack Velocity =	1089	1094	1061	1057
Isokenetic estimated (I')	0.99	0.90	1.09	1.04
C	1.17	1.18	1.11	1.10
I = I' x C	1.16	1.06	1.20	1.14
gm/acf	0.0440	0.0517	0.0283	0.0338
gm/sm^3	1.55	1.83	1.00	1.19
sc	0.965	0.966	0.962	0.962

Table 30. (Continued)

(1) Pitot $\Delta P = 0.06$ Date 7/11/76
SAP = 20 psi (2) $P_{bar} = 29.05$ in Hg

Sample #	569	570	571	572
(3) Δp HEPA	0.5	0.5	0.5	0.5
(4) $P_{Stack} = (2) - (3)/13.6$	29.01	29.01	29.01	29.01
(5) Stack T (C)	58	54	58	65
Wire Feed Rate	30	30	40	40
MAP	55	50	55	45
Open Voltage	27	29	29	25
(6) CF	0.368	0.374	0.357	0.361
(7) Time	1 min	1 min	1 min	1 min
T_{Meter}	82	82	82.25	83
(8) Nozzle Velocity =	1080	1097	1047	1059
(9) Stack Velocity =	1059	1053	1059	1070
Isokenetic estimated (I')	1.02	1.04	0.99	0.99
C	1.10	1.09	1.10	1.12
$I = I' \times C$	1.12	1.13	1.09	1.11
gm/acf	0.0327	0.0319	0.039	0.0346
gm/sm^3	1.15	1.13	1.38	1.22
sc	0.962	0.962	0.961	0.960

Table 30. (Continued)

(1) Pitot ΔP = 0.06 Date 7/11/76

SAP = 20 psi (2) P_{bar} = 29.05 in Hg

Sample #	573	581	575	576
(3) Δp HEPA	0.5	0.5	0.5	0.5
(4) P_{Stack} = (2) - (3)/13.6	29.01	29.01	29.01	29.01
(5) Stack T (C)	68	80	76	76
Wire Feed Rate	50	60	60	50
MAP	40	55	45	50
Open Voltage	29	25	27	25
(6) CF	0.360	0.309	0.372	0.356
(7) Time	1 min	1 min	1 min	1 min
T_{Meter}	83.5	83.75	84	84
(8) Nozzle Velocity =	1056	906	1091	1044
(9) Stack Velocity =	1074	1094	1087	1087
Isokenetic estimated (I')	0.98	0.83	1.003	0.96
C	1.13	1.17	1.16	1.16
I = I' x C	1.11	0.97	1.16	1.11
gm/acf	0.0406	0.0513	0.0392	0.0413
gm/sm^3	1.43	1.81	1.38	1.46
sc	0.959	0.959	0.958	0.958

Table 31. Mass data orthogonal experiment

(1) Pitot $\Delta P = 0.05$ Date 8/9/76

SAP = 20 psi (2) $P_{bar} = 28.91$ in Hg

Sample #	700	701	702	703
(3) Δp HEPA	0.4	0.4	0.4	0.4
(4) $P_{Stack} = (2) - (3)/13.6$	28.88	28.88	28.88	28.88
(5) Stack T (C)	70	72	90	72
Wire Feed Rate	45	45	55	45
Map	50	40	50	40
Open Voltage	30	28	30	30
(6) CF	0.236	0.236	0.165	0.216
(7) Time	77/100	72/100	50/100	71/100
T_{Meter}	72	72	72	72
(8) Nozzle Velocity =	986	989	1015	989
(9) Stack Velocity =	899	961	968	892
Isokenetic estimate (I')	0.91	0.97	0.95	0.90
C	1.16	1.17	1.23	1.17
I = I' x C	1.06	1.13	1.17	1.05
gm/acf	0.04	0.0408	0.0603	0.0428
gm/sm^3	1.41	1.44	2.13	1.51
sc	0.975	0.975	0.975	0.975

Table 31. (Continued)

(1) Pitot $\Delta P = 0.05$ Date 8/9/76
SAP = 20 psi (2) $P_{bar} = 28.91$ in Hg

Sample #	704	705	706	707
(3) Δp HEPA	0.4	0.4	0.4	0.4
(4) $P_{Stack} = (2) - (3)/13.6$	28.88	28.88	28.88	28.88
(5) Stack T (C)	80	95	85	85
Wire Feed Rate	45	55	55	55
MAP	50	40	40	50
Open Voltage	28	30	28	28
(6) CF	0.217	0.205	0.236	0.192
(7) Time	60/100	72/100	67/100	65/100
T_{Meter}	72	72	72	72
(8) Nozzle Velocity =	948	970	1008	1008
(9) Stack Velocity =	1061	835	1033	867
Isokenetic estimate (I')	1.12	0.86	1.03	0.86
C	1.20	1.25	1.21	1.21
$I = I' \times C$	1.34	1.08	1.25	1.04
gm/acf	0.043	0.0485	0.0408	0.0481
gm/sm^3	1.52	1.71	1.44	1.70
sc	0.975	0.975	0.975	0.975

Appendix D-1 Latin Square

The Latin Square Design is considered an economic, balanced design. Extraneous variables can be tested for any effect on the dependent variable in this design. The variability produced by the extraneous variables is separated from the variability produced by the main independent variables (9). A thorough presentation is included in references 9 and 11.

A F-statistic is used to test the null hopothesis that the effect of the variable is equal to zero. The independent, extraneous, and a replicate statistic are found. Table 32 presents short cut formulae and definitions of terms necessary for the calculation of the F-statistic (9). This statistic is compared to a tabulated F-value with the specified degrees of freedom and confidence limit. If the calculated F-value is greater than the chosen tabulated F-value, then the effect of the variable is not equal to zero.

Table 33 shows calculation table and Latin Square Summary table. Tables 24 and 25 show the equivalence of the SAS ANOVA procedure for analysis of variance and the short cut Latin Square procedure; the F values are essentially equal.

Table 32. Formula and definitions for latin square analysis of variance

Source of Variation	Degrees of Freedom	Sum of Squares	Mean Square	F
Treatments (wire feed rate)	n-1	$SS(T_R)$	$\frac{SS(TR)}{n-1}$	$\frac{MS(TR)}{MSE}$
Rows	n-1	SSR	$\frac{SSR}{n-1}$	$\frac{MSR}{MSE}$
Columns	n-1	SSC	$\frac{SSC}{n-1}$	$\frac{MSC}{MSE}$
Replicates	r-1	SS(Rep)	$\frac{SS(Rep)}{r-1}$	$\frac{MS(Rep)}{MSE}$
Error	(n-1)(rn+r-3)	SSE	$\frac{SSE}{(n-1)(rn+r-3)}$	
Total	rn^2-1	SST		

$$C = (T\ldots)^2/r-n^2$$

$$SS(T_R) = \frac{1}{r\cdot n}\sum_{k=1}^{n} T_{(k)}^2 - C$$

r = Number of replicates

$$SSR = \frac{1}{r\cdot n}\sum_{i=1}^{n} T_{i..}^2 - C$$

n = Number of factors

$$SSC = \frac{1}{r\cdot n}\sum_{j=1}^{n} T_{j..}^2 - C$$

$$SS(Rep) = \frac{1}{r\cdot n}\sum_{l=1}^{r} T_{..l}^2 - C$$

$$SST = \sum_{i=1}^{n}\sum_{j=1}^{n}\sum_{l=1}^{n} Y_{ij(k)l}^2 - C$$

$$SSE = SST - SS(TR) - SSR - SSC - SS(Rep)$$

Table 33. Calculation table for latin square design

Replicate 1 (gm/sm^3)

MAP (psi)

Vo (Volts)	40	45	50	55	
25	A 0.92	B 1.11	C 1.37	D 1.03	4.43
27	B 1.19	C 1.28	D 1.74	A 0.81	5.02
29	C 1.51	D 1.77	A 1.07	B 1.48	5.83
31	D 1.70	A 1.05	B 1.31	C 1.18	5.24
	5.32	5.21	5.49	4.50	

Replicate 2 (gm/sm^3)

MAP (psi)

Vo (Volts)	40	45	50	55	
25	A 1.00	B 1.22	C 1.46	D 1.81	5.49
27	B 1.50	C 1.55	D 1.83	A 1.15	6.03
29	C 1.43	D 1.38	A 1.13	B 1.38	5.32
31	D 1.67	A 1.19	B 1.92	C 2.16	6.94
	5.60	5.34	6.34	6.50	

Wire Feed (Rate %)	Σ Rep 1	Σ Rep 2	ΣT... 44.30
A-30	3.85	4.47	
B-40	5.09	6.02	
C-50	5.34	6.60	
D-60	6.24	6.69	

Appendix D-2 T Test Procedures

The student t-test is based on a random variable having the student-t distribution with n-1 degrees of freedom. Where n is the sample, x is the sample mean, s is the sample standard deviation, and μ is the expected mean of a normal population, the value of the t-statistic is given by

$$t = \frac{x - \mu}{s/\sqrt{n}}$$

The testing of the hypothesis concerning two means with unknown population variances is based on the t-statistic. If the variances are equal by the F-test, the t-statistic that is used for decision-making is the Student-t.

The t-statistic for comparing two means is found with the formula

$$t_{cal} = \frac{(\bar{x}_1 - \bar{x}_2) - \delta}{S_{\bar{x}p}} \qquad (1)$$

where

$$\frac{1}{S_{\bar{x}p}} = \left(\frac{n_1 n_2 (n_1 + n_2 - 2)}{(n_1 + n_2)[(n_1 - 1)S_1^2 + (n_2 - 1)S_2^2]} \right)^{-1/2} \qquad (2)$$

The value of δ is set equal to zero when testing the hypothesis that the means are not different. If the variances are unequal, then the Smith-Satterthwaite t-statistic is used (9) where

$$t'_{cal} = \frac{(\bar{x}_1 - \bar{x}_2) - \delta}{\sqrt{\frac{S_1^2}{n_1} + \frac{S_2^2}{n_2}}} \qquad (3)$$

and

$$df' = \left(\frac{S_1^2}{n_1} + \frac{S_2^2}{n_2}\right) \div \left(\frac{(S_1^2/n_1)^2}{n_1-1} + \frac{(S_2^2/n_2)^2}{n_2-1}\right) \quad (4)$$

The equivalent mean hypothesis tests in this report are based on the assumption that $\delta = 0$.

$$H_o: \; V_1 - V_2 = \delta = 0$$

$$H_A: \; V_1 - V_2 \neq 0$$

The criterion for rejecting H_o, where $t\alpha/2$ is equal to the tabulated t-value with $(n_1 + n_2 - 2)$ degrees of freedom and Type I error equal to α, is given by

$$\text{Reject } H_o: \; V_1 - V_2 = 0$$

$$\text{if } t_{cal} < -t\,\alpha/2$$

$$\text{or } t_{cal} > t\,\alpha/2 \quad (5)$$

The F-statistic given by $F_{cal} = S_1^2/S_2^2$ is used to determine equality of sample variances. If F_{cal} is less than a tabulated F statistical, then the variances are equal. If the variances are unequal, then the Smith-Satterthwaite t-statistics are used in the hypothesis test.

The following are example Agglomerate T Test Calculations.

Given: $x = 0.41\ \mu m$ $\quad s = 0.53\ \mu m$ $\quad n_1 = 300$

$x_2 = 0.40\ \mu m$ $\quad s_2 = 0.54\ \mu m$ $\quad n_2 = 282$

with equation (1)

$$t_{cal} = \left(\frac{0.41\ \mu m - 0.40\ \mu m}{\frac{(300)(282)(300+282-2)}{(300+282)[(294)(0.53)^2+(281)(0.54)^2]}} \right)^{1/2}$$

$t_{cal} = 0.225$ df - 300 + 282 - 2 = 580

with equation (3)

$$t'_{cal} = \frac{0.41\ \mu m - 0.40\ \mu m}{\sqrt{\frac{(0.53)^2}{300} + \frac{(0.54)^2}{282}}}$$

$t'_{cal} = 0.225$

from equation (4)

$$df' = \left(\frac{(0.53)^2}{300} + \frac{(0.54)^2}{282} \right)^2 \div \left[\frac{(0.52)^2/300)^2}{299} + \frac{(0.54)^2/282)^2}{281} \right]$$

$df' = 576.3$

In either case, equivalent variances or not, the t_{cal} value is 0.225. The df are approximately 580; this degree of freedom for all practical calculations is equal to infinity. With the tabulated t value (alpha equals 0.10 and df equals infinity) being 1.645, the hypothesis test (5) shows the means not different.

In Table 34, the SAS T Test Calculates both the general t-statistic and the Smith-Satterthwaite t-statistic. The differences in the calculated by hand and calculated by computer t-values are a consequence of rounding and truncating errors.

Table 34. SAS T test table

Variable: **X, agglomerated particle diameter.**

REPP	N	Mean	STD Dev.	STD Error
1	300	0.41	0.53	0.036
2	282	0.40	0.54	0.032

Minimum	Maximum	Variances	T	DF	PROB>!T!
0.087	2.61	Unequal	0.1938	575.5	0.8464
0.091	2.74	Equal	0.1939	580.0	0.8463

For HO: Variances are equal. F' = 1.05 with 281 and 299 DF

PROB > F' = 0.565

Appendix D-3 ANOVA

The SAS ANOVA procedure uses a matrix manipulation technique to determine the analysis of variance in a collection of samples. The procedure finds the analysis of variance sum of squares for each variable in the selected model as well the sum of squares of the error in the data. A comparison of the average drop in the sequential sum of squares to the average drop in the sum of squares of the error terms is used to determine if the independent variable helps explain the variability of the data.

The F-statistic in formula expression is

$$F = \frac{SSR/p-1}{SSE/n-p}$$

where SSR is the sequential sum of squares for the particular variable, SSE is the error sum of squares for the data, p is the number of variables in the selected model, and n is the number of samples. This statistic is shown to the right of the variable names in Table 25. The ANOVA procedures also calculates the F-statistic associated with examining the data fit of the model. This statistic is shown to the right of the model source in Table 23. The term below this statistic, PR>F, gives the probability that the model is fitting noise. Other statistics are shown in the ANOVA table.

Appendix D-4 Stepwise Procedure

One of the search methods for arriving at a "best" set of independent variables from the total variables available is the stepwise regression method (15,11). This set of variables will best describe as well as predict the relation between the independent and dependent variables. The stepwise procedure determines the variables which have an observed effect on the outcome at a certain level of significance. The variable which explains most of the variability in the data is first added to the set of best independent variables.

After the first variable is chosen, a second best variable is chosen (with the assumption that the first variable explained a portion of the variance in the data), and then a statistical test determines if the first variable (actually, any and all prior variables chosen) should be eliminated from the set of "best" variables. If both of the choices are kept in the set, the procedure continues to add to and check for deletion of best variables until all the variables in the set are "best" with a certain confidence. The SAS default confidence is 90%. The deleted variables do not significantly explain the outcome therefore they are dropped.

The SAS STEPWISE procedure calculated the best variables that describe (predict) the collection of mass concentration data. The analysis printout format is presented in Table 35. This stepping procedure took four steps. The wire feed rate variable was added first and the best variable set contained the wire feed rate and open voltage variables.

Table 35. Stepwise regression procedure for dependent variable Y, mass concentration

STEP 1	Variable WF Entered	R Square = 0.43				
		DF	Sum of Squares	Mean Square	F	PROB>F
	Regression	1	1.69	1.69	29.1	0.0001
	Error	38	2.21	0.06		
	Total	39	3.91			
		B Value	STD Error	Type II SS	F	PROB>F
	Intercept	0.52				
	WF	0.02	0.0037	1.69	29.1	0.0001
STEP 2	Variable V Entered	R Square = 0.54				
		DF	Sum of Squares	Mean Square	F	PROB>F
	Regression	2	2.09	1.05	21.4	0.0001
	Error	37	1.81	0.05		
	Total	39	3.91			
		B Value	STD Error	Type II SS	F	PROB>F
	Intercept	-0.81				
	WF	0.019	0.0034	1.63	33.3	0.0001
	V	0.048	0.017	0.4	8.1	0.0070

Table 35. (Continued)

STEP 3	Variable P Entered	R Square = 0.543				
		DF	Sum of Squares	Mean Square	F	PROB>F
	Regression	3	2.12	0.71	14.3	0.0001
	Error	36	1.79	0.090		
	Total 39	39	3.91			
		B Value	STD Error	Type II SS	F	PROB>F
	Intercept	-1.05				
	WF	0.019	0.003	1.6	33.1	0.0001
	V	0.048	0.017	0.40	8.2	0.0070
	P	0.0047	0.006	0.03	0.56	0.4605

STEP 4	Variable P Removed	R Square = 0.53				
		DF	Sum of Squares	Mean Square	F	PROB>F
	Regression	2	2.09	1.05	21.4	0.0001
	Error	37	1.81	0.04		
	Total	39	3.91			
		B Value	STD Error	Type II SS	F	PROB>F
	Intercept	-0.81				
	WF	0.01	0.003	1.6	33.3	0.0001
	V	0.04	0.017	0.40	8.1	0.0070

All variables in the model are significant at the 0.1000 level.

Appendix D-5 GLM and Residual Plots

The SAS GLM (General Linear Model) procedure functions much as the SAS ANOVA procedure. The GLM procedure is more powerful than the ANOVA procedure because it can be applied to virtually any data set; the ANOVA procedure requires the data to be balanced. Since the GLM procedure outputs the needed statistics, the GLM procedure was used to calculate residuals for standardized residual plots.

A residual is the difference between the predicted out come from the regression model developed from the observations and the observed out come at the same point. A standardized residual is the residual at a point divided by the square root of the mean sum of squares (the standardized deviation) of the error. The standardized residuals from a well fitting model should be evenly dispersed about the zero residual line because they are normally distributed variables if the model adequately describes the independent-dependent variable relationship (11).

The GLM table is presented in Table 36. The model F-statistic value indicated that the model is fitting valid independent variable induced variability. The F-value for the wire feed rate and open voltage indicates that these variables significantly influenced the outcome. The next table presents the parameter (B_1) estimates for the linear model: $Y = B_o + B_1 (WF) + B_2 (V)$. The t-statistic for acceptance of the beta parameter is indicative of the confidence in the predictive ability of the variable. The next table shows the observed data, the predicted data using the model and beta parameters, and the residuals. The standardized residuals are plotted against various variables in Figures 12, 13, 14, and 15.

Table 36. SAS GLM table including residuals

```
Dependent Variable Y, mass concentration

Source                   DF    Sum of Squares      Mean Square       F Value

Model                     2        2.09               1.05             21.4

Error                    37        1.81               0.04             PR > F

Corrected Total          39        3.90                                0.0001

                         R-Square          C.V.
                          0.54             15.5

                         STD Dev.         Y Mean
                          0.22             1.43

Source    DF     Type I SS     F Value    PR > F    DF     Type IV SS     F Value     PR > F

WF         1        1.69         34.6     0.0001     1        1.63          33.3       0.0001
V          1        0.40          8.1     0.0070     1        0.40           8.1       0.0070

          Parameter            Estimate         T for HO:          PR > !T!     STD Error of
                                                Parameter = 0                   Estimate

          Intercept             -0.81             -1.64              0.1085         0.49
          WF                     0.02              5.77              0.0001         0.003
          V                      0.048             2.85              0.0070         0.017
```

Table 36. (Continued)

OBSERVATION	OBSERVED VALUE	PREDICTED VALUE	RESIDUAL
1	1.51	1.54	-0.03
2	1.31	1.44	-0.13
3	1.11	1.15	-0.04
4	1.28	1.44	-0.16
5	1.18	1.64	-0.460
6	1.70	1.83	-0.13
7	0.81	1.06	-0.25
8	1.05	1.25	-0.20
9	1.19	1.25	-0.06
10	1.77	1.73	0.03
11	1.37	1.35	0.02
12	1.07	1.15	-0.08
13	0.92	0.96	-0.04
14	1.74	1.64	0.10
15	1.03	1.54	-0.51
16	1.48	1.35	0.13
17	1.50	1.25	0.25
18	1.92	1.44	0.48
19	2.16	1.64	0.52
20	1.87	1.83	-0.16
21	1.55	1.44	0.11
22	1.83	1.64	0.19
23	1.00	0.96	0.04
24	1.19	1.25	-0.06
25	1.15	1.06	0.09
26	1.13	1.15	-0.02
27	1.38	1.35	0.03
28	1.22	1.15	0.07
29	1.43	1.54	-0.11
30	1.81	1.54	0.27

Table 36. (Continued)

OBSERVATION	OBSERVED VALUE	PREDICTED VALUE	RESIDUAL
31	1.38	1.73	-0.35
32	1.46	1.35	0.11
33	1.41	1.49	-0.08
34	1.44	1.40	0.04
35	2.13	1.68	0.45
36	1.51	1.49	0.02
37	1.52	1.40	0.12
38	1.71	1.68	0.03
39	1.44	1.59	-0.15
40	1.70	1.59	0.11

Dependent Variable: Y

Sum of Residuals	0.00
Sum of Squared Residuals	1.81
Sum of Squared Residuals - Error SS	-0.00
First Order Autocorrelation	0.15
Durbin-Watson D	1.69

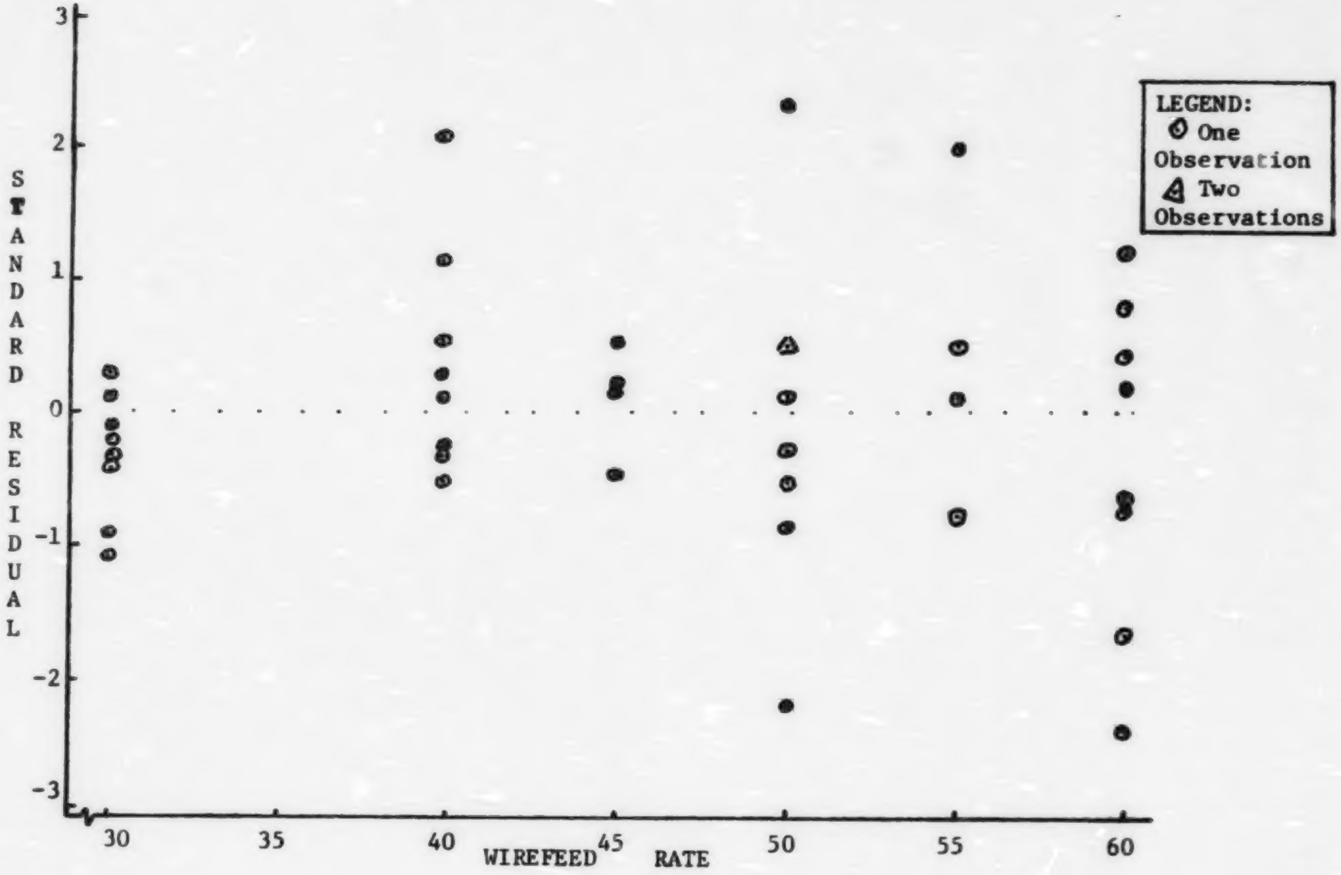

Figure 12. Standard Residual versus Wirefeed Rate

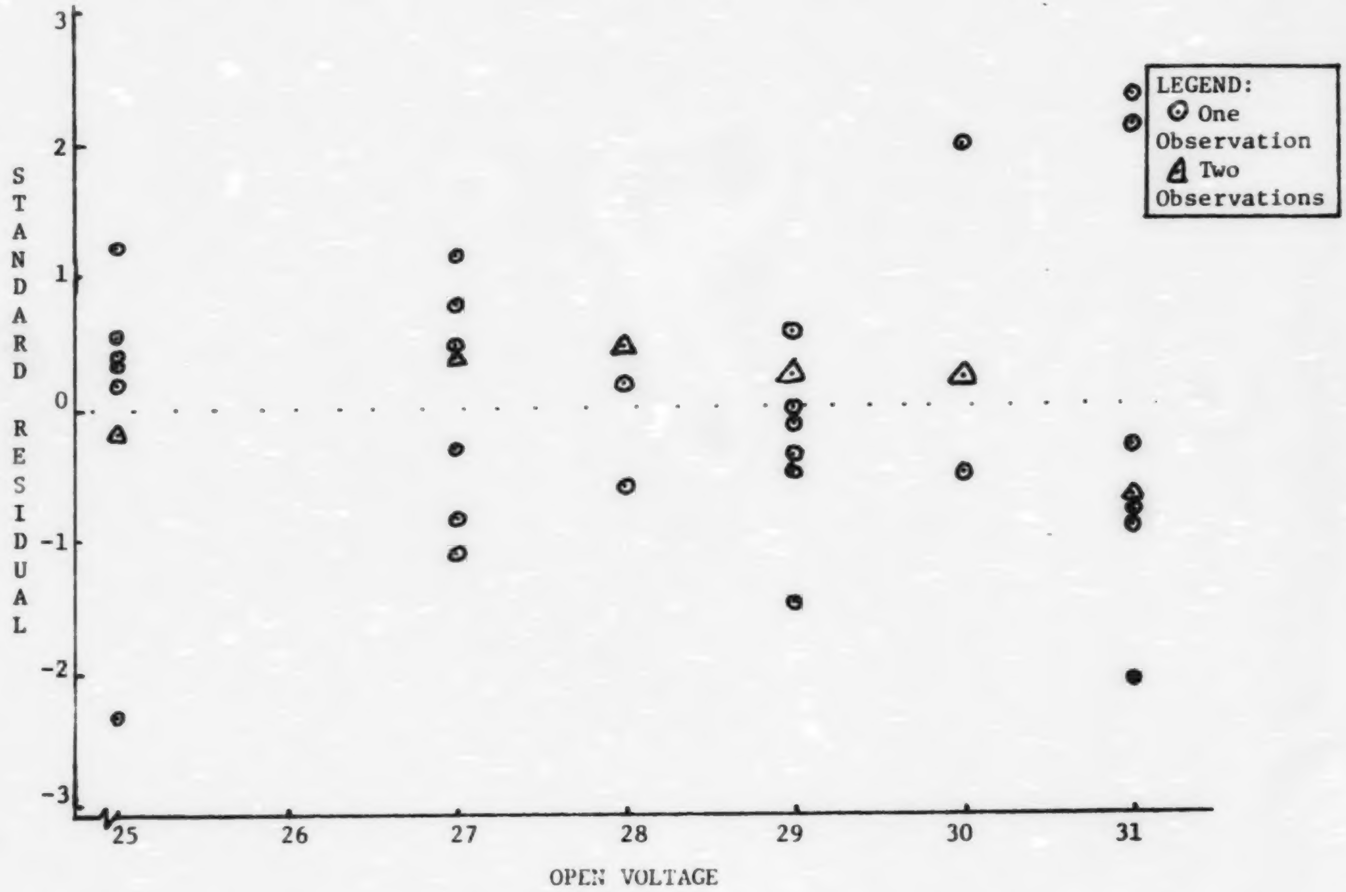

Figure 13 Graph: Standard Residual versus Open voltage

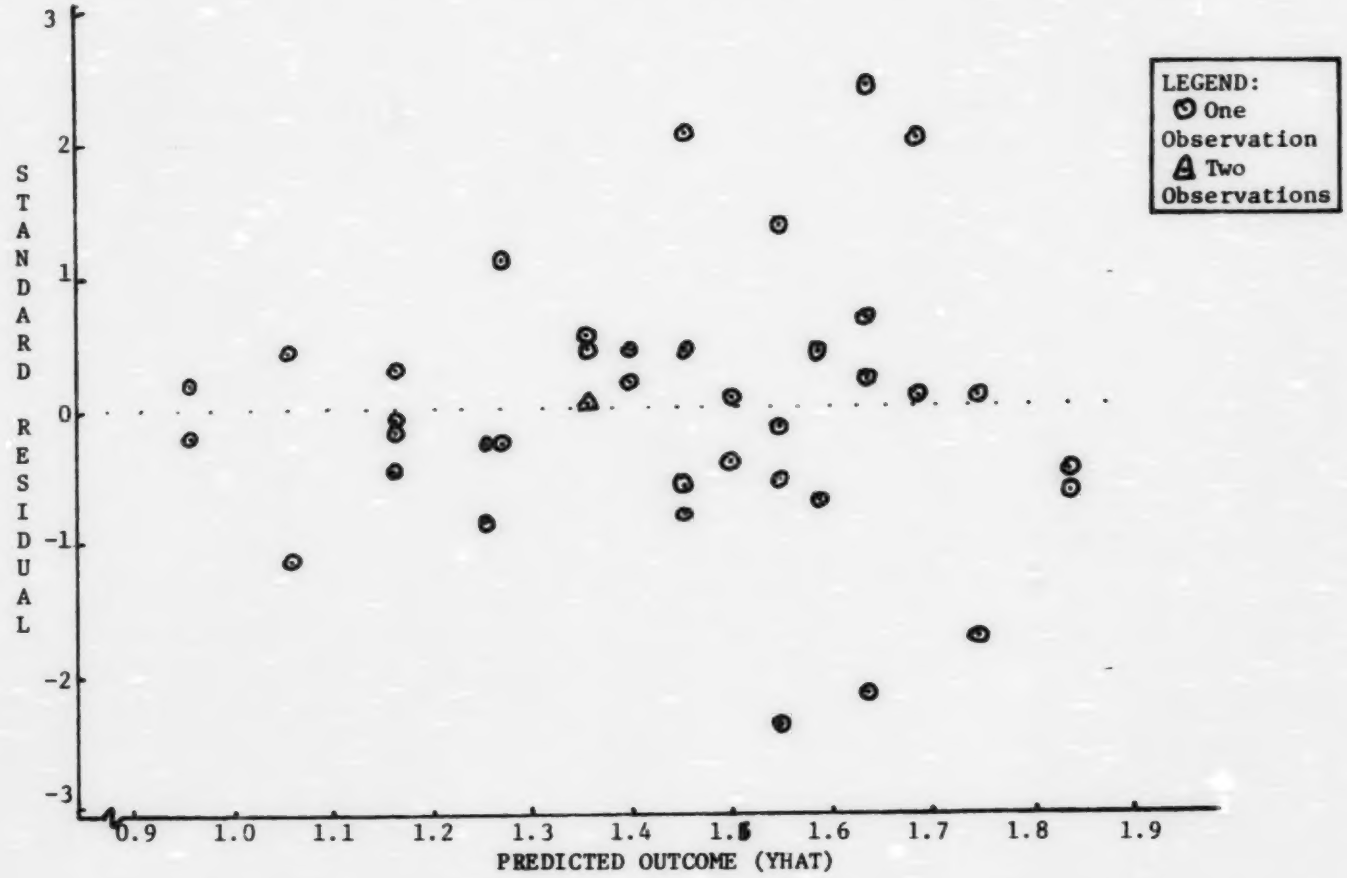

Figure 14. Graph: Standard Residual versus Predicted Outcome(Yhat)

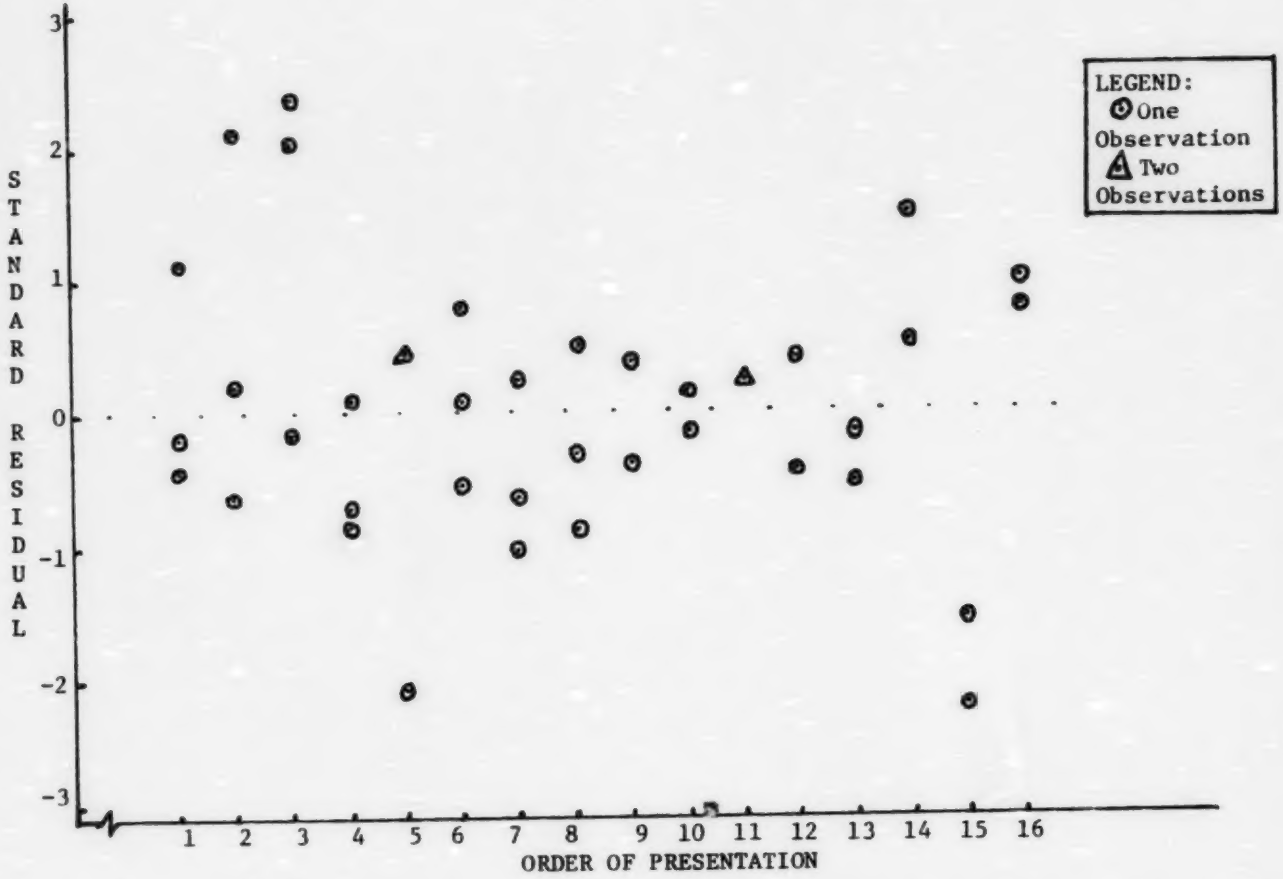

Figure 15. Graph: Standard Residual versus Order of Presentation

Appendix E

The wire feed rate is a unitless dimension on the metallizer unit. The rate of feed is dependent on the wire feed rate setting and the amount of material that is being feed. Time trials at various settings with Walcomonoy #10 wire were used to graph a wire feed rate. This graph is shown in Figure 16.

Using the developed equation for the converted mass of the aerosol:

$$Y = -0.81 + 0.01\ (WF) + 0.048\ (V)$$

a relation between increased metallizer wire feed rate and the percentage of converted mass can be found. Assuming the open voltage to be 31 volts and a ductwork volumetric flow of 5.6 m^3/min., the predicted percent conversion for the various wire feed rates is given by the following expression:

$$\%\ \text{conversion} = \frac{[-0.81+0.048(31) + 0.01(WF)]\ 5.6}{\text{mass input @ wire feed rate, WF}} \times 100$$

Table 37. Relating wire feed rate and percent of mass converted

Wire Feed Rate	Percent Conversion
30	14.8%
40	11.6%
50	9.6%
60	8.3%

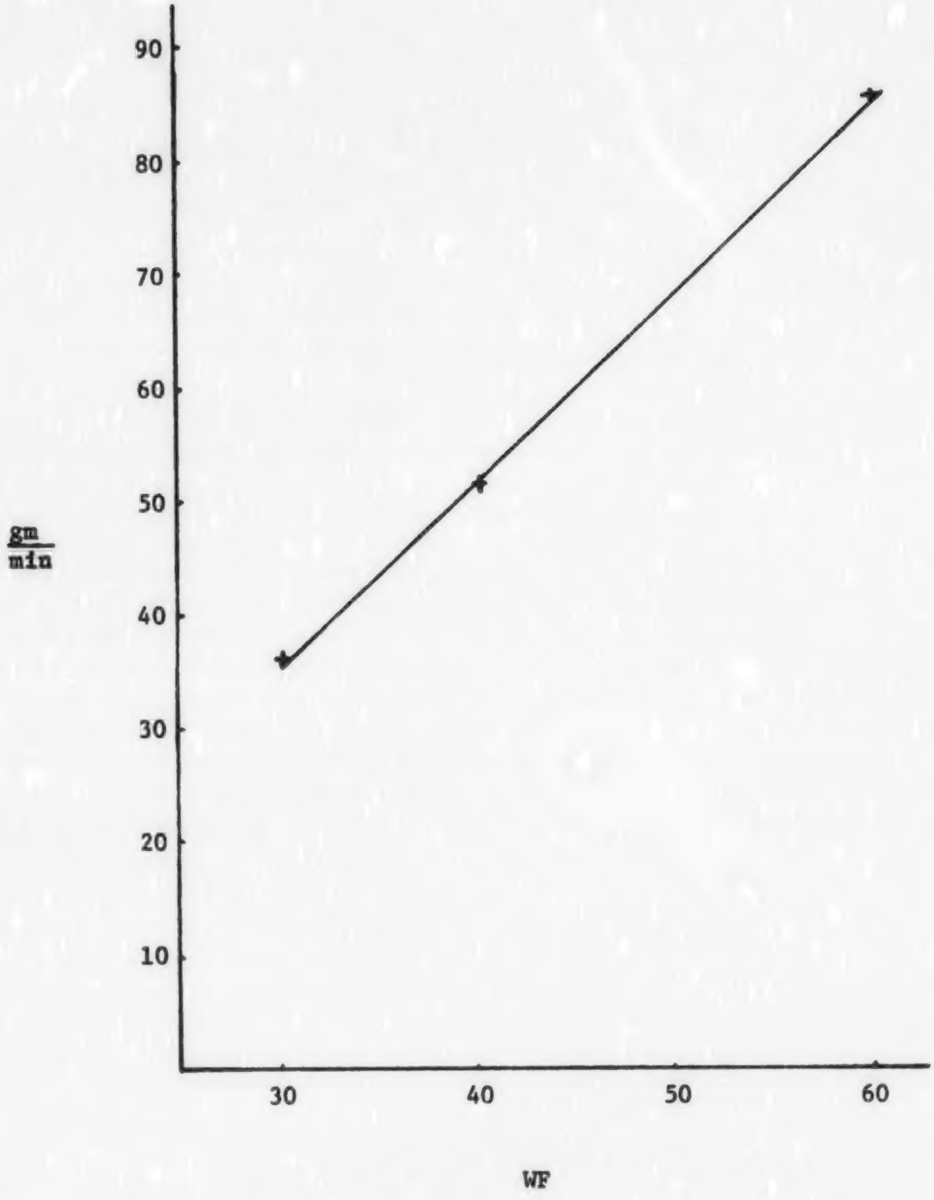

Figure 16. Wire Feed Rate Calibration